River flood reconstruction in the Lower Rhine valley and delta

Water levels and discharges in past landscape contexts

Reconstructie van rivieroverstromingen in de Benedenrijnse laagvlakte en Rijndelta

Waterstanden en afvoeren in vroegere landschapscontexten

(met een samenvatting in het Nederlands)

Proefschrift

ter verkrijging van de graad van doctor aan de
Universiteit Utrecht
op gezag van de
rector magnificus, prof. dr. H.R.B.M. Kummeling,
ingevolge het besluit van het college voor promoties
in het openbaar te verdedigen op

vrijdag 22 oktober 2021 des middags te 2.15 uur

door

Bas van der Meulen

geboren op 9 september 1991
te Amersfoort

Promotor:

Prof. dr. H. Middelkoop

Copromotor:

Dr. K.M. Cohen

The work in this thesis was financially supported by the Dutch Research Council (Nederlandse Organisatie voor Wetenschappelijk Onderzoek, project 14506).

Utrecht Studies in Earth Sciences 236

River flood reconstruction in the Lower Rhine valley and delta

Water levels and discharges in past landscape contexts

Bas van der Meulen

Utrecht 2021

Faculty of Geosciences, Utrecht University

Examination committee:

Prof. dr. G. Benito, CSIC Madrid
Prof. dr. J. Herget, University of Bonn
Prof. dr. S.J.M.H. Hulscher, University of Twente
Prof. dr. J.C.J. Kwadijk, Deltares
Prof. dr. J. Renes, VU Amsterdam

ISBN 978-90-6266-603-4

Published by Faculty of Geosciences, Utrecht University, the Netherlands, in:
Utrecht Studies in Earth Sciences, ISSN 2211-4335

DOI:10.33540/879

Printed by Ipskamp, the Netherlands

Cover: Lower Rhine flood extents on a historic map and in a numerical model result.
Historic map: *Gelders Archief* (Übersichtskarte des Rheinstroms und des Terrains zwischen Wesel und Arnheim in Beziehung auf die Überschwemmung des Jahres 1784).
Reconstructed topography: *Geomorphology* (van der Meulen et al., 2020).
Palaeoflood simulation: *Earth Surface Processes and Landforms* (van der Meulen et al., 2021).

Contents

Preface

Over the past four years, I learned a lot about geography and geology, about history and hydrology, but most importantly about myself. This was the first time I actually had to ask for support, both professionally and in my personal life, which wasn't easy. Here, I thank all the people who helped me during my research, providing data and insights that contributed to this thesis. Moreover, I thank my family and friends, without whom I would have definitely drowned in my flood research and possibly in life – I am glad that you kept me afloat.

First, I thank my supervisors Kim Cohen and Hans Middelkoop for creating the PhD opportunity and always trusting me to bring it to completion. During the first three and a half years of my research, you gave me all the freedom in the world, which allowed me to thoroughly follow my interests across disciplines. Near the end of my project, I received more supervision, and without your advice and guidance during this period, I would not have been able to finish. Kim – despite your sometimes chaotic working and supervising styles, you imparted a great deal of knowledge and research skills on me. Hans – your specific feedback on my manuscripts was always useful. I thank both of you for the memorable times we shared at conferences and in the field, in the Netherlands and abroad. During these trips, we got to know each other on a more personal level, and I fondly look back on those moments.

Second, I thank all members and advisors of the Floods of the Past, Design for the Future project – Anke Becker, Anouk Bomers, Ysbrand Graafsma, Frans Hoefsloot, Suzanne Hulscher, Menne Kosian, Rita Lammersen, Hans Renes, Ralph Schielen, Willem Toonen, Walter van Doornik, and Ellen Vreenegoor. Willem – during my bachelor, I conducted a variety of laboratory and software analyses in your PhD project. This was a great experience and I have always appreciated the connection with my own research. Anouk – we collaborated well, despite our different backgrounds in geology and engineering. We regularly met in Utrecht or Enschede, and all meetings ended on a positive note. I am proud of the two excellent papers that we produced together, both focused on the combination of landscape reconstruction and flood modelling. Everyone – thank you for the input and involvement during our half-yearly user meetings. The sincere interest you showed in my work and the discussions after (or during) my presentations often motivated me.

During my PhD research, I collaborated with many other scientists besides the Floods of the Past, Design for the Future project team. Although most are thanked in the acknowledgement sections of the individual chapters, I want to mention a few people in particular. Marco van Egmond – thank you for introducing me to the world of historical cartography. In addition to helping me find crucial data, you supported me to attend a course on the subject and to present at a specialized conference, both of which were very enlightening. Willem Overmars (†) – we met several times early on in my project, sharing common interests in fluvial morphology and historic river maps. I learned a lot from you during those meetings. Martijn Defilet, Leo Tebbens, Marieke van Dinter, and others – whenever I wanted to dive into archaeological research, you were willing to help me

out. Gerben Zielman – thank you especially for giving me the opportunity to collaborate with you on the Jansbeek report. Jürgen Herget – thank you for guiding me through the upstream part of my study area. The trip around Bonn and Cologne was a wonderful experience and on top of that greatly increased my familiarity with the region. Livio Ronchi – I visited you in Padova multiple times after supervising the student fieldwork, which made the yearly trip to Italy even more fun. Jasper Candel, Hessel Woolderink, and many others – thank you for the good times at the various conferences where we ran into each other. Thinking back brings up many nice memories of dinners, drinks, and, of course, insightful discussions.

Besides doing research, I spent a lot of time on teaching, including numerous courses, excursions, and fieldworks. In particular, I enjoyed supervising students and cooperating with them during their research projects, whether BSc honours project, BSc thesis, MSc guided research, MSc thesis, or bright minds assistantship. Tessa Deggeller, Roy Dierx, Yorick Fredrix, Liam Hall, Silke Meijdam, Jelle Olthuis, Jari Wouters, and Jip Zinsmeister – thank you for your efforts, your enthusiasm, and the in-depth discussions on your respective subjects. Each of you worked on an innovative topic and produced interesting results, some of which found their way into my thesis. Jip – I wish you the best of luck with your PhD in Leuven on floodplain evolution.

Without naming everyone, I want to acknowledge all my (former) colleagues at the department of Physical Geography. Maarten Zeylmans – I am grateful for the extensive help with GIS and for the opportunity to provide guest lectures in your MSc course. Harm Jan Pierik – the landscape reconstruction aspects of my research benefited from your input. Furthermore, I enjoyed sharing an apartment with you during the INQUA congress in Dublin. Maarten Kleinhans, Menno Straatsma, Esther Stouthamer, Wim Hoek, and several others – thank you for checking in with me at times despite not being directly involved in the project. It is nice to experience some support during the often individualistic PhD trajectory. Most of all, I acknowledge my fellow PhD candidates, who provided distraction and focus, and sometimes both at the same time. Thank you for being there – Anne Baar, Muriel Brückner, Jana Cox, Job de Vries, Willem-Jan Dirkx, Fabian Ercan, Ed Jones, Bas Knaake, Lonneke Roelofs, Teun van Woerkom, Steye Verhoeve, Steven Weisscher, Tim Winkels, Danghan Xie, and all others. Tim – thanks for taking me on many small field trips and showing me the ins and outs of coring. Fabian – thanks for being a great roommate in the 'aioquarium' and in the Zonneveldvleugel. For those of you still working on your projects – best of luck and please don't hesitate to contact me if I can be of any help!

Last but not least, I thank my family and friends for their love and support. To start, I thank my parents Marjan and Aarnout, my twin brother Joris, my younger sister Paulien, and my younger brother Kees. Mama and papa – you instilled the fascination for the natural environment in me, bestowed me with a critical mind, and learned me to 'read the landscape' during family holidays. In short, you unwittingly provided me already in childhood with the motivation and skills necessary to obtain a PhD in physical geography. Joris – we share the same DNA, which creates a dynamic that most people can impossibly comprehend. This has led to many conflicts, but also to some wonderful moments of connection – thank you for those. Paulien and Stephan – thank you for the regular mountainbike rides. Your company, going out in nature, and getting some exercise all meant a lot to me during the final stages of my PhD. And, of course, my baby niece Julia – thank you for simply existing! Kees – thank you for always being my 'little' brother and for being an overall top bloke. I sincerely hope you have as good a time as I had studying Earth Sciences. Many thanks also to my grandmothers and late grandfathers – love you.

A big hug to all my friends – including everyone that I do not mention here. I look forward to seeing each of you more often now that my mind is liberated from constantly thinking about my thesis. Niels – the fieldworks that we conducted together and our road trips in the USA are amongst my best memories. We have many shared interests, which is absolutely fantastic. Roel, Luc, Carlijn – our friendships deepened over the years, for which I am very grateful. Thank you for the pleasant dinners and walks. Cindy, Levi, Karin, Simon, David, Jesse, Stefan, Robin, and many others – thank you for all the fun (online) board game nights and weekends. Michiel, Jetze – I always enjoy our light-hearted banter and I am glad that we still keep in touch. Floris – thank you for the weekly running sessions that often turn into more talking than walking. There has always been a great deal of natural trust between us, which is incredibly valuable. Lisanne – you are the nicest person and on top of that one of the best scientists I know. Thank you for being my everything for so long.

Utrecht, summer 2021

BvdM

Chapter 1

Introduction

Measure what can be measured, and make measurable what cannot be measured.

Galileo Galilei

1.1 Relevance

Major river floods are amongst the most destructive natural hazards worldwide. In northwest Europe, flood risk and impact have increased and will continue to do so, due to climate change and economic growth (Benito et al., 2015; Winsemius et al., 2016; Blöschl et al., 2017; 2019). In the Lower Rhine valley and delta (Fig. 1.1), many large and disastrous floods occurred throughout historic times (Weikinn, 1958–1963; Gottschalk, 1971–1977; van de Ven et al., 1995; Buisman, 1995–2019; Glaser and Stangl, 2003). At present, an extreme flood may do considerably more damage than in the past, because the low-lying floodplain areas have become densely populated. To determine which preventive measures are necessary, it is essential to constrain magnitude–frequency relations of extreme river discharge. Such calculations generally rely on instrumental measurement records and improve by incorporating older flood magnitudes, especially for the largest events (e.g. Benito and Thorndycraft, 2005; Toonen et al., 2016; Reinders and Muñoz, 2021). Therefore, it is important to study past extreme floods, which is the subject of this thesis.

1.2 Project

My research is part of the project *Floods of the Past, Design for the Future*, led by Utrecht University and the University of Twente, supported by several partners in government and consultancy. The aim of this project is to constrain past flood magnitudes in the transboundary Lower Rhine region (Fig. 1.1) and use that information to improve assessments of future extreme discharges (Cohen et al., 2016a). Earlier and overlapping PhD research in the project focused on hydraulic and statistical modelling (Bomers, 2020), whereas my PhD research focused mainly on flood level and landscape reconstructions over the past centuries to millennia. I approached all aspects of my research in a multidisciplinary way, applying geological, geomorphological, archaeological, and historical geographical techniques whenever relevant (Section 1.5). In addition, my research encompassed numerical simulations of past floods thanks to collaboration within the project.

1.3 Research context

Determining absolute discharge magnitudes of past river floods requires reconstruction of water levels combined with hydraulic calculations (see overviews of palaeoflood studies in Baker, 2008; Benito and Díez-Herrero, 2015; Benito et al., 2020). The large majority of these studies have been carried out in settings with stable morphology, such as bedrock-incised river canyons. Settings with dynamic morphology require reconstruction of channel and floodplain geometry as an additional step prior to hydraulic calculations (e.g. Sudhaus et al., 2008; Toonen et al., 2013; Machado et al., 2017). Without accounting for the landscape context, reconstructed water levels cannot provide conclusive insights into the discharge magnitudes of past floods in dynamic alluvial settings. The Lower Rhine valley and delta are geomorphologically dynamic, similar to most other lowland regions, and on top of that heavily influenced by anthropogenic activities (e.g. Kalweit et al., 1993; Hudson et al., 2008; van der Meulen et al., 2020). Therefore, any palaeoflood calculations in this study area demand a proper reconstruction of the terrain.

Most palaeoflood studies rely on cross-sections and are thus one-dimensional (Webb and Jarrett, 2002). This is usually stated explicitly when it comes to the hydraulic calculations, but essentially also applies to the reconstructions of flood levels and morphology. Upscaling the methodology to

more than one dimension (spatially continuous reconstructions combined with a two-dimensional modelling approach) is considered beneficial, but highly uncommon due to data requirements and time and budget constraints (see discussions in England et al., 2010; Herget et al., 2014). Although the 'traditional' one-dimensional approach is appropriate for most fluvial reaches, any laterally extensive valley and delta setting, such as the study area of this thesis (Fig. 1.1), necessitates research in two dimensions.

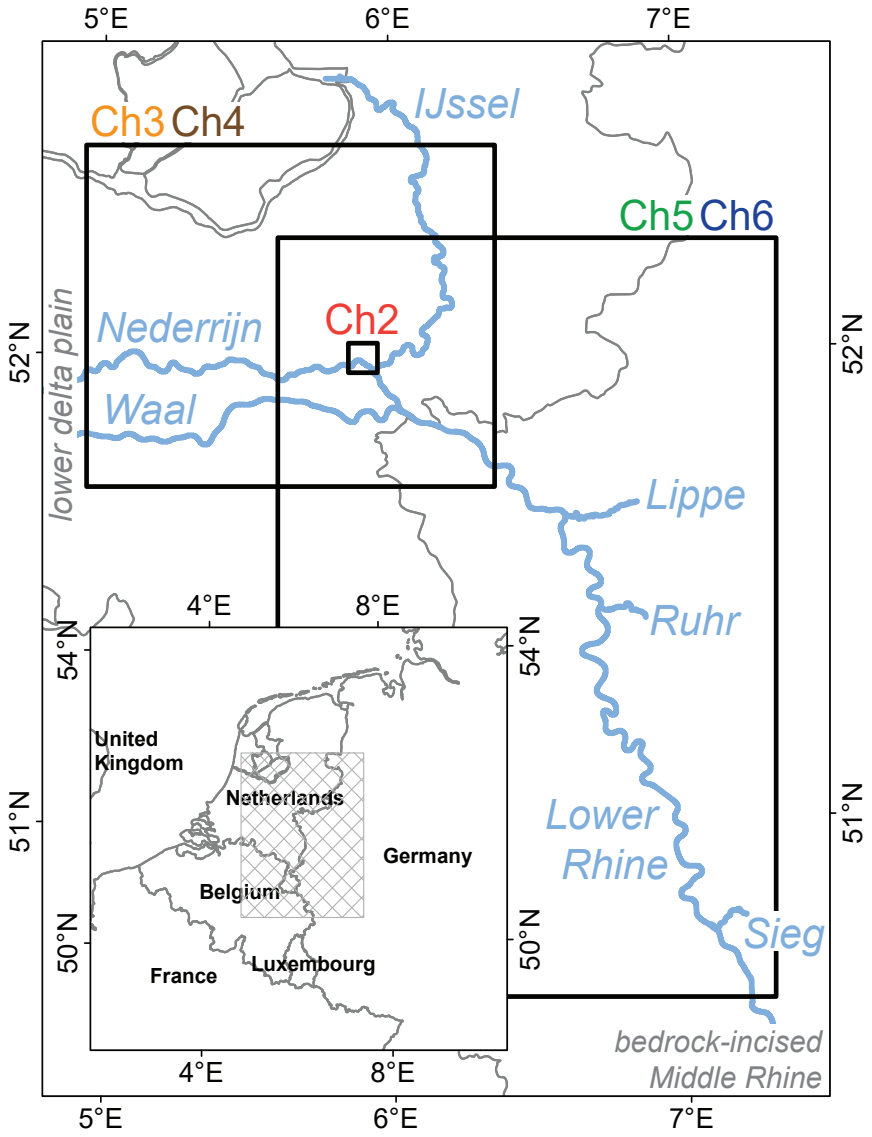

Fig. 1.1. Study area covering the Lower Rhine valley and delta in Germany and the Netherlands. The boxes indicate the approximate spatial extents of the different chapters in this thesis.

Reliable flood risk assessments are very important for the densely populated Lower Rhine region. Therefore, several studies already focused on past floods of this river. These include two cross-sectional analyses, one for the Middle Holocene period (Toonen et al., 2013) and one for the late medieval period (Herget and Meurs, 2010), both applying a single flood level reconstruction and a simple landscape reconstruction. Furthermore, grain-size variations in fluvio-lacustrine sediments have been applied to determine recurrence times and associated relative magnitudes of past floods of the Lower Rhine (Toonen et al., 2015; Cohen et al., 2016; Minderhoud et al., 2016). In addition, historical written records have been used to determine relative flood magnitudes based on intensity indicators such as damage descriptions (Glaser and Stangl, 2003; Toonen, 2015). This thesis builds upon these existing studies by determining the water levels reached during past floods across the Lower Rhine region and by calculating absolute flood magnitudes using a two-dimensional hydraulic modelling approach in the reconstructed landscape context. As such, it also contributes to quantitative palaeoflood research in general by unravelling the necessary conditions for upscaling the methodology from stable confined to dynamic unconfined fluvial settings.

1.4 Objectives

The overarching goal of my research is to determine absolute magnitudes of the largest historic floods in the Lower Rhine valley and delta in two dimensions. This requires three major steps, namely (1) determining past flood levels, (2) reconstructing river and floodplain landscape contexts, and (3) conducting hydraulic calculations. I aim to implement every aspect at unprecedented levels of detail and completeness. Separated by step, the objectives of my research are to:

1. *Determine the water levels reached during the largest floods in pre-instrumental times.*
2. *Reconstruct the river and floodplain morphology at different times in the past by accounting for both natural and anthropogenic changes.*
3. *Define palaeoflood patterns and magnitudes by hydraulic simulations in the past landscape context.*

All three of these steps have never been conducted for the full study area. Consequently, my research aims to contribute a large amount of new data products. Furthermore, it aims to explore and push the limits of different palaeoflood hydrological research methods, which have rarely been applied to low-gradient alluvial settings (Section 1.3). Overall, my research aims to advance current insights into past flooding patterns of the Lower Rhine river, which is of both scientific and societal relevance (Sections 1.1 and 1.2).

1.5 Outline

Deriving from the objectives, my research approach comprises flood level reconstruction, river and floodplain landscape reconstruction, and extreme discharge reconstruction. Chapters 2 and 3 deal with flood levels, Chapters 4 and 5 deal with river and floodplain morphology, and Chapter 6 deals with discharge magnitudes. The main focus areas of the different chapters are summarized in Fig. 1.2. Their positions in the flooded fluvial system are illustrated in Fig. 1.3.

More specifically, *Chapter 2* presents an overview of late medieval extreme flood levels extracted from geological-archaeological and historical data, with the city of Arnhem as main case (Fig. 1.1). This chapter already stresses the importance of accounting for morphological changes in palaeoflood

research, and the importance of incorporating more than one dimension in a delta setting. The next two chapters report on historical geographical data collection campaigns and subsequent analyses. These cover the upper and central delta (Fig. 1.1). *Chapter 3* provides an overview of flood levels obtained from epigraphic marks. This is the first time these marks are systematically collected and measured in the Rhine delta. *Chapter 4* is about landscape reconstruction using historic maps and measurement data, with a focus on fluvial morphology. The results of this chapter have been successfully applied in historic flood simulations.

Chapters 5 and 6 together illustrate the combination of landscape reconstruction and palaeoflood simulation envisioned in the project (Section 1.2), for the entire Lower Rhine river valley and upper delta region (Fig. 1.1). *Chapter 5* explores the construction of a high-resolution palaeo-DEM (Digital Elevation Model of a past situation) and pushes the limits of terrain reconstruction far beyond current standards. *Chapter 6* uses this palaeo-DEM, together with new reconstructions of roughness values and palaeoflood levels, to estimate the Late Holocene millennial flood magnitude by 1D–2D coupled hydraulic modelling. The thesis ends with a synthesis (*Chapter 7*) that provides the main findings and overarching insights, recommends future research opportunities ('next steps'), and discusses further scientific and societal implications.

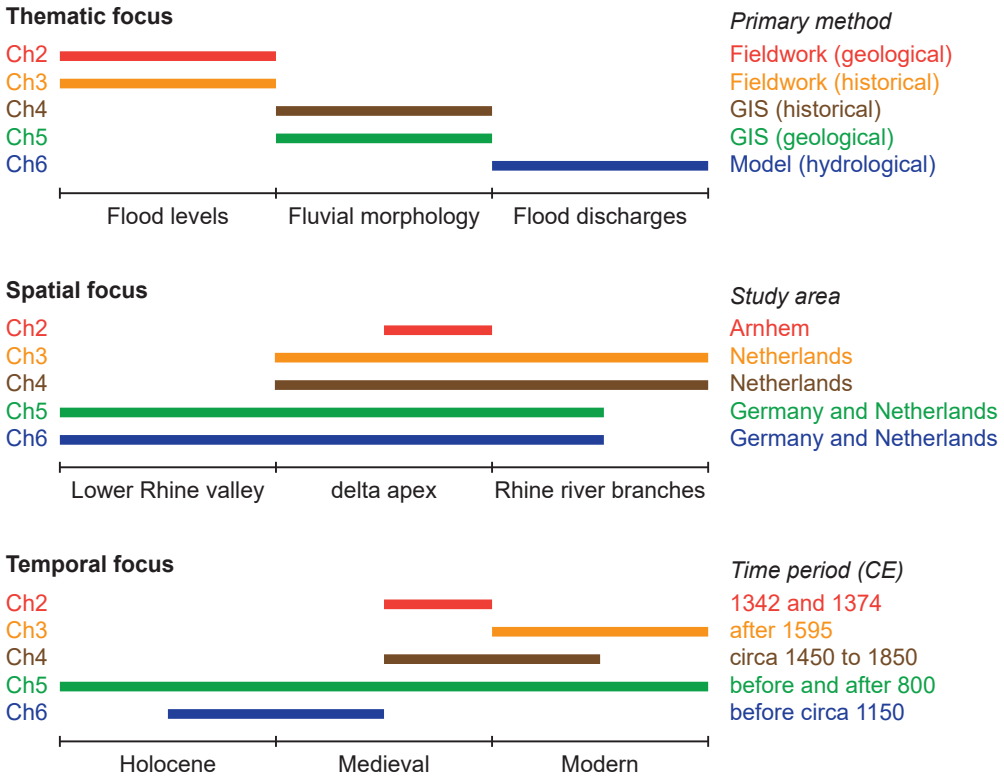

Fig. 1.2. Thematic, spatial, and temporal focus areas of the different chapters in this thesis.

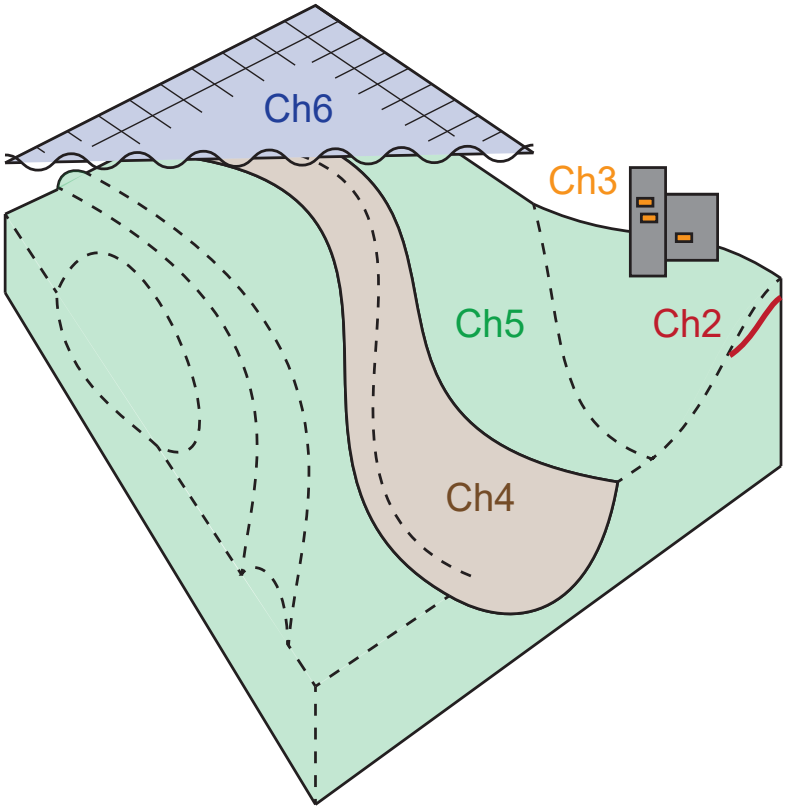

Fig. 1.3. Elements of the river and floodplain system addressed by the different chapters in this thesis, covering flood levels in the geological-archaeological record (Chapter 2), flood marks on buildings (Chapter 3), river bathymetry (Chapter 4), floodplain topography (Chapter 5), and flood wave propagation (Chapter 6).

Chapter 2

Medieval extreme flood levels

this chapter is based on

van der Meulen, B., Defilet, M.P., Tebbens, L.A., Cohen, K.M., 2021 (submitted). Palaeoflood level reconstructions in a lowland setting from urban archaeological stratigraphy, Rhine river delta, the Netherlands. Catena, under review.

– Ons land is natuurlijk klein, maar de bodem is bijzonder gevarieerd.
– Dat verbeeldt men zich bij u, omdat er op iedere vierkante meter een geoloog staat met een microscoop.

Willem Frederik Hermans – Nooit meer slapen (1966)

Abstract

Reconstructing water levels reached during past floods contributes to fluvial system understanding and flood risk assessments. For methodological restrictions, this type of research is usually conducted in confined valley settings. In this study, we expand upon that geomorphological context by reconstructing extreme flood levels in a lowland delta setting. We used the archaeological stratigraphy of medieval river cities in the Rhine delta to determine water levels for the largest historic flood in the year 1374. We obtained minimum estimates by identifying thin fluvial deposits interbedded with anthropogenic layers, and further constrained peak flood levels using fourteenth-century raised ground layers directly overlying these deposits. First, we tested the proposed method for extracting flood levels from urban archaeological stratigraphy in the city of Arnhem. Then, we complemented those results with archaeological and historical data in other cities to arrive at a complete overview for the Rhine delta. This overview shows that the 1374 flood levels exceed the highest levels in the instrumental record along the northern distributary (IJssel river), but not along the western distributaries in the central delta (Nederrijn and Waal rivers). This pattern is explained by changes in the discharge division over the different river branches and by the rise of embankments since late medieval times, which considerably decreased the flooded area. Thus, this study demonstrates not only the potential of palaeoflood reconstructions in lowland floodplain settings, but also the pitfalls, resulting from spatially complex flooding patterns and anthropogenic terrain modifications.

2.1 Introduction

Determining magnitudes of pre-instrumental extreme floods improves risk assessments and geomorphological understanding of fluvial systems (Baker, 2008; Benito and Díez-Herrero, 2015; Wilhelm et al., 2019; St. George et al., 2020). The most important parameter in quantifying past floods is the maximum water level reached during the event (Herget et al., 2014), which can be obtained from various sources. For floods in recent centuries, instrumental measurement records and epigraphic marks provide direct indications of maximum water levels (Pinter et al., 2006; Macdonald, 2007; Balasch et al., 2019). In the absence of these types of data, the reconstruction of older flood levels relies on historical or geological data (Benito et al., 2004). Combining documentary and sedimentary records reduces the uncertainties associated with each approach (Sheffer et al., 2003; Thorndycraft et al., 2006; Schulte et al., 2019; Herget, 2020).

Written sources such as administrative data (e.g. city financial accounts) and descriptive data (e.g. chronicles) often provide information on floods, for example regarding their dates, durations, and intensities (Witte et al., 1995; Glaser and Stangl, 2003; Kjeldsen et al., 2014; Barriendos et al., 2019; Li et al., 2020). However, written records rarely provide direct indications of flood level. The extraction of quantitative levels requires sources that describe the exceedance or non-exceedance of a datum such as a bridge or city gate by the flood waters (Benito et al., 2004; 2015; Kadetova and Radziminovich, 2020). Through geographical and historical surveys, such records can then be appended with absolute height values (Wetter, 2011; Elleder et al., 2013; Wetter et al., 2017).

Geological methods for reconstructing flood levels predominantly rely on the identification of fine-grained slack-water deposits at high positions along a river (Kochel and Baker, 1982; Zhang et al., 2014; Lam et al., 2017; Machado et al., 2017). The elevation of such a flood bed provides

a minimum estimate of the local water level during flooding, as water depth and flow velocity were sufficient to transport suspended sediment load. The actual maximum water level exceeds the elevation of the deposit, but the difference between the two is difficult to quantify and varies with hydraulic setting (Guo et al., 2017). Reported differences range from a few decimetres up to two metres (Benito et al., 2004). In fact, the relation between flood beds and actual water-surface elevations is one of the principal sources of error in palaeoflood research and requires further research (Jarrett and England, 2002; Benito and Díez-Herrero, 2015; Benito et al., 2020).

Traditionally, palaeoflood deposits are collected in geomorphologically stable fluvial settings such as bedrock-incised river reaches, where a relatively small increase in discharge results in a significant rise of water levels and the stable morphology enables calculating past discharges from water levels without accounting for changes in channel bathymetry and floodplain topography. In dynamic lowland settings, the rise of water level with discharge is modest and reconstruction of past morphology is complex (van der Meulen et al., 2020). Hence, alternative methods for palaeoflood reconstruction have been developed for alluvial reaches that focus on relative magnitudes and circumvent the requirement of knowing past flood levels (Toonen et al., 2015; Munoz et al., 2018; Peng et al., 2019; Toonen et al., 2020). Still, in light of recent advances in palaeoflood modelling (van der Meulen et al., 2021), it is particularly relevant to reconstruct flood levels for alluvial settings, as these are generally characterized by dense population and high flood risk.

This study focuses on the extreme flood of the year 1374 in the Rhine delta (Fig. 2.1). It also discusses the flood of the year 1342, which for several rivers in central Germany (including some Rhine tributaries) was the largest event in historic times (Herget et al., 2015). However, along the Lower Rhine river and in the Rhine delta, the winter flood of 1374 was even larger than the summer flood of 1342, and resulted in the highest water levels not affected by ice jams over the

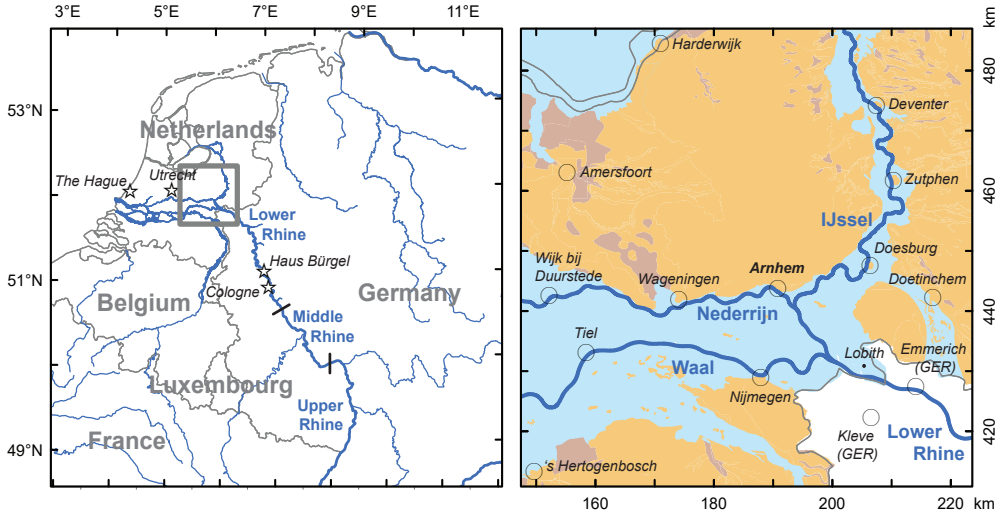

Fig. 2.1. Left: Location of the study area (upper part of Rhine delta). Right: Simplified geological map of the study area, distinguishing between Holocene fluvial and marine deposits (blue), Holocene peat (brown), and Pleistocene glacial and aeolian deposits (yellow).

past millennium in Cologne (Weber, 1977; Herget and Meurs, 2010; Krahe and Larina, 2010). The 1374 flood event triggered the meander cut-off near Zons, placing the Roman and medieval site Haus Bürgel on the right-hand side of the Lower Rhine (Zimmermann et al., 1930; Hansmann et al., 1973; Strasser, 1992). Allegedly, people sailed in a straight line from the city of Utrecht in the central delta to the city of The Hague at the coast (Fig. 2.2; van der Monde, 1835). This account is likely based on contemporary historical sources (Gottschalk, 1971; Buisman, 1996). Moreover, the extreme flood of 1374 possibly was the largest in the entire Holocene, according to sedimentary records in the delta apex region providing relative flood magnitudes based on grain sizes (Toonen, 2013; Cohen et al., 2016). Despite the numerous historical mentions and sedimentological evidence, a detailed study addressing medieval flood levels in the Rhine delta is lacking.

The overall aim of this study is to reconstruct historic extreme flood levels in the Rhine delta at multiple locations. To do this, we present a method for identifying flood signatures in medieval urban archaeological contexts, which largely derives from traditional palaeoflood hydrological approaches. We collect a series of fourteenth-century flood signatures in otherwise anthropogenic stratigraphy, which provide minimum water level estimates. Moreover, we propose the hypothesis that artificially raised ground layers were placed as a reaction to the extreme flood event, and thus provide maximum water level estimates. We test this hypothesis by compiling existing and new data in the city of Arnhem, and complement the flood level results obtained there with similar observations in nearby cities and with historical mentions that we convert into absolute flood heights. In addition to thoroughly constraining water levels for the 1374 flood in the Rhine delta, this study advances the methodological aspects and spatial applicability of palaeoflood hydrological research to lowland alluvial settings.

2.2 Materials and methods

To determine the water levels reached during the 1374 flood in the Rhine delta, we targeted medieval cities located at the edges of the delta plain (Fig. 2.1; Fig. 2.3). The manuscript focuses on new data obtained in the city of Arnhem, where extensive archaeological research has been carried out in recent years (e.g. reports by: van der Mark, 2016; van Engeldorp Gastelaars, 2019; Baetsen and Zielman, 2020). We used these data in combination with our own field surveys to test the applicability of archaeological stratigraphy in reconstructing maximum flood levels. Then, we complemented the Arnhem results with archaeological and historical data in other cities.

1374. 13 Januarij. Het water, in eene groote hoe-veelheid van boven uit het gebergte gekomen, overstroomde door de doorbraken in de Rijkerwaard, de Lek en meer andere dijken, veel land, waardoor geheel Holland onder water stond, zoo dat men dezen dag van Utrecht tot in 's Gravenhage regt over het land voer, daar alles was onder geloopen

Fig. 2.2. Example of a note on the 1374 flood event by a nineteenth-century gazetteer (van der Monde, 1835). The text states that Holland was largely submerged ("geheel Holland onder water") so that people sailed across in a straight line ("regt over het land"), as everything was flooded ("alles was onder geloopen").

We acquired available archaeological results from digital archives (easy.dans.knaw.nl) and through contacts with municipal archaeologists working in the targeted areas. For relevant historical information, we consulted established chronological overview studies on flood events and weather history in the Netherlands (Gottschalk, 1971; Buisman, 1996). We extracted flood levels from these sources through geological interpretation of the archaeological documentation and geographical analysis of historical references on relative flood heights.

2.2.1 Site selection

From a geomorphological perspective, potential sites are restricted to the Pleistocene grounds bordering the Holocene floodplain and isolated patches of high grounds within the floodplain. Given their elevations, and under a first assumption that medieval extreme floods reached levels similar to the highest values in instrumental data series (e.g. Toonen, 2015: events of 1809 and 1926), these areas flooded only very incidentally. Thus, these sites may have recorded maximum water levels of the very largest events.

From a historical perspective, sites of interest are restricted to cities founded before the fourteenth century. Unlike uninhabited sites and small towns, medieval cities have the available research context necessary to start a targeted search for past flood information. Within the selected cities, the areas with natural substrate elevations close to maximum observed flood heights usually coincide with the medieval urban centre (vicinity of main church, market square, city administrative buildings).

The geomorphological and historical preconditions largely overlap, as localities just outside the flooding regime have long been the preferred sites for human settlement. In the study area, medieval cities are mostly located on high grounds bordering the river, either on push-ridge relief inherited from the penultimate glacial period (e.g. Arnhem, Nijmegen, Fig. 2.1; also in Germany: Kleve, Xanten), on inland dune ridges inherited from the last glacial (e.g. Doesburg, Zutphen, Fig. 2.1; also in Germany: Emmerich, Wesel), or on Late Holocene levee complexes at former bifurcation points of Rhine river branches (e.g. Lobith, Tiel, Fig. 2.1).

2.2.2 Data inventory – Arnhem

From the available archaeological information, we determined the general stratigraphy beneath the medieval city centre. Reports of excavations provide stratigraphic features in horizontal planes and vertical profiles, which administer the archaeological finds such as pottery shards and coins. The connection between finds and stratigraphic features provides the primary dating control for strata and buried surfaces in the urban archaeological setting, sometimes complemented with geological dating (^{14}C, OSL), dendrochronology, or historical dating (e.g. documented building phases). We used the general stratigraphy to identify the areas with medieval surface elevations close to the highest measured water levels.

Detailed stratigraphic data for these areas do not directly reveal potential extreme flood deposits such as thin clay beds. In general, archaeological profiles differentiate natural and anthropogenic layers at cm to dm-scale, but thin (mm to cm-scale) layers are rarely registered (Fig. 2.4). Therefore, in our explorative analysis of the available information, we first looked for artificially raised ground

layers dated to the fourteenth century. Raised grounds are usually well-dated based on artefacts in these layers and in the surrounding strata and structures. Then, we searched for flood signatures below the raised ground both in field surveys (vicinity of Eusebius church, Fig. 2.3) and in archived data of earlier excavations (Musiskwartier, Fig. 2.3).

2.2.3 Field surveys – Arnhem

During a series of site visits in 2017–2019, we described temporary sections with attention to suspected palaeoflood signatures. The visits took place during excavations related to large inner city restoration projects, including the reintroduction of a duct for the Jansbeek stream (Fig. 2.3; Baetsen and Zielman, 2020). These excavations, executed by commercial archaeological subcontracting companies under municipal authority (Netherlands implementation of Valetta 1992 EU treaty), removed post-war building foundations and WWII-damage top strata, allowing us to collect geological-geomorphological data at the desired but normally hard to investigate locations in the paved and overbuilt city centre of Arnhem. Besides conducting our field activities, we frequently contacted the archaeological investigators to exchange preliminary data before, during, and after visits.

The field research steps consisted of inspecting exposed sections, prospective hand coring (Edelman auger and gauge), and local trenching to obtain detailed profiles. This strategy aimed to identify Rhine flood deposits (fine-grained, calcareous, homogenous, artefact-free, laterally traceable) interbedded with anthropogenic strata. We constrained the ages of flood layers using archaeological

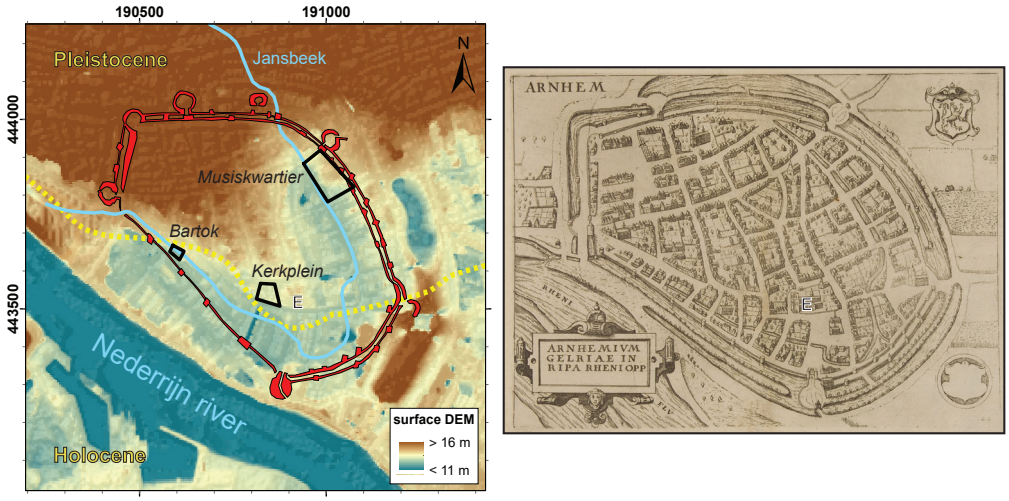

Fig. 2.3. Left: Interpolated ground level DEM of Arnhem with hill-shade overlay. The dashed yellow line is the approximate boundary between Pleistocene and Holocene deposits, as in Fig. 2.1. The blue line is the medieval canalized course of the Jansbeek and the red outlines are the former city walls obtained from sixteenth-century historic maps (Kosian et al., 2016). The black polygons are the locations of archaeological excavation campaigns of which results are shown in Fig. 2.4. Right: Historic map of Arnhem (L. Guiccardini, circa 1565). E = Eusebius church.

dating information obtained locally from underlying and overlying strata and from the already studied reports, verifying whether the highest identified deposits indeed date to the fourteenth century and thus relate to the 1374 millennial flood event. Further, we examined the raised ground directly above the flood bed to determine whether it was placed shortly after the event (relatively

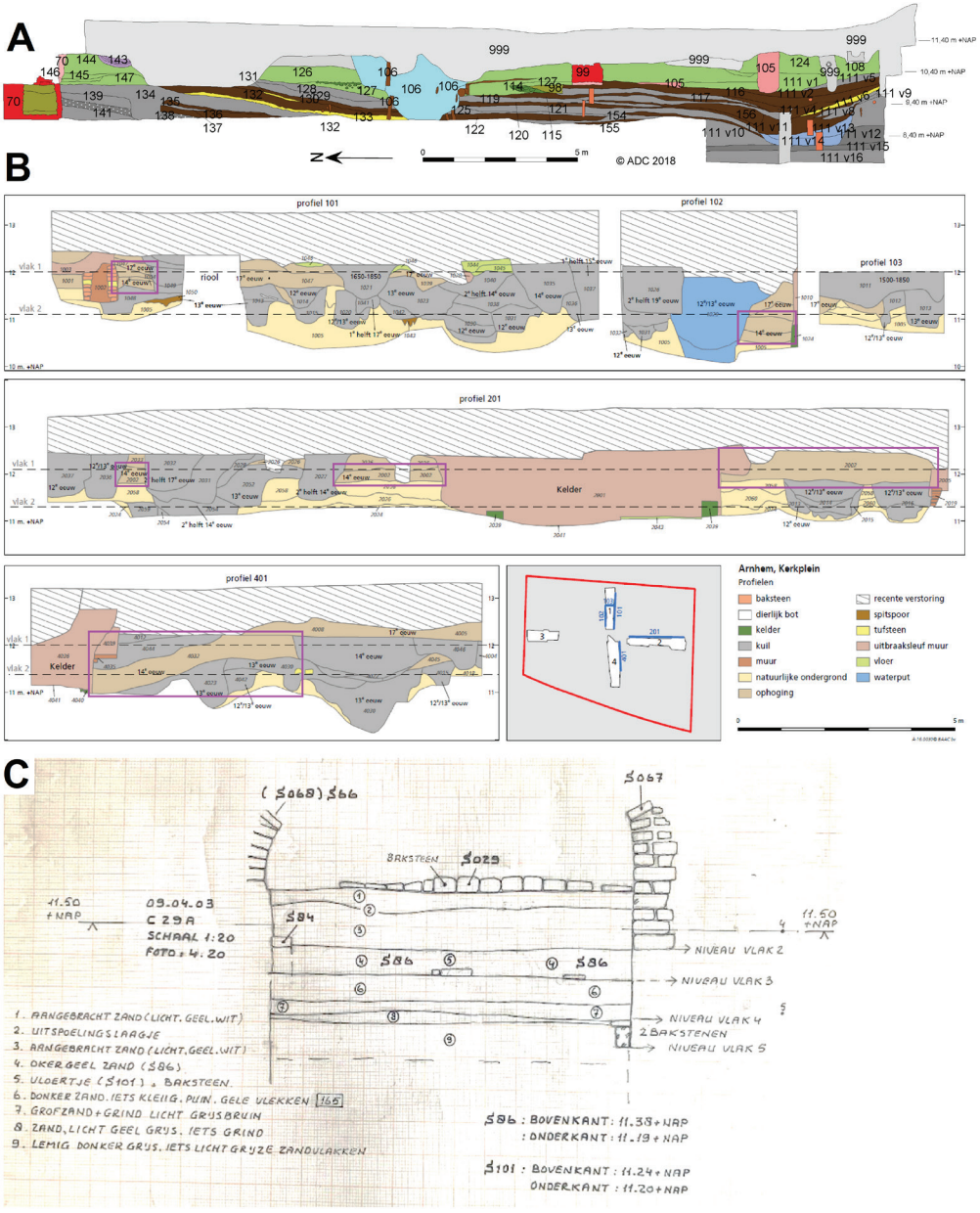

Fig. 2.4. Description on next page.

uniform appearance, not containing artefacts younger than the late fourteenth century). In this way, we tested our hypothesis that the ground surface in critical areas was raised as a reaction to the event, most likely to the level of the flood water, thus providing a better indication of the maximum flood level than the actual deposits.

Elevations and layer thicknesses were recorded with total stations and differential GPS at all locations, allowing us to identify the highest occurrences of flood deposits. We combined the results for the visited sites in the Eusebius church area with unpublished field sketches from the Musiskwartier. In this part of the city, the topography is defined by the valley of the Jansbeek (Fig. 2.3). This small stream, seepage-fed from the Pleistocene push-ridge complex and predominantly transporting sand and organics, may have acted as a back-flooded tributary during medieval extreme floods of the Rhine (Supplementary Information).

2.2.4 Regional upscaling

For the selected other medieval cities and river towns in the Rhine delta, we analysed existing archaeological descriptions at sites with estimated substrate elevations close to highest water levels in measurement records. In cities located on large topographic elements well above the floodplain such as Nijmegen (Fig. 2.1), the areas within target elevations are smaller than in Arnhem, limiting the local applicability of our research strategy. More suitable were cities positioned on inland dune outcrops, notably Doesburg and Zutphen (Fig. 2.1), where archaeological studies indicate thick raised ground layers dating to the fourteenth century. For medieval river towns located in the floodplain, where archaeological stratigraphy overlies natural levee deposits such as in Lobith (Fig. 2.1), the top of the fluvial succession only provides a very minimum estimate of flood level. Still, raised ground with adequate dating control may suggest a correlation to a medieval extreme flood event and thus provide an estimate for its maximum water level.

Besides the geoarchaeological examinations, we reviewed historical information to complement the 1374 flood level reconstructions where possible. Historic flood marks inscribed on stones in buildings or landmarks (epigraphic records; Macdonald, 2007) do not date back to before the sixteenth century in the Netherlands. Therefore, we relied on documentary sources, targeting references that specifically mention relative water height. Contemporary data for the medieval

Fig. 2.4. Selected examples of archaeological profiles in the medieval city of Arnhem. A: Profile at Bartok archaeological site (van Engeldorp Gastelaars, 2019), showing sand and clay deposits in respectively yellow and dark grey, peat and peaty clay layers in dark brown, medieval raised ground layers in green, and recent disturbed grounds in light grey; ^{14}C dates for the peaty layers yield calibrated ages in the tenth to thirteenth centuries. B: Profiles at Kerkplein archaeological site (van der Mark, 2016), showing Pleistocene sand deposits (natural subsurface) in yellow, and artificially raised ground layers in light brown; layers dated to the fourteenth century are highlighted by purple rectangles. C: Profile (field sketch) at Musiskwartier archaeological site (Supplementary Information; van der Mark et al., 2006), showing a 'washed-out layer' (layer 2, 'uitspoelingslaagje') in between two sandy raised ground layers (layers 1 and 3, 'aangebracht zand'); pottery shards collected from layer 6 date to 1250–1525; building remnants above layer 1 date to 1400–1425. Excavation locations indicated in Fig. 2.3.

study period are limited to administrative sources and chronicles. We traced relevant original sources starting from historical scientific overview studies (Gottschalk, 1971; Buisman, 1996). Other studies mentioning the fourteenth-century flood events, such as gazetteers (Fig. 2.2) and books on local history, rarely provide original sources and are considered less reliable (Brázdil et al., 2006). For the medieval cities of Deventer and Tiel, we found reliable historic references to water level in relation to buildings and other landmarks. We visited and measured (GPS, LiDAR) the locations described, and consulted available historical information to establish past dimensions of mentioned features such as streets and city walls, thereby deriving absolute flood heights for 1374.

2.3 Results

Here, we describe the results for each site that provided quantitative information on the 1374 flood. We first present all results for the city of Arnhem, where we obtained abundant palaeoflood data within the urban archaeological context. Then, we give the results for the other sites, extracted from both archaeological and historical sources, and compare our estimates of maximum flood levels in 1374 to the levels of the largest twentieth-century flood in 1926.

2.3.1 Flood levels in Arnhem

The city of Arnhem is located on the right-hand side of the Nederrijn river (Fig. 2.1). This area was already inhabited before the Bronze Age. Arnhem was first mentioned in the year 893 and was granted city rights in 1233. The medieval urban centre is for the most part located on an outwash fan of a Middle Pleistocene ice-pushed ridge, which consists almost completely of coarse sand with some gravel. To the south, this geomorphological unit borders Rhine fluvial deposits, consisting mostly of clay. The margin of the Holocene floodplain is locally recognisable in the topography, but largely obscured by anthropogenic modifications to the terrain (Fig. 2.3). In the north-eastern part of the medieval centre, a small valley is present created by the Jansbeek stream originating from the ice-pushed ridge. The highest flood levels at Arnhem observed in the instrumental period are about 13 m NAP (Normaal Amsterdams Peil, the national vertical datum; 0 m NAP is approximately mean sea level). Presuming that past extreme floods reached a roughly similar level, the parts of the city best suitable for collecting potential flood levels are where the top of the Pleistocene substrate is below and the present surface above 13 m NAP.

In the southernmost part of the medieval city centre (present surface elevation ~12.5 m NAP, Pleistocene surface elevation <8.5 m NAP), relatively thick fluvial deposits occur that are slightly inclined and thicken in southward direction (Fig. 2.4A). The top of these floodplain clay deposits is at 10.4 m NAP. The high organic content in some layers may suggest agricultural use of the floodplain in early medieval times (van Engeldorp Gastelaars, 2019). The upper fluvial strata are overlain by anthropogenic raised ground layers up to 11 m NAP, above which the ground is recently disturbed (Fig. 2.4A). This area was flooded regularly in medieval times and thus only provides a very minimum estimate of the water level reached during the largest floods. In the central part of medieval Arnhem (present surface elevation >16 m NAP; Pleistocene surface elevation >13 m NAP), anthropogenic layers directly overlie Pleistocene glacial sand and lack any suggestion of Rhine flooding (Defilet and van den Berghe, 2011). Therefore, we focused on the area in between these locations. This is the area near the city its main church, located very close to the floodplain edge (Fig. 2.3).

The available archaeological results in the targeted area show thick (up to 1 m) raised ground layers at elevations around 12 m NAP dating to the late fourteenth century (Fig. 2.4B; van der Mark, 2016; Spitzers and van der Venne, 2020). We found this same thick raised layer in our cores, conducted from a late medieval ground level uncovered during excavation and dated to before the fifteenth century by abundant pottery shards (Fig. 2.5). Directly below the raised ground layer, which is more homogenous than other anthropogenic layers, we found a fine-grained (silty clay) deposit of up to 5 cm in thickness (Fig. 2.5; Fig. 2.6). Opposed to the overlying and underlying sandy and sometimes peaty layers, this silty clay layer contains a calcareous fraction (reaction with 5% HCl), indicating a relatively young fluvial origin (no pedogenic decalcification). These characteristics warrant lithogenetic interpretation as a flood sediment unit. The unit has an irregular base (Fig. 2.6), possibly indicating an erosive contact, caused by the energy of the flood water, or wet sand deformation. The homogeneity of the raised ground layer, consisting mostly of locally available sand, and its position directly above the flood bed, strongly suggest that the ground was raised as a reaction to the flood, either directly after the event or not long after, when new buildings were built in this part of the city. Therefore, the top of the raised layer likely gives a good indication of the water level reached during the event.

In a complex stratigraphy preserved directly underneath the southern nave aisle of the Eusebius church, a temporary exposure showed a distinct layer at 11.5 m NAP that we identify as a flood deposit (Fig. 2.7). Similar to the flood beds observed west of the church (Fig. 2.5; Fig. 2.6), this layer had a fine-grained and homogenous texture, contained no artefacts or charcoal, and reacted

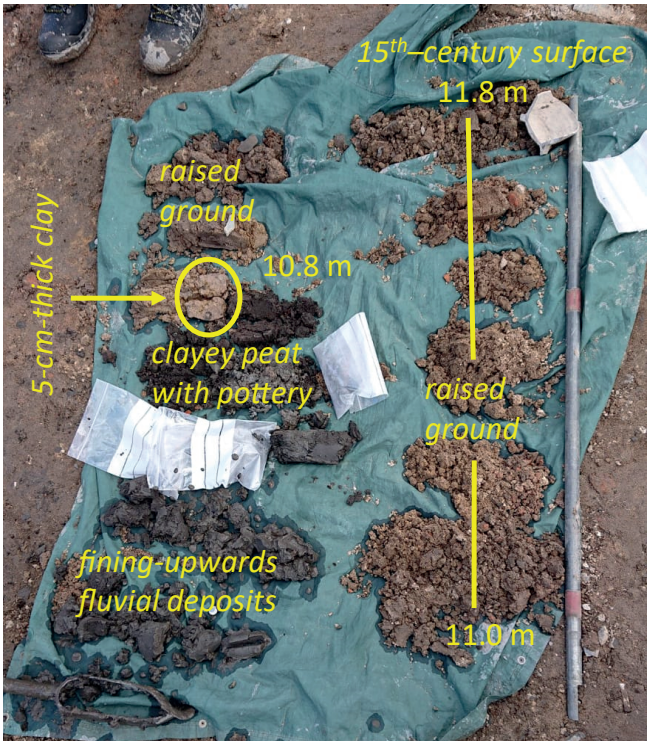

Fig. 2.5. Photograph of a hand coring (UU.2019.02.002) showing a flood clay deposit overlain by raised ground. The coring was conducted from an excavated floor level, archaeologically dated to the fifteenth century based on abundant characteristic white-coloured pottery shards (e.g. top right of photograph).

with HCl, in sharp contrast to all surrounding layers. This confirms the identification of the layer as a flood deposit. The profile shows many anthropogenic disturbances predating and postdating deposition of the flood bed, as expected in the centre of a medieval city. This complicates lateral tracing of the flood bed and finding the highest position where it occurred. The upper part of the profile is disturbed and no raised layer is preserved above the flood bed (Fig. 2.7). Still, the considerable thickness (up to 10 cm) of the deposit implies that the actual water level was significantly higher and that 11.5 m NAP is a minimum estimate of 1374 flood level in Arnhem.

An archaeological profile from the Musiskwartier reports on two clay drapes ('kleibandjes') that are not documented as individual strata (Fig. A1a). Based on the lithology, the minor thickness and the position in the lower brook valley, we interpret these drapes as slack-water deposits. The fact that these were only mentioned as annotations and not drawn and labelled in the field sketch profile (Fig. A1a), signifies the complexity of extracting palaeoflood levels from archaeological results without additional surveys. The age constraints for these flood beds are scarce, as no artefacts were recovered below the clay drapes, nor in the raised ground layers directly overlying the beds. A younger feature in the profile dates to circa 1500, based on recovered glass artefacts (Fig. A1b). It is thus likely that the beds correspond to the 1342 and 1374 floods events, providing elevations of 10.8 m NAP (clay drape) to 10.9 m NAP (top of raised ground) for the first and 10.9 m NAP (clay drape) to >11.1 m NAP (truncated top of raised ground) for the second event (Fig. A1a).

Another profile in the Musiskwartier documents a 'washed-out layer' at an elevation at 11.6 m NAP (Fig. A2a), for which archaeological-historical dating evidence points towards the fourteenth

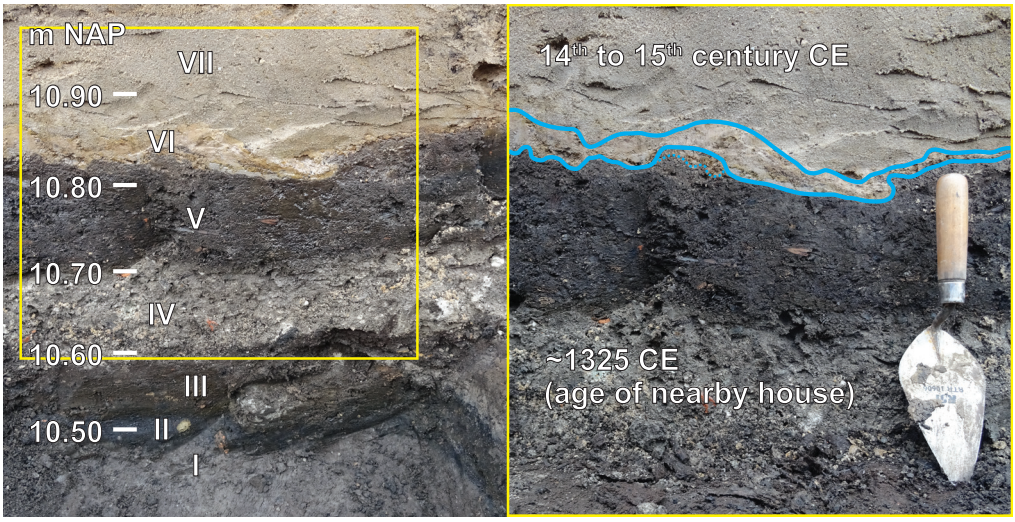

Fig. 2.6. Detailed photographs of a trenched profile (Broerenstraat site, west of Eusebius church) showing the same sequence as the coring in Fig. 2.5. Archaeological age constraints for layers I to V are early medieval to early fourteenth century. Layer VII is largely devoid of artefacts but predates the fifteenth century based on pottery above this layer (Fig. 2.5). The flood clay deposit (layer VI) is outlined in blue in the right-hand photograph.

century (Fig. A2b). This description in itself does not justify an interpretation as a flooded horizon. However, taking into account the focus of the original research (large-scale excavation to describe overall development and human history, research conducted without expectation of potential fluvial signatures), such an interpretation may be appropriate in this stratigraphic context. Attribution to the 1374 flood satisfies considerations regarding the irregularity of the layer and its position directly below a raised ground layer (Fig. A2a). Further, a nearby infill dated to 1280–1400 contains a distinct light-coloured grey-brown layer (texture not specified) that may be a flood deposit (compare field sketch Fig. A3a to photograph Fig. 2.7). Given that a late fourteenth-century age for the layer is well possible, although this is based on a single find (Fig. A3b), we interpret this deposit as a flood signature for the 1374 event, yielding a local minimum water level of 11.7 m NAP.

Two Musiskwartier profiles document strata with a clay component (Supplementary Information). Available age constraints for the layer at 11.8 m NAP in Fig. A4a show that it is located directly below a late sixteenth-century floor level (Fig. A4b). Likely, the clay has a fluvial origin, but at these

Fig. 2.7. Complex anthropogenic stratigraphy in a pocket of ground between foundation structures of the Eusebius church southern nave face. No layers in this profile react with hydrochloric acid, except for the light-coloured yellowish deposit indicated as a flood bed. The hatched layers fill the pits dug to construct the brick columns and arch during the church expansion and rebuilding phase between circa 1450 and 1550 (den Hartog and Glaudemans, 2013), supporting a late fourteenth-century age for the flood bed. The present street level at this location is approximately 13 m NAP.

sites it is not encountered in situ. Instead, it was displaced and used together with other locally available material to raise the ground, which explains the mixed nature and thickness (up to 30 cm) of the layer. The layer at 11.7 m NAP in Fig. A5a may be a flood deposit based on its appearance (thickness up to a few cm, thinning out with increasing elevation). However, as it is described as a mixture of clay and sand, it probably also resulted from sediment mixing owing to human activities. The archaeological age constraints for this layer are very broad (Fig. A5b).

In short, the Arnhem reference case shows that medieval urban archaeological stratigraphy can record extreme floods and serve to constrain the water level reached during the event. The results support our hypothesis that thick raised ground layers directly above flood sediment beds were placed as a reaction to the extreme flood event and can be used as an estimate for the maximum water level, in addition to the minimum value that flood deposits provide. Finding multiple indicators with adequate dating in different parts of the city shows that our observations are robust signals. The highest and often only recorded flood bed was deposited in 1374, which corroborates the unusual magnitude of this flood event indicated by historical data in Cologne (Krahe and Larina, 2010) and geological records in the delta apex region (Toonen, 2013). The water levels of the 1374 flood in Arnhem exceeded 11.5 m NAP (actual flood signatures; Fig. 2.4C; Fig. 2.7; Fig. A1a) and most likely reached about 12 to 12.5 m NAP (top of raised ground layers above flood deposits; Fig. 2.4B; Fig. 2.5; Fig. 2.6; Fig. A2a). This is lower than the maximum flood level in the twentieth-century instrumental record (Table 2.1).

2.3.2 Flood levels in additional sites

Deventer
Deventer is amongst the oldest medieval cities in the Netherlands, founded in early medieval times and formally receiving city rights in 1123. Deventer is located on the right-hand side of the IJssel river on an inland dune complex, similar to Doesburg and Zutphen (Fig. 2.1). According to old ecclesiastical accounts (Kapittel van Deventer), the water levels during the unprecedented flood in January 1374 reached a height of 3 feet (about 1 m) inside the Lebuinus church (Buisman, 1996). According to Gottschalk (1971), these accounts correspond well to the expenses and notes listed in the contemporaneous financial records of the city. The current floor level of the church is over 8 m NAP, but building history and archaeology show that the late medieval floor level of the church was about 7.4 m NAP (van der Wal, 2015), thus providing an estimate of 8.4 m NAP for the local maximum water level in 1374. This value considerably exceeds the highest twentieth-century water level in 1926 (Table 2.1).

Doesburg
Doesburg received city rights in 1237, relatively shortly after it was founded. The original layout of the city changed in 1343, when it was granted permission to extent in a different direction, in a duke's charter mentioning damage by the river in the year before as the reason (Haans, 2008). An archaeological exposure in the medieval city centre (Doesburg Gemeentehuis; unpublished data archived in 1995; partially published in Haans, 2008; Harenberg, 2008; van Wees, 2020) shows a fourteenth-century sandy raised ground sequence with a thin clay layer at its base and a washed-out contact about halfway (Fig. 2.8). The thin clay layer at 11.2 m NAP is interpreted as an extreme flood deposit (Harenberg, pers. comm.; Cohen et al., 2016). It overlies the thirteenth-century oldest town surface layer and underlies two phases of raised ground. The first phase raised the ground

to a new town surface level at 11.5 m NAP and the second phase to a late fourteenth-century surface at 11.9 m NAP (van Wees, 2020). An archaeological excavation conducted 50 m to the north duplicated these findings (Fermin and Groothedde, 2008). Based on the age constraints, the clay bed at the base of the lower raised ground layer may be attributed to the flood of 1342 and the upper raised ground layer as a response to the flood of 1374 (Cohen et al., 2016). Similar to the argumentations adopted for the Arnhem results, we consider 11.5 m NAP a minimum exceedance limit for the 1374 flood in Doesburg and the top of the raised ground at 11.9 m NAP a best estimate for the maximum flood level (Table 2.1). The flood bed at 11.2 m NAP and the intermediate raised ground top at 11.5 m NAP represent minimum and maximum estimates for the preceding event in 1342.

Lobith

The late medieval toll station and town of Lobith is located on the right-hand side of the Lower Rhine river close to the Dutch-German border (Fig. 2.1). It was established next to the delta apex bifurcation of the thirteenth and fourteenth centuries (Noordzij, 2008; Kleinhans et al., 2011; Overmars, 2020), on an artificial mound with present surface at 16.5 m NAP ('Dorpsdijk'). This site was occupied from late medieval times onwards (Schabbink et al., 2006), but the scarce documentation of the mound its archaeological stratigraphy does not allow for the conclusive identification of a representative level corresponding to the medieval raised surface. The top of the natural fluvial succession is at 12.7 m NAP (Schabbink, 2006) and nearby at 13.2 m NAP (Flokstra

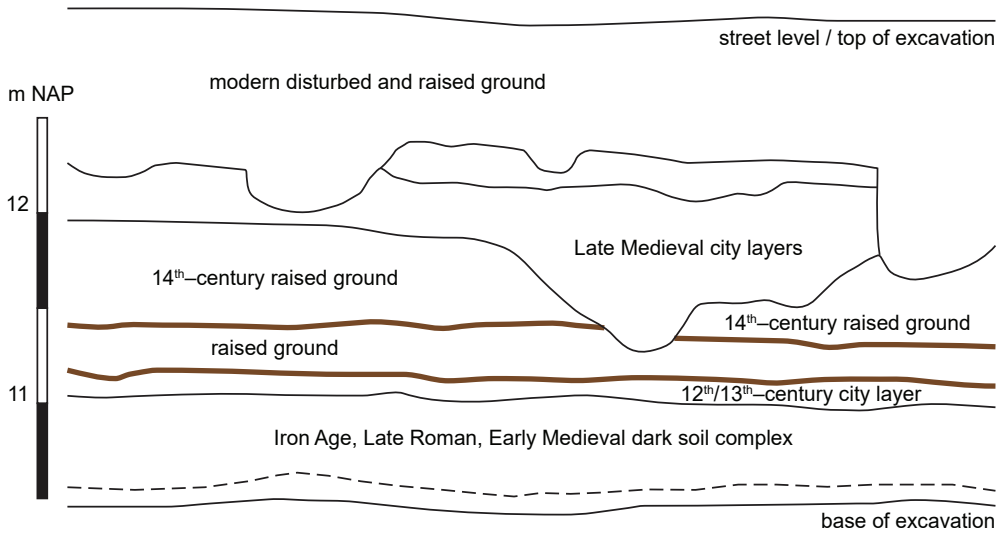

Fig. 2.8. Archaeological profile in Doesburg (Ph. Gastelaarstraat, 'vindplaats C'). The lower brown layer represents a fluvial clay drape and the upper brown layer an intermediate raised ground level with a small-scale undulating surface, buried by further raised ground in the fourteenth century. We interpret these as exceeded levels for the 1342 and 1374 floods. The drawing is based on an annotated photograph of the 1995 exposure in Haans (2008), Cohen et al. (2016), and van Wees (2020).

and Schuurman, 2008; van Renswoude and van Kampen, 2019). Therefore, 13.2 m NAP is a conservative minimum estimate for the 1374 flood water level. We use 16.5 m NAP as a tentative upper bound (Table 2.1). The highest instrumentally recorded water level at Lobith, which is the primary gauge for modern river management in the Netherlands, is 16.9 m NAP in 1926.

Nijmegen

Nijmegen has been an urban centre since Roman times (first century CE). The river front is located at the foot of a steep hill slope to the 10–15 m higher Pleistocene push ridge hosting the actual city (e.g. de Roode and Kuppens, 2012; de Roode, 2018). City walls and bastion towers lined the narrow river front in the thirteenth to fourteenth centuries. Along a main tower at the upstream river front, a fourteenth-century second row of bricks against the original thirteenth-century brick walls reaches up to 11.3 m NAP and likely indicates reinforcement to repair flooding damage ('Bastei' site, de Roode, pers. comm.). Behind the city walls, a lowest fourteenth/fifteenth-century brick house floor is observed at 13.4 m NAP on top of colluvial and Roman archaeological strata. Contemporary city accounts report that the downstream river-facing corner tower ('Rode Toren') and adjacent walls and gates were reinforced in 1382 (Gorissen, 1956). In the direct vicinity, underground-preserved late medieval wall structures reach up to 12.8 m NAP (de Roode, 2018). Thus, based on construction evidence for the medieval city walls, and supported by less precise urban stratigraphic and historic documentary information, the fourteenth-century highest water levels at Nijmegen exceeded 11.3 m NAP, but likely did not exceed 13.4 m NAP (Table 2.1). We use 13 m NAP as a tentative best estimate for the 1374 flood level at Nijmegen.

Tiel

Tiel is located in the central delta at the former bifurcation of the Waal and Linge rivers. It was an important early medieval trade town, flourishing around 850–1100, and was granted formal city rights in the thirteenth century (the precise date is unknown). The Chronicon Tielense, written and compiled from older sources in the fifteenth and sixteenth centuries, mentions the flood events of 1342 and 1374 (van Leeuwen, 1789; Kuys et al., 1983). For 1342, it reports that only three locations in the Betuwe area (central delta between Waal and Nederrijn rivers) were not flooded, namely the city of Tiel, the village of Drumpt next to Tiel, and part of the nearby village of Wadenoijen. Considering the current elevations of these settlements, the water level reached about 6.0 m NAP

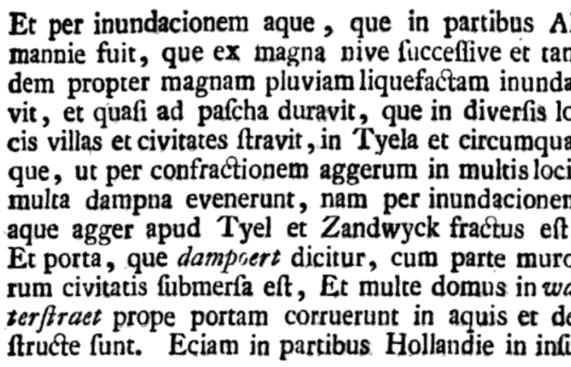
Et per inundacionem aque, que in partibus Almannie fuit, que ex magna nive ſucceſſive et tandem propter magnam pluviam liquefactam inundavit, et quaſi ad paſcha duravit, que in diverſis locis villas et civitates ſtravit, in Tyela et circumquaque, ut per confractionem aggerum in multis locis multa dampna evenerunt, nam per inundacionem aque agger apud Tyel et Zandwyck fractus eſt, Et porta, que *dampoert* dicitur, cum parte murorum civitatis ſubmerſa eſt, Et multe domus in *waterſtraet* prope portam corruerunt in aquis et deſtructe ſunt. Eciam in partibus Hollandie in inſu-

Fig. 2.9. Note on the 1374 flood event in the medieval chronicle Chronicon Tielense, reprinted by van Leeuwen (1789). The text reports on a flood caused by extreme and prolonged snow and rainfall ("magna nive successive et tandem propter magnam pluviam liquefactam") that greatly damaged ramparts, destroyed many houses, and overtopped ("submersa") a gate named Dampoort with parts of the city walls.

near Tiel. This level is archaeologically corroborated by the top of a fourteenth-century dike just northwest of Tiel (van den Brink and van Renswoude, 2017). For 1374, the reported flooding was considerably more severe (Fig. 2.9). Continuous precipitation and large amounts of melt water coming from upstream flooded many cities, including Tiel. The water overtopped the Dampoort ('Dam gate') and some of the city walls (Fig. 2.9). We conservatively estimate a level of 9.5 m NAP for the walls at the river-facing side of the city in the fourteenth century (about 2 m below the present wall elevations at this location). If the walls were indeed overtopped, as suggested by the documentary evidence, this is a minimum estimate for the flood level. However, given the large difference with the estimated level for 1342, the 1374 flood level is likely an overestimate (Table 2.1). This may be explained by an historically exaggerated description of the impact of the event, or by our interpretation of "submersa" as fully overtopped (Fig. 2.9).

Zutphen

Zutphen is located on an inland dune directly along the IJssel river (Fig. 2.1). It has an even older start of continuous site occupation than Deventer, with Merovingian-Carolingian rulership roots (Groothedde, 2013). Zutphen long featured a ring wall, and was granted city rights in 1190. Archaeological profiles in the northern part of the medieval city centre reveal a late medieval cobble street at 8.9 m NAP, just 60 cm below the present surface, overlying a thick raised ground layer (Fermin et al., 2006). The artefacts recovered from this layer date to the fourteenth century. Below the raised ground is an organic-rich anthropogenic layer with a truncated top at 7.9 m NAP (Fig. 2.10). Based on the erosive nature of that contact, and the thickness and age of the overlying raised layer, we interpret the level at 7.9 m NAP as a minimum flood level indicator for 1374. The organic layer overlies a washed-in sand bed at 7.7 m NAP, which may be related to an earlier flood, similar

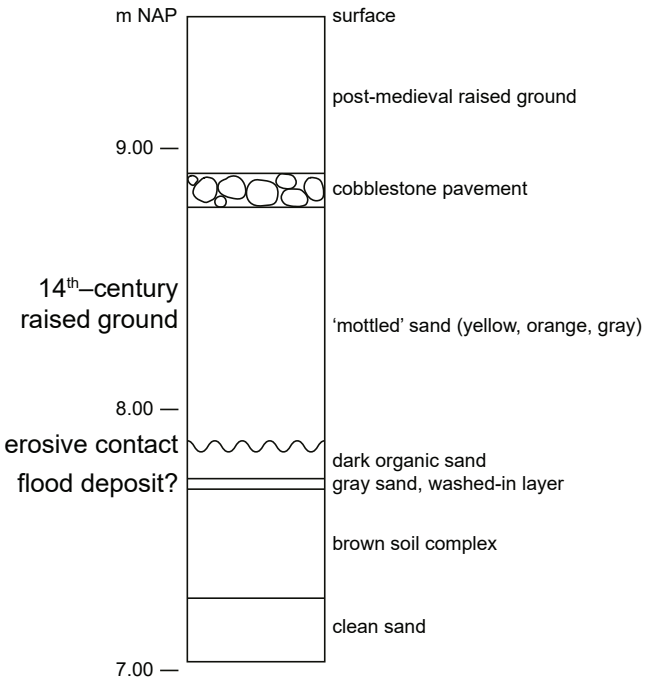

Fig. 2.10. Archaeological profile in Zutphen (Nieuwstad, Oude Wand 20/22). We interpret the washed-in sand layer and the erosive contact ('afgetopt', truncated) as exceeded levels for the 1342 and 1374 floods. Based on a profile description in Fermin et al. (2006).

to the reasoning at Doesburg. Wood fragments in the organic layer date to the thirteenth century, which favours attribution of the sand bed to an older event, but cannot exclude a correlation to the 1342 flood. The soil complex below the washed-in layer is considerably older, containing pottery from the fifth or sixth century (Fermin et al., 2006), which again suggests a correlation to an older flood, possibly in early medieval times (e.g. in the year 602; Jansma, 2020). Based on the results for Zutphen, the best estimate for the maximum water level in 1374 is 8.9 m NAP (top of raised ground above flooded horizon including the cobblestone street; Fig. 2.10). This is comparable to the maximum water level in 1926 (Table 2.1).

2.4 Discussion

Up till now, only qualitative historical studies documented the extreme flood of 1374 in the Rhine delta. This study considerably expands upon those by adding quantitative information in the form of reconstructed flood levels. We obtained these from archaeological stratigraphy in medieval city centres along the margins of the Holocene floodplain, and added levels reconstructed from historical mentions of relative flood heights. In contrast to stratigraphy, historical information is susceptible to inheriting exaggeration of the event (see Tiel in Section 2.3.2). Therefore, we recommend to reconstruct past flood levels not only based on written sources, but to complement these with geological-geomorphological indicators from the same region. The medieval urban archaeological stratigraphy provides an excellent starting point to find such indicators.

Table 2.1. Reconstructed flood levels for the extreme events in 1374 (largest in historical and geological record) and 1342, compared to measured flood levels in 1926 (largest in instrumental record). All values are in m NAP.

	January 1374		**January 1926**
	Minimum	***Maximum***	***Maximum***
Arnhem	11.7	12.5	13.4
Deventer	N/A	8.4	7.3
Doesburg	11.5	11.9	10.8
Lobith	>13.2	<16.5	16.9
Nijmegen	11.3	<13.4	13.8
Tiel [a]	>6.0	9.5	10.1
Zutphen	7.9	8.9	8.8
	July 1342		**January 1926**
	Minimum	***Maximum***	***Maximum***
Arnhem	10.8	11.0	13.4
Doesburg	11.2	11.5	10.8
Tiel	N/A	6.0	10.1
Zutphen [b]	7.7	>7.9	8.8

[a] *Likely, the maximum flood level for 1374 in Tiel results from a historical exaggeration and is thus an overestimate, given the large difference with the flood level for 1342 at the same location.*

[b] *Possibly, these levels corresponds to an earlier medieval flood.*

2.4.1 Flood signatures in archaeological profiles

In general, geological indicators provide minimum estimates of past flood levels rather than actual maximum water levels reached during peak discharge (Kochel and Baker, 1982; Springer and Kite, 1997; Benito et al., 2004). This is a suboptimal result, as the application of such minimum elevations in palaeoflood model calculations results in underestimating past discharges by up to 20% (Lam et al., 2017). Determining actual flood heights is arguably of even more importance in lowland settings, where the wider floodplain reduces the sensitivity of flood height to discharge, i.e. significant increases in discharge lead to only small increases in water levels (van der Meulen et al., 2021). Moreover, the actual water column height above a flood deposit may be higher in low-gradient settings such as the Rhine delta than in steep upstream sections, as lower overall flow velocities decrease the sediment transport capacity.

Various methods have been established to determine the water column height above a flood deposit based on its properties (Baker, 1987; Benito et al., 2003; Guo et al., 2017), but these methods are limited to specific hydraulic settings and sediment types, and certainly not suited to the delta setting we focus on. The relatively thin layers of fine-grained alluvium and subtle erosive features that we identified high along the rim of the delta plain provide minimum water levels reached during flooding, but hardly inform on the height of the water column. The flood beds in Arnhem are up to 10 cm thick (Fig. 2.6; Fig. 2.7; Supplementary Information) and likely resulted from backwash gathered in local ponds and ditches, given the low-angle sloping relief of the site away from the river (Fig. 2.3), whereas the flood bed in Doesburg is only about 0.5 cm thick, but appears more extensive (Fig. 2.8) and likely resulted from settling in standing flood waters inundating most of this medieval city, given its location on the top of an inland dune.

The archaeological stratigraphy that we used to find flood deposits provides a unique indication of local water column height. A raised ground layer directly overlying such a deposit may have been placed as a reaction to incidental extreme flooding. Additional constraints on the raised ground that warrant such an interpretation are a relatively homogeneous composition (Fig. 2.5; Fig. 2.6) and a reasonable archaeological age control that matches the historic mentions (Fig. 2.4; Supplementary Information). Of course, ground raising as a reaction to an extreme flood only happened at locations where this was feasible given the available resources (man power, organisation, excessive sand) and a felt need for diminishing flood risk (built-up parts of inner cities). In this light, it should be noted that the cities of Arnhem, Doesburg, and Zutphen were approaching the top of their wealth in the fourteenth to fifteenth centuries.

From these findings arises the recommendation to archaeologists working on sites at floodplain edges to specifically scout for thin fine-grained deposits either on top of the substrate (in the case of the Rhine delta: Holocene soil developed in Pleistocene sand) or interbedded between anthropogenic layers. This can be incorporated in the planning and processing of prospective coring and monitored excavation campaigns. Many medieval cities and towns have the potential to record past extreme flood levels in their archaeological stratigraphy, because relatively elevated grounds close to the river have been preferred settlement locations in lowland areas throughout history (e.g. Arnaud-Fassetta et al., 2010; Bini et al., 2015; Pennington et al., 2016; van Dinter et al., 2017; Pierik and van Lanen, 2019; Syrovatko et al., 2019). Requirements for reliable identification of a fine-grained layer as a flood deposit besides its lithology are its appearance (colour, thickness)

and chemical composition, lateral continuity (although likely interrupted by anthropogenic disturbances), and homogeneity (no artefacts, not mixed with sand; e.g. Fig. A4a). The combination of these characteristics can be established with more confidence from direct observations (Fig. 2.5; Fig. 2.6; Fig. 2.7) than from reported data (Fig. 2.8; Fig. 2.10; Supplementary Information).

Besides their palaeohydrological significance, flood signatures in archaeological profiles can provide precise dating constraints and allow for correlations between different sites (event stratigraphy). Sedimentary palaeoflood records are generally affected by decadal to century-scale uncertainties (Wilhelm et al., 2019; Benito et al., 2020). The age constraints on a flood bed can improve by the use of archaeological materials collected from surrounding strata (Benito et al., 2003; Thorndycraft et al., 2006; Huang et al., 2011). A correlation to a historically-known event can further constrain the dating accuracy to the year or even to a specific period within a year (Medialdea et al., 2014; Toonen et al., 2015). This specific age can then be used to improve dating of the surrounding layers in the profile, which is useful for further archaeological and historical interpretations. Furthermore, the flood signatures and their surrounding stratigraphy improve the knowledge on the ways in which people responded to natural disasters in past times (ground raising, potentially site abandonment or relocation; e.g. Kiss and Laszlovszky, 2013; Fontana et al., 2020).

As the central parts of medieval river cities were only flooded by very rare events, the method of extracting flood levels from archaeological profiles is limited to the most extreme floods, similar to palaeohydrological reconstruction methods for natural settings (Baker, 1987; 2008; Benito et al., 2020). The largest events are precisely those that require quantification most, as these are of primary importance for flood frequency analyses (e.g. St. George and Mudelsee, 2019) and for public awareness of flood risks (e.g. Baker et al., 2002). In valley settings, flood beds are expected at locations where flow decelerates, for example in caves along bedrock channels (Springer and Kite, 1997; Sheffer et al., 2003; 2008; Dezileau et al., 2014). The urban setting similarly provides areas of flow obstruction and local widening, explaining the occurrence of flood sediments in the archaeological stratigraphy. In the case of Arnhem Musiskwartier (Supplementary Information), back-flooding in the Jansbeek tributary valley likely contributed to flow deceleration. Another common issue in palaeoflood studies is the preservation potential and thereby the chances of identifying a flood bed (e.g. House et al., 2002). Here, the urban archaeological setting introduces both an advantage and a caveat, as the artificial cover on top of the flood deposit may enhance its preservation, but anthropogenic disturbances in later centuries may erase most of the bed and the overlying raised ground layer (Fig. 2.4B; Fig. 2.7).

2.4.2 Palaeoflood reconstruction in a delta setting

Our study has specified flood levels for the Lower Rhine millennial event of 1374 at seven sites in the inland part of the Rhine delta (Fig. 2.11). These results allow us to cross-check between historical and geoarchaeological reconstructions, and to contrast the medieval flood of record to the largest flood in the instrumental period. Since historical records may be inaccurate, it is important to use sources that are original (based on contemporary accounts; Brázdil et al., 2006; Herget, 2020) and written without a potential incentive to exaggerate (preferably no documents asking for financial support; van de Ven et al., 1995; Herget, 2020). Even though the historical data that we used fulfil these criteria, the reconstructed level for 1374 in Tiel is likely an overestimate, given the major difference with the level specified for 1342 at the same location (Table 2.1). The 1374 flood

level in Deventer of 8.4 m NAP considerably exceeds the highest measured level of 7.3 m NAP (Table 2.1), and thus may seem an exaggeration as well. Still, it is a plausible value considering that a similar height difference was observed upstream along the same river in Doesburg (Fig. 2.11), reconstructed from sedimentological and archaeological evidence. This signifies the importance of including multiple and different types of sources in past flood reconstructions whenever possible. Although the 1374 flood levels in Doesburg and Deventer are considerably higher than the 1926 flood levels, the levels for the two events in Zutphen are comparable (Table 2.1). Possibly, our reconstruction for Zutphen is an underestimate, as the data were extracted from a single profile, and both the flood level indicator and the top of the fourteenth-century raised ground may be higher in other parts of the city. Furthermore, the indicators in Zutphen consist of sand and an erosive contact (Fig. 2.10), implying higher-energy depositional conditions than for the clay layers in Arnhem (Fig. 2.6) and Doesburg (Fig. 2.8), and thus higher water columns above the levels of flood layer formation.

In the delta apex and in the central delta, reconstructed maximum water levels for 1374 are on average 0.7 m lower than the maxima observed in the instrumental period (Fig. 2.11). Although the water level reconstructions in Lobith and Nijmegen are somewhat tentative (Section 2.3.2), the values in Arnhem are well constrained (Section 2.3.1). Furthermore, as mentioned, the 1374 flood level in Tiel is likely an overestimate, yet it is still below the 1926 flood level (Fig. 2.11). At first sight, these lower levels for 1374 than for 1926 are remarkable, since the water level in Cologne was about 2.5 m higher in 1374 than in 1926 (Krahe and Larina, 2010). However, Cologne is located in in the terraced upstream stretch of the Lower Rhine valley, with an active floodplain width of just a few km. Between Cologne and the Rhine delta, the floodplain widens considerably (e.g. Erkens et al., 2011; van der Meulen et al., 2020). Thus, although the amount of water received in the delta

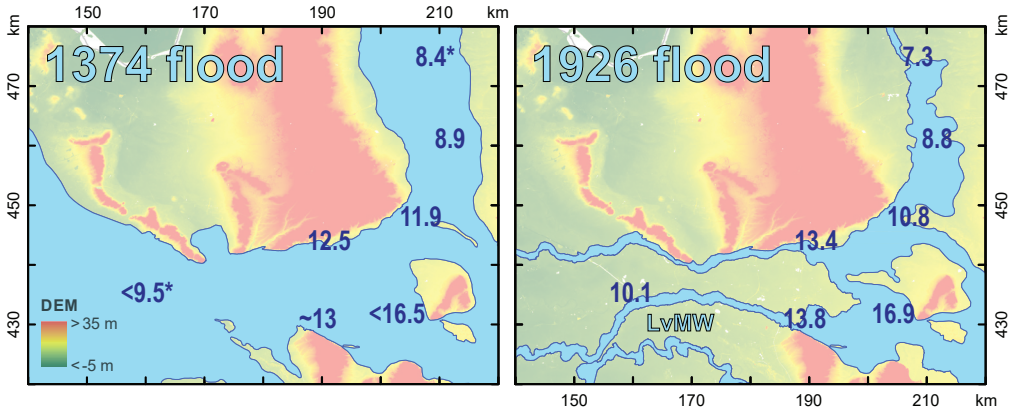

Fig. 2.11. Maximum water levels and flood extents for the extreme events in 1374 and 1926. The 1374 levels are extracted from urban archaeological stratigraphy or from historical sources (indicated by an asterisk); the 1926 levels are measured values (Rijkswaterstaat waterinfo). The 1374 extent is approximated based on the topography (AHN2), supported by historical sources; the 1926 extent is obtained from a contemporary report (Departement van Waterstaat, 1926). In 1926, the Land van Maas en Waal (LvMW) was also flooded, but only from the south by the river Meuse. All values are in m NAP.

may have been comparable to the discharge passing at Cologne, the much wider area carrying flood water considerably lowered the corresponding water levels. This effect was significantly greater in medieval times, when flow was hardly constricted by embankments. The embankments that were already present in the fourteenth century were still rather low (1–2 m compared to >5 m at present; van den Brink and van Renswoude, 2017; Rondags, 2019; Willemse, 2019) and thus easily overtopped during the most extreme floods. We can safely assume, supported by documentary evidence (Section 2.1), that all currently embanked low-lying areas were flooded in 1374 (left panel of Fig. 2.11). However, in the twentieth century, the stronger and higher embankments prevented flooding in the central delta, resulting in a greatly diminished area for overbank flow and consequently higher flood levels (right panel of Fig. 2.11). Thus, the findings for Arnhem, Lobith, Nijmegen, and Tiel (1374 flood levels below 1926 flood levels) do not imply that the discharge of the 1374 'millennial' event was lower than that of the 1926 'centennial' event.

Along the upper reaches of the IJssel river, large parts of the floodplain were inundated in 1926 (Departement van Waterstaat, 1926; Fig. 2.11). Consequently, the approximately 1 m higher flood levels in 1374 compared to 1926 in Deventer and Doesburg may be indicative for the natural difference between a 'millennial' and a 'centennial' flood in the upper delta. This is still 1.5 m less than the difference in Cologne, about 200 km upstream. The discrepancy between the central delta and IJssel floodplain is further complicated by the pathways that routed and diverted the river waters from the Lower Rhine valley into the Rhine delta. During large floods before major human interventions, Lower Rhine flood waters flowed freely in northward direction to the IJssel river around Doesburg (Fig. 2.11), whereas in the present embanked situation the IJssel river only receives water at the Nederrijn bifurcation point (Fig. 2.1). In 1926, some water flowed through the alternative pathway (Departement van Waterstaat, 1926; Fig. 2.11), following dike failure near the German-Dutch border, but the contribution to downstream water levels was likely modest. Potentially further complicating the interpretation of flood levels, the IJssel river channel was larger and received more water under bankfull conditions in the fourteenth century than at present (Hesselink, 2002; Cohen et al., 2016).

From these results, it is evident that interpreting palaeoflood levels in a delta setting requires careful consideration of flood dynamics and flow division. Therefore, the conversion of reconstructed water levels into a past flood discharge requires the application of spatially continuous model software (e.g. Apel et al., 2009; Cook and Merwade, 2009; Shen et al., 2015) rather than one-dimensional models that are usually applied in palaeoflood research (e.g. Webb and Jarrett, 2002; Herget et al., 2014; Benito et al., 2020). In addition, any comparisons to recent floods need to account for potentially major changes in floodplain capacity related to river embankment, which significantly affects maximum water levels at a regional to national scale (Fig. 2.11). The integration of multiple sites and sources, as done in this study, is especially important in lowland settings as relatively small (dm-scale) accuracies in palaeoflood levels may significantly affect the outcomes of extreme discharge calculations (van der Meulen et al., 2021). Since discharge is the preferred variable for use in statistical analyses of flood frequency and associated risk (e.g. Benito et al., 2004; Kjeldsen et al., 2014; Toonen, 2015), future research on the 1374 flood should include numerical modelling to convert the reconstructed flood levels into a discharge and further constrain the estimated magnitude of the event (Herget and Meurs, 2010; Toonen, 2013). This requires both an accurate reconstruction of the terrain (e.g. Schmidt et al., 2018; van der Meulen et al., 2020) and a series of historic flood simulations (e.g. Bomers et al., 2019; van der Meulen et al., 2021).

2.5 Conclusion

Determining maximum water levels of past extreme floods is essential for improving flood risk assessments and public awareness of such risks. Of particular importance are events with magnitudes exceeding those observed in the instrumental period. Past flood levels are usually obtained from sedimentary data such as flood deposits or from historical data such as documentary evidence. In this study, we demonstrate the potential of urban archaeological stratigraphy to extract past extreme flood levels. Geomorphological and hydrological data support the detection of a flood bed, and the archaeological context provides age constraints that correlate an identified bed to a historic event. Raised ground directly overlying a flood bed likely represents a reaction to witnessing the event and its top therefore approximates the actual water level that was reached, whereas flood bed elevations only provide a minimum indications of palaeoflood level. The opportunity to derive a maximum flood level indicator is an important benefit of the urban archaeological context.

The presence of fourteenth-century raised ground layers with a clear flood bed at their base in multiple river-bordering cities in the Rhine delta strongly suggests that these sites were raised in response to the extreme floods the Lower Rhine in 1342 and 1374. We reconstructed flood levels for these events in the Netherlands by integrating archaeological and historical sources. The results provide a consistent overview of water levels in the Rhine delta and confirm that the flood of 1374 was the largest in medieval times. We then compared the reconstructed levels of this 'millennial' flood to the measured levels of a twentieth-century 'centennial' flood. This geographical comparison demonstrates that differences between medieval and recent flood levels cannot be directly converted into differences in discharge magnitudes, mainly because floodplain width reduction by embankments has greatly affected flooding patterns in the lowland upper delta setting.

Acknowledgements

This work is part of the research programme 'Floods of the Past, Design for the Future' with project number 14506, financed by the Dutch Research Council (NWO). We thank Michael Bot (ADC), Leo Smole (Arnhem municipality), René van der Mark (BAAC), Marieke van Dinter (ADC), and Gerben Zielman (RAAP) for providing and explaining results on several past and ongoing excavations in Arnhem. Hans Middelkoop (UU) is thanked for comments on earlier versions of the manuscript.

BvdM, MPD, LAT, and KMC conducted the field research in Arnhem. BvdM and MPD examined the Musiskwartier archived data; LAT visited the site during excavation. BvdM and KMC examined the data for Doesburg, Lobith, and Nijmegen; KMC visited the Doesburg and Nijmegen sites during excavation. BvdM examined the data for Deventer, Tiel, and Zutphen. The author contributions to conceptualization, data collection, data analysis, and writing are BvdM (70, 50, 60, 80), MPD (0, 15, 20, 5), LAT (0, 15, 0, 5), and KMC (30, 20, 20, 10).

Chapter 3

Flood marks on buildings

part of this chapter is based on

van der Meulen, B., 2021. Historic flood level inventory from epigraphic marks in the Rhine river delta. DANS dataset. DOI:10.17026/dans-2zz-kpka

We have GPS and yet, we're still lost.

The Lonely Island – Incredible Thoughts (2016)

Note

This chapter presents an inventory of historic flood levels marked on buildings and other structures in the Rhine delta. These flood marks provide maximum water levels across the area from the late sixteenth to twentieth centuries, complementing instrumental measurement records in both space and time. The main goals of the chapter are to explain how I created this inventory and to unlock the resulting flood level dataset for future hydrological analyses.

3.1 Introduction

Historic data, such as descriptions and images, have been widely used to inform on past flood events (overviews of studies: Brázdil et al., 2006; 2012; Benito et al., 2015a). A special category of historic data are epigraphic marks: inscriptions in stone or other materials. When such engravings depict a water level reached during a flood event, they are referred to as flood marks. In many European countries, epigraphic records of flood levels have been collected and analysed for historical geographical or hydrological purposes (e.g. *Czech Republic*: Munzar et al., 2006; Elleder et al., 2013; *France*: Naulet et al., 2005; Piotte et al., 2016; *Germany*: Deutsch et al., 2006; Roggenkamp and Herget, 2014; *Great Britain*: Macdonald et al., 2006; Lewin, 2013; Macdonald, 2013; *Norway*: Engeland et al., 2018; *Poland*: Cyberski et al., 2006; *Spain*: Barriendos et al., 2014; Machado et al., 2015; *Slovakia*: Pekárová et al., 2013; *Switzerland*: Wetter, 2011; Wetter et al., 2017). For the Rhine river branches in the Netherlands, however, no such study exists.

Compared to the Middle Rhine river reach with abundant flood marks (e.g. Witte et al., 1995; Herget, 2012; own observations), the Rhine delta holds relatively few marks. Thanks to extensive river management ('normalisation' – see Chapter 4), large discharges did not induce serious disasters over the past ~150 years, lowering the need to mark water levels. The last flood of the Rhine that inundated a significant part of the Netherlands dates back to 1861 (e.g. van de Ven et al., 1995; Tol and Langen, 2000; van Heezik, 2007). The largest flood in the instrumental record, in 1926, inundated a relatively small area as Rhine river dikes in the central delta did not breach. The last major flood in 1995 did not result in any dike breaches in the Netherlands. Moreover, many old flood marks in the Netherlands may have been removed due to widespread urban growth and city renewal. Still, the remaining flood marks provide a valuable collection of maximum water levels that complement instrumental measurement records both in space (flood marks occur not only along rivers, but also in floodplain areas) and in time (flood marks on buildings often predate measurement records). Furthermore, the maximum water levels provided by flood marks are valuable in light of recent advances in river landscape reconstruction (van der Meulen et al., 2018; 2020) and flood hydraulic modelling (Bomers et al., 2019; van der Meulen et al., 2021) that have enabled the simulation of historic flood events in the Rhine delta.

3.2 Materials

In order to create an inventory of flood marks in the Rhine delta (Fig. 3.1), I based myself on a combination of (1) nineteenth-century technical reports, documenting early levelling campaigns, (2) twentieth-century books and journals, dealing with regional history, geography, and water management, and (3) twenty-first-century websites. In addition, I undertook many reconnaissance visits throughout the area, where I checked old buildings, churches, and city walls and gates for

flood marks. After this collection phase, I measured the vertical positions of the marks using the appropriate equipment (Section 3.3), thereby creating a dataset of water levels with respect to NAP (Normaal Amsterdams Peil = Dutch ordnance datum, in which 0 m is approximately twentieth-century mean sea level).

The flood marks in the Netherlands come in many shapes. In the simplest form, they are stones or commemorative plaques with the year of flooding inscribed and a horizontal indicator of the water level reached during the event. Often, the base of the stone is this indicator. Many flood marks have additional text, for example regarding the location and date of a dike breach (only in the case of marks located inland of dikes; e.g. Fig. 3.2, Fig. 3.3) or simply to liven up the mark (e.g. Fig. 3.4). Some flood marks are more exceptional in shape, but still meet the basic specification of providing both a year and a water level (e.g. Fig. 3.5). An important subdivision for hydrological purposes is the distinction between individual flood marks (a single event level marked at a location) and series of flood marks (multiple event levels marked at a location, e.g. Fig. 3.6, Fig. 3.7). The latter are often located in cities directly adjacent to the river, whereas individual marks occur much more scattered throughout the delta (Fig. 3.1).

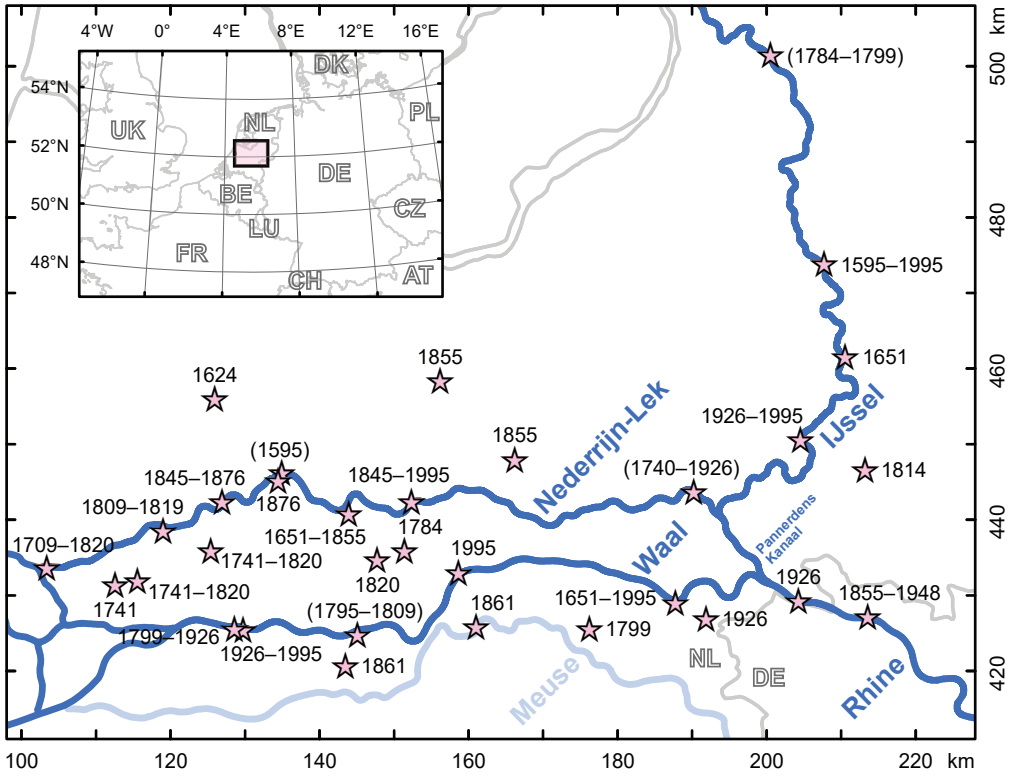

Fig. 3.1. Overview of flood marks in the Rhine delta, indicated by the year of the recorded event or the range of years in the case of multiple marks in one town. Indications between brackets represent disappeared flood marks.

Fig. 3.2. Example of a flood mark in Culemborg. The stone informs on the water level (base of stone as indicated by the index finger of the depicted hand), and on the location and date of dike breaching (Ochten, 3 March 1827).

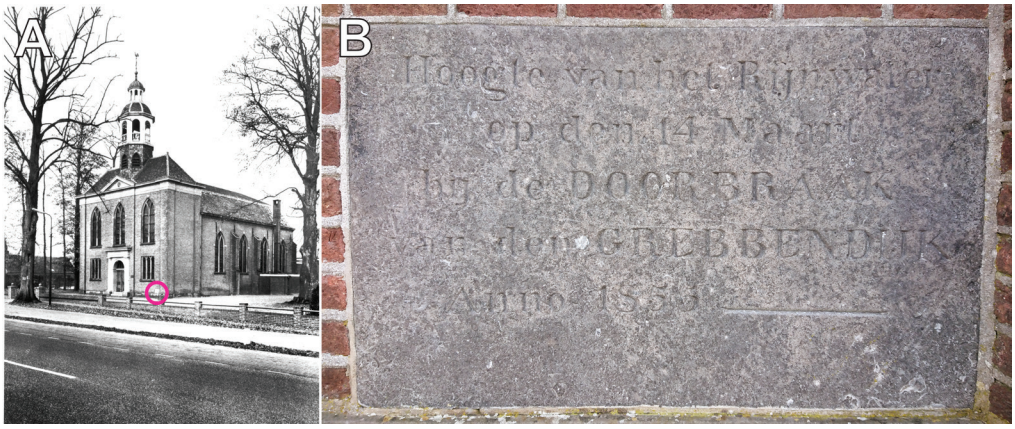

Fig. 3.3. Example of a flood mark in Leusden. A) Position of mark on church, indicated on a photograph from 1962. Source: Rijksdienst voor het Cultureel Erfgoed. B) Close-up of mark. The stone informs on the water level (horizontal line), and the location and date of breaching (Grebbedijk, 14 March 1855).

Fig. 3.4. Examples of flood marks in Molenaarsgraaf. The inscriptions are small verses.

Fig. 3.5. Memorial column in Veenendaal that serves as a flood mark. A) Reveal of the monument following its construction in 1955, precisely 100 years after the flood. Source: Nationaal Archief, obtained from www.veenendaalsekrant.nl. B) The top of the column represents the local water level reached in 1855.

3.2.1 Not all marks are flood marks

Particular for the Netherlands is the presence of reference stones that are sometimes thought to be flood marks (Fig. 3.8). These reference stones ('peilmerkstenen') indicate a level with respect to NAP (or AP, the precursor of NAP) and were placed during levelling campaigns in the nineteenth and early twentieth centuries (e.g. Waalewijn, 1979; 1987). They occur throughout the country and do not relate to flooding. The reference stones are actually rather easy to tell apart from other types of marks, because of their standardized size (width 36 cm, height 24 cm) and lay-out (Fig. 3.8).

In rare cases, older stones that appear to be flood marks may not directly refer to actual water levels. Instead, they mark the heights of dikes or nearby spillways (e.g. Fig. 3.9). The indicated levels may indirectly relate to floods that actually occurred, but this cannot be concluded with certainty. Such marks were therefore not included in the results, nor used in further analyses.

Fig. 3.6. Example of a series of flood marks in Deventer. Note that the mark of 1595, the oldest recorded year, is precisely in the middle of the main stone. Thus, the stone was very likely placed in that year, with the intention to record future extreme flood levels in the space above and below. Further note that for some years, the month and day of flooding are indicated in between the century and decade numbers. This way of denoting the date of flooding has been observed for a number of marks across the delta.

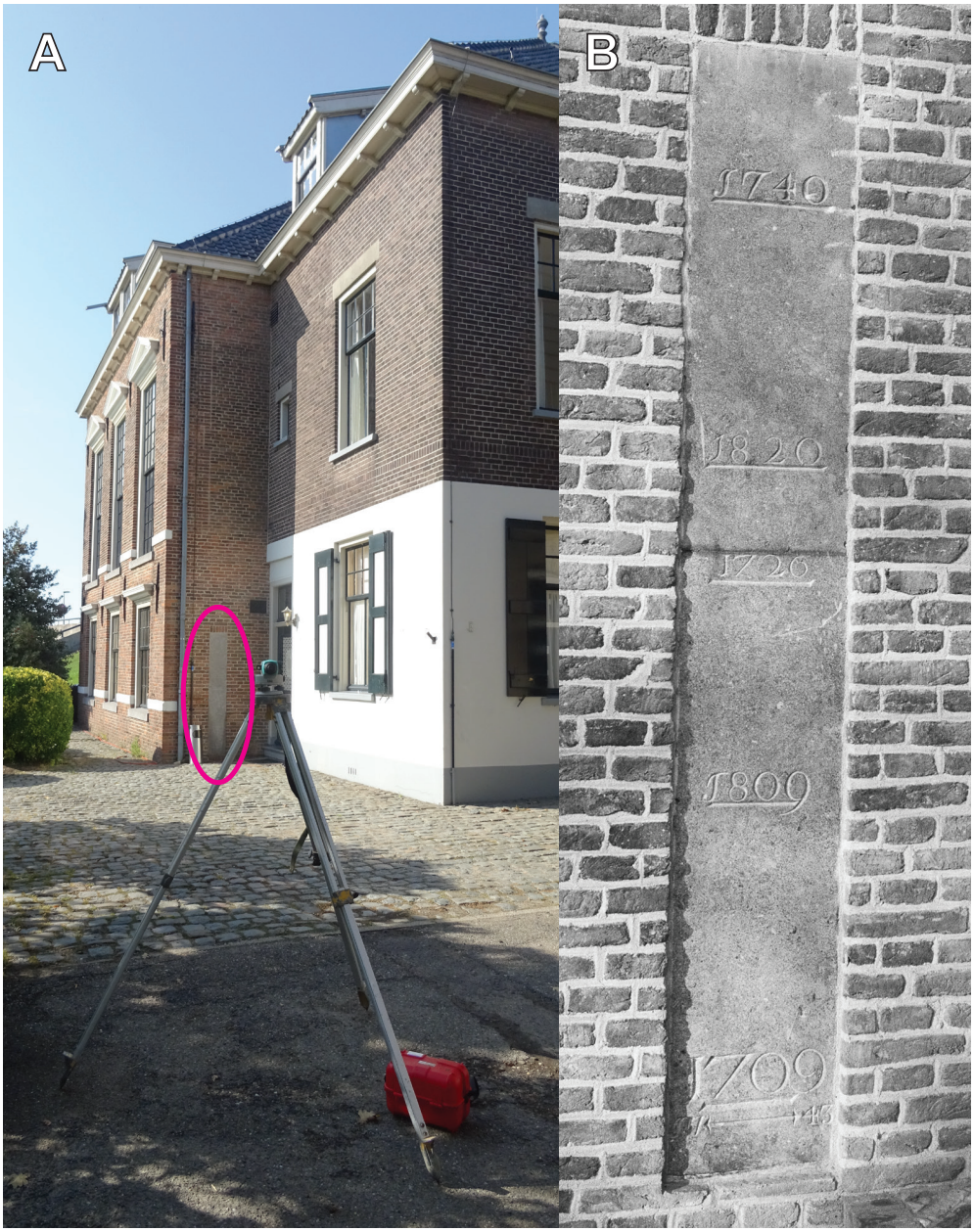

Fig. 3.7. Example of a series of flood marks in Kinderdijk. A) Position of marks on former water board building. B) Close-up of marks on a photograph from 1984. Source: Rijksdienst voor het Cultureel Erfgoed. Note that the record covers two stones. As 1709 is the earliest recorded year, the lower stone was likely placed in that year, with space above to record future events. There was just enough space to record the level in 1726. The upper stone was most likely placed in 1740, when the flood level considerably exceeded the height of the then present stone.

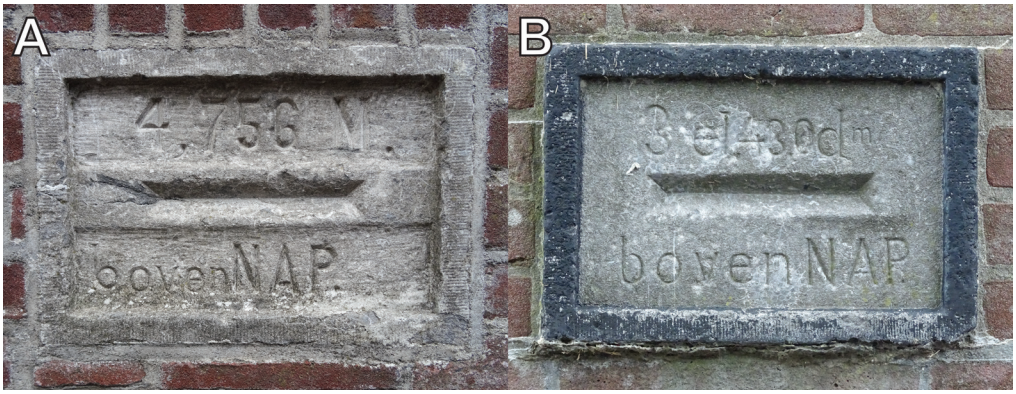

Fig. 3.8. Examples of standardized vertical reference stones ('peilmerkstenen') that are found throughout the Netherlands and do not represent water levels. A) Waterpoort, Woudrichem. B) Koepoort, Woudrichem.

Fig. 3.9. Stone in the city wall of Leerdam that resembles a flood mark, as it depicts both a year and a horizontal level. However, it likely does not indicate an actual water level, as no flood occurred in 1660. Instead, the stone refers to an agreed-upon water level for piercing a dike during flooding in order to protect one polder area at the cost of another (this agreement was still in use circa 150 years later; Ewijk, 1809). Note that major floods occurred in 1651 and 1658, and the mark may relate to a water level reached in those years, although it is positioned remarkably high (above the water level reached during the major flood of 1809).

3.2.2 Disappeared flood marks

The inventory contains a few flood marks that have disappeared. These marks are reported in old (mid-nineteenth century) technical reports, but cannot be found in the field. For a few cases (disappeared flood marks in Vreeswijk, Zaltbommel, and Zwolle), the old reports document the levels of the marks with respect to AP, which I included in the dataset. For one particular location, in Arnhem next to the Nederrijn, old photographs show a series of flood marks (Fig. 3.10). The building that held these marks was destroyed in the second world war and the entire area has since been overbuilt by a large road junction (Roermondsplein). Nevertheless, it was possible to assign absolute elevations to the marks, because the photographs also depict a measurement gauge relating to the Dutch ordnance datum (Fig. 3.11).

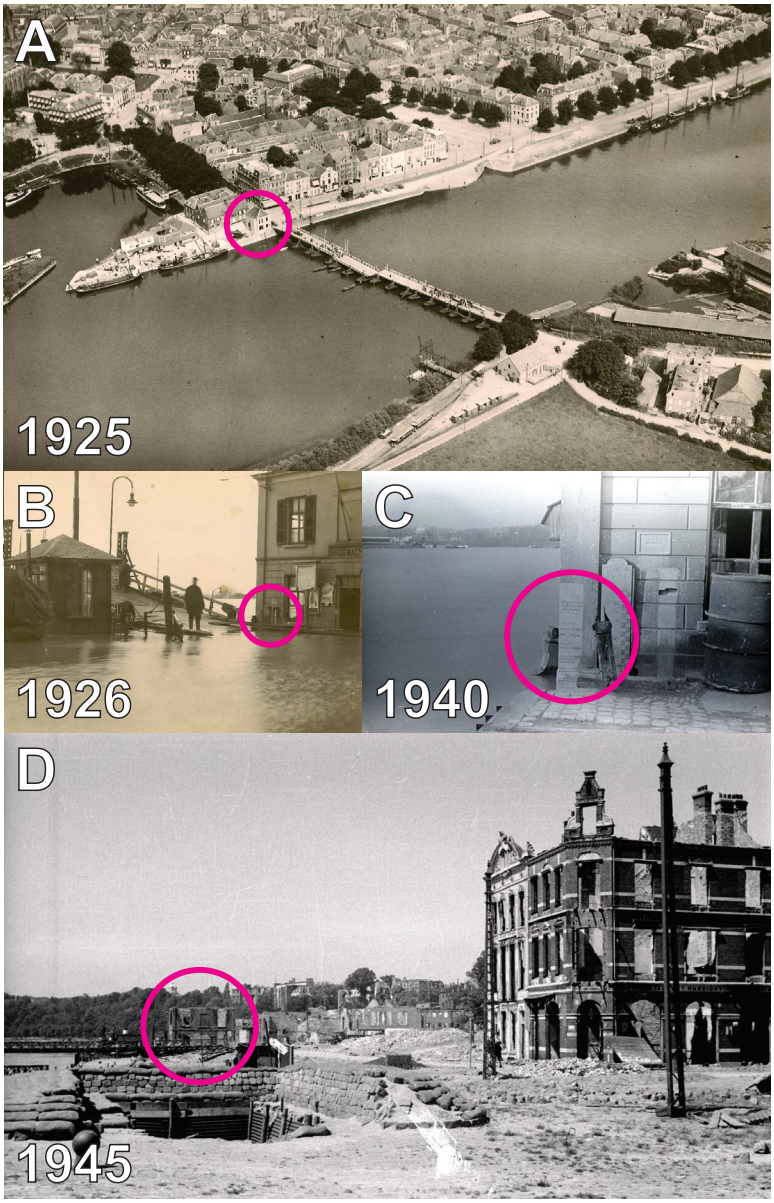

Fig. 3.10. Disappeared flood marks in Arnhem. A) Aerial photograph taken from the southwest, depicting the former Brugwachtershuis at the head of the former pontoon bridge. Source: KLM Aerocarto NV, collection B. Mohr, obtained from Oud-Arnhem (PB). B) Photograph of the former Brugwachtershuis during flooding in January 1926, depicting the epigraphic marks on the southeast face of the building. Source: collection B. Mohr, obtained from Oud-Arnhem (PB). C) Photograph of the epigraphic marks during flooding in February 1940. Source: F.W. Holleman, obtained from Gelders Archief. D) Photograph of Arnhem river front in June 1945, depicting the largely destroyed Brugwachtershuis. Source: Nico Kramer, obtained from Gelders Archief.

3.3 Geographical survey

Obtaining the levels of the flood marks was done using a three-step process (Fig. 3.12). First, I measured the street level at a location away from buildings where RTK-DGPS reception was good (vertical error <3 cm), using a Trimble system on a 2.000 m pole (Fig. 3.13A). Then, I positioned the levelling instrument at a spot from which both the GPS and the flood mark were visible, and measured its height above the street level at the GPS location (Fig. 3.12). The last step consisted

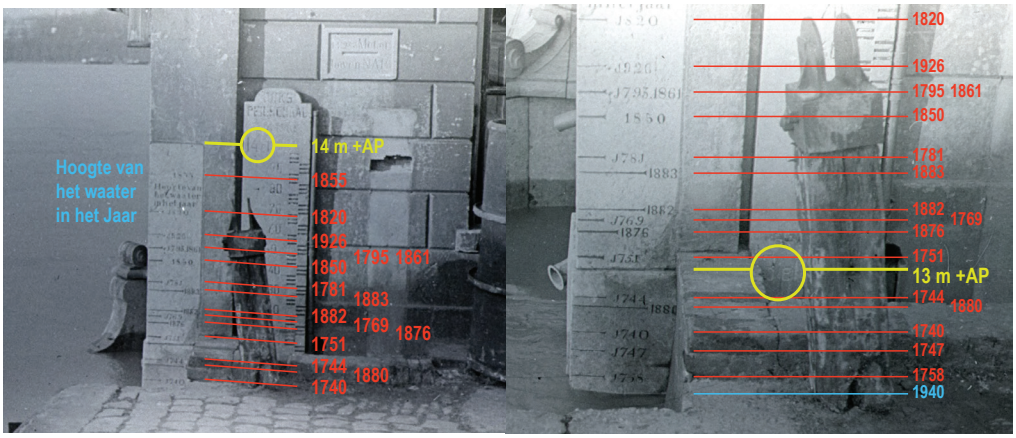

Fig. 3.11. Procedure for obtaining flood levels from historical photographs in Arnhem. Source of photographs: F.W. Holleman, obtained from Gelders Archief.

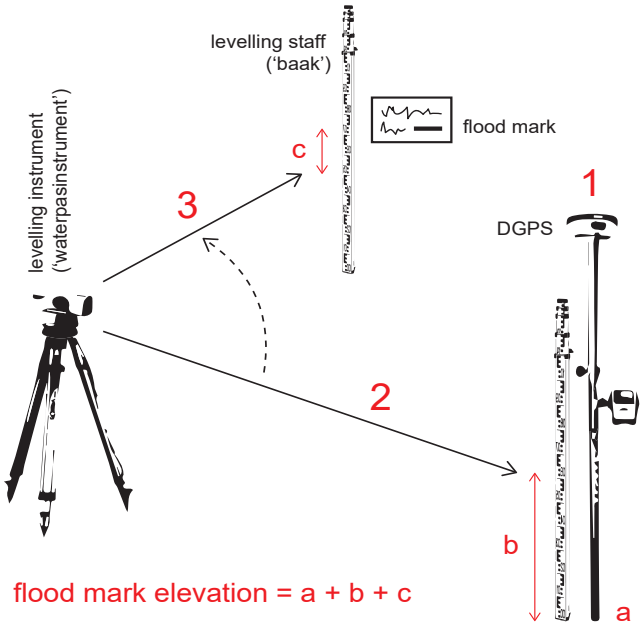

Fig. 3.12. Measurement steps of the geographical survey. First, the ground level above NAP is measured at a site with good DGPS reception (a). Second, the levelling instrument, placed at a location from which both the GPS equipment and the flood mark are well visible, is used to measure its height above the ground level (b). Third, after rotating the levelling instrument, the height difference with the flood mark is measured (c). Combining the measurements provides the absolute elevation of the flood mark.

of rotating the levelling instrument to the wall holding the flood mark and measuring the height difference between the instrument and the mark (Fig. 3.13B). The flood mark elevation then derived from simply adding the GPS ground level measurement, the height of the levelling plane above this level, and the height difference with the mark (which may be a negative value). The uncertainty induced by the single levelling step is negligible (<1 mm), so the total uncertainty of the reported levels is <0.03 m. For many flood marks I conducted multiple measurements, which reproduced and confirmed this good accuracy.

Besides the elevations of the flood marks, I measured their exact locations, which I later verified using different maps in ArcGIS to arrive at a spatial accuracy <1 m. Further, I documented the types and estimated ages of the constructions holding the marks, which is important for assessing whether the flood marks are in their original positions. This affects the reliability of the water levels obtained from the marks. I verified the ages of the constructions using the 'Basisregistratie Adressen en Gebouwen' and other governmental information websites (such as www.rijksmonumenten.nl). During the surveys, I also transcribed the inscriptions of the marks, which was sometimes difficult due to weathering (e.g. Fig. 3.14). The location, construction information, year, level in cm above NAP, and inscription for each flood mark are presented in Table 3.1.

3.4 Reliability of epigraphic levels

The largest potential problem associated with historic flood levels obtained from epigraphic marks is displacement of commemorative stones. When structures holding flood marks are demolished or rigorously renovated and the stones are re-used, these may not be placed at their original elevations (e.g. Herget, 2012; 2020). During the survey I accounted for this problem by checking the types and ages of all buildings holding flood marks, which led to the exclusion of some marks in the measurement steps (no NAP value given in Table 3.1). Other potential errors, such as vertical inaccuracies during the original placement, are likely small. Presumably, most flood marks were placed soon after the event (e.g. Macdonald, 2007), although some were placed many years later (e.g. Fig. 3.5). Marks were presumably placed at the observed maximum water level, which is well visible after flooding as a horizontal line on built structures. This level may not precisely represent the flood water surface due to wave and capillary action (e.g. Neal et al., 2009; Wetter et al., 2011), but such inaccuracies are considered minor (cm-scale) and negligible compared to the potential errors induced by renovation of the building holding the mark.

Series of flood marks occasionally reveal information regarding the history of placement. For example, in Deventer, the earliest recorded year is positioned precisely in the vertical middle of the main stone (Fig. 3.6). Thus, the stone was very likely placed following the flood event in that year, with space below and above to record potential future floods (which indeed occurred). To avoid overlapping engravings, new stones were placed to the right of the main stone in 1784, 1883 (difficult to read), and 1926. The flood mark series in Kinderdijk provides another example. Here, the earliest recorded year is positioned near the base of the lower of two stones, about 20 cm above ground level (Fig. 3.7). Later flood events were recorded in the space above, and an additional stone was placed circa 30 years later to record an event exceeding the height of the original stone. A similar template, with space above to record future flood levels, is visible for the nearly 300-year younger stone in Wijk bij Duurstede with event levels of 1993 and 1995 (Fig. 3.15). A peculiar problem with this stone is that the inscribed NAP values are somewhat lower than the actual

elevations of the marks (Table 3.1). Moreover, the inscribed values differ by 20 cm while the marks are only 7 to 8 cm apart (Fig. 3.15). This example shows that even very recent flood marks are not devoid of inaccuracies, with potential errors amounting to between 10 and 20 cm.

3.5 Results

In total, the inventory contains 131 flood marks from 46 locations spread across 32 towns (Table 3.1). It includes 2 marks from the sixteenth century, 8 marks from the seventeenth century, 34 marks from the eighteenth century, 56 marks from the nineteenth century, and 31 marks from the twentieth century (Fig. 3.16). The increasing number of flood marks over the centuries is in line with the expected preservation bias and likely also resembles increased efforts to mark water levels, as flood disasters in the late eighteenth to early nineteenth centuries were particularly severe (e.g. Driessen, 1994; note that many of these events were caused by ice jams related to the colder climate conditions at the end of the Little Ice Age). The smaller number of marks in the twentieth century compared to the previous two centuries is in line with the absence of destructive flood disasters in recent times (e.g. Tol and Langen, 2000).

Fig. 3.13. Measurement steps 1 and 3 of the geographical survey. A) Identifying a location with good satellite reception in Culemborg. Photograph by Maarten Zeylmans. B) Difficult levelling measurement of a flood mark in Nijmegen.

Many flood marks occur in the downstream part of the study area in between the Waal and Nederrijn-Lek (Fig. 3.1). This area has the potential for the highest water levels with respect to the terrain, as a dike failure upstream can lead to a sustained rise of water levels given the gently decreasing elevation of the delta towards the sea. In addition to this 'sloping bath-tub effect', the

Fig. 3.14. Example of a heavily weathered flood mark in Kerkwijk. A) Position of mark on church. B) Close-up of mark. The nearly erased inscription reads 'WATERVLOED – 1861'. C) Artificial refuge hill located opposite of the church, created as a reaction to the flood. GPS ground level measurements on top of the hill reveal that it was raised to almost exactly the local flood level as indicated by the mark.

spread of flood marks is likely related to other vulnerability aspects. Towns in the upper delta located on Pleistocene relief are generally less susceptible to flooding than towns in the central and lower delta. Furthermore, some of the spatial patterns may simply be explained by the spread in population density (many large river cities hold series of flood marks) and possibly by copying behaviour (placement inspired by the presence of flood marks in a neighbouring town; e.g. similar flood marks for the same years in Molenaarsgraaf and Noordeloos).

Not only the total number of flood marks, but also the distribution along the three major distributaries of the Rhine (Waal, Nederrijn-Lek, IJssel) changes with time (Fig. 3.17). Overall, flood marks along the Waal become more prevalent over time relative to flood marks along the Nederrijn-Lek. Increased discharge diversion towards the Nederrijn following construction of an artificial bypass in the delta apex (Pannerdens Kanaal; e.g. van de Ven, 1976) may have contributed to high water levels along this branch in the eighteenth century. In addition, the temporal distribution may be influenced by societal factors, with more attention to commemorative stones nearby the relatively wealthy lower-delta provinces of Holland and Utrecht. The larger number of flood marks along the Waal in the twentieth century may be explained by the large size of this river with relatively narrow floodplains, resulting in an impressive water mass under high water conditions. Thus, in the absence of dike breaches, water levels are more likely to be marked along the Waal than along the other two river branches.

3.6 Hydrological interpretations

Comparing the temporal distribution of flood marks to historical records of flood intensity reveals that in general the most extreme events led to the placement of the most marks (Fig. 3.16). Extreme discharge peaks before the instrumental period occurred in 1595, 1651, and 1658 (Gottschalk,

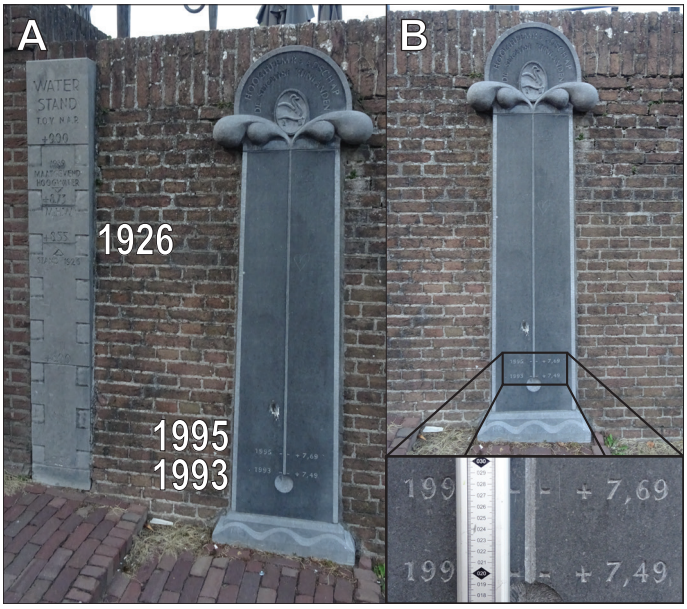

Fig. 3.15. Relatively recent flood marks in Wijk bij Duurstede. A) Two separate stones record the maximum water levels of 1926, 1993, and 1995. The left stone also depicts a former design flood level ('maatgevend hoogwater'). B) Stone with flood marks of 1993 and 1995, with space above to record future flood levels. The close-up shows that the difference between the inscribed values (20 cm) does not match with the vertical distance between the two marks (8 cm).

1977; Toonen, 2015). Each of these years is characterized by a relatively large number of flood marks, taking into account that these marks must have been preserved over three centuries. Further

Table 3.1. Inventory of flood marks and their levels in the Rhine delta.

Location		Coordinates				Structure		Flood mark		Notes	Inscription
river	town	RD_x	RD_y	latitude	longitude	type	age	year	level (cm +NAP)		
Lower Rhine	*Emmerich (GER)*	*213608*	*427242*	*51.8307*	*6.2375*	river face of flood wall	20th century	*1861*	*1783*	likely placed post-datum or displaced, considering destru	Hochwasser 30.1.1861
/ Niederrhein								*1926*	*1779*		3.1.1926
/ Bovenrijn								*1882*	*1749*		29.11.1882
								1855	*1748*		4.3.1855
								1930	*1713*		26.11.1930
								1948	*1713*		3.1.1948
	Tolkamer	*204284*	*429367*	*51.8507*	*6.1025*	coupure in dike	20th century	*1926*	*1693*	placed post-datum, level inscribed on plate	Hoogte van deze dijk NAP + 19.10 m | Hoogst bekende w
Waal	*Beek*	*191883*	*426987*	*51.8303*	*5.9223*	building (outside)	1923	*1926*	*1362*	level inscribed on stone, not placed at local water level, t	WATERSNOOD 1926. 5 JANUARI - 13.62 + N.A.P. PEILSCH
	Nijmegen	*188074*	*429054*	*51.8491*	*5.8672*	building (outside)	17th century	*1861*	*1444*		1861. Tot hier, aan dezen steen, stond den verbolgen vlo
	Nijmegen	*187811*	*429110*	*51.8496*	*5.8634*	building (outside)	1986	*1861*	*1441*	present level 1341 cm +NAP, but displaced (stone origina	IN 1860 & 1 WAS DE NOODKREET ALGEMEEN TOEN HET
	Nijmegen	*187769*	*429099*	*51.8495*	*5.8628*	building (inside)	17th century	*1820*	*1450*	estimates, based on pictures and information at www.no	18(23/1)20
								1861	*1430*		18(1/2)61
	Nijmegen	*187756*	*429110*	*51.8496*	*5.8626*	building (outside)		*1820*	*no meas.*	disappeared, photograph at studiezaal.nijmegen.nl (Foto	in 1800-10 en 10 was het water hier aan te zien
	Nijmegen	*187399*	*429209*	*51.8505*	*5.8574*	wooden pole	20th century	*1926*	*1384*	levels read from scale on pole	1926 - 1384
								1995	*1362*		1995 - 1362 - 1 Februari
								1993	*1340*		1993 - 1340 - 25 December
								1970	*1332*		1970 - 1332 - 27 Februari
								1988	*1310*	metal plate is missing (September 2019)	
	Nijmegen	*187964*	*428816*	*51.8469*	*5.8656*	formerly in crane, now in memorial wall		*1651*	*no meas.*	displaced	1651 Maert het water sonder opstovwinge van ijs onder
								1740	*no meas.*	displaced	
								1784	*no meas.*	displaced	
								1799	*no meas.*	displaced	
								1820	*no meas.*	displaced	op den 23ste January 1820 stond het water aan deze ste
	Nijmegen	*185467*	*428083*	*51.8405*	*5.8293*	church (outside)	16th century	*1799*	*1179*		1798 & 1 STONT HET WAATER AAN DEZE STEEN
	Tiel	*158662*	*433098*	*51.8864*	*5.4404*	coupure in city wall (riv	19th century	*1995*	*1028*	level inscribed on stone	10.28 M + N.A.P. 1995
	Zaltbommel	*145110*	*424870*	*51.8124*	*5.2438*	former city gate (inside	16th–17th centu	*1809*	*768*	destroyed, levels obtained from Krayenhoff, C.R.T., 1813.	Verzameling van hydrographische en topographische wa
								1795	*728*		
	Loevestein	*129763*	*425451*	*51.8171*	*5.0212*	gate in castle wall	16th century (pa	*1809*	*546*		1809 EN 1825
								1825	*546*		1809 EN 1825
								1861	*541*		1861
								1799	*516*		1799 EN 1820
								1820	*516*		1799 EN 1820
								1926	*514*		1926
								1883	*510*		1883
								1817	*505*	Meuse river flood	1817
								1882	*502*		1882
								1876	*500*	Meuse river flood	1876
								1920	*494*		1920
								1995	*493*		1995
								1881	*487*		1881
								1827	*411*		1827
Land van Maas e	*Leur*	*176236*	*425676*	*51.8193*	*5.6952*	church (inside)	16th century (ch	*1799*	*960*	estimate, based on pictures at www.oudegeldersekerken	TOT AAN DEZEN STEEN STOND HET WATER BY DE HOOGI
	Alphen aan de M	*161017*	*425847*	*51.8212*	*5.4745*	building (outside)	19th century (ac	*1861*	*887*	(location next to Meuse, but flooding by Waal)	ANNO 18(4/2)60 en EEN STOND de VLOED AAN DEZEN S
Bommelerwaard	*Kerkwijk*	*143465*	*420736*	*51.7752*	*5.2201*	church (outside)	12th century	*1861*	*604*	weathered	WATERVLOED 1861
Merwede	*Woudrichem*	*128589*	*425610*	*51.8185*	*5.0042*	coupure in city wall	19th century	*1926*	*504*	inscribed levels are accurate, 1 cm offset between measu	1926 Hoogte t.o.v. NAP +5.05
								1995	*465*		1995 +4.66
								1993	*441*		1993 +4.42
								1953	*394*	North Sea storm surge	1953 +3.95
Nederrijn	*Arnhem*	*190222*	*443695*	*51.9805*	*5.8999*	building (outside)	circa 1880, repla	*1855*	*1385*	disappeared in WWII, levels determined from photograpl	1855
								1820	*1367*		Hoogte van het waater in het Jaar 1820
								1926	*1354*		1926
								1861	*1348*		1861
								1795	*1348*		1795
								1850	*1341*		1850
								1781	*1330*		1781
								1883	*1326*		1883
								1882	*1316*		1882
								1769	*1313*		1769
								1876	*1310*		1876
								1751	*1303*		1751
								1744	*1291*		1744
								1880	*1288*		1880
								1740	*1281*		1740

								1747	1276		1747
								1758	1269		1758
								1940	1265	flood water surface on photographs	
	Wijk bij Duurstea	152342	442482	51.9708	5.3485	city wall (city side)	19th century	1845	892	possibly displaced	WATER STAND A: APRIL 1845
	Wijk bij Duurstea	152345	442477	51.9707	5.3486	coupure in city wall (riv	19th century	1926	867	inscribed level is inaccurate, 10 cm offset between meas	WATER STAND T.O.V. N.A.P. +8.55
	Wijk bij Duurstea	152346	442477	51.9707	5.3486	coupure in city wall (riv	19th century	1995	779	inscribed levels are inaccurate, 10 cm offset between me	HOOGHEEMRAADSCHAP DE STICHTSE RIJNLANDEN +7,69
								1993	771		+7,49
Gelderse Vallei	Veenendaal	166202	448051	52.0207	5.5505	memorial column	1955	1855	904	monument erected 100 years after flood, top of column	[...] DE BOVENKANT VAN DEZE ZUIL WIJST AAN HOE HOO
	Leusden	156188	458382	52.1137	5.4045	church (outside)	1828	1855	320		Hoogte van het Rijnwater op den 14 Maart bij de DOORB
Betuwe	Buren	151375	435914	51.9117	5.3345	building (outside)	circa 1700	1784	557	weathered, info sign ANWB	Dit - is de hoogte van de vloed [...]de [...] 1784 [...]
	Tricht	147755	434736	51.9011	5.2819	wall connected to build	19th century	1820	574	replaced, but according to owners not displaced	1820 VLOEDLIJN
Lek	Culemborg	143932	440874	51.9562	5.2262	building (outside)	1617	1820	607		DOORBRAKEN bij Oosterhout en Elden, den 23, 24 en 25
								1741	535	difficult to measure, moat between street and building	INBREUCK VAN BEMMEL EN ELDEN DEN 3 JANNUA ANNC
								1658	512		Inbreuck van D[oornick], Oosterholt E[n Loenen] A° 16(2,
								1726	506		INBREUCK VAN OCHTEN en PASWAEY. {2/2} A°. 1726
								1651	486		Inbreck va Holthuise en Oosterholt, by de Rietkamer A° 1
								1651	478		Weder inbreck van Holthuisen 1651
								1769	478		DOORBRAAK : BY HUISSEN : DEN 28 DECEMBer 1769
	Culemborg	143926	440865	51.9561	5.2261	building (outside)	1909	1809	608	difficult to measure, moat between street and building,	Doorbraak van Loenen en Oosterholt den 14 January 180
								1784	563		Doorbraaken tot Ogten en Bemmel, den 1 en 3 Maart 17
								1799	500		[Doorbraken te] Doornenburg en Doornik den 7en en 21
	Culemborg	143734	441002	51.9573	5.2233	building (outside)	1350 (BAG) or 15	1827	618		Doorbraak te Ochten den 3den Maart 1827
								1855	562		Doorbraken te Lienden, Ingen en te Maurik den 5den Ma
	Vreeswijk	134970	446250	52.0043	5.0955	former sluice	1373, restored m	1595	485	likely removed during restorations, level obtained from K	Den 4 Martii waerachtich stont het water boven dezen st
	Vianen	134436	445203	51.9948	5.0878	bridge in front of castle	17th century	1876	620	level inscribed on stone	WATERHOOGTE VAN 16 MAART 1876 6.20 Mr +AP.
	Harmelen	125927	456013	52.0916	4.9630	bridge	19th century	1624	no meas.	displaced, information at shhv.info (Stichts-Hollandse His	DE HOECTE VAN DE LECK 1624
	Jaarsveld	126945	442402	51.9693	4.9789	gauge installation (insic	1896 (www.rijksr	1876	no meas.	inside historic 'peilschaalhuisje'	WATERHOOGTE 18 MAART 1876
								1845	no meas.		
	Nieuwpoort	119006	438611	51.9348	4.8638	building (outside)	restored in 1985	1819	no meas.	info sign ANWB	
								1809	no meas.		
	Kinderdijk	103383	433697	51.8894	4.6374	building (outside)	1644	1740	247		1740
								1820	199		1820
								1726	179		1726
								1809	139		1809
								1709	84		1709
								1743	81		J. 1743
	Kinderdijk	103389	433679	51.8892	4.6375	unconnected wall, hold	20th century	1809	no meas.	displaced	HOOGTE VAN HET VLOEDWATER 1809
Alblasserwaard	Noordeloos	125420	435942	51.9112	4.9573	building (outside)	1614	1741	235	base of stone	1741.
								1820	173	base of stone	1820.
								1809	116	base of stone	1809.
	Noordeloos	125154	435529	51.9075	4.9535	building (outside)	1880	1741	no meas.	building younger than floodmark, displaced (van Groning	1740 EN EEN STOND HET WATER AAN DESEN STEEN
								1820	no meas.		1819 EN EEN REES HET WATER AAN DESEN STEEN
								1809	no meas.		1809 IS HET WATER AAN DEES STEEN GESTEGEN
	Molenaarsgraaf	115557	431951	51.8747	4.8144	building (outside)	1741	1741	253	base of stone	1740 EN EEN STOND HET WATER AAN DESEN STEEN.
								1820	195	base of stone	1819 EN EEN STOND HET WATER AAN DESEN STEEN
								1809	137	base of stone	1809 IS HET WATER AAN DESEN STEEN GESTEGEN
	Molenaarsgraaf	115158	431779	51.8731	4.8087	building (outside)	1600	1741	no meas.	displaced (van Groningen, 2012)	ANNO 1740 EN EEN STOND HET WATER AAN DESEN STEE
								1809	no meas.		IN FEBRUARY 1809, STOND HET WATER HIER TEEGEN. N:
	Bleskensgraaf	112585	431388	51.8694	4.7713	building (outside)	1980	1741	195	building younger than flood mark	WATER-HOOGTE 1741
Oude IJssel	Hummelo	213210	446659	52.0053	6.2350	building (outside)	1955	1814	no meas.	building younger than flood mark	Gedenkteken van 't hooge Rijn water a: 1814
IJssel	Dieren	204542	450637	52.0418	6.1093	memorial stone	1998	1995	1042	placed post-datum, no offset between measurements an	HOOG WATER AAN 'T VEER | BUURTSCHAP VAN DIEREN
								1993	1028		26-12-1993
								1926	1025		05-01-1926
								1983	1022		01-06-1983
	Zutphen	210542	461639	52.1401	6.1986	building (outside)	circa 1300	1651	935		IN JANUARIO ALLES GODES WERCK ANNO EENDUISENT S
	Deventer	207755	473859	52.2502	6.1598	piece of wall at locatior	buildings on both	1658	808	construction possibly younger than flood mark	1658
								1635	780		1635
								1784	758		17{4/3}84
								1595	753		1595
								1814	722		18{2/16}14
								1754	696		17{2/1}54
								1926	690		19{7/1}26
								1883	682		18{?/?}83
	Deventer	207452	473904	52.2507	6.1553	building (outside)	19th century	1926	732		MR. N. BOLKESTEIN FONDS | 19{7/1}26
								1995	709		19{2/2}95
								1993	692		19{27/12}93
	Zwolle	200500	501500	52.4993	6.0573	fortification work ('Kate	17th century	1799	478	estimated location, likely removed, levels obtained from	Krayenhoff, C.R.T., 1813. Verzameling van hydrographisch
								1784	448		

extreme discharges occurred in 1809, 1920, 1926, and 1995. These years are similarly represented by many flood marks, with the notable exception of 1920 (Fig. 3.16).

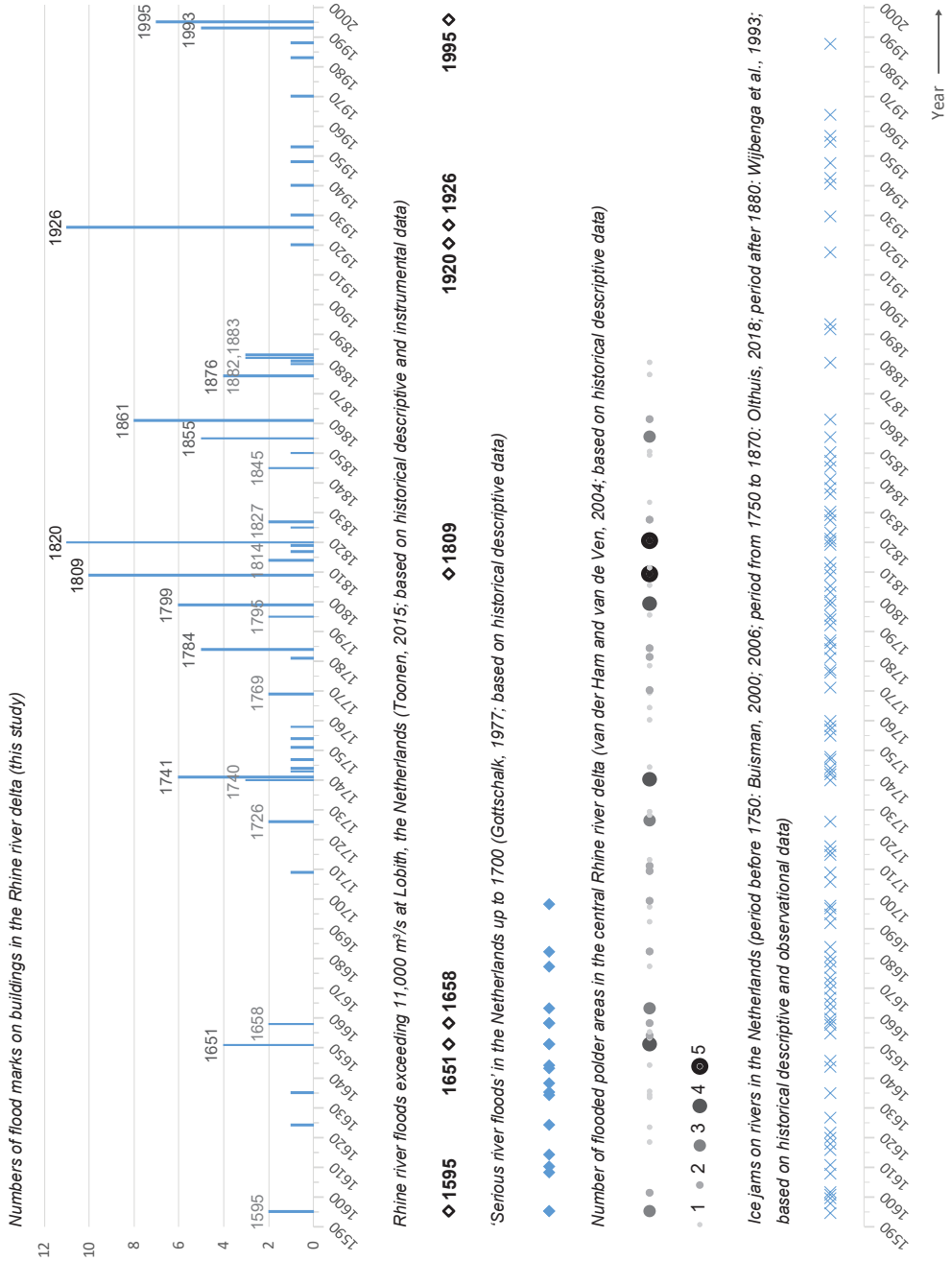

Fig. 3.16. Temporal distribution of flood marks in the Rhine delta. The results are plotted together with historical records of flood intensity and ice jam occurrence (Gottschalk, 1977; Wijbenga et al., 1993; Buisman, 2000; 2006; van der Ham and van de Ven, 2004; Toonen, 2015; Olthuis, 2018).

For the period up to 1900, there is a strong correlation between the number of flood marks and the number of flooded areas in the central delta reported in historical sources (van der Ham and van de Ven, 2004). Several contemporary maps corroborate the extents of flooding extracted from historical written records (e.g. Fig. 3.18; Fig. 3.19). The floods of 1809 and 1820 resulted in the largest amount of flooded areas, and are represented by the largest numbers of flood marks from that century (Fig. 3.16). Other events with multiple reported flooded areas are similarly documented by relatively large numbers of marks (1595, 1651, 1658, 1726, 1740, 1784, 1799, 1827, 1855, 1861). The correlation between numbers of flood marks and flooded areas ceases in the twentieth century, because by then high water levels hardly resulted in flooding of embankment-protected polder areas thanks to extensive river normalization and dike strengthening.

The relatively large numbers of flood marks in the eighteenth and nineteenth centuries may be linked to extreme winter conditions at the time. Especially in the early nineteenth century, ice jams formed on the Rhine river branches in many years (Wijbenga et al., 1993; Buisman, 2000; 2006; Olthuis, 2018). In several cases, such ice jams were responsible for dike failure, resulting in particularly sudden and locally highly destructive floods (e.g. Driessen, 1994). Many of the years with a large number of flood marks were characterized by ice jams, such as 1784, 1799, 1809, 1820, 1855, and 1861 (Fig. 3.16). This correlation signifies the potential impact of this type of flood. Ice jams are furthermore responsible for some years with flood marks but without flooded polder areas, as they can influence the discharge distribution over the different Rhine branches. For example, due to a large ice jam on the Waal near Hulhuizen in 1845, the Nederrijn-Lek had very high water levels, illustrated by flood marks in Jaarsveld and in Wijk bij Duurstede (Fig. 3.20).

3.6.1 Differences between river branches

Similar to the explanation for the marks of 1845, detailed interpretations of flood mark distribution would require careful historical analysis of each event. For example, flood marks of 1814 occur only along the IJssel, not along the Waal or along the Nederrijn-Lek (Table 3.1). Literature research reveals that in this year the 'Liemerse overlaat', a former spillway in the delta apex region, operated

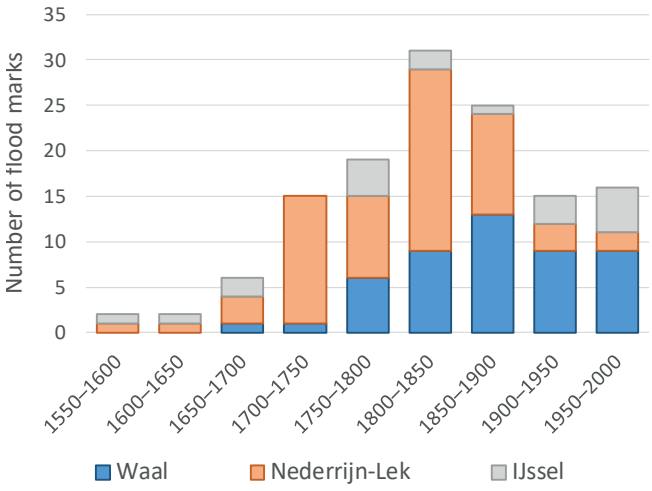

Fig. 3.17. Temporal distribution of flood marks, seperated by Rhine river branch, in fifty-year intervals.

for the first time (van der Ham and van de Ven, 2004), which resulted in controlled local flooding north of the Lower Rhine and east of the IJssel. This clearly explains the anomalous distribution of flood marks for this year.

The spatial distribution of flood marks for the more extreme events with relatively many marks informs on the flooding patterns in those years. For example, water levels of 1855 are marked along the Nederrijn-Lek and in the Gelderse Vallei north of this river (Fig. 3.21). In Arnhem, the level of 1855 is the highest mark on the stone, positioned even above the inscribed title (Fig. 3.11). In contrast, water levels of 1861 are marked mainly along the Waal and in the polder areas south of this river (Fig. 3.21). Extraordinary high water levels occurred in the Bommelerwaard polder area, which led to the construction of raised mounds serving as refuge hills (e.g. Berendsen, 1986). These reached to more than 3 m above their surroundings, up to the local water levels reached during the flood (Fig. 3.14). The flood events of 1855 and 1861 were both characterized by ice jams (e.g. Mijnssen-Dutilh, 2006), explaining the regionalized flooding patterns.

Two events that were explicitly not affected by ice jams are those of 1740–1741 and 1926. The flood of 1926 is marked throughout the Rhine delta (Fig. 3.21). The large number of marks may be explained by the temporal bias (increased preservation and increased awareness), but also signifies the exceptional magnitude of the event (it is the largest in the discharge measurement record, which started in 1901). In the winter of 1740–1741, extraordinary high water overtopped the dikes before a period of freezing commenced. At that time, when dikes were still smaller than at present, dike overtopping without the presence of ice jams was already highly unusual (van Zellem, 2003).

Fig. 3.18. Historic map showing Rhine flood extent in 1809. The blueish colour indicates that not only the lands along the Lower Rhine were flooded, but also all the polders in the central delta (Overbetuwe, Nederbetuwe, Tielerwaard, Bommelerwaard, Alblasserwaard) and the lands along the IJssel. Source: Gelders Archief.

The flood mark distribution of this event reveals that the flood caused the largest problems in the Alblasserwaard polder area in the downstream part of the study area (Fig. 3.21). Here, 1740 and 1741 are the highest recorded event levels at multiple locations (Fig. 3.4; Fig. 3.7), suggesting a magnitude that warrants interpretation as an extreme event, despite not being recognized as such based on historical indices of flood-related damages (Toonen, 2015). The historical record in Cologne corroborates the unusual magnitude of the 1740–1741 flood event, as it shows that the maximum water level of 1740 even slightly exceeded that of 1651 (Krahe and Larina, 2010).

3.6.2 Flood level series

The water levels obtained from the epigraphic marks provide an overview of flood levels in the Rhine delta from the late sixteenth to late twentieth centuries (Table 3.1). Combining the levels of multiple years and locations provides new insights into the historic flood dynamics of the Rhine river branches. For example, the data along the Waal reveal that differences between event levels decrease in downstream direction. In Nijmegen, the early nineteenth-century levels exceed the late twentieth-century flood levels by about 1 m, whereas in Loevestein this difference is about 0.5 m (Fig. 3.22). However, it should be noted that such differences are considerably smaller than the potential rise in local water levels due to ice jams (e.g. Wijbenga et al., 1993; Lindenschmidt et al., 2018; Olthuis, 2018)

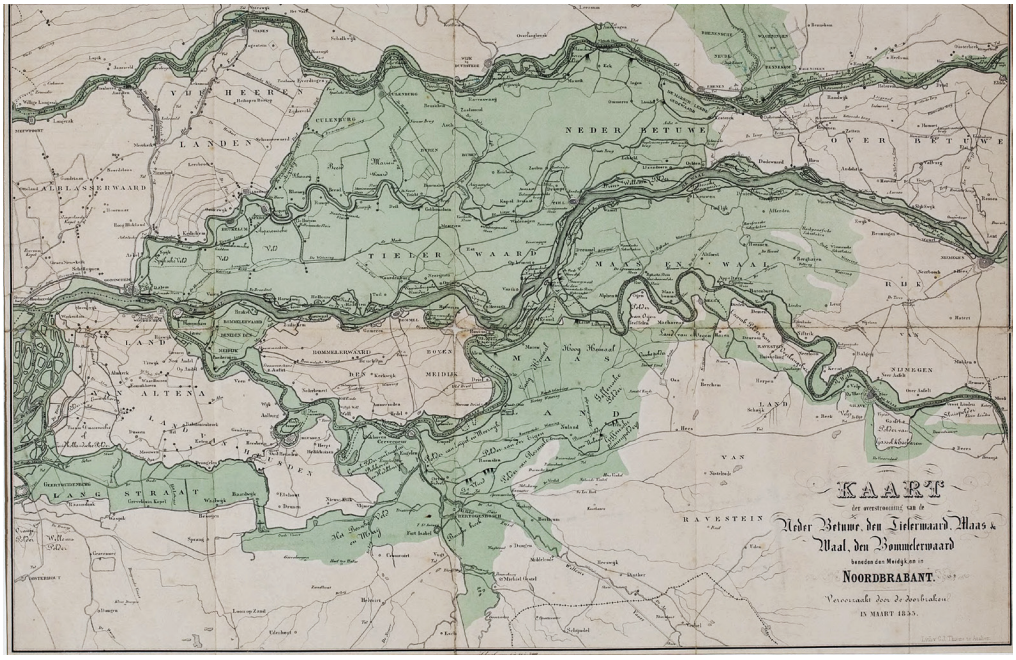

Fig. 3.19. Historic map showing Rhine flood extent in 1855. The greenish colour indicates that a few polders in the central delta were flooded. It further indicates northward flooding at the entrance of the Gelderse Vallei, which is corroborated by flood marks north of the Nederrijn (Fig. 3.1; Fig. 3.3; Fig. 3.5). Source: Gelders Archief.

The historic flood levels along the Waal and Nederrijn-Lek show a remarkable overall increase over time up to the early nineteenth century, which is followed by an abrupt decrease around 1870 (Fig. 3.23). This pattern very clearly follows the increasing frequency and intensity of flood disasters, which peaked in the beginning of the nineteenth century and greatly lessened after normalisation in the beginning of the second half of this century (e.g. van de Ven et al., 1995). My results show that not only the number of flood disasters, but also the associated water levels increased over the centuries leading up to normalisation. This increase is partly explained by sedimentation in between the embankments, leading to an overall rise in floodplain elevation and thus a decrease in conveyance capacity (e.g. Middelkoop, 1997; Hudson et al., 2008; Hobo, 2015). A similar trend is convincingly observed in a series of flood marks along the Po river in Italy, although that

Fig. 3.20. A flood mark in Wijk bij Duurstede. The inscription reads 'WATER–STAND A: APRIL 1845'. The horizontal line in between the words 'WATER' and 'STAND' represents the maximum water level.

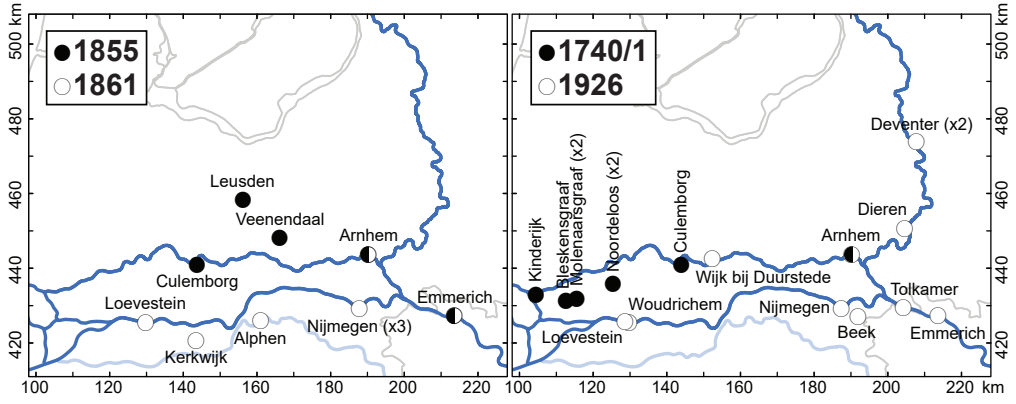

Fig. 3.21. Spatial distribution of flood marks for the ice-jam events in 1855 and 1861, and for the ice-free events in 1740–1741 and 1926.

observation is limited to a single location (Camuffo et al., 2020). The river normalisation works that started around 1850 considerably decreased the potential for ice jam formation, thanks to the removal of sand banks and the construction of regular arrays of groynes. This very likely contributed to the sudden reduction in maximum water levels after the period 1850–1870 (Fig. 3.23).

Interestingly, the notion of increasing flood mark elevations up to the mid-nineteenth century only applies to the Waal and Nederrijn-Lek. The flood levels marked along the IJssel show a different trend, exhibiting an overall decrease from the seventeenth century onwards (Fig. 3.23). Apparently, this distributary carried relatively large amounts of water during floods in the sixteenth and

Fig. 3.22. Flood marks in Loevestein. A) Detail of the marks. B) Position of marks in western gate of fortification wall. C) Location of gate, close to the Waal. Source: Google Street View.

seventeenth centuries, contrasting with a loss of discharge under normal flow conditions (e.g. van de Ven, 1976; Overmars, 2020). The explanation for this dynamic is likely related to flood water routing near the German–Dutch border area. Presumably, dikes were still low in this area and more prone to failure than in later centuries. Any water that overtops the northern embankments in the apex region enters the floodplain areas that connect to the Oude IJssel valley and onwards to the IJssel river, contributing to water level raising along this branch. The flooding pattern that arises resembles the controlled flooding in 1814. Historical sources indeed explicitly report on severe dike breaches along the Lower Rhine near Wesel and Emmerich in 1595 and 1651 (Gottschalk, 1977), corroborating the above explanation for the disparate trend in flood levels along the IJssel compared to the other two river branches. Similar patterns of flooding during the most extreme discharges were identified for early medieval times based on model results (Chapter 6) and for late medieval times based on geoarchaeological data (Chapter 2).

3.7 Further implications

The water levels obtained from the flood marks predate the onset of water level measurement records in the Rhine delta by almost two centuries (Schoor et al., 1999; Glaser and Stangl, 2003; Toonen, 2015; Toonen et al., 2016). In addition to extending the instrumental record back in time, the epigraphic marks provide water levels at locations that do not have measurement stations. These data may be of particular societal importance, as they provide tangible evidence of historic flood events and thereby have the potential to raise awareness of flood risk (Baker et al., 2002; Deutsch et al., 2006; Munzar et al., 2006). In many central floodplain locations in the Rhine delta, water levels during nineteenth-century extreme floods exceeded the street level by more than 2 m (e.g. Fig. 3.3; Fig. 3.4; Fig. 3.14). Especially since these locations are not located close to a river, which may lead to a perceived feeling of safety from flooding, the effect of showing the extremity of historic events may provide both incentive and support for flood-protective measures. This is very important for a delta setting which for a large part consists of flood-prone yet densely inhabited lands.

Furthermore, the flood marks can act as a reliability check on peak levels provided by measurement records, especially for events in the nineteenth century (records obtained from waterinfo.rws.nl). For this period, it is difficult to assess the accuracy of measurements. The highest water level in the measurement record of Nijmegen is in 1820 and agrees very well with an observed flood mark elevation in the city centre (measurement record: 1446 cm; flood mark: 1450 cm). However, the maximum water level in the measurement record for the flood event of 1861 is over a meter lower than that of 1820 (Table 3.2), whereas the flood mark data indicate a difference of only about 10 cm (Table 3.3). This level is constrained by no fewer than three different flood marks in Nijmegen city centre, thus it is safe to infer that the peak value given by the measurement record is inaccurate. The large height of the 1861 flood in Nijmegen is further corroborated by marks in other locations along the Waal (Fig. 3.20). In Loevestein, at the downstream end of the river, the level of 1861 is close to that of 1820 (Fig. 3.22). In Emmerich, just upstream of the Waal bifurcation, the 1861 flood level is the highest in the record, although earlier events are not indicated (Table 3.1).

The reason for the error in the water level measurement record is unclear. Possibly, the measurement was hampered due to the severe flooding. The water level may have exceeded the then present gauge equipment. Another likely contributing factor concerns the timing of measurements, which presumably happened at a set time in the morning of each day. Therefore, an extraordinarily rapid

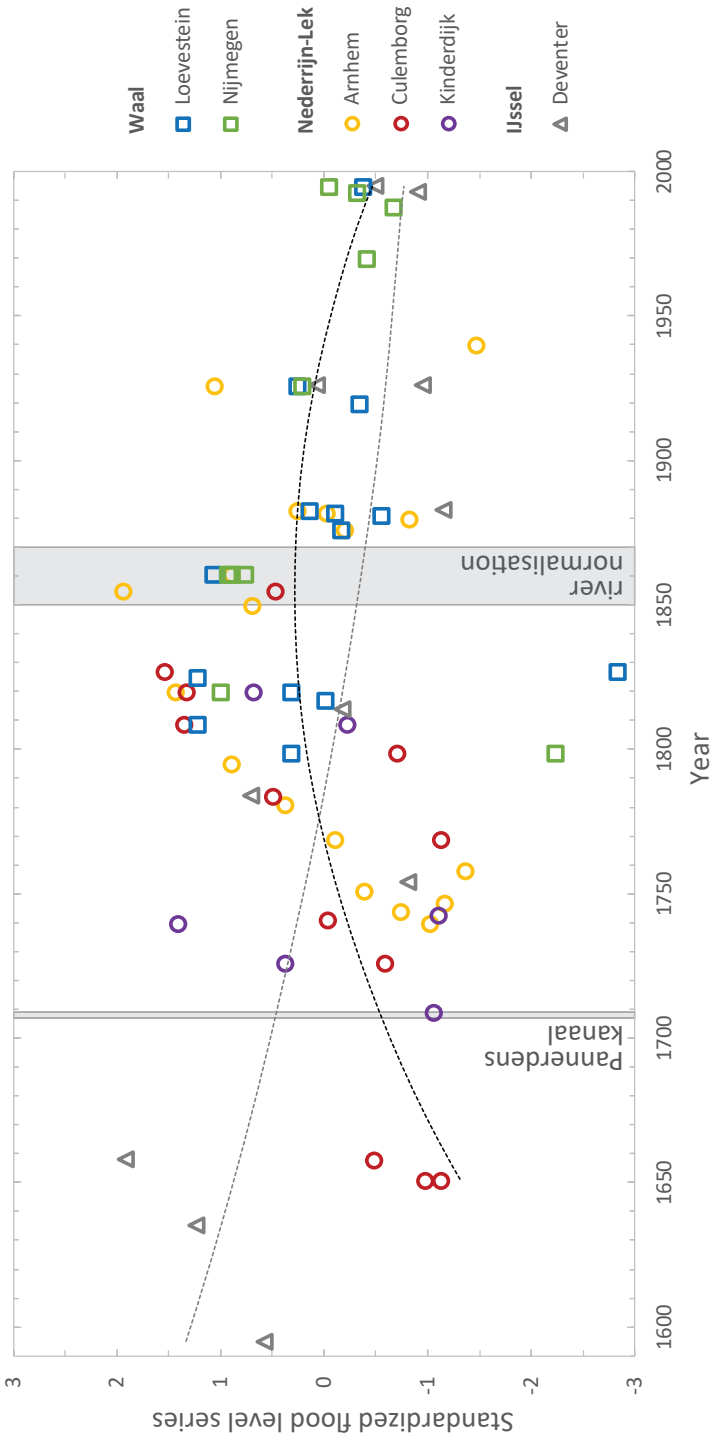

Fig. 3.23. Standardized records for sites with more than five flood marks. The squares and circles are records along respectively the Waal and the Nederrijn-Lek. The triangles are a record along the IJssel. The lines are second-order polynomial trend lines for the combined western branches (black) and for the northern branch (grey). Note that these trend lines are shown to indicate the contrast between the two distributary systems, not to represent the actual development in flood levels, since no trend line can account for the step that occurs around 1870 in the records of Waal and Nederrijn-Lek flood levels.

rise and fall in water level, for example caused by ice jam formation and dike breaching, may be missed in a historical measurement record. It should be noted that the average errors of water level measurement records are likely very small; only peak levels during extreme events were not always recorded accurately. Still, precisely those extremes are the most important for further hydraulic calculations and flood risk assessments, thus necessitating confidence in their values.

Through hydraulic calculations, historic water levels such as those presented in this study can be converted into discharges (e.g. Elleder et al., 2013; Herget et al., 2014; Wetter, 2017). These historic discharges can in turn be used in statistical analyses to constrain future extreme flood magnitudes (e.g. Macdonald, 2013; Pekárová et al., 2013; Engeland et al., 2018). For hydraulic models of

Table 3.2. Top ten years with the highest water levels in the measurement record of Nijmegen (since the onset of measurements in 1772). Source: waterinfo.rws.nl.

Year	Level (cm +NAP)
1820	1446
1809	1407
1799	1378
1830	1375
1926	1374
1781	1367
1805	1352
1995	1352
1861	1345
1784	1344

Table 3.3. Elevations of flood marks on commemorative stones in Nijmegen city centre.

Year	Level (cm +NAP)
1820	1450
1861	1444
1861	1441
1861	1430

historic flood events in the Rhine delta (e.g. Hesselink et al., 2003; Bomers et al., 2019), flood marks can serve as a check on the measured peak values (Table 3.2; Table 3.3). Furthermore, they provide model validation points at additional locations besides the measurement stations (Fig. 3.1). Last but not least, they allow for the quantitative study of floods that precede the instrumental measurement record, for example the events in 1651 and 1740–1741.

Acknowledgements

Jürgen Herget introduced me to flood marks along the Rhine in Germany, sparking my enthusiasm to undertake this study. Hans Renes and Ton Markus kindly shared unpublished overview maps of anthropogenic landscape elements in the central delta (Hans Harten, 1980s–1990s), which helped me to complete my dataset. The inventory phase greatly benefited from the online map 'Hoogwatermarkeringen in Nederland' (Dik Brijs), which shows about two-thirds of the flood marks in the Rhine delta and an impressive amount of storm surge marks in the coastal region. For their assistance in the field, I thank Maarten Zeylmans, Willem-Jan Dirkx, Teun van Woerkom, Kees Nooren, and Marcel van Maarseveen. In addition, I sincerely acknowledge the many local inhabitants that I met during the field surveys, who often provided valuable information on the flood marks and local water management history.

The main dataset of this chapter (Table 3.1) and selected images (Fig. 3.1; Fig. 3.16; Fig. 3.23) are available (open access) in table format (.xlsx) and vector format (.pdf) at the KNAW DANS archive website (DOI:10.17026/dans-2zz-kpka).

Chapter 4

Historic river morphology

part of this chapter is based on

Bomers, A., van der Meulen, B., Schielen, R.M.J., Hulscher, S.J.M.H., 2019. Historic flood reconstruction with the use of an Artificial Neural Network. Water Resources Research 55, 9673–9688. DOI:10.1029/2019WR025656

No man ever steps in the same river twice, for it is not the same river and he is not the same man.

Heraclitus

Note

This chapter describes a reconstruction I made of the Rhine river branches and their surrounding floodplains based on historic maps and measurement data. The results have been used in numerical simulations of an early nineteenth-century extreme flood event [Bomers, A., van der Meulen, B., Schielen, R.M.J., Hulscher, S.J.M.H., 2019. Historic flood reconstruction with the use of an Artificial Neural Network. Water Resources Research 55, 9673–9688.]. The reconstruction covers all relevant river landscape elements in the delta, but the focus of this chapter is on the historical morphology of the river branches.

4.1 Introduction

Historic maps and measurement data provide information on river geometry and fluvial processes at time scales of centuries, bridging shorter-term high-resolution approaches using modern data such as aerial photographs (e.g. van Denderen et al., 2018) and longer-term low-resolution approaches based on geological deposits (e.g. Berendsen and Stouthamer, 2000). Many studies apply historic maps to reconstruct the planform geometry of rivers, which serves various geomorphological and historical geographical purposes (e.g. Hesselink, 2002; Uribelarrea et al., 2003; Wolfert and Maas, 2007; Zanoni et al., 2008; Hobo et al., 2014; Furlanetto and Bondesan, 2015; Quik and Wallinga, 2018; Arnaud et al., 2020; Overmars, 2020). Three-dimensional reconstructions incorporating bathymetry are rare, due to available data limitations, but necessary for hydraulic calculations (Hesselink et al., 2006). Existing studies often cover only a small stretch of river, introducing potential problems for modelling purposes as results are affected by boundary conditions (Montes Arboleda et al., 2010; Le et al., 2020).

In the Netherlands, there is a wealth of maps depicting rivers from the fifteenth century onwards. These maps are broadly categorized based on their original purpose (Donkersloot–de Vrij, 1981; Koeman, 1983). River maps created for juridical purposes such as land ownership (Fig. 4.1, Fig. 4.2) were especially prevalent until the mid-seventeenth century (e.g. Overmars, 2020), whereas river maps created for engineering purposes such as artificial cut-offs (Fig. 4.3, Fig. 4.4) became more common between the seventeenth and nineteenth centuries (e.g. van de Ven, 1976; van den Brink, 1998). Especially maps of the latter category are suitable to reconstruct channel morphology, as these can be considered accurate and sometimes contain depth measurement information (Fig. 4.4). This category is dominated by the first edition of the *Algemene Rivierkaart* ('General River Map'), created in the nineteenth century to aid regulation and channel bed fixation (normalization) of the Rhine river branches (Boode, 1979; van der Ham and van de Ven, 2004; van Heezik, 2007).

The nineteenth-century interventions in the river bed dramatically altered channel flow patterns (e.g. Lambeek and Mosselman, 1998; Hudson et al., 2008). Even though embankments were present long before normalization, as were (wooden) groynes in some river stretches (e.g. Fig. 4.2; Fig. 4.3), the Rhine river branches were still semi-natural and dynamic (Frings et al., 2009; Hobo et al., 2014). This rapidly changed with the construction of regular arrays of (stone) groynes in the late nineteenth century. Since the first edition of the *Algemene Rivierkaart* predates these major interventions that constricted and fixated the river channels, a reconstruction based on this map series is largely representative for the morphology of the Rhine in historic times up to ~1850. For that reason, such a reconstruction can connect local historical and geomorphological studies using

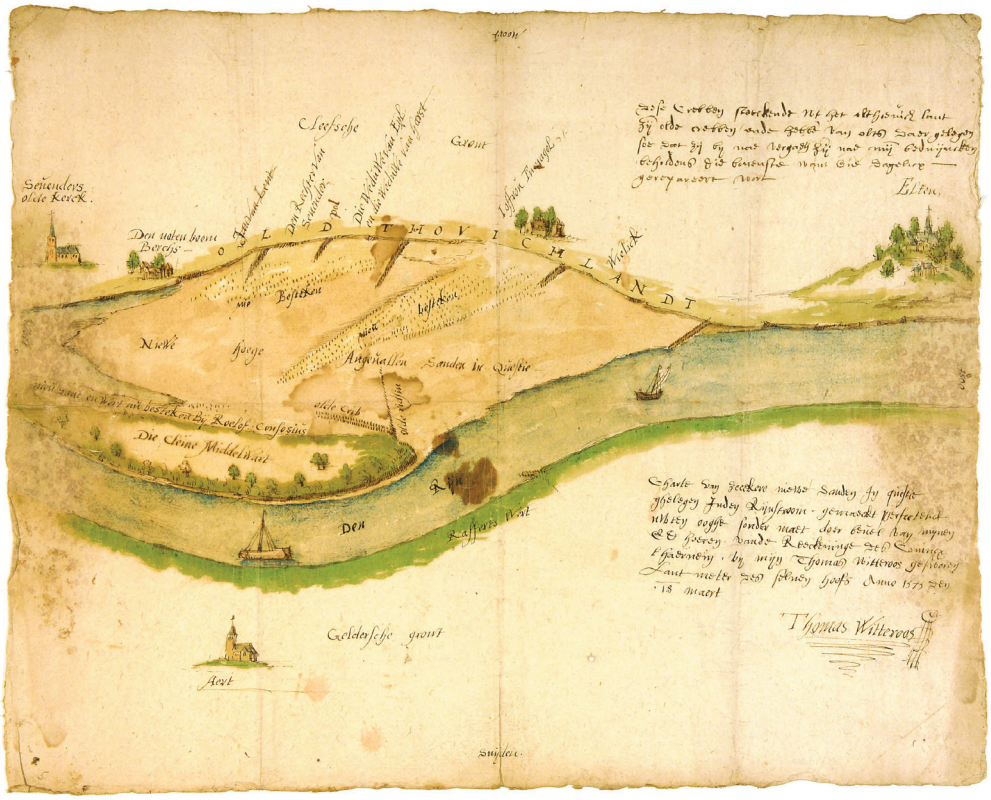

Fig. 4.1. Example of a river map created for juridical purposes (T. Witteroos, 1575).

Fig. 4.2. Example of a river map created for juridical purposes (N. van Geelkercken, 1634).

historic maps (e.g. Middelkoop, 1997; Hesselink, 2002; Overmars, 2020) to numerical modelling studies that cover the entire delta but are limited to twentieth-century or present landscape settings. This in turn can enable the simulation of large flood events that occurred in historic times before the onset of discharge measurements.

4.2 Materials

The *Algemene Rivierkaart* map series covers the large rivers in the Netherlands over their full lenghts at a scale of 1:10,000. The first edition map sheets of the Rhine river branches (Waal, Nederrijn-Lek, IJssel) were produced by B.H. Goudriaan and L.J.A. van der Kun in the 1830s and early 1840s (van den Brink, 2002), before the onset of river normalization around 1850 (Ploeger, 1992; van Heezik, 2007). Thus, the maps depict a river morphology that considerably differs from the current engineered channels (Fig. 4.5, Fig. 4.6). The early nineteenth-century triangulation network by C.R.T. Krayenhoff formed the geometrical basis for the *Algemene Rivierkaart* (Koeman, 1983). The maps were drawn in the Bonne projection with the meridian at 4°53'01.95" longitude (Westertoren, Amsterdam) and the perpendicular at 51°30' latitude (Boode, 1979).

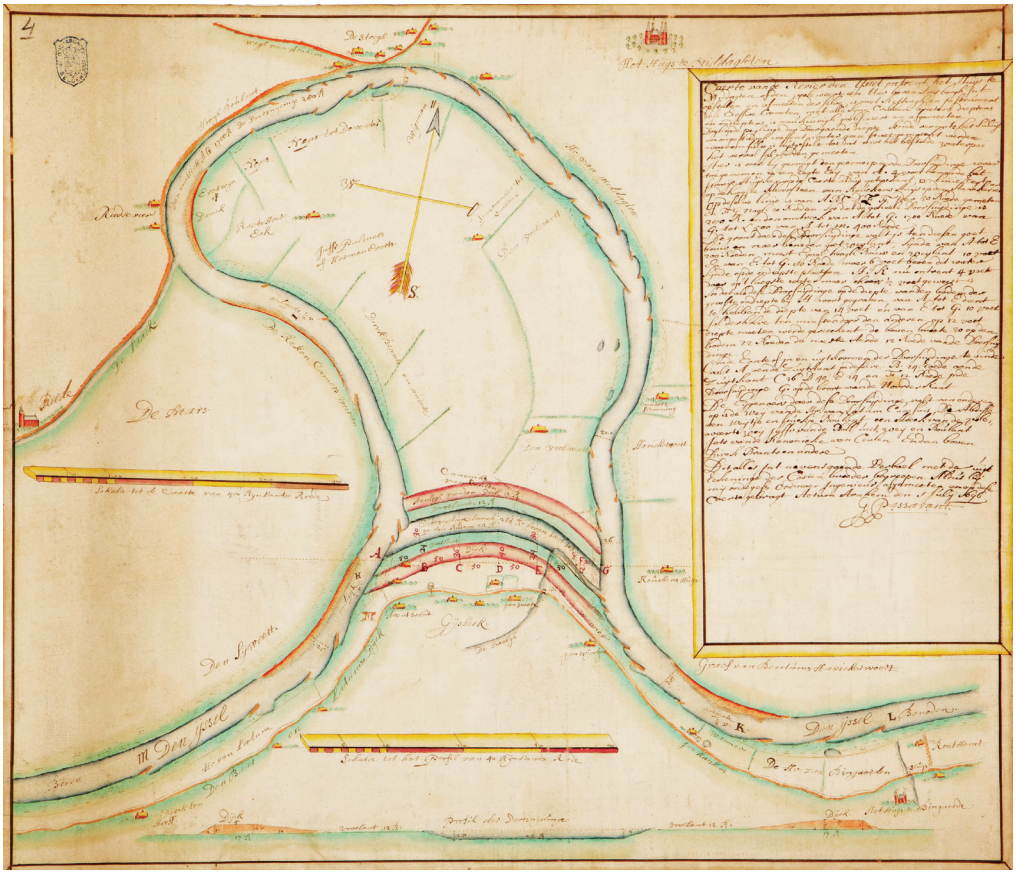

Fig. 4.3. Example of a river map created for engineering purposes (G. Passavant, 1696).

Fig. 4.4. Example of a river map created for engineering purposes (F. Beijerinck, 1767).

The maps show profile lines at regular intervals of 1 km along the rivers (Fig. 4.5, Fig. 4.6). At all of these locations, water depths were measured across the river. The measurement data accompanied the maps in separate registers, which were considered lost (Wierda and Zweerus, 1994), until recently (van der Meulen et al., 2018). The registers contain for each river km location a table with information (orientation of profile, date of measurement, description of floodplain characteristics and engineering works) and about 30 to 120 data rows with measurements (Fig. 4.7). These consist of depth values corrected to 'Middelbare Rivierstand' (MR) and distances between depth measurement points. The registers define MR as the average water surface in summer (between May 1 and October 31) over a period of 29 years in the early nineteenth century.

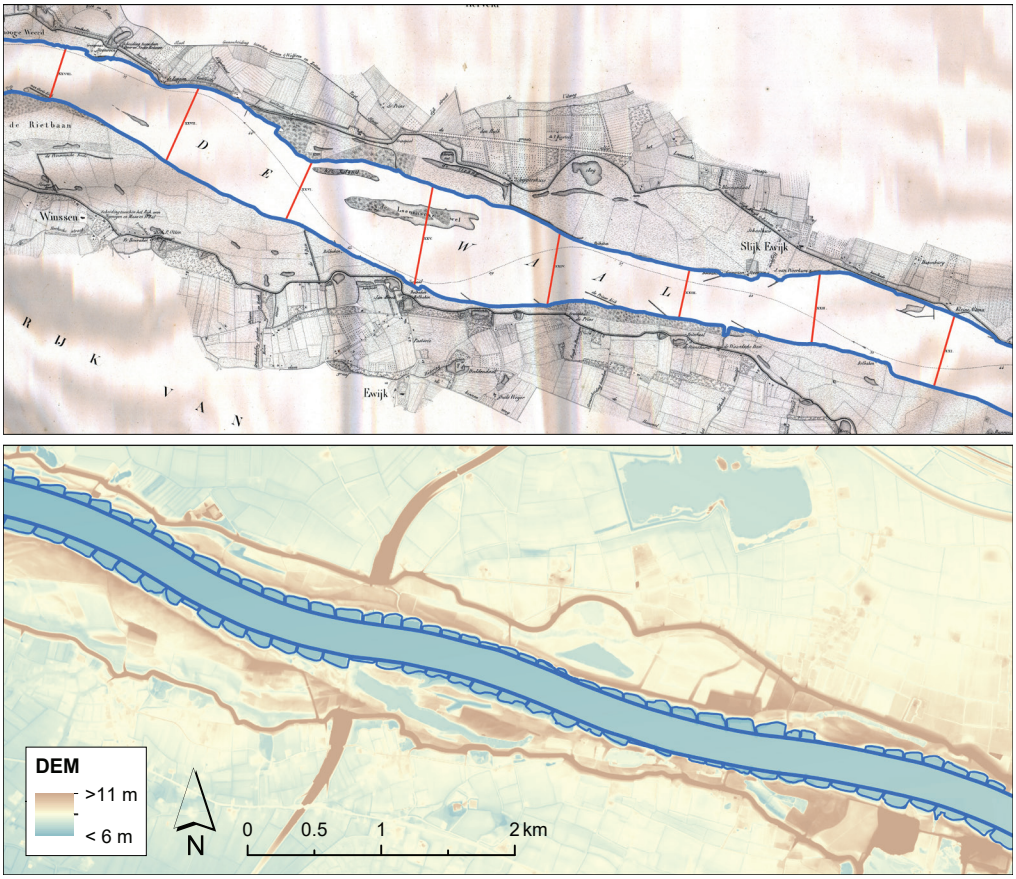

Fig. 4.5. Comparison of Waal river morphology between circa 1835 and the present. Above: *Algemene Rivierkaart* map sheet Herveld showing a stretch of river in its semi-natural state before normalization. Note the presence of islands and major variations in channel width. The blue and red lines are the digitized river shores and profile locations. Below: LiDAR ground level DEM showing current morphology. The blue lines are the river shores obtained from the RWS Baseline dataset.

4.3 Georeferencing and vectorising

Digital scans of the *Algemene Rivierkaart* map sheets were available at the library of Utrecht University. To project the individual maps onto their correct geographical positions, I tested two different methods. The first method used the original coordinate system, depicted on the map sheets themselves (Fig. 4.8). The second method used manually identified locations as ground control points, linking the historic maps to modern data products. The maps have a high degree of geometric accuracy, which made further conversion relatively straightforward. Thus, I applied affine (first order polynomial) transformations to all map sheets, which means that the scanned maps were not deformed, only shifted, scaled and rotated.

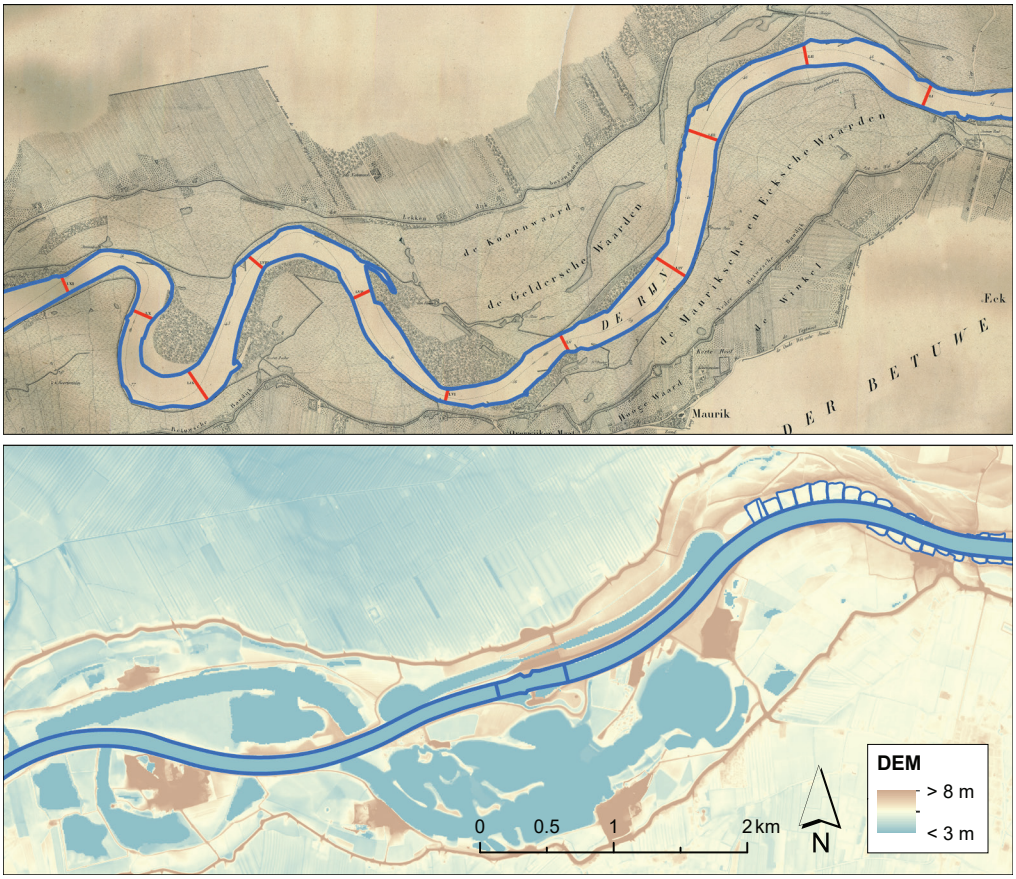

Fig. 4.6. Comparison of Nederrijn river morphology between circa 1835 and the present. Above: *Algemene Rivierkaart* map sheet Maurik showing a stretch of river in its semi-natural state before normalization. Note the variations in river width and the sinuous character with relatively sharp meander bends. The blue and red lines are the digitized river shores and profile locations. Below: LiDAR ground level DEM showing current morphology. The blue lines are the river shores obtained from the RWS Baseline dataset.

PEILRAAI N°. XXI.

VERKENNINGSPUNT. Aan den regteroever der rivier op de binnenkruin des dijks, bij dijkpaal N°. 134, in den eersten inwendigen hoek bovenwaarts het huis toebehoorende aan en bewoond door J. Janssen, gemerkt B, 56; zijnde uit dit punt waargenomen de hoeken:

Slijk-Ewijk .	
Beuningen .	57° 18′.
Peilraai . . .	23° 55′.
Weurth . . .	53° 48′.

RIGTING. De peilraai maakt in het verkenningspunt, met Slijk-Ewijk een hoek van 81° 13′, met Beuningen van 23° 55′ en met Weurth van 53° 48′.

OEVERS. De regteroever bij *MR* of peiling N°. 1, is op 58 ellen afstands uit het verkenningspunt. De linkeroever of peiling N°. 83, op 630 ellen uit hetzelfde punt. De breedte der rivier bij *MR* is dus 572 ellen.

NOMMERS DER PEILINGEN.	ONDERLINGE AFSTANDEN.	DIEPTEN BENEDEN *MR* GEREDUCEERD.	NOMMERS DER PEILINGEN.	ONDERLINGE AFSTANDEN.	DIEPTEN BENEDEN *MR* GEREDUCEERD.	NOMMERS DER PEILINGEN.	ONDERLINGE AFSTANDEN.	DIEPTEN BENEDEN *MR* GEREDUCEERD.	NOMMERS DER PEILINGEN.	ONDERLINGE AFSTANDEN.	DIEPTEN BENEDEN *MR* GEREDUCEERD.
1		0.00	22		2.85	43		3.45	64		4.45
	12.0			8.0			8.0			8.0	
2		0.65	23		2.85	44		3.45	65		4.45
	5.0			5.0			6.0			10.0	
3		0.85	24		2.85	45		3.45	66		4.35
	5.0			5.0			6.0			5.0	
4		1.05	25		2.95	46		3.75	67		3.95
	3.0			10.0			10.0			5.0	
5		1.45	26		2.95	47		3.85	68		3.95
	3.0			5.0			6.0			3.0	
6		2.45	27		3.05	48		3.65	69		3.95
	3.0			5.0			10.0			10.0	
7		3.95	28		3.05	49		3.45	70		3.95
	3.0			8.0			5.0			5.0	
8		3.85	29		3.05	50		3.45	71		3.95
	4.0			10.0			10.0			5.0	
9		3.45	30		3.25	51		3.95	72		3.85
	6.0			7.0			10.0			7.0	
10		2.95	31		3.05	52		3.95	73		3.45
	4.0			7.0			10.0			5.0	
11		3.45	32		3.45	53		4.05	74		3.45
	7.0			10.0			5.0			5.0	
12		2.45	33		3.45	54		3.95	75		3.45
	5.0			8.0			4.0			5.0	
13		2.45	34		3.45	55		4.05	76		3.25
	10.0			8.0			8.0			5.0	
14		2.45	35		3.25	56		4.05	77		3.05
	4.0			10 0			10.0			10.0	
15		2.45	36		3.35	57		3.85	78		2.95
	4.0			7.0			3.0			5.0	
16		2.25	37		3.35	58		4.45	79		2.85
	5.0			10.0			15.0			10.0	
17		2.45	38		3.35	59		4.45	80		2.65
	5.0			10.0			10.0			10.0	
18		2.45	39		3.45	60		4.45	81		2.45
	6.0			5.0			3.0			8.0	
19		2.45	40		3.45	61		4.45	82		1.45
	10.0			6.0			5.0			7.0	
20		2.45	41		3.45	62		4.25	83		0.00
	10.0			6.0			9.0				
21		2.65	42		3.85	63		4.45			
	10.0			10.0			7.0				

WATERSTANDEN GEDURENDE DE PEILINGEN.

De peilingen in raai N°. XXI zijn gedaan den 30 Julij 1830, bij eenen rivierstand aan de peilschaal te Nijmegen, van 3.49 duim boven nul of boven *MR* 0.61 duim.

Algemeene Opmerkingen en Omschrijving der Werken.

De stroom rigt zich, tot aan de rijzenbol, hoofdzakelijk langs den *linkeroever*, doch van daar verder naar benedenwaarts wijkt dezelve weder daarvan af. Die oever is dan ook over het algemeen eenigzins afnemende. De genoemde rijzenbol heeft eene lengte van 17 el 20 duim, breedte van 93 ellen en hoogte aan de rivier van 0.75 en van achteren van 2.25 boven *MR*.

Langs den *regteroever*, die aanwinnende is, heeft men de navolgende werken, als:

Eene puinstorting tot beveiliging van het eerste huis buitendijks, beneden peilraai N°. XXI genaamd *de kleine Altena*, over 56 ellen lengte, tot de hoogte van 2.70 boven *MR*.

Aan het einde dezer puinstorting heeft men een rijsbeslag, behoorende aan het dorp Slijk-Ewijk, lang 53 el, hoog 2.60 boven *MR*.

Ongeveer 165 ellen beneden de kleine Altena, heeft men eene krib behoorende aan het dorp Slijk-Ewijk, lang 80 ellen, breed 3.60, hoog aan den oever 1.20 en aan den kop 0.10 boven *MR*, zijnde, op 18 ellen afstands uit den kop, aan dezelve eene rits verbonden, lang 290 ellen, hoog gelijks *MR*, achter welke eene slijkplaat is aangewassen.

63 ellen beneden laatstgenoemde krib, heeft men een dito krib, behoorende als voren en insgelijks aan den kop met de reeds genoemde slijkplaat verbonden; deszelfs lengte is 32 el, breedte 4.50 en hoogte aan den oever zoo wel als aan den kop 0.05 boven *MR*.

Eindelijk heeft men, een weinig verder benedenwaarts, eenige overblijfselen van voormalige, thans geheel vervallene, rijswerken bespeurt.

Fig. 4.7. Example of a profile description in the registers belonging to the *Algemene Rivierkaart*.

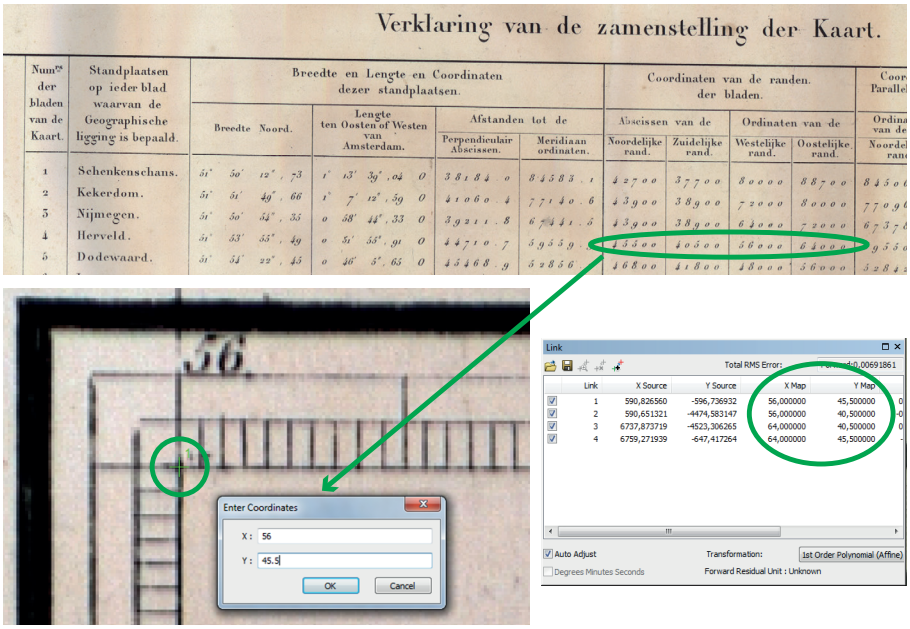

Fig. 4.8. Method for georeferencing using the original coordinate system. After changing the projection settings in ArcGIS, I simply selected the map edges and typed in their coordinates.

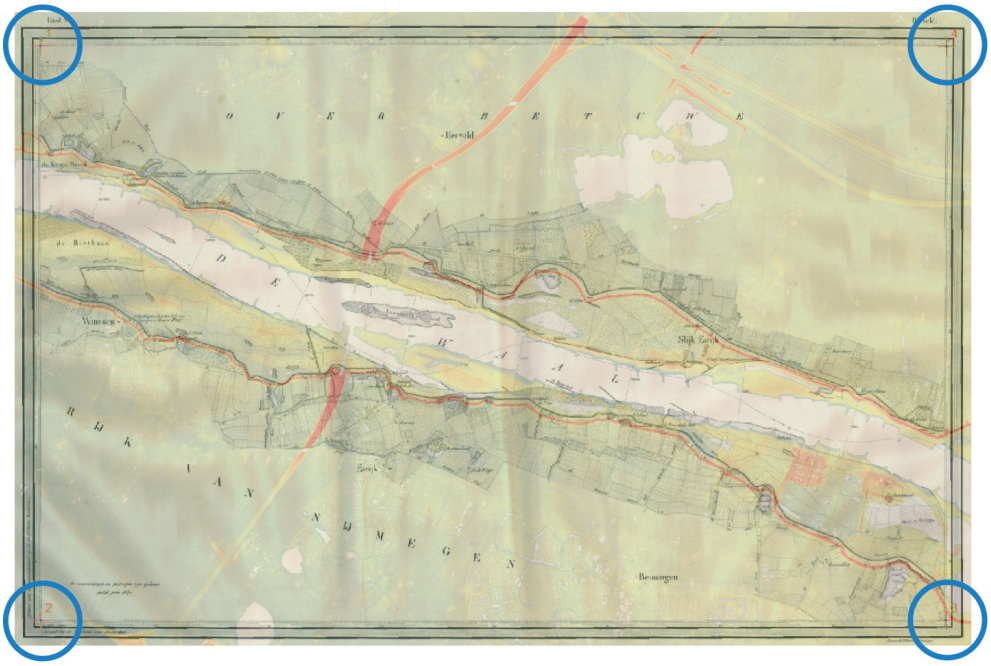

Fig. 4.9. *Algemene Rivierkaart* map sheet Herveld georeferenced using the original projection.

For the georeferencing method using the depicted coordinate information, I changed the projection settings in ArcGIS to Bonne and subsequently displaced the central meridian to 4.883875 degrees (4°53'01.95" longitude) and the standard parallel to 51.5 degrees (51°30' latitude). Then, I precisely selected the edges of the *Algemene Rivierkaart* map grids and simply entered their indicated values as x and y coordinates to place the maps at their desired locations (Fig. 4.8; Fig. 4.9).

For the more conventional georeferencing method using ground control points, I selected locations of semi-permanent elements on the historic maps and linked these to their locations selected in modern digital map products (Fig. 4.10). This requires elements of which the positions have not changed since the period of mapping, such as road intersections and church towers (Kreßner, 2009; Grabowski and Gurnell, 2016; Overmars, 2020). Distinct bends and inflections in the river dikes turned out to be the most suitable for this purpose, because these remained largely intact over the past centuries and are easily recognisable in the LiDAR ground level DEM (Fig. 4.5, Fig. 4.6). Moreover, the linear nature of the dikes allowed to easily check without additional information where their positions did or did not change, which is an important benefit compared to individual point features commonly used for georeferencing. Furthermore, given their relevance for river management purposes, the dikes on the *Algemene Rivierkaart* were likely mapped with great precision, which is a requirement for reliable ground control points.

To check the results of both methods, the georeferenced map sheets were overlain semi-transparent on the LiDAR ground level DEM to visually inspect and digitally measure deviations between features that should align (Fig. 4.9, Fig. 4.10). On average, such deviations were small (about 10 to

Fig. 4.10. *Algemene Rivierkaart* map sheet Herveld georeferenced using ground control points.

20 m) in both methods, but for some map sheets the deviations amounted up to 150 m in the first method using the original coordinate system (Fig. 4.9). The second method using ground control points achieved significantly better results (Fig. 4.10), with maximum deviations below 50 m for all map sheets. The uncertainties can be attributed to inaccuracies in the original mapping and printing processes, and to folds in the maps that were not completely flattened during scanning.

Because of the improved accuracy, I used the second method for all map sheets, even though it was more time-consuming, requiring about 5 to 15 carefully identified selections per map compared to 4 straightforward selections in the first method. After successful georeferencing, I created vector datasets of river shores and islands by manually tracing these in ArcGIS ('on-screen digitizing'). In addition, I traced the profile lines depicted on the maps (Fig. 4.5, Fig. 4.6), as these were necessary to append the resulting planform geometry with depth information.

4.4 Bathymetry reconstruction

After digitizing the measurement data provided by the registers, I assigned geographical locations to the depth values by linking them to their respective profile lines vectorised on the georeferenced maps (Fig. 4.5, Fig. 4.6). In this process, the distances between the measurements were converted into percentages to ensure that the total distance for each profile matched the length of the drawn line. This resulted in a detailed depth profile at every km along the rivers (Fig. 4.11). Subsequent interpolation between the profiles produced a fully three-dimensional reconstruction of the river branches (for details, see Bomers et al., 2019).

To convert the standardized depth values provided by the registers (below MR; Fig. 4.7) to the current vertical datum (above NAP, in which 0 m is approximately mean sea level), I traced the original calculation of MR, which I found in the results of the first national levelling campaign (see Appendix). This source provides values for both MR and AP (precursor of NAP) at multiple water level measurement stations ('peilschalen') along the river branches, which allowed me to convert between the two vertical measurement systems (see Appendix). Because AP is a horizontal surface similar to NAP, while MR is a river water surface consisting of a series of inclined slopes, I linearly interpolated along the rivers (river km coordinates) between the stations where both MR and AP levels were available. With this series of steps, NAP levels were calculated for all depth values along all transects.

4.5 Additional steps and implications

In the early nineteenth century, the Rhine river branches had wider bends than in the present, and particularly the river Waal was characterized by the occurrence of islands and river bars (Fig. 4.11). This different morphology had major negative impacts on navigation and flood risk (e.g. Bosch and van de Ven, 1993; Crosato and Mosselman, 2020). The reconstruction I made forms a good representation of the river morphology between 1775 (artificial cut-off at IJssel bifurcation) and 1850 (onset of normalization), and is thus appropriate for numerical analysis of flood events in the late eighteenth and early nineteenth centuries (many large floods with the presumed largest event in 1809: Driessen, 1994; Toonen, 2015). Besides river position and bathymetry, hydraulic models require floodplain topography, including dimensions of river dikes, and floodplain roughness values. These were reconstructed from various historical data sources.

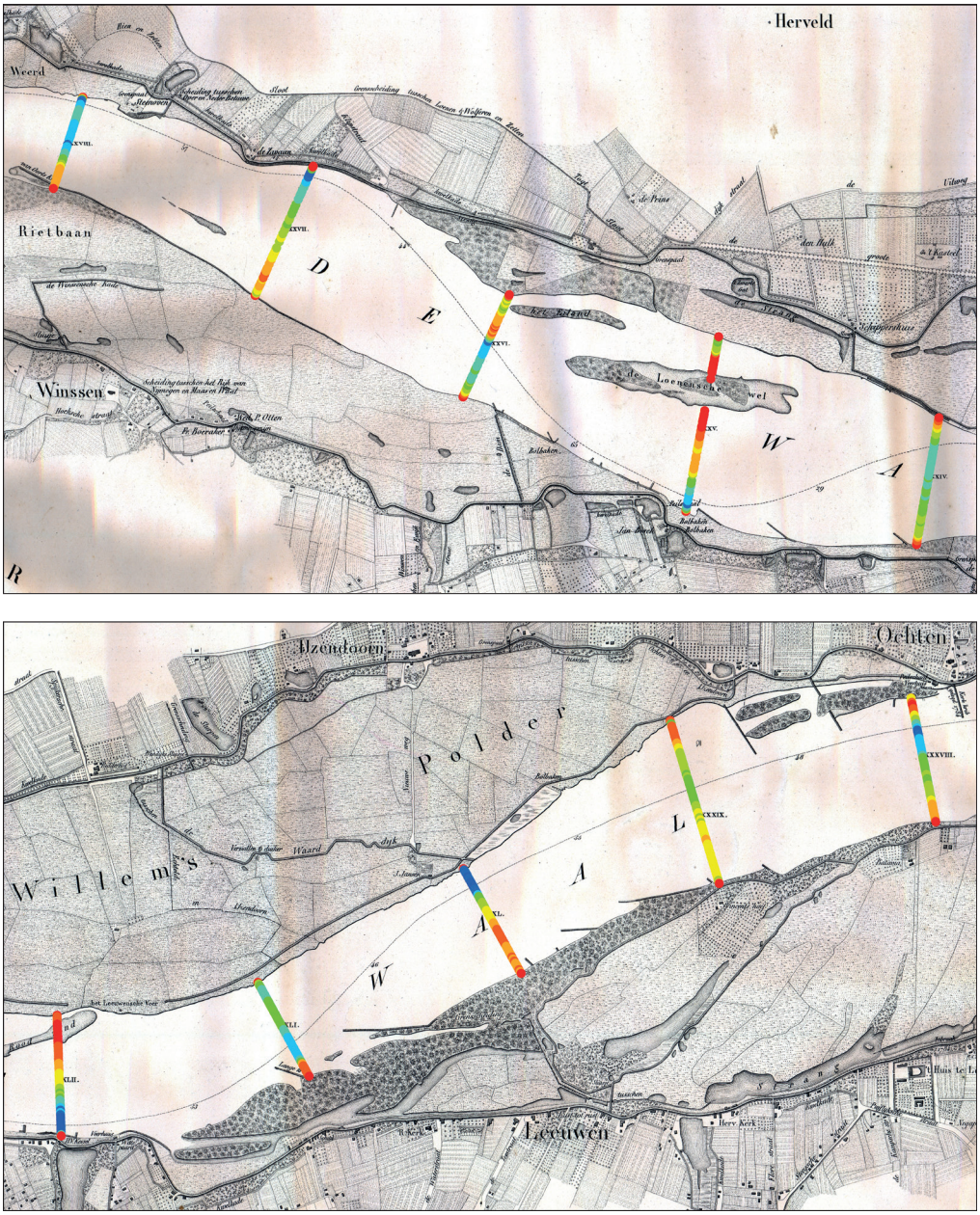

Fig. 4.11. Profiles showing nineteenth-century depth values copied from the measurement data tables in the registers (Fig. 4.7), plotted at their correct geographical locations on the georeferenced *Algemene Rivierkaart* map sheets, across the river at regular distance intervals of 1 km. Blue-green-yellow-orange-red points indicate deep to shallow measurement values. Above: Waal river between Rhine km 892 and 896 (map sheet Herveld). Below: Waal river between Rhine km 906 and 910 (map sheet Leeuwen).

For the topography of both the river-bordering ('uiterwaard') and protected (polder) areas, I used a collection of elevation measurements obtained between 1950 and 1965. As this period predates major anthropogenic changes such as land levelling for agricultural practices and the construction of highway embankments, these elevations approximate the early nineteenth-century topography (Hesselink et al., 2003; Alkema and Middelkoop, 2005). The point data were converted into a digital elevation model (DEM) by simple point-to-raster conversion in ArcGIS, with a relatively large cell size of 500 × 500 m to smooth out potential inaccuracies in the historic data (Fig. 4.12).

For the river dikes, I again used the first edition of the *Algemene Rivierkaart*, complemented with the first edition of the *Waterstaatskaart* ('Water Management Map'). From the georeferenced *Algemene Rivierkaart* map sheets, dike locations were reconstructed as vector lines in ArcMap. These locations have remained largely unchanged up to the present (Fig. 4.12). The first edition of the *Waterstaatskaart* map series dates to the late nineteenth century and covers the entire Netherlands at a scale of 1:50,000 (Heere and Storms, 2002; Blauw, 2005). The map sheets that cover the study area, produced between 1871 and 1879, provide information on dike heights. These were on average about 1 m lower than present values. The nineteenth-century heights were put into ArcGIS and used for linear interpolation along the reconstructed dike vector lines.

To supply the hydraulic model with historic roughness values, I obtained land use reconstructions based on early (circa 1900) topographic maps of the Netherlands (Knol et al., 2004). The land use classes provided by these maps were converted into Manning's roughness coefficients (for details, see Bomers et al., 2019). The underlying assumption (the land use situations around 1800 and around 1900 are comparable) is fair, as the largest changes to land use in the study area occurred in early historic times, when the entire area was taken into agricultural use, and in the twentieth century, when cities and road networks expanded. Especially areas that have been converted into residential locations in the past century have higher roughness values in the reconstructed situation than in the present.

The assembly of results provides a complete landscape reconstruction for the upper and central parts of the Rhine delta in the nineteenth century. Compared to the present situation, the reconstructed landscape shows a semi-natural river morphology and a considerably 'softer' floodplain terrain, without large pits and highway embankments (Fig. 4.12). The results are particularly detailed for the river channels (positions, widths, bathymetries), which makes the reconstruction especially suitable for the envisioned purpose of hydraulic simulations. Further potential applications of the historic bathemetry with absolute elevations are in the fields of ecology, including river and floodplain rehabilitation studies (e.g. Nienhuis et al., 2002), and engineering, including channel incision studies relevant to navigability and river management (e.g. Ylla Arbós et al., 2021).

Acknowledgements

For help with locating data and many stimulating discussions on historical cartography, I thank Marco van Egmond, Bram Vannieuwenhuyze, Willem Overmars, Menne Kosian, and Maarten Kleinhans. This work would not have been possible without the data processing support (digitizing tables, vectorising map features) and technical assistance (scripting in Python and MATLAB) of Tessa Deggeller, Silke Meijdam, Lisanne Braat, and Yorick Fredrix.

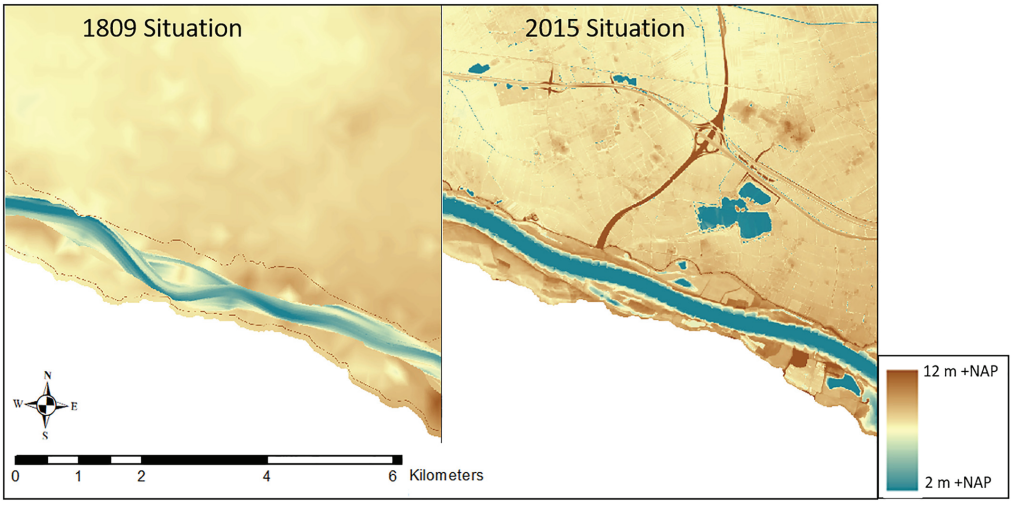

Fig. 4.12. Details of reconstructed and present terrain (topography, dikes, bathymetry) along the Waal between Rhine km 888 and 897 (as depicted in Bomers et al., 2019).

Chapter 5

Digital Elevation Model reconstruction

this chapter is based on

van der Meulen, B., Cohen, K.M., Pierik, H.J., Zinsmeister, J.J., Middelkoop, H., 2020. LiDAR-derived high-resolution palaeo-DEM construction workflow and application to the early medieval Lower Rhine valley and upper delta. Geomorphology 370, 107370. DOI:10.1016/j.geomorph.2020.107370

'The universe,' said Arthur, 'is big enough and old enough to look after itself for half an hour.'

Douglas Adams – Life, the Universe and Everything (1982)

Abstract

Reconstruction of past topography in palaeo-DEMs serves various geomorphological analyses. Constructing a palaeo-DEM by stripping young elements from a LiDAR DEM can provide results for large study areas at high resolution. However, such a 'top-down' approach is more suited to recent periods and geomorphologically static parts of the landscape than to geomorphologically dynamic areas and periods farther back in time. Here, we explore this approach by reconstructing the early medieval (circa 800 CE) topography of the Lower Rhine river valley and upper delta in Germany and the Netherlands. The large (~4,500 km^2) study area contains abundant anthropogenic terrain modification and stretches across geomorphologically active as well as inactive zones. We first removed all anthropogenic relief elements from the LiDAR DEM, using separate procedures for linear and non-linear elements. These steps were sufficient to obtain the palaeotopography of the inactive zone, characterized by inherited natural relief. Then, we reconstructed the topography and bathymetry in the fluvially-reworked active zone by incorporating geological and historical geographical information. We present and evaluate zonal averages of elevation differences between the modern and past valley floor topography in this densely populated area with complex land-use history, which allows us to approximate total anthropogenic volumetric change. Further comparisons with the modern LiDAR DEM indicate large changes in floodplain negative-relief connectivity, demonstrating the importance of palaeo-DEMs for research into past river floods. Our palaeo-DEM construction workflow is deployable at diverse spatial scales and widely applicable to other lowland areas, because of its top-down and generic nature. The relative importance of different workflow aspects depends on the time period that is targeted. Beyond a target age of 10–15 ka, large valley floors are considered geomorphologically dynamic and a top-down approach to palaeo-DEM construction is no longer advisable.

5.1 Introduction

The geomorphology of many parts of the world has been altered by humans (Tarolli and Sofia, 2016; Brown et al., 2017). For this reason, a Digital Elevation Model (DEM), even with non-ground points such as buildings and canopies filtered out, for a typical inhabited area does not represent a natural state of the topography. This is especially true for lowland river areas, which often are densely occupied, with long histories of human modifications to the terrain, and lose natural relief quickly because of modest elevation differences (Lewin and Ashworth, 2014). The present topography, altered by human as well as fluvial activity, is not readily applicable in quantitative analyses of past landscapes and landscape processes. Instead, such analyses require a palaeo-DEM that represents the topography of a historical or natural situation.

The need for palaeo-DEMs is widespread across geomorphological studies focusing on reconstruction or modelling, on both short (<10^3 yr) and longer (>10^3 yr) time scales, and at a variety of spatial scales. At a regional scale, palaeo-DEMs help to understand the historical and geomorphological evolution of an area (Werbrouck et al., 2011; Vermeer et al., 2014; Pierik et al., 2017; Briant et al., 2018; Pierik and van Lanen, 2019), and aid in landscape-archaeological regional inventories and archaeological modelling (Cohen et al., 2017; van Lanen et al., 2018; van Lanen and Pierik, 2019; Willmes et al., 2020). At a local scale, palaeo-DEMs are key to identify past natural and artificial drainage network elements (Baubiniene et al., 2015; Kirchner et al., 2017; Schmidt et al., 2018), and to map the geomorphological contexts of early settlements and urban

centres (Schneider et al., 2017; Mozzi et al., 2018; Grimm and Heinrich, 2019; Pröschel and Lehmkuhl, 2019). Further, lowland palaeo-DEMs are essential in numerical simulations of past extreme flood events such as tsunamis (Röbke et al., 2016; Wronna et al., 2017) and large river floods (Hesselink et al., 2003), although recent river-flood palaeohydrological research so far has relied on one-dimensional cross-sectional analyses (Herget and Meurs, 2010; Toonen et al., 2013; Herget et al., 2014; Benito and Díez-Herrero, 2015).

Two contrasting approaches exist for constructing a palaeo-DEM (Fig. 5.1). The first is to reconstruct the past terrain 'bottom-up' from interpolating point observations on sedimentary surfaces derived from geological, pedological, and archaeological data (e.g. Kirchner et al., 2017). The second is to reconstruct the past terrain 'top-down' from a modern DEM, removing young relief elements and interpolating the resulting voids to obtain the past topography (e.g. Schmidt et al., 2018). Often, a combination is used (e.g. Pierik et al., 2017). The bottom-up approach demands specific data, such as sedimentary profiles with good age constraints, and is sensitive to differences in observation density and quality across the study area. It is primarily useful for small areas (<1 to 10s km^2) where sufficient data are available to achieve the resolution and accuracy needed for the palaeo-DEM application in mind. A key benefit of the top-down approach is that the required data are often regionally collected and publicly available, most notably a LiDAR ground level DEM and digital datasets of infrastructure and land use. For this reason, the top-down approach is the more suitable method for reconstructions of larger areas (>10s km^2). Only a few studies have provided a generic workflow to construct palaeo-DEMs (Werbrouck et al., 2011; Vermeer et al., 2014; Pierik et al., 2017; Schmidt et al., 2018) and, so far, limits and trade-offs concerning the resolution and temporal reach of different approaches have not been evaluated.

The aim of our study was to develop a workflow for palaeo-DEM construction and apply this to reconstruct the early historic topography (target age circa 800 CE) along the Lower Rhine at high spatial resolution (50 × 50 m) to be useful in mapping and modelling applications in fluvial geomorphology and palaeohydrology. The target age of the palaeo-DEM shortly predates the onset

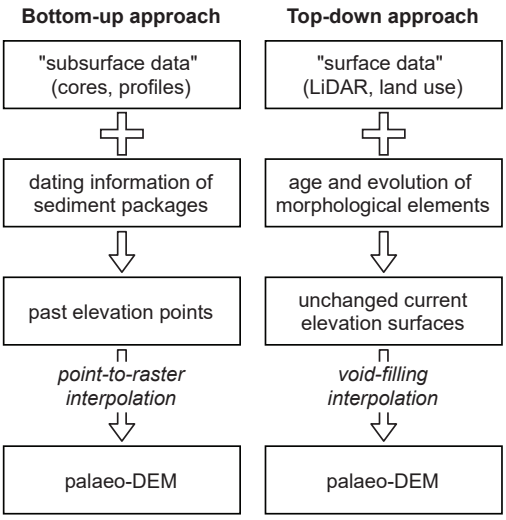

Fig. 5.1. Workflow outlines for two main takes on palaeo-DEM construction, contrasting the 'bottom-up' and 'top-down' approaches.

of river dike construction in the Rhine delta. Because river dikes were the first major anthropogenic relief elements in the study area, the period around 800 CE represents a last semi-natural state of the river and floodplain without direct human modifications. This implies that elevations differences with the present siutation provide volumetric quantifications of medieval-to-modern net anthropogenic topographic changes. Presenting results on this was a secondary aim of the study, partly because it is a way to evaluate the quality of the palaeo-DEM.

The study area covers the full width of the Lower Rhine valley and upper delta. This large lowland region is an excellent case for exploring and evaluating large-area high-resolution palaeo-DEM construction for three reasons. First, the area contains many anthropogenic modifications to the terrain. Second, there are geomorphologically dissimilar zones, with and without fluvial activity since the target age of the palaeo-DEM. Third, abundant data are available from multiple disciplines on for example floodplain ages (e.g. Klostermann, 1992; Erkens et al., 2011; Cohen et al., 2012) and past river positions (e.g. Hoppe, 1970), which are of use in the reconstruction.

We describe the workflow for palaeo-DEM construction in detail, highlighting the generic aspects of each step. The workflow is a dominantly top-down approach, based on LiDAR DEM adaption rather than geological methods. The most important steps concern stripping anthropogenic features, i.e. reconstruction by removal and subsequent void-interpolation. Additional steps account for fluvial processes that have affected the topography, after demarcating the zone within which the river laterally migrated and cut off meander bends since the target age. Our workflow, consisting of both automated and manual steps, is applicable to lowland settings at different spatial scales and resolutions. We first show how we applied the workflow to the Lower Rhine study area and then analyse the resulting palaeo-DEM on aspects relating to human and fluvial activity as well as the role of the floodplain in the fluvial system. Next, we evaluate the workflow and the implications of our choices on the accuracy of the palaeo-DEM. We end with a discussion of the wider applicability of the workflow and provide a detailed framework for adjusting the workflow to different, earlier or later, time periods.

5.2 Study area

The study area of approximately 4,500 km^2 covers the Lower Rhine valley and upper delta in Germany and the Netherlands (Fig. 5.2). The area has been a strategic barrier and corridor for millennia. It functioned as the border for the Roman Empire between circa 50 BCE and 450 CE, for the Carolingian Empire after 843 CE, and on and off in all historic periods since then including WWII (e.g. Begbie and Roberts, 2014). The crossings of the 'barrier' of the Rhine by warring parties, whether for the purpose of military conquest or retaliation, are repeatedly mentioned in historical accounts ever since the Gallic wars of Julius Caesar around 50 BCE (e.g. Breeze et al., 2018), and are part of the narrative of the Unesco heritage status nomination (Polak et al., 2019) for the Roman military border infrastructure archaeological legacy. The Rhine valley was a transportation corridor to humans in prehistory and history alike. Neolithic agriculture and the tribes that introduced it spread into the study area along the Lower Rhine (Louwe Kooijmans, 2007; Denis et al., 2019). Roman-age military patrolling roads and forts guarded the Rhine as a shipping route (Polak et al., 2019 and abundant sources therein). Early and high medieval land and river trade (notably at Duisburg; Krause, 1997, Krause, 1999, Krause, 2003) continued to use the existing routes (e.g. van Lanen et al., 2016). Medieval tolling privileges were manifold, such as

fourteenth-century Guelders Lobith/Tolkamer and Cleves Griethausen at the later Dutch-German border (Overmars, 2020), when river trade became managed by the Hanseatic league.

The population density of the study area is high and the land use in the Lower Rhine valley and upper delta plain today is a complex patchwork characterized by industry, intensive farming, and dense urbanization. Consequently, the area features abundant anthropogenic modifications to the pre-industrial topography and original natural geomorphology of the valley floor (active and abandoned meandering channels, variable floodplain topography, flood-free terraces). Positive anthropogenic relief is formed by dikes, embankments for highways and railroads, mining and waste dump sites, and other raised grounds. Negative anthropogenic relief is formed by clay and gravel quarries and pits, harbours, and other dug features. Particular forms of human-induced negative relief area are coal mining-related subsidence bowls that developed during the twentieth century (e.g. Harnischmacher and Zepp, 2014).

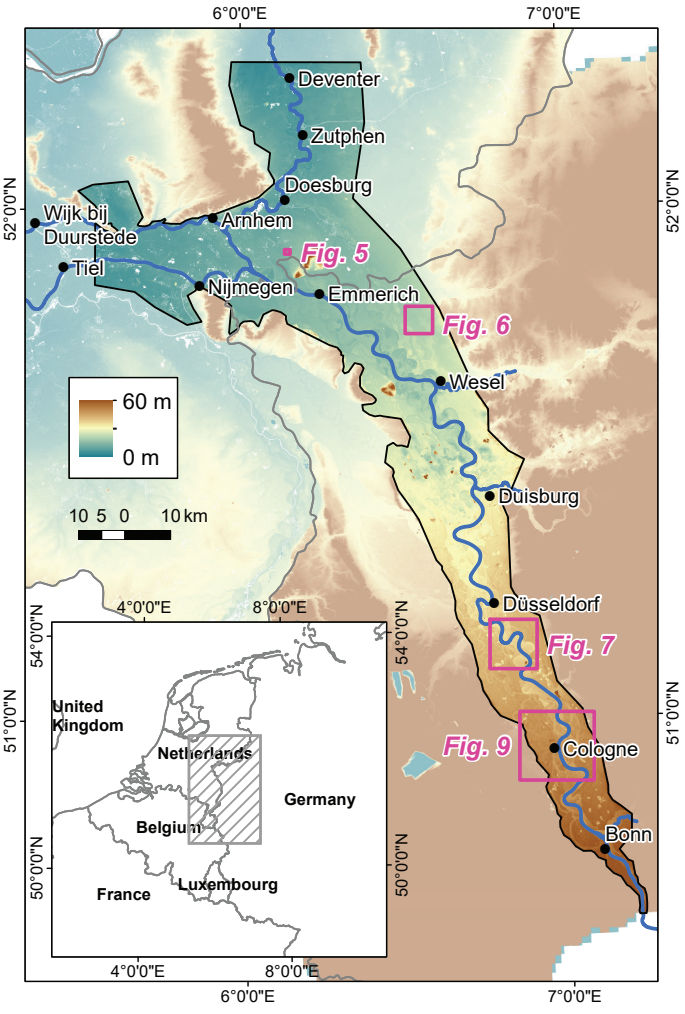

Fig. 5.2. Extent of the study area covering ~4,500 km^2 in North Rhine-Westphalia (Germany) and the Netherlands. Background is the LiDAR ground level DEM (DGM1-BrK, 2017; AHN2-RWS, 2013) as merged for the two countries (as merged for the two countries (resolution: 1 × 1 m original download; 5 × 5 m processing; 50 × 50 m post-processing and foreseen usage).

The axial zone of the study area is occupied by the Lower Rhine, which was a freely meandering river up to historic times, when it became increasingly human-modified. In the nineteenth century, extensive river training measures were carried out that confined the flow and halted lateral migration along the entire river course (Kalweit et al., 1993). In the north of the study area, close to the German-Dutch border, the Lower Rhine valley floodplain grades into the Rhine delta plain (Klostermann, 1992; Erkens et al., 2011). Here, the Lower Rhine bifurcates into the distributaries Waal and Nederrijn (Fig. 5.2). The history of the delta apex is well known from earlier geological, sedimentological, and historical work, including studies focusing on past oscillations in channel sizes and related discharge division (van de Ven, 1976; Kleinhans et al., 2011). At present, discharge partitioning between the river branches Waal and Nederrijn is 2:1 and engineering-controlled. Partitioning before 1500 CE was in favour of the Nederrijn (>50%), indicated by first millennium CE meander morphology, geoarchaeological finds, and classic historical accounts (e.g. Verhagen et al., 2017). Near the city of Arnhem, a second bifurcation results in the Gelderse IJssel distributary (Fig. 5.2). This northward river branch began avulsing between 600 and 800 CE and reached a full size between 1100 and 1500 CE (Makaske et al., 2008; Groothedde, 2010; Cohen et al., 2012).

The upstream boundary of the study area is placed 15 km upstream of the city of Bonn, where the Rhine river leaves the bedrock-confined zone of the Middle Rhine and enters the alluvial reaches of the Lower Rhine valley (Klostermann, 1992; Erkens et al., 2011). The downstream boundaries are placed at the transition of the upper delta plain to the lower delta plain, where river flow and water levels come within reach of tidal influence (e.g. Berendsen and Stouthamer, 2001; Gouw and Erkens, 2007). The lateral boundaries of the study area are placed at the flanks of Middle Pleistocene (Saalian) landforms. In the upstream part of the study area, these are the lowest middle terraces (cf. Klostermann, 1992); in the downstream part, these are ice-pushed ridges and glacio-fluvial outwash landforms. The lateral boundaries define a maximum floodplain extent that, from the river channel outwards, includes the modern floodplain, all former Holocene floodplains and channels, and the surfaces of Late Pleistocene terraces (Fig. 5.2).

5.3 Materials

Here, we declare the various materials incorporated and otherwise made use of in the palaeo-DEM construction (Fig. 5.3; Table 5.1). We started with airborne LiDAR data of North Rhine-Westphalia (DGM1, available as open data since 2017) and the Netherlands (AHN2, available as open data since 2013), in which buildings and vegetation are filtered out so that grid-cell values represent the ground surface. Together, these data products provided land surface elevations over the full study area (Fig. 5.2). The bathymetry of the river bed was obtained from survey data of river managing authorities (part of the RWS-LANUV Baseline dataset). Further, we obtained a dataset of elevation changes in the Ruhr area, based on historical survey data from nineteenth-century topographic maps (Harnischmacher and Zepp, 2010; 2014). The six western-most map sheet tiles of this dataset overlap with our study area. Relatively accurate results were obtained for this subarea of near-horizontal valley floor (regional gradient = 0.2–0.3 m/km; e.g. Erkens et al., 2011; Toonen et al., 2013), where the error associated with nineteenth-century contour mapping is regarded <<1 m (Harnischmacher and Zepp, 2014; their Fig. 5.3). From these elevation data, we isolated depressions caused by underground coal-mining to correct for the related subsidence. The above datasets, after some merging, resampling, and warping operations (Section 5.4.1) allowed us to prepare an input DEM at 5 × 5 m processing resolution.

Next, we incorporated land-use datasets identifying anthropogenic elements to supply the workflow steps that strip these features from the LiDAR data. We mainly used OpenStreetMap, since this dataset is in vector format and one of the few high-resolution datasets that covers more than a single country, and uses nearly consistent feature attributes across nation boundaries. Initial tests and visual inspections confirmed that this volunteer-generated open dataset is accurate in our study area for the infrastructure features targeted within the dataset. River dike positions in vector format were supplied from the previously mentioned Baseline dataset that provides these in a consistent format at both sides of the border, and supplemented with dike elements from the digital geomorphological map of the Netherlands (Koomen and Maas, 2004). Further, we used satellite and aerial imagery for visual reference in the identification of anthropogenic landforms.

Last, we incorporated data from different disciplines providing information on the development of the Rhine river (Fig. 5.3; Table 5.1). These allowed us to identify the zone within which the river has migrated in the last 500 years (historic maps), 500–1000 years (medieval settlements and written descriptions including position and dates for bend cut-offs), 1000–1500 years (geoarchaeology, scarce older descriptions, some radiocarbon dating), 1500–2000 years (archaeology, few classic roman texts, some radiocarbon dating), and so on (some archaeology, mostly geomorphology, pedology, and Quaternary geology). This constrained and informed the palaeo-DEM construction workflow for the active zone: the part of the study area where the landscape has been reworked by natural processes (besides human activity) since the target age. Given the extent of the study area, the developed state of prior research, and the volumes of potential raw data to be incorporated, we used earlier-compiled map datasets as starting points rather than primary observational data consisting of individual point observations. For example, Klostermann (1992) and Cohen et al. (2012) provide referenced ages for individual meander segments with superregional coverage. These enabled us to digitally select the active meandering zone for a given time period in order to demarcate the active zone, with geological-geomorphological studies of sub-regional coverage providing further detail (references 4–8 in Table 5.1). Many datasets were created before the availability of LiDAR DEM data. This meant that using them required some re-digitizing to improve the accuracy of digital mapping of floodplain-edge scarps. Within the active zone, by definition and implication, direct superficial geomorphological features of target-age river channel positions are lost to younger reworking. Still, historical, historical geographical, and archaeological studies (references 21–32 in Table 5.1) provided sufficient information to address past positions of the river channels, either by inference from archaeological data or by interpretations of historical written information (e.g. first settled ages, settlement abandonment dates, meander cut-off years and locations).

5.4 Methods

5.4.1 Preparing the input DEM

As first steps, preceding palaeo-DEM construction, we merged the LiDAR data (AHN2: 0.5 × 0.5 m resolution in the Netherlands National Grid; DGM1: 1 × 1 m resolution resampled from the German to the Netherlands Grid) and inserted the RWS-LANUV Baseline channel bathymetry. We then clipped this assemblage to the study area. One region within the area is affected by underground mining-caused subsidence, so we pre-treated the LiDAR DEM for this subarea before starting the generic workflow deployed along the entire valley. From the grid of elevation

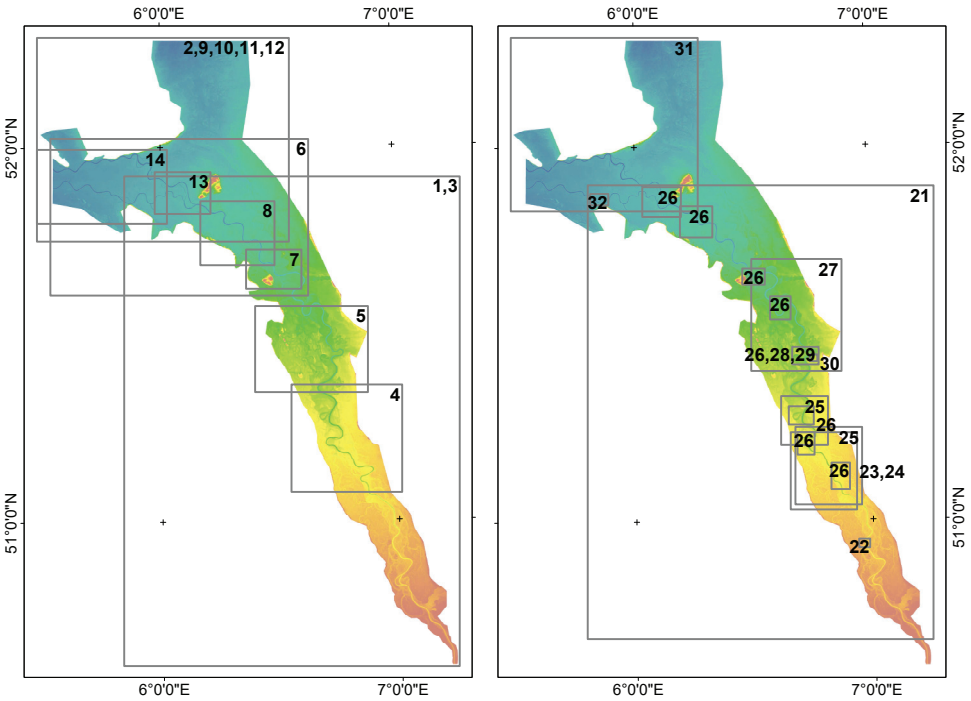

Fig. 5.3. Overview of materials, with spatial extents indicated by rectangles, depicted on the input DEM. The left panel shows geological-geomorphological information sources (numbered 1–14) and the right archaeological and historical sources (numbered 21–32). Not indicated are starting-point resources covering the complete study area (satellite imagery, OpenStreetMap vector data, RWS-LANUV Baseline vector data). The sources are referenced in Table 5.1.

Table 5.1. References of materials used. Spatial extents are indicated in Fig. 5.3.

A. Geology and geomorphology		**B. Archaeology and historical geography**	
No.	Reference	No.	Reference
1	DGM1-BzK, 2017	21	Schneider, 1886
2	AHN2-RWS, 2013	22	Höltken and Wagner, 2014
3	Klostermann, 1992; Erkens et al., 2011	23	Straßer, 1989
4	Zhou, 2000	24	Gerlach, 2006
5	Shala, 2001	25	Scheller, 1965
6	Toonen, 2013	26	Hoppe, 1970
7	Klostermann, 1986	27	Harnischmacher and Zepp, 2010–2014
8	Heine and Siebertz, 1980	28	Scheller, 1957; Krause, 1997–2003; Meurers-Balke et al., 1999
9	Berendsen and Stouthamer, 2001	29	Bechert, 2007
10	Koomen and Maas, 2004	30	Gerlach, 2003
11	Cohen et al., 2012	31	Cohen et al., 2014
12	Cohen et al., 2017	32	Heunks and van Hemmen, 2016; Willemse, 2019
13	Kleinhans et al., 2011		
14	Pierik et al., 2017		

differences between nineteenth-century and modern elevations (Harnischmacher and Zepp, 2010), we selected all cells with negative elevation change and made further masking deselections (harbour canal linear elements, surficial aggregate-mining pits) to isolate bowl-shaped depressions in areas with otherwise unaltered relief (e.g. on map sheet Rheinberg 4405: 1–2 km in diameter, up to 6 m subsidence in the centre, near 0 m at the edges). We deployed void-fill techniques to interpolate the subsidence patterns in deselected areas, applied a low-pass smoothing filter, and used the result as a warping grid to bring depressed areas in the merged LiDAR+bathymetry DEM to a representative present elevation. This provided the input DEM used as the starting point of our palaeo-DEM construction workflow (Fig. 5.4). We down-sampled the input DEM to a resolution of 5x5 m for further processing to ensure lower digital data storage and computational demands, and lower accuracy demands on the different vector datasets used to demarcate the active zone and strip anthropogenic features.

5.4.2 Demarcating the inactive and active zones

A key step in the workflow is to distinguish a geomorphologically inactive distal floodplain zone and a geomorphologically active fluvially-reworked zone. To demarcate these zones, the workflow requires a decision on the palaeo-DEM target age. Specific age information is not required in the first steps of the workflow, encompassing the stripping of anthropogenic features (Section 5.4.3), but is again required for positioning the target-age river channel in the active zone (Section 5.4.4).

In the inactive zone, by definition and implication, the terrain surface is defined by anthropogenic topographic signatures superimposed on the relief inherited from times before the palaeo-DEM target age. In our valley-floor setting, quasi-natural processes such as superficial net erosion on tilled fields and net sedimentation owing to occasional larger floods (when embankments were overtopped) are very modest over most of the gently sloping valley floor and upper delta plain (hence the label 'inactive'), and vertically much smaller than the anthropogenic overprints that we target to remove. The active zone, on the other hand, is characterized by abundant natural and quasi-natural geomorphic processes that have continued to alter the relief in recent times. Here, the natural terrain surface has been shaped by erosion and sedimentation processes since the target age. Human influence has also played a major role in modifying the terrain in the active zone, but recent fluvial activity dominates. Creating a palaeo-DEM for the active zone thus requires additional reconstruction steps compared to the inactive zone, where stripping all anthropogenic elements from the LiDAR DEM provides a good representation of the early historic geomorphology. Thus, 'top-down' stripping methods (Fig. 5.4: upper part) suffice to transform the input DEM starting point to the palaeo-DEM end product in the inactive zone, whereas additional methods for restoration (Fig. 5.4: lower part) are required in the active zone.

We demarcated the active zone from the inactive zone by querying existing geological mapping data products to obtain the areas considered geologically younger than the palaeo-DEM target age. In this way, we selected a ribbon-shaped polygon representing the post-800 CE channel belt of the Rhine, i.e. the zone of meander migration activity. Overview maps of the area typically identify a Late Holocene channel belt (e.g. Klostermann, 1992), and local geological and historical geographical studies (various sources in Table 5.1) provide abandonment ages for individual meanders based on radiocarbon dating, historical sources, and cross-cutting relationships. Dating accuracy for individual meanders in the common era along the Rhine is quite good, owing to

archaeological attention to the Roman occupation (50 BCE to 450 CE) of the left bank of the Lower Rhine. The accuracy is 'to the year' in the best cases (back to the fourteenth century CE), to ±100 years in most cases, and to ±200 years in the poorest age-control cases. To further improve the demarcation of the active zone, we confronted the applied geological data products with the LiDAR imagery. This revealed feature-boundary mapping inaccuracies locally exceeding 50 m where data products had been created prior to LiDAR availability. For this reason, we updated the initial zone polygon outlines to match morphological scarps more closely (within 5 m). At locations where anthropogenic landforms overlie scarps delimiting the active zone, it was enlarged to fully include the anthropogenic form.

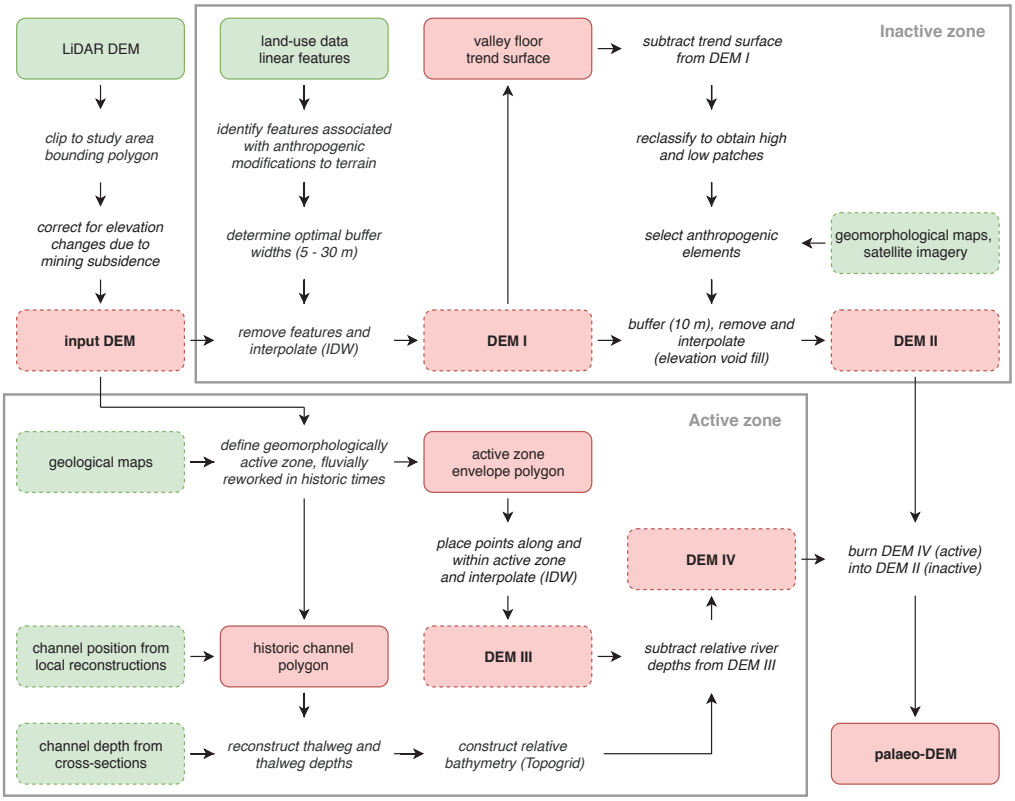

Fig. 5.4. Workflow for valley-floor palaeo-DEM construction using a dominantly top-down approach. The upper part of the workflow depicts the steps for removing anthropogenic features, with the resulting DEM II sufficing for the geomorphologically inactive areas. The lower part of the workflow depicts the additional steps for restoring the terrain in the geomorphologically active areas characterized by younger-than-target age river meandering activity besides anthropogenic overprints. Data products are shown in coloured boxes. Operations are shown in italics. Input products are shown in green, with dashed borders indicating non-essential input used indirectly as guidance. Output products are shown in red, with dashed borders indicating intermediate output.

5.4.3 DEM stripping

We deployed a two-step method to remove all anthropogenic elements larger than 50 m as well as most smaller elements. The first step, leading to DEM I (Fig. 5.4), involved land-use datasets, from which we selected linear features associated with significant anthropogenic modifications to the terrain, such as major roads and railroads (these are commonly built on embankments; Fig. 5.5A). Then, we placed buffers around the selected elements defining the sizes of terrain modifications (Table 5.2). Buffer widths were chosen large enough to fully mask out the sloping sides of features, but at the same time as small as possible to minimise the introduction of interpolation artefacts. Determining buffer widths therefore required some scrutiny and varied per feature type. In the buffer zones (white area in Fig. 5.5B), we replaced LiDAR-derived elevations with interpolated values, applying Inverse Distance Weighting (IDW, power 2) as a simple and fast interpolation method applicable to fill small voids (e.g. Reuter et al., 2007). In general, abundant remaining LiDAR elevation data surrounded the linear removal zones. Together with the relatively small buffer widths, this data abundance explains the good results produced by the IDW interpolation (Fig. 5.5C).

The second step proceeded from DEM I, i.e. after the removal of anthropogenic features derived from land-use datasets (Fig. 5.6A; Fig. 5.6B). This step, leading to DEM II (Fig. 5.4), concerned the removal of any remaining anthropogenic relief modifications. These are of various types, ages, and dimensions, and mostly non-linear in shape, and it is difficult to select such features from existing high-resolution national-scale datasets, which tend to classify on e.g. usage, rather than on origin (natural versus anthropogenic) or age. Thus, rather than selecting these non-linear anthropogenic features by dataset queries, we manually selected them in a DEM-of-difference between DEM I and a second-order polynomial trend surface calculated over DEM I. In the calculation of this trend surface, we excluded insular areas of elevated non-floodplain terrain so that it represented the average height of the valley floor (Late Pleistocene terraces and younger valley features, i.e. the extended Holocene floodplain). We reclassified the DEM-of-difference at 0.5 m vertical intervals to obtain discrete patches of low and high grounds (Fig. 5.6C), which we

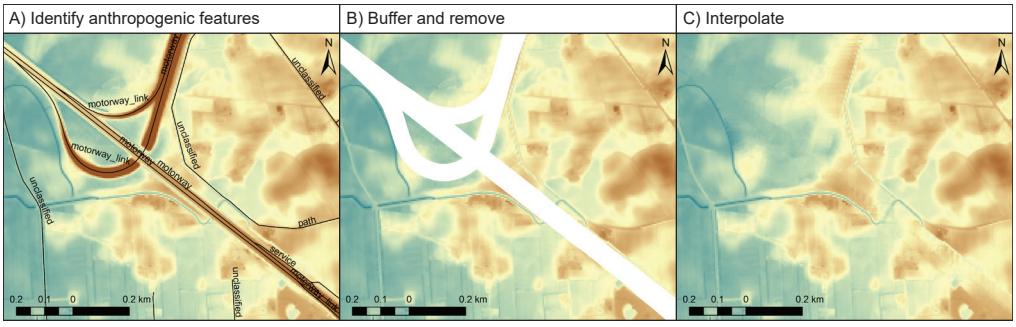

Fig. 5.5. Automated removal of highway-related elevated grounds from the LiDAR ground level DEM. Panel A shows infrastructure vector lines from OpenStreetMap. Panel B shows the applied buffers (widths specified in Table 5.2; see main text for details). Panel C shows the result. Location indicated in Fig. 5.2.

converted to polygons. These were used to manually select the 'natural' (to remain in the DEM) and anthropogenic (to strip from the DEM) elements based on geomorphological expert judgement, aided by geomorphological maps and satellite imagery (Fig. 5.6D). Location and planform morphology of low and high elements in the DEM was also taken into account as part of the judgement. For example, a rectangular shaped lake in the proximal floodplain is likely the result of quarrying (anthropogenic relief), whereas an irregular curved lake is presumably a natural feature such as a residual channel remnant (natural topography). More generally, steep slopes indicate anthropogenic influence whereas gentle and irregular slopes suggest the presence of natural phenomena. After selecting the anthropogenic elements, we placed buffers around the polygons and removed them (Fig. 5.6E). A fixed buffer width of 10 m turned out sufficient to remove identified anthropogenic features completely. For relatively large voids, IDW produces poor results. Therefore, we interpolated the resulting gaps in the DEM using the elevation void fill function in ArcGIS, generating a surface inside each void based on all its surrounding cells (Fig. 5.6F).

5.4.4 Reconstruction of topography and bathymetry in the active zone

In the active zone, constructing a palaeo-DEM requires the insertion of a restored topography and bathymetry for the target age, which replaces all younger relief (Fig. 5.7A). To achieve this, we first produced an interpolated terrain from a manually-created set of elevation points (Fig. 5.7B), and then burned in a reconstructed river channel of prescribed thalweg depths. The locations of the elevation points inside and along the boundaries of the active zone were carefully selected, incorporating geomorphological interpretation of the fluvial landforms to avoid point placement in present and former channels, and favouring areas with remaining alluvial ridge-and-swale relief. We iteratively increased point density (note density variations in Fig. 5.7B) and visualised preliminary interpolations (IDW, power 0.6) until satisfying results were obtained in the to-be-replaced active zone. This method produced a smoothed but otherwise representative palaeo-DEM (DEM III in Fig. 5.4) for lower floodplain subareas of the active zone as well as for terrace rims in places where the river eroded these in historic times (Fig. 5.7D).

Table 5.2. Buffer widths for anthropogenic linear elements used in DEM stripping.

Feature	Source	Buffer (Germany)	Buffer (Netherlands)
Highway	OpenStreetMap	30 m	30 m
Trunk road	OpenStreetMap	20 m	20 m
Primary road	OpenStreetMap	25 m	25 m
Secondary road	OpenStreetMap	20 m	10 m
Tertiary road	OpenStreetMap	5 m	5 m
Railway	OpenStreetMap	30 m	30 m
Bandijken (main river dikes)	RWS-LANUV Baseline	–	30 m
Kades (artificial levees)	RWS-LANUV Baseline	30 m	–
Hoge dijk (high dike)	Alterra GKN	–	15 m
Middelhoge dijk (medium high dike)	Alterra GKN	–	15 m
Lage dijk (low dike)	Alterra GKN	–	15 m

The last steps consisted of reconstructing the circa 800 CE river position and inserting a bathymetry representative for this target age. This reconstruction integrated data from various studies (Fig. 5.3B) that usually provided information at a detailed scale of one to a few meander bends. As Fig. 5.7C exemplifies, reconstructed channel positions reported in pre-LiDAR studies align well with residual channels and other fluvial geomorphology visible in the LiDAR DEM. To decide on palaeochannel widths and thalweg depths, we used existing geological data (thicknesses of Late Holocene channel fills; e.g. Erkens et al., 2011; Kleinhans et al. 2011; Toonen et al., 2012) and historical information (depth measurements presented on maps that predate modern river engineering and can be considered historical analogues for the river in our palaeo-DEM; e.g. Hesselink et al., 2006; van der Meulen et al., 2018; Overmars, 2020). Over river stretches in between locations allowing for explicit reconstructions, we assumed similar meander geometries and thalweg depths, i.e. gradual morphological changes.

The thalweg depth values inferred for the target age situation were 8 m, 6 m, and 7 m for respectively the undivided Lower Rhine (Late Holocene representative value), and the deltaic

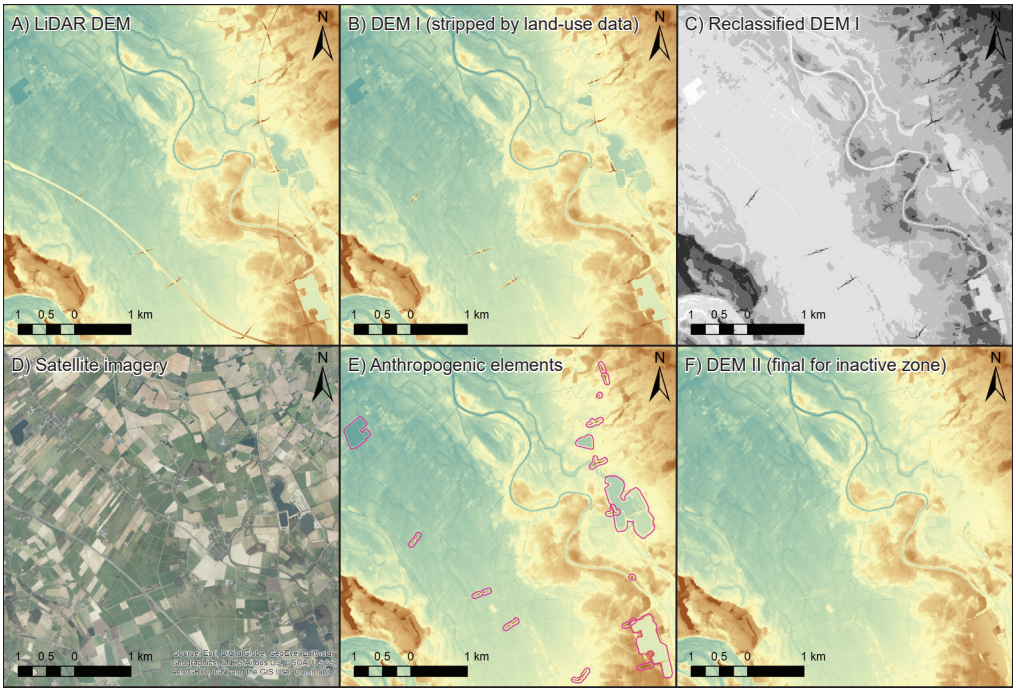

Fig. 5.6. Removal of diverse anthropogenic elements using a detrended, reclassified DEM. A) LiDAR input DEM. B) Result after stripping linear features such as major roads (DEM I in Fig. 5.4). C) Detrended, reclassified DEM I (DEM-of-difference between DEM I and trend surface; see main text for details). D) Satellite and aerial photography used for reference. E) polygons selected from the reclassified DEM, manually identified as anthropogenic elements. F) Result with selected elements of panel E removed and subsequently void-filled (DEM II in Fig. 4). Location indicated in Fig. 5.2.

branches Waal (then smaller) and Nederrijn (then larger). We attributed these depth values to thalweg lines, which we positioned close to outer bends inside the reconstructed channel polygons, and interpolated between these lines and the channel edges (depth value = 0 m) using the Topogrid algorithm (Hutchinson, 1993; Topo to Raster tool in ArcGIS). We subtracted these depths from the active zone topography and burned the result into the stripped DEM (Fig. 5.7D). The active zone of the IJssel branch is treated differently (Section 5.4.5), because at the time of the target age this third distributary was not yet a full river (Section 5.2).

5.4.5 Post-processing and preparation for method and product evaluations

The methods for the inactive and active zones described above produced a palaeo-DEM for the Lower Rhine valley and upper delta for circa 800 CE (Fig. 5.8). For the delta region, two earlier palaeo-DEM products were available, both at 100 × 100 m resolution. Pierik et al. (2017: main text) used a 'bottom-up' approach, starting from geological and archaeological borehole and find data to produce a palaeo-DEM for the levee landscape between the river branches Waal and Nederrijn for 100 CE (representative for the middle Roman period). Interpolation between this and a present surface DEM was used to derive a palaeo-DEM for 900 CE (Pierik et al., 2017: appendices), which we regarded a target equivalent to our palaeo-DEM. Along the IJssel river branch, Cohen et al. (2017) derived a palaeo-DEM product for 900 CE by combing gridded 3D shallow-geological mapping data products (GeoTOP model) with reconstructions of past natural deltaic groundwater tables (Cohen, 2005; Koster et al., 2017) that include a large active zone void (IJssel channel belt; Cohen et al., 2012). We resampled these products constructed subregionally from subsurface data to our production resolution and integrated them with where appropriate, selecting the highest elevation values to include in our palaeo-DEM. The void originating from the IJssel channel belt was filled in using the active zone method described in Section 5.4.4 and Fig. 5.7B, but without the bathymetry insertion. These solutions for the upper delta 'central' (Pierik et al., 2017) and the 'apex and IJssel' subareas are labelled as 'hybrid' methods in our tabulated results in the next section and are reported separately from the ordinary inactive zone (floodplain rim) and active zone (embanked floodplain) in the upper delta (Fig. 5.8; Table 5.3).

We resampled the final palaeo-DEM to a resolution of 50 × 50 m, in order to generate aggregated results relatively fast computationally and remove small artefacts caused by vector-to-grid conversions and interpolation procedures. We deployed Zonal Statistics and Zonal Histogram operations to summarize the elevation differences between the palaeo-DEM and the present. For these analyses, we distinguished between (1) the Lower Valley South, Lower Valley North, and Upper Delta (Fig. 5.8), (2) the inactive and active zones, (3) the non-stripped and stripped areas (linear anthropogenic features, negative anthropogenic relief, positive anthropogenic relief), and (4) the elevation differences caused by underground mining-related subsidence (changes from LiDAR DEM to input DEM; Fig. 5.4) and superficial anthropogenic relief-modifying activities (input DEM to final DEM; Fig. 5.4).

To quantitatively compare the palaeo-DEM to the present, we calculated the mean value of elevation change for each subarea zonation and the associated standard error, calculated as a sum of error contributions. The first component contributing to the error was based on the standard deviation reported in the cell statistics of the difference-DEM and calculated as $STD \times (N_{cells} - 1)^{-0.5}$, where N_{cells} is the number of cells that contributed to the difference (e.g. all subsidence-corrected

cells, all void-filled cells). The second component was the uncertainty of the LiDAR surface, set to 0.05 m at 5 × 5 resolution, and multiplied by $(M-1)^{-0.5}$ for operations where we resampled the

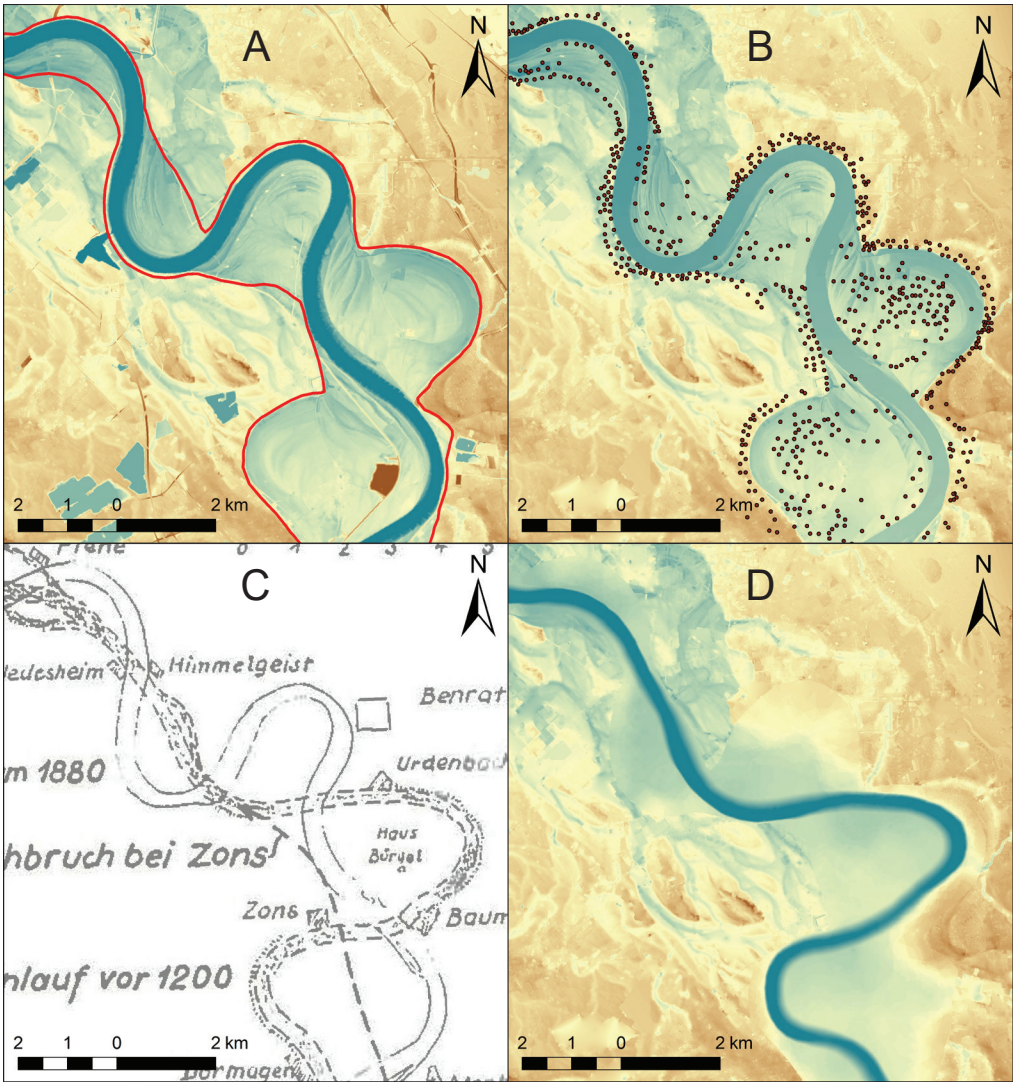

Fig. 5.7. Reconstruction of floodplain topography in the fluvially reworked area. A) Input DEM and active zone boundary for meander activity since the target age. B) Intermediate 'stripped' DEM II and manually-placed elevation points along and inside the active zone. C) Example of an earlier reconstruction showing former Rhine river positions (Scheller, 1965), used as input for target-age palaeochannel positioning. D) Final palaeo-DEM, after interpolating the points in panel B (DEM III) and inserting paleochannel bathymetry from a secondary interpolation (between channel edges and thalweg, DEM IV). Location indicated in Fig. 5.2.

raster, with M representing the number of 5 × 5 m cells. The third component was the uncertainty associated with interpolations deployed in void-filled areas and the active zone. This was set to 2 m at 5 × 5 m resolution for the cells affected, and multiplied by $(M-1)^{-0.5}$ at resampled resolutions. The reported standard errors for the subareas were calculated as the root sum of squares of the three error components. For accumulations of subareas to larger regions, we calculated area-weighted means of the standard errors. Besides elevation change, we calculated volumetric change per subarea to allow further DEM cross-comparison, propagating the errors (Table 5.3).

For a palaeohydrological-oriented evaluation of our reconstruction, we quantified connected floodplain areas in both the present LiDAR ground level DEM and the palaeo-DEM. We detrended the DEMs with the second-order polynomial trend surface created earlier and sliced the resulting rasters at vertical intervals of 0.5 m. For each interval, we identified all cells of the DEM below the slice and subsequently separated the patch of cells connected to the river. The surface area of this patch was used to approximate potential inundation in the two situations. For this analysis, we reused the trend surface created in the workflow to detect positive and negative anthropogenic relief. As this trend surface was fitted on the extended floodplain, excluding island remnants of Middle Pleistocene elevated terrain and linear elements of anthropogenic origin (Section 5.4.3), it serves as a first-order approximation of the flood water surface during the passage of a high-discharge event.

5.5 Results

Here, we compare the past and present morphology of the Lower Rhine valley and upper delta. First, we quantify the amounts of anthropogenic modifications to the terrain, (Section 5.5.1). Then, we provide simple analyses of fluvial dynamics (Section 5.5.2) and floodplain negative-relief connectivity (Section 5.5.3).

5.5.1 Elevation change and volume of anthropogenic elements

Fig. 5.8 and Table 5.3 show a tri-partitioned study area that is further subdivided based on treatment in the palaeo-DEM construction workflow. The inactive zone covers 79% of the study area (3,545 km^2) and the active zone 21% (942 km^2). In total, 707 km^2 (15.8% of surface area; Table 5.3) was removed by LiDAR DEM stripping, i.e., the first half of the workflow (Fig. 5.4). Of this area, 310 km^2 was removed as linear voids (roads, railroads, dikes), 223 km^2 as negative relief non-linear voids (digging, extracting), and 174 km^2 as positive relief non-linear voids (raising, dumping). These steps corrected topography throughout the study area with modest differences between southern and northern subzones, but more in the areas close to the river (Table 5.3: 14% of the inactive zone, 22% of the active zone), and also more in densely populated areas (Fig. 5.8: shades of grey). This is mainly because these areas host more surface modifications such as harbour complexes and have denser infrastructure networks, e.g. in and around the city of Cologne (Fig. 5.9).

In the inactive zone, DEM stripping resulted in a very minor net mean elevation change of +0.02 ± 0.09 m for the full study area (Table 5.3). This is the result of a cancelling-out effect between the southern and northern parts. In fact, the Lower Valley South ('Cologne') shows a net removal (negative elevation change) of –0.10 ± 0.05 m, whereas the central parts of the Upper Delta plain ('Betuwe') show a net accumulation (positive elevation change) of +0.23 ± 0.05 m. The latter is

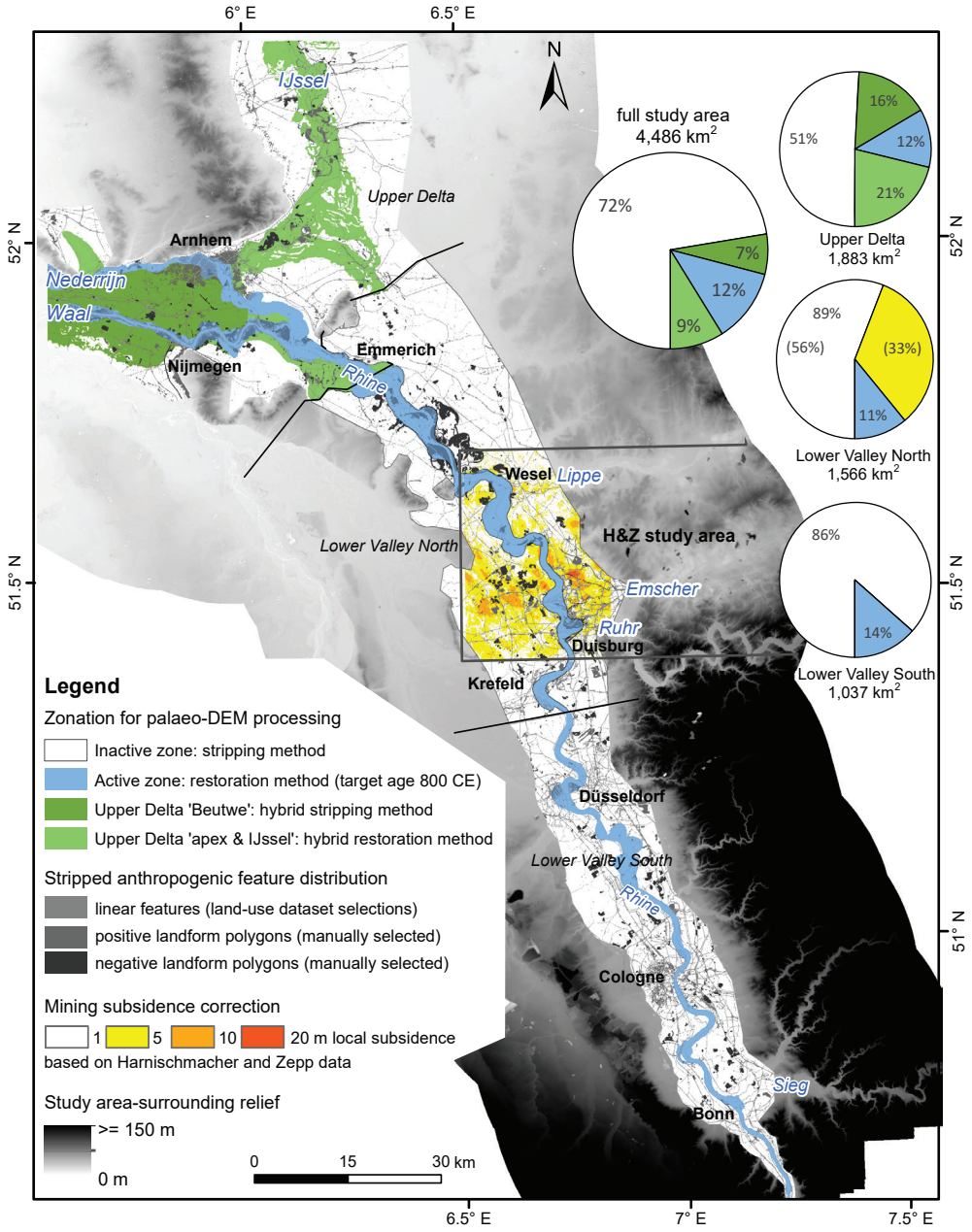

Fig. 5.8. Evaluation of elevation differences between the present DEM and the palaeo-DEM, executed at 50 × 50 m resolution. The map shows subzones as used in Table 5.3 and inset charts. White: inactive zone. Blue: active zone. Green: upper delta 'central' and 'IJssel' subzones (hybrid methods deployed; see main text for details). Shades of grey: stripped features. Shades of yellow–orange: subsidence caused by underground mining in area overlapping the Harnischmacher and Zepp (2010; 2014) dataset.

Table 5.3. Regionally-summarized differences between the present and the palaeo-DEM.

Study area subdivision ('zonation')	Surface area		Void-filled subarea		Elevation difference *		Cell-based statistics at 50 x 50 m				Volumetric change *		Interpretative remarks
	Sum (km^2)	% total	Sum (km^2)	% subarea	Mean (m)	STE (m)	STD (m)	MIN (m)	MAX (m)	# cells	Sum (km^3)	STE (km^3)	[–]: palaeo-DEM above present (on average, in the zone considered) [+]: palaeo-DEM below present (on average, in the zone considered)
Full study area: modern DEM versus palaeo-DEM cross-comparison													
Inactive zone	3,545	79	503	14	0.02	0.09					0.02	0.05	
Lower Valley South ('Cologne')	897	20	180	20	–0.10	0.05	1.67	–18.9	36.0	358,501	–0.09	0.04	[–]: net removal/deepening: building activity, aggregate mining pits
Lower Valley North ('West-Ruhr')	1,394	31	198	14	(–0.66) 0.04	0.13	2.57	–31.4	73.6	556,313	0.06	–0.06	[+]: net accumulation/raising: building activity, coal mining dumps
Upper Delta plain ('floodplain rim')	958	21	78	8	0.05	0.03	0.59	–14.3	28.2	372,920	0.04	0.03	[+]: net accumulation/raising: floods and dike breaches, building activity
Upper Delta plain centre ('Betuwe')	296	7	47	16	0.23	0.05	0.90	–4.1	27.3	112,648	0.07	0.01	[+]: net accumulation/raising: floods and dike breaches, building activity
Active zone	942	21	204	22	0.32	0.42					0.07	0.13	
Lower Valley South ('Cologne')	140	3	24	17	–0.82	0.42	4.45	–13.7	33.8	56,188	–0.12	0.06	[–]: net removal/deepening: river bed erosion, river management
Lower Valley North ('West-Ruhr')	172	4	43	25	(–0.60) 0.86	0.43	3.96	–12.5	39.2	68,917	0.15	0.08	[+]: net accumulation/raising: sedimentation, harbour works Ruhrort/Duisburg
Upper Delta ('apex and IJssel')	399	9	61	15	–0.03	0.42	0.93	–11.2	31.5	149,107	–0.01	0.17	[–]: net removal/deepening: incision after IJssel avulsion
Upper Delta ('embanked floodplain')	230	5	77	33	1.23	0.43	2.96	–7.0	19.6	76,604	0.28	0.10	[+]: net accumulation/raising: sedimentation, anthropogenic raised grounds
Full study area	4,486	100			0.09	0.19					0.09	0.13	
Non-stripped area (coal-mining subs.) *	3,779	84			(–0.25) 0	0.07	1.56	–31.4	31.5	1,480,264			combination of 'West-Ruhr' subsidence and active zone interpolation net –0.25 m
Stripped and void-filled (linear features)	310	7			(0.31) 0.56	0.24	2.36	–28.9	18.7	124,106	0.17	0.07	[+]: net accumulation/raising: raised roads and dikes >> entrenched roads
Stripped and void-filled (pos. relief areas)	223	5.			(1.7) 2.0	0.58	4.30	–14.3	73.6	85,484	0.45	0.13	[+]: net accumulation/raising: urban and industrial terrains near the river, dump sites
Stripped and void-filled (neg. relief areas)	174	4			(–2.7) –2.5	0.58	3.55	–18.0	12.8	61,344	–0.43	0.10	[–]: net removal/deepening: harbours, aggregate mining near and away from the river
Stripped and void-filled (all features)	707	16			0.27	0.46	3.27	–29	74	270,934	0.19	0.10	[+]: net accumulation/raising
Lower Valley North: H&Z cross-comparison and coal mining subsidence correction													
Raw elevation difference 1892–2010 (obtained from H&Z dataset, overlaps 39% of Lower Valley North)													
Inactive + active zone	611	14			–1.49	0.21							
Inactive zone (overlap area)	516	12			–1.35	0.17	3.92	–27.0	74.4	206,506	–0.69	0.09	[–]: net removal/deepening
Active zone (overlap area)	94	2			–2.28	0.39	3.81	–12.1	38.5	37,674	–0.21	0.04	[–]: net removal/deepening
Coal mining-attributed subsidence component (elevation change in non-stripped subarea, representative for entire H&Z overlap area)													
Inactive zone (overlap area)	518	12			–1.83	0.11	2.42	–27.0	0.0	207,159	–0.95	0.06	[–]: accommodation space created since 1892
Active zone (overlap area)	94	2			–2.86	0.31	2.97	–12.1	0.0	37,695	–0.27	0.03	[–]: accommodation space created since 1892
Residual elevation change in H&Z overlap area (raw minus coal mining-attributed subsidence component) *													
Inactive + active zone	611	14			0.50	0.25							
Inactive zone (overlap area)	517	12			0.49	0.20	*calculated, not queried*				0.25	0.11	[+]: dominantly positive-relief anthropogenic landforms since 1892
Active zone (overlap area)	94	2			0.58	0.50	*calculated, not queried*				0.05	0.05	[+]: dominantly positive-relief anthropogenic landforms since 1892
Remaining part of Lower Valley North (outside H&Z overlap area, 61% of Lower Valley North) *													
Inactive + active zone	955	21			–0.10	0.25							
Inactive zone (non overlap area)	877	19			–0.22	0.22	*calculated, not queried*				–0.19	0.19	[–]: net removal/deepening
Active zone (non overlap area)	78	2			1.20	0.66	*calculated, not queried*				0.09	0.05	[+]: net accumulation/raising

* Mean elevation and volumetric change estimates are negated for coal mining-attributed subsidence affecting modern elevations in the Lower Valley North. Where applicable, raw elevation difference values are given in brackets. Note that elevation and volumetric change estimates still include substantial negative relief of surficial aggregate mining and positive relief of mining waste dumps.

attributable to sedimentation by floods besides anthropogenic sediment import. The determination of mean elevation change for the middle part of the study area ('West-Ruhr') is more complex, due to the mining-related subsidence component. Raw quantification suggests a net lowering of –0.66 ± 0.13 m over the full Lower Valley North (1,394 km^2). This value is to –1.35 ± 0.17 m for the 'West-Ruhr' industrial subarea (516 km^2) where our study area overlaps the dataset of Harnischmacher and Zepp (2010; 2014).

Based on the difference between the LiDAR DEM and the subsidence-corrected input DEM (Fig. 5.4), and on our areal subdivisions in 'natural' (not stripped) and modified topography, we split the subsidence (sampled in the natural area and held representative for any neighbouring stripped areas) from the total elevation change. This yields a minor net change of +0.04 ± 0.13 m in the inactive zone of the Lower Valley North (+0.49 ± 0.20 m in the subsidence-affected area, cancelled out by –0.22 ± 0.22 m in the remainder of the Lower Valley North). The subsidence-attributed component is separated in the tabulated results (Table 5.3) to allow for comparisons of mean elevation changes resulting from direct anthropogenic modifications to the topography. Being able to separate human-induced subsidence from direct human modifications to the terrain ratifies our choice to correct for mining-related subsidence before further reconstruction. In addition, it illustrates one of the advantages of having clearly defined steps and intermediate output in the workflow (Fig. 5.4).

All in all, the inactive zone shows a modest loss of relative elevation since early medieval times in the southern Lower Rhine valley (urbanized terraced valley floor), lots of activity and complications of subsidence but near-zero net change in the middle reaches (urbanized and industrialized valley floor), and a modest gain in the downstream deltaic reaches (flooding-protected urbanized upper delta plain). This result is in line with general expectations when evaluating mean values of anthropogenic change between a palaeo-DEM and a present-day DEM over very large areas of river valley, as throughout history many of the bulk resources to raise terrains were obtained from within the valley floor. This is best illustrated by the volumetric break-down of elevation change to the zonations of the DEM-stripping steps. Cells representing positive-relief anthropogenic landforms total 0.45 ± 0.13 km^3 above the void-filled palaeo-DEM surfaces, and linear features (raised roads, dikes) add another 0.17 ± 0.07 km^3 (Table 5.3). The counter-balance volume extracted from negative landforms totals 0.43 ± 0.10 km^3, which we consider a minimum value because many sand pits are deeper in reality than in the input DEM.

5.5.2 Active zone and river position

The active zone covers ~20% of the study area (Fig. 5.8). The width of the active zone is approximately 1 km in the southern part of the Lower Rhine valley and increases to 2 to 3 km in the northern part. The active zone splits in the delta, where the three parts of the active zone each measure 1 to 2 km in width . Similar to the active zone, the extended floodplain (the study area itself) is less wide along the terraced upstream reach of the Lower Rhine than it is in the delta apex region. In most of the study area, about 15% of the width has been reworked by fluvial activity since 800 CE.

Quantification of net elevation change in the active zone bears greater uncertainties than in the inactive zone, and the interpretation is more complex because aspects of channel migration and

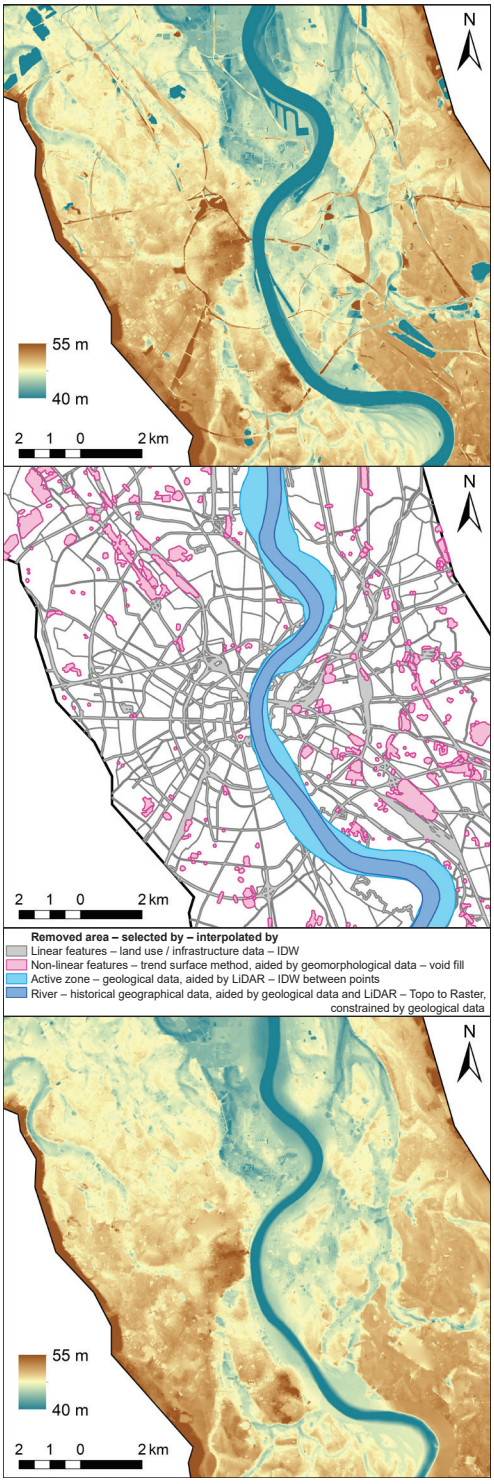

Fig. 5.9. Detail of study area around Cologne with LiDAR ground level DEM (top), altered surface areas separated by method (middle), and palaeo-DEM (bottom).

anthropogenic activities interplayed. Averaged over the study area, the active zone shows a modest positive elevation change of +0.32 ± 0.42 m (Table 5.3), but this value differs considerably when broken down for upper, middle and lower reaches. In the Lower Valley South ('Cologne'), the active zone lost floodplain and bed elevation (–0.82 ± 0.42 m), matching insights regarding channel bed incision in this reach (Erkens et al., 2011; Frings et al., 2019). Contrarily, the active zone in the Lower Valley North shows a net raising of the surface (+0.86 ± 0.43 m), which can be partly attributabed to fluvial deposition in the proximal floodplain. However, for a larger part this should be regarded as an outcome of human action (Duisburg-Ruhrort main inland harbour complex; e.g. Krause, 2003). The embanked floodplains in the Upper Delta show a net gain in surface elevation of +1.23 ± 0.42 m. This large change is the result of floodplain sedimentation in between the dikes, which even necessitated further raising of these dikes (e.g. Hudson et al., 2008). The implied surface elevation change in the IJssel branch subzone is modestly negative, which should be seen as the effect of comparing a situation without an incised river channel to one with a mature channel.

The reconstructed river position provides an overview of Lower Rhine meander dynamics in North Rhine-Westphalia and the Netherlands (Fig. 5.10). As already known from geological mapping at a longer Holocene time scale (Klostermann, 1992; Erkens et al., 2011), lateral meander migration was restricted in the southern part of the study area, but considerably increased downstream. This

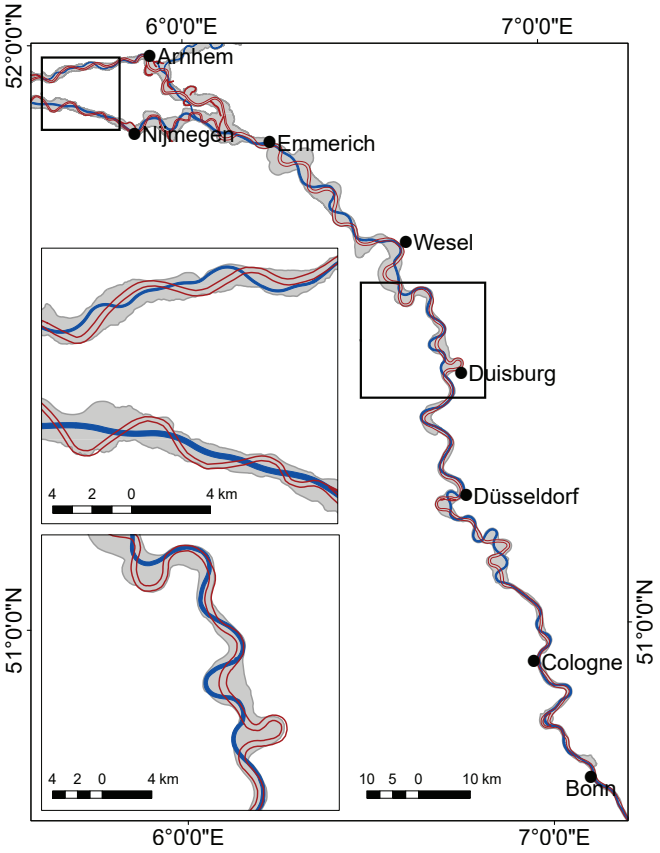

Fig. 5.10. Reconstructed river positions for the target age (red, hollow) and present river positions (blue, solid) within the active zone (grey). The insets show the active zone and the river positions in more detail for a middle part and a downstream part of the study area.

explains both the downstream increase in river position change and the widening of the active zone (Fig. 5.10). Especially in the Dutch-German border region, the Rhine and its branches were dynamically meandering, with bends migrating downstream and repeatedly cutting themselves off (Hoppe, 1970; Kleinhans et al., 2011; Verhagen et al., 2017; Overmars, 2020). Beyond the apex region, i.e., downstream of Nijmegen and Arnhem, the active zones are essentially equal to the embanked floodplain areas between the rivers and the dikes. Here, the active zone width narrows and straightens compared to upstream in the delta apex (Fig. 5.8; Fig. 5.10). This is partly because of the discharge division over multiple branches and deltaic substrate characteristics (Berendsen and Stouthamer, 2001; Stouthamer et al., 2011), but more importantly because of the early onset of river embankment in this part of the study area which confined meander activity.

5.5.3 Floodplain connectivity

In the present situation, many low-lying areas are separated from the proximal floodplain of the Rhine and from each other by dikes and other types of artificial features. These features form topographic barriers by crossing flat terrain and low corridors such as residual channels in Late Pleistocene terraces (Fig. 5.9A). This is not the case in the palaeo-DEM, where the absence of anthropogenic structures implies that floodplain connectivity was much higher (Fig. 5.9C). Indeed, the surface area that is connected at varied inundation levels greatly differs between the present and past situations (Fig. 5.11). When the detrended DEMs are sliced at 4 m below the trend surface, only the river channels themselves and isolated basins are at the inundated level, and the surface area connected to the river is similar in the present and past situations (Fig. 5.11A). At higher inundation levels, increasingly larger parts of the floodplain are connected to the river in the palaeo-DEM compared to the present situation. Even though the total area below the detrended surface is roughly similar in both DEMs (Fig. 5.11B), there is a large difference in the size of the area connected to the river (dark blue patch in Fig. 5.11B; 0.67×10^3 versus 2.11×10^3 km^2). This illustrates a considerable difference in potential inundation extents between early medieval and recent times.

Especially in the northern half of the study area with extensive dike networks, inundated floodplain areas were much larger around 800 CE than at present. Along the downstream reaches of the Lower Rhine and in the delta, large proportions of surface area were flooded regularly in early medieval times. This confirms geological, archaeological, and historical information on past flood extents (e.g. references in Table 5.1). These spatial differences have important implications for the mapping and intercomparison of human settlement and overbank sedimentation patterns within the study area. Simple trend surface-slicing and subsequent connectivity analysis (Fig. 5.11) does not take into account many important hydraulic control factors such as surface roughness and flow patterns. Still, our exploratory results already demonstrate the importance of incorporating palaeotopography in hydraulic modelling studies aimed at quantifying past flooding patterns, flood water levels, and discharge magnitudes. The analysis of connectedness and inundation can be greatly refined by the application of 2D palaeoflood hydraulic models (e.g. Hesselink et al., 2003; Alkema and Middelkoop, 2005). These require as main input an accurate reconstruction of floodplain topography, such as we present here. In addition, the trend-sliced surfaces can provide floodplain landscape zonation templates, which are useful in vegetation reconstruction (e.g. Brouwer Burg, 2013), which in turn is required to provide palaeoflood model scenarios with spatially-distributed hydraulic roughness values.

5.6 Discussion

Here, we first evaluate the different steps in our workflow (Section 5.6.1). Then, we describe the implications of the methodological choices on the accuracy of the palaeo-DEM, and potential opportunities for validation (Section 5.6.2). We end with specifying how the workflow can be repeated for different river valleys and for earlier or later target periods (Section 5.6.3).

5.6.1 Information intake in palaeo-DEM construction methods

The workflow outlined in Section 5.4 serves to construct palaeo-DEMs of large lowland areas, intended for mapping and modelling applications in fluvial geomorphology and palaeohydrology. The first part of the workflow consists of stripping the LiDAR DEM from anthropogenic relief elements, and provides largely sufficient results (DEM II in Fig. 5.4) for the geomorphologically inactive zone. This part of the workflow is a fully top-down approach, also called retrogressive (Werbrouck et al., 2011) or deductive (Schmidt et al., 2018). The DEM stripping steps utilise datasets on current features with no or implicit age information. As such, the result represents a landscape before direct anthropogenic impacts on the topography, without a more specific time stamp associated to it. This is an appropriate reconstruction for the inactive zone of our study area in early medieval times, but not for considerably older or younger periods (Section 5.6.3).

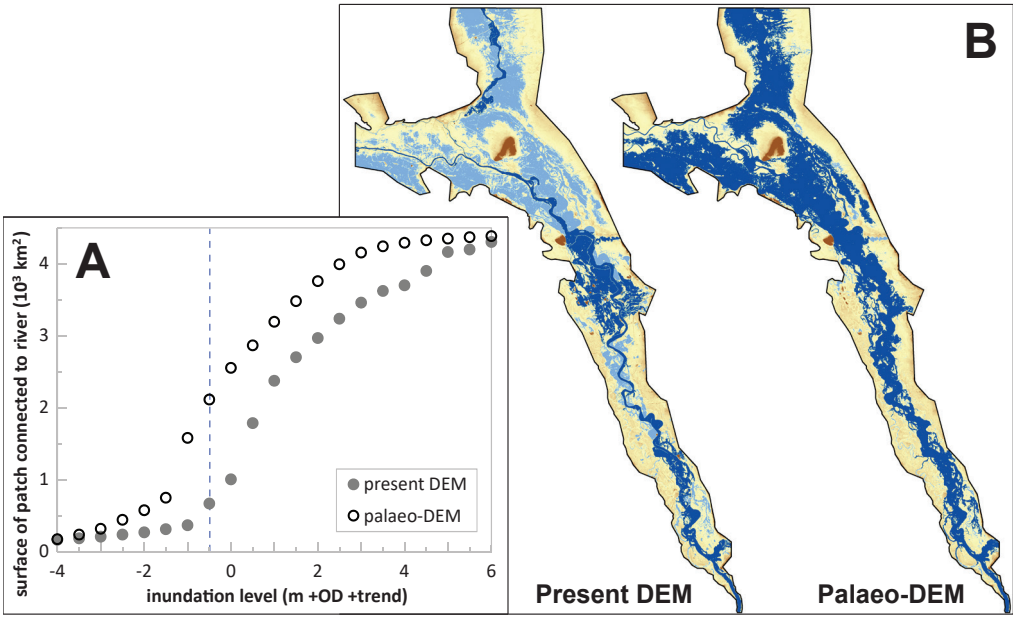

Fig. 5.11. A) Surface area of detrended floodplain connected to the river at varied inundation levels for both the present and the palaeo-DEM. B) Detrended floodplain at an inundation level of −0.5 m (near-maximum difference in connectivity between present and palaeo-DEM). Blue patches are below this level, with dark blue indicating the area connected to the river.

Applying land-use datasets to query anthropogenic features is the preferred method for DEM stripping, because it can be automated after determining buffer widths manually. For a large study area, however, choice and availability of land-use datasets are limited by their uniformity, completeness, and precision. The geometry of the features should be precise to remove only the undesired parts from the LiDAR product, and at least as accurate as the cell size of the DEM that is stripped (5 × 5 m in our case). We largely overcame any initial problems with dataset inaccuracies by resampling the end result to cell sizes an order of magnitude coarser (50 × 50 m). Another limitation is that typical land-use datasets are not primarily classified by morphology and therefore often do not provide accurate boundaries of anthropogenic terrain elements. In our study area, this is not a problem for the linear features. In particular, the infrastructure vector lines obtained from OpenStreetMap almost perfectly follow the middles of entrenched and raised segments (Fig. 5.5). Based on this experience, we regard the OpenStreetMap infrastructure data well-suited for use in automated DEM-stripping, probably also in other geomorphological environments. Despite the considerable number of other land-use datasets available for Germany and the Netherlands, our workflow does not make direct automated use of these. Due to the lack of explicit morphological attributes in common land-use datasets and difficulties in homogenizing partial datasets by different makers, the remaining anthropogenic features are stripped from the DEM by trend surface-aided manual identification (Fig. 5.6).

The trend surface method relies on the detection of anthropogenic elements based on their deviating elevation, and can in theory be used to remove all anthropogenic elements from the topography. However, in the workflow this step follows the automated stripping of features by land-use datasets. This is convenient for three reasons. First, the trend surface improves when some anthropogenic elements are already removed. Second, the trend surface method is relatively time-consuming, so this order decreases the amount of work required for palaeo-DEM construction. Especially linear features may show up as a multitude of smaller elements in a detrended and reclassified DEM. Third, this workflow order restricts the somewhat subjective manual identification to a smaller number of elements. Although it is generally straightforward for a geomorphologically-trained eye to determine whether an element on a DEM is natural or anthropogenic, and this process is aided qualitatively by cross-referencing between the detrended LiDAR DEM and satellite imagery, the number of elements can be overwhelming and mistakes are possible.

The methods for reconstructing the active zone (Fig. 5.4: lower half of workflow) are of a restorative nature and, in contrast to the methods for the inactive zone, demand an explicit specification of the palaeo-DEM target age. Although the resultant terrain still derives from the present morphology (Fig. 5.7), our methods for demarcating the active zone and for reconstructing the river geometry incorporate various types of additional data (Fig. 5.3; Table 5.1) and reasoning. The results for the active zone are more uncertain than those for the inactive zone. This outcome was clear from the start of the research. The need to distinguish between active and inactive zones is evident from the proportionally larger volumetric differences between the palaeo-DEM and the present (Table 5.3). The additional information intake for active zone reconstruction besides the input DEM (used to manually sample point elevations to interpolate a floodplain topography) mainly consists of geological and archeological mapping products (used to define the active zone edges and palaeochannel dimensions). As those products are largely based on subsurface data, the workflow steps for the active zone can be framed as a hybrid between bottom-up and top-down approaches (similar to the framing of the methodology for the deltaic parts in the study area; Section 5.4.5).

5.6.2 Accuracy of palaeo-DEM and outlook on validation

We present the final palaeo-DEM at a downsampled resolution of 50 × 50 m. The main reason for downsampling is that the palaeo-DEM at its 5 × 5 m production resolution still reveals minor anthropogenic features such as shallow ditches and small roads that were not removed in the DEM stripping procedures (Fig. 5.5C; Fig. 5.6F). In theory, however, either stripping method can be applied at a small spatial scale to eliminate this reason for downsampling. For a study area of 12.5 km^2 in southern Germany, Schmidt et al. (2018) constructed a palaeo-DEM, with the isolation of a subtle local topographic saddle as the goal, using a removal and subsequent void-filling approach that also removed many minor anthropogenic elements, for example by buffering field boundaries. However, a risk associated with removing many buffered features is that void-interpolation becomes difficult (Reuter et al., 2007). A large proportion of voids generally leads to a smooth palaeo-DEM, which may not represent a realistic state of the landscape. The reconstructed terrain in our active zone is relatively smooth for a similar reason. This is hard to avoid for areas where palaeotopography is missing due to erosion (Schneider et al., 2017). For applications where field-scale feature isolation is not the goal, downsampling a stripped DEM is the practical solution, since the elevation differences of minor anthropogenic elements with respect to their surroundings are typically small (Fig. 5.5C; Fig. 5.6F), and the material dug from ditches is often incorporated in the elevation of the surrounding land. For envisioned applications such as valley-scale palaeohydrological modelling, a resolution of 50 m is still significantly finer than typical grid sizes of numerical models.

The vertical resolution at which the reconstruction is accurate is less straightforward to assess than the horizontal resolution. For the method of DEM stripping by land-use datasets, the vertical accuracy of the intermediate result (DEM I) is as good as that of the LiDAR DEM, which is in the order of 0.05 m. Section 5.4.5 and Table 5.3 report how this uncertainty propagates into zonal elevation-difference averages and volumetric totals. Additional uncertainties in the accuracy of the palaeo-DEM vary considerably across the study area, because (1) different stripping and associated void-interpolaton methods were applied, and (2) subareas differ in history and degree of anthropogenic modifications. For grid cells affected by the trend surface-based stripping method (Fig. 5.6), the vertical accuracy depends on the choices made in the reclassification step and on the size of the interpolated voids. Since we reclassified the detrended DEM at 0.5 m height intervals, anthropogenic elements deviating less than 0.5 m were not identified nor removed in this step. Within the active zone, the restorative terrain interpolations produce relatively smooth floodplain landscapes (Fig. 5.7D), which include eroded terrace scarps but do not account for detailed variations in topography such as point-bar ridge-and-swale topography. The relatively smooth active zone palaeo-DEM could be used as starting point to simulate such micro-relief when an application demands it.

Local validation of the palaeo-DEM is theoretically possible for interpolated surfaces that are currently buried below younger relief. Here, the reconstruction can be validated in an excavation or in boreholes, or against existing detailed cross-sections encountered occasionally in literature (e.g. Krause, 2003). However, for the majority of removed and interpolated cells, such as the areas of negative relief and the complete active zone, validation is impossible because the palaeo-DEM results from restorative operations. Quantitative trust in the quality of the palaeo-DEM for these areas thus needs to derive from zonal averaged and intercompared elevation differences as presented in Fig. 5.8 and Table 5.3.

The largest areas of anthropogenic positive elevation remaining in the palaeo-DEM are those underneath the centres of towns and cities. Many of these were founded in medieval times and postdate the target age of the palaeo-DEM, although Cologne is a marked exception of Roman age. Since our methods cannot easily correct for uniform raising of the ground, the inner parts of large old cities likely are the locations where the vertical accuracy is lowest. Here, upgrading the cell-by-cell accuracy of the palaeo-DEM is possible, but requires a bottom-up approach utilising detailed archaeological stratigraphy with dating control throughout the city centres. Given the large size of our study area, this is not feasible. Improving the accuracy at this resolution is necessary for small-scale applications, such as mapping past urban topography (Gerlach, 2003; Krause, 2003; Baubiniene et al., 2015; Mozzi et al., 2018), but for typical regional-scale applications such level of detail is not required (e.g. Section 5.5.3).

In the most downstream parts of the study area, we deployed hybrid methods of palaeo-DEM construction (Section 5.4.5). These involved corrections for gradual aggradation of the floodplain in areas outside the active zone (complying with Pierik et al., 2017), a process that largely ceased after embankment. Because our target age is close to the moment of embankment in the delta, the resulting corrections and their vertical inaccuracy are small (in the order of centimeters, locally up to decimetres close to the river). Especially in these areas, the palaeo-DEM can be verified and potentially improved by integrating newly-processed subsurface data to determine the thicknesses of historic sediment packages at many locations (e.g. Vermeer et al., 2014; Pierik et al., 2018). This would change the hybrid workflow from a dominantly top-down approach to a dominantly bottom-up approach, significantly increasing data requirements (Section 5.1). Furthermore, the specifics of bottom-approaches are expected to differ strongly between the valley and delta settings in the study area, whereas the top-down approach performs well across the entire area in a rather uniform way.

5.6.3 Applicability to other study areas and time periods

Our workflow is generic in set-up and therefore transferable to other study areas and target ages. However, the relative importance of the different workflow steps and the required data may change (Fig. 5.12). The methods can be applied to construct palaeo-DEMs of any lowland region, provided that a high-resolution LiDAR DEM is available. In addition to being the starting point for stripping the present topography, the LiDAR DEM helps to define the active zone in combination with geological data, and to reconstruct the river position in combination with historical information. The removal of anthropogenic elements was the most important step in our reconstruction of the Lower Rhine valley and upper delta, and we expect this to be similar in other cases, because lowland areas are generally densely populated with long settlement histories, resulting in abundant anthropogenic modifications to the terrain. DEMs stripped from such features can provide valuable starting points for archaeological prediction maps (e.g. Cohen et al., 2017) and modelling studies focusing on human-landscape interactions in deltas (e.g. Groenhuijzen and Verhagen, 2017; van Lanen et al., 2018). Consideration of the active zone is important for large study areas centred around meandering rivers. For this zone, geological data to demarcate the active zone and geomorphological insights to fill the active zone void with restored terrain are indispensable tools for reconstruction. Still, we recommend to conduct DEM stripping before starting other operations in the active zone, because this improves the recognisability of natural geomorphological features (Fig. 5.7; Fig. 5.9).

Our workflow is designed to construct a palaeo-DEM that represents the time before major anthropogenic modifications to the terrain. The timing of this moment depends on the study area, as it relates to population density and technological developments. For example, in most of the Americas, significant anthropogenic modifications did not start before 1800 CE, whereas in some parts of Africa, Asia, and Europe, the first large (visible in a 50 × 50 m cell-size DEM) anthropogenic geomorphological elements are considerably older than 800 CE. The timing of this moment and its relation to the palaeo-DEM target age are important for assessing which procedures and data are relevant in the reconstruction (Fig. 5.12). For example, these factors determine whether the preferred resources to reconstruct the active zone consist of historical data or geological data. In the case of the Lower Rhine valley, target ages in Roman to medieval time periods imply using a combination of both (Fig. 5.4). This is methodologically illustrative, altough it has necessitated steps in the workflow that may not be relevant to readers having palaeo-DEMs for either the youngest centuries or for many millennia older in mind (hence, Fig. 5.12).

Historical data will play an increasingly important role when elements of the workflow are applied to younger periods. For recent periods (circa 1850 and later), a palaeo-DEM may be constructed based solely on historical elevation and bathymetry data. This possibility depends on the availability of such data and cannot be used to correct for elements older than the data itself; for example, the river dikes in our study area predate any quantitative measurement data by many centuries. The accuracy and effective resolution of the resulting DEM will reflect those of the historical data. In general, historical data may prove especially useful for the otherwise difficult reconstruction of geomorphologically active zones (van der Meulen et al., 2018; Overmars, 2020) and urban environments (Krause, 2003; Wronna et al., 2017).

When DEM-stripping methods are deployed to periods younger than the oldest anthropogenic modifications, the removal of anthropogenic elements should be conducted selectively (Fig. 5.12). Although most anthropogenic changes to the terrain occurred during the nineteenth and twentieth centuries, there are major exceptions such as dikes, raised settlements, and canals (e.g. Schmidt et al., 2018). Determining which features were present, and reconstructing their correct dimensions, requires integration with historical insights on the ages of elements as well as their geometrical evolution over time (Fig. 5.1). A higher temporal resolution is required for more recent historical periods, when rates of anthropogenic alterations increased. Thus, our top-down workflow concepts are well applicable to palaeo-DEM construction for younger time periods, but the stripping steps will require more attention (Fig. 5.12). The active zone, on the other hand, will be easier to reconstruct, as the effects of geomorphological processes such as erosion are smaller over shorter time scales.

Farther back in time, a larger area has been reworked and the zone that should be considered active is more extensive. As a result, restoration of the active zone requires more assumptions, and geological and geomorphological information play an increasingly important role for older palaeo-DEM target periods (Fig. 5.12). The reconstruction of the inactive zone on the other hand does not require any additional input when targeting older periods. Moreover, it becomes smaller at the expense of the active zone.

For target ages predating the Holocene, we reckon that the top-down approach loses its benefits compared to bottom-up approaches. In our study area, this is because the active zone then covered a

major part of the valley floor, and only few preserved remnants can still be considered indicative of the palaeotopography (e.g. Erkens, 2009). Furthermore, such a reconstruction should also consider geomorphological processes of a different nature besides fluvial reworking, like periglacial colluvial and aeolian activity. For study areas in different parts of the world, geomorphological responses to external changes in climate and base level determine the adequate lower time limit of the top-down approach. In most lower river reaches this is a moment between the Last Glacial Maximum (circa 21 ka) and the Mid-Holocene optimum (circa 7 ka), because for earlier palaeo-DEM target ages most of the region has to be considered active (e.g. Briant et al., 2018).

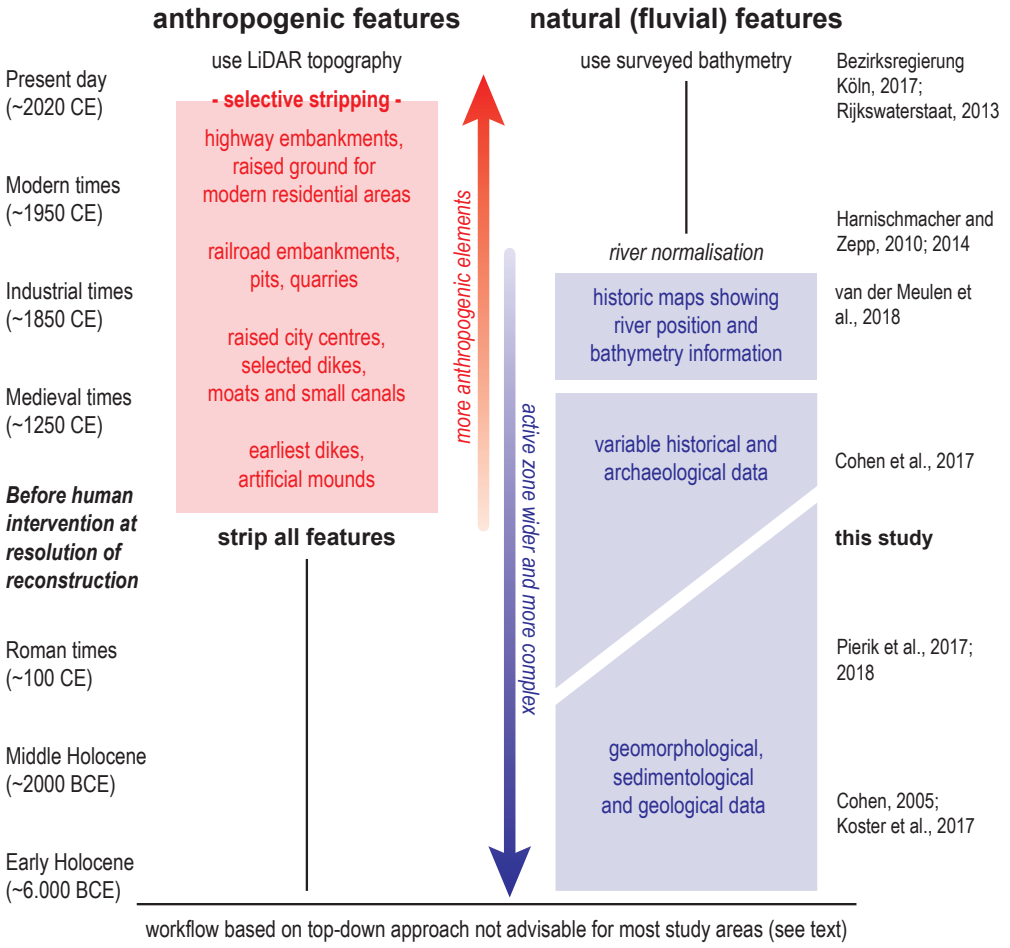

Fig. 5.12. Overview of changes to the workflow and data intake when it is applied to older or younger time periods. The periodization varies per study area; therefore, the left column gives this in broad terms, with ages in brackets indicating the specific timing in the Lower Rhine valley. The references in the right-most column are earlier studies relevant to palaeo-DEM construction in the study area.

5.7 Conclusion

We present a workflow for LiDAR-derived high-resolution palaeo-DEM construction, developed for the case of the Lower Rhine valley and upper delta. Our workflow is suitable to reconstruct the topography of large valley-floor areas (>1000 km^2) at high resolution (5 × 5 m processing resolution; 50 × 50 m output resolution), because it mainly relies upon LiDAR DEM adaption ('top-down' approach). The first steps of the workflow consist of removing anthropogenic relief elements and filling the resulting voids. These DEM-stripping steps are sufficient to reconstruct the topography of the distal floodplain defined by inherited relief with many anthropogenic modifications, with little explicit demand for detailed age information on the removed features. The reworked proximal floodplain requires additional steps involving geomorphological process insights, with greater demands on age information for landscape features, obtainable from diverse geological, archaeological, and historical sources. Distinguishing these geomorphologically distinct 'inactive' versus 'active' zones is important for reliable palaeo-DEM construction.

The palaeo-DEM is regarded accurate at a horizontal resolution of 50 m and at a vertical scale of approximately 0.5 m, though considerably better in non-stripped areas and potentially worse locally in the restored active zone. The total volume of anthropogenic modifications in the Lower Rhine floodplain area is in the order of 10^9 m^3. Positive and negative topographic changes largely cancel out over the total valley surface, with a net volumetric change of about 10^8 km^3 (excluding mining-subsidence-related accommodation space). A simple palaeohydrological analysis demonstrates large differences in floodplain connectivity between the present and past situations, highlighting the importance of incorporating the past topography in palaeoflood research. The palaeo-DEM and the assessment of its accuracy can be verified locally. However, over 20% of the study area is an informed restorative product that cannot be verified by observational data, but might be validated through its further use in modelling work.

The workflow developed in this study is widely applicable to other lowland areas at different spatial scales and resolutions. In addition, we provide a framework for adjusting the workflow to younger or older palaeo-DEM target periods. Reconstructions for younger periods require selective stripping of the LiDAR DEM, which demands historical or archaeological data to determine the ages and past dimensions of anthropogenic elements. In contrast, reconstructions for older periods require no additional DEM stripping, but have to increasingly rely on restorative approaches taking in geological and geomorphological information. The overall workflow methodology is limited to geologically recent time periods (end of Pleistocene and younger), because of its top-down approach using the present morphology for interpolative construction of a palaeo-DEM.

Acknowledgements

This study was funded by STW (now NWO-TTW), project 14506. We thank Hessel Woolderink and Maarten Zeylmans for help with processing raw LiDAR data. Stefan Harnischmacher kindly provided digital data for the Ruhr area. We thank the organising committees of the Fluvial Archives Group (FLAG) 2018 and International Union for Quaternary Research (INQUA) 2019 meetings, where we presented and discussed our methods and preliminary results. Two anonymous reviewers and the SI editor S. Cordier are thanked for their advice on an earlier draft of this manuscript, and journal editor S. Lecce is thanked for editorial corrections. The palaeo-DEM, intermediate output

products, and all automatic and manually created feature-selection data files used in the process are archived and will be made available as open data.

Chapter 6

Palaeoflood simulation

this chapter is based on

van der Meulen, B., Bomers, A., Cohen, K.M., Middelkoop, H., 2021. Late Holocene flood dynamics and magnitudes in the Lower Rhine river valley and upper delta resolved by a two-dimensional hydraulic modelling approach. Earth Surface Processes and Landforms 46, 853–868. DOI:10.1002/esp.5071

Als de werkelijkheid er niet zou zijn, dan zou de wereld er heel anders uitzien.

Theo Maassen – Functioneel naakt (2002)

Abstract

Palaeoflood hydraulic modelling is essential for quantifying 'millennial flood' events not covered in the instrumental record. Palaeoflood modelling research has largely focused on one-dimensional analysis for geomorphologically stable fluvial settings, because two-dimensional analysis for dynamic alluvial settings is time-consuming and requires a detailed representation of the past landscape. In this study, we make the step to spatially continuous palaeoflood modelling for a large and dynamic lowland area. We applied advanced hydraulic model simulations (1D–2D coupled set-up in HEC-RAS with 950 channel sections and 108 × 10^3 floodplain grid cells) to quantify the extent and magnitude of past floods in the Lower Rhine river valley and upper delta. As input we used a high-resolution terrain reconstruction (palaeo-DEM) of the area in early medieval times, complemented with hydraulic roughness values. After conducting a series of model runs with increasing discharge magnitudes at the upstream boundary, we compared the simulated flood water levels to an inventory of exceeded and non-exceeded elevations extracted from various geological, archaeological and historical sources. This comparison demonstrated a Lower Rhine millennial flood magnitude of approximately 14,000 m^3/s for the Late Holocene period before late medieval times. This value exceeds the largest measured discharges in the instrumental record, but not the design discharges currently accounted for in flood risk management.

6.1 Introduction

Palaeoflood analysis informs current and future flood risk (Wilhelm et al., 2019; St. George et al., 2020). Identifying past flooding patterns helps to determine areas at risk under different management scenarios (Alkema and Middelkoop, 2005; Remo et al., 2009), and quantifying past flood magnitudes helps to assess future discharge extremes (Benito and Thorndycraft, 2005; Schendel and Thongwichian, 2017). Many studies on past floods aim to quantify the peak discharge reached during specific events (Herget and Meurs, 2010; Toonen et al., 2013; Hu et al., 2016) or a non-exceeded discharge over a prolonged time period (Ely et al., 1993; England et al., 2010). Traditionally, palaeoflood modelling studies have been conducted in geomorphologically stable fluvial settings such as bedrock canyons, where calculating a representative discharge is relatively straightforward (Kochel and Baker, 1982; overviews in Baker, 2008 and Benito and Díez-Herrero, 2015). In settings where the fluvial landscape has changed due to natural fluvial processes and anthropogenic activities, however, the floodplain topography and channel bathymetry must be reconstructed prior to calculations of palaeoflood discharges (Herget and Meurs, 2010; Toonen et al., 2013; Machado et al., 2017).

Palaeoflood reconstructions by hydraulic models have been largely limited to one-dimensional (1D) calculations, applied to a single or a few consecutive valley cross-sections (Webb and Jarrett, 2002; Busschers et al., 2011; Benito and Díez-Herrero, 2015). Although major advantages of deploying 1D hydraulic models are computational speed and little required input, these models cannot resolve spatial aspects of flooding such as floodwater dispersal patterns over the floodplain. Therefore, 1D modelling produces first-order calculations of palaeoflood peak magnitudes rather than actual palaeoflood simulations. Introducing a two-dimensional (2D) model component lessens the assumptions in the modelling step of palaeoflood research and yields more realistic output than a 1D model (see discussion in Herget et al., 2014), providing stages and discharges at different points in time over the entire model area. Many studies discuss the performance of 2D hydraulic models

for present landscape situations (Dottori et al., 2013; Bomers et al., 2019b; Czuba et al., 2019), and the importance of applying these in palaeoflood research is often emphasised, but the actual use is usually outside time and budget constraints (England et al., 2010; Benito and Dièz-Herrero, 2015).

Besides computing power limits, the main problem associated with 2D modelling of past floods is a requirement for accurate high-resolution input data, most notably a reconstruction of the terrain. Generating this input involves the use of geological and geomorphological field data, and experimental GIS techniques (van der Meulen et al., 2020). A few studies have applied 2D models to simulate relatively recent floods, occurring in the nineteenth century (Calenda et al., 2003; Hesselink et al., 2003; Skublics et al., 2016; Bomers et al., 2019) and the twentieth century (Denlinger et al., 2002; England et al., 2007; Ballesteros et al., 2011; Masoero et al., 2013; Bomers et al., 2019a; Stamataki and Kjeldsen, 2020). For such recent events, abundant data are available for model schematisation and validation. Changes in morphology can be regarded as either insignificant or well-documented and readily incorporated. Simulations of older floods in larger alluvial reaches, such as the Lower Rhine, are lacking due to terrain reconstruction demands. However, these reaches are usually densely populated, warranting detailed assessments of river flood risk. For such regions, it would be of interest to simulate extreme events in earlier historic or prehistoric times, thereby constraining peak discharges over longer time periods that are usually the focus of palaeoflood research.

The Lower Rhine is a large and economically important meandering river, which transitions into the Rhine delta near the German-Dutch border (Fig. 6.1). Here, it divides into three main distributaries: the Waal, the Nederrijn, and the IJssel. These river branches have been embanked since late medieval times (Hesselink, 2002). Across the valley and delta, the river and floodplain have been heavily modified by anthropogenic activities (Kalweit et al., 1993; Lammersen et al., 2002; Hudson et al., 2008; van der Meulen et al., 2020). Throughout the Holocene, Lower Rhine floods have left scattered geological and geomorphological traces in the landscape (Gouw and Erkens, 2007; Toonen et al., 2013; Minderhoud et al., 2016; Pierik et al., 2017; Willemse, 2019). In historic times, large floods were a recurring threat for the inhabitants of the area (Tol and Langen, 2000), and at present, considerable resources are dedicated to develop and maintain flood protection structures. A major challenge lies in determining appropriate safety standards for river management works and underlying magnitude-frequency relationships of extreme events (Hegnauer et al., 2014; 2015; van Alphen, 2016).

Previous palaeohydrological research in the delta apex region has provided estimates of Lower Rhine flood frequencies and relative magnitudes over the past centuries to millennia based on sedimentary archives obtained from oxbow-lake fills (Toonen, 2013; Toonen et al., 2015; Cohen et al., 2016; Toonen et al., 2017). These studies have shown that between 4.2 and 0.8 ka (kiloannum: thousands of years ago), i.e. in the Late Holocene up to embankment along the downstream reaches, five flood events with recurrence times close to 1,000 years occurred. The largest of these was dated to 785 CE based on a tentative correlation between radiocarbon-dated flood deposits and historical sources (Toonen, 2013; Cohen et al., 2016). Recently, a palaeo-DEM has been constructed for the Lower Rhine river valley and upper delta in the first millennium CE (van der Meulen et al., 2020). The present research builds upon these studies by applying a hydraulic model to the palaeo-DEM, resolving absolute magnitudes of extreme floods in the Late Holocene period preceding the onset of river embankment in late medieval times.

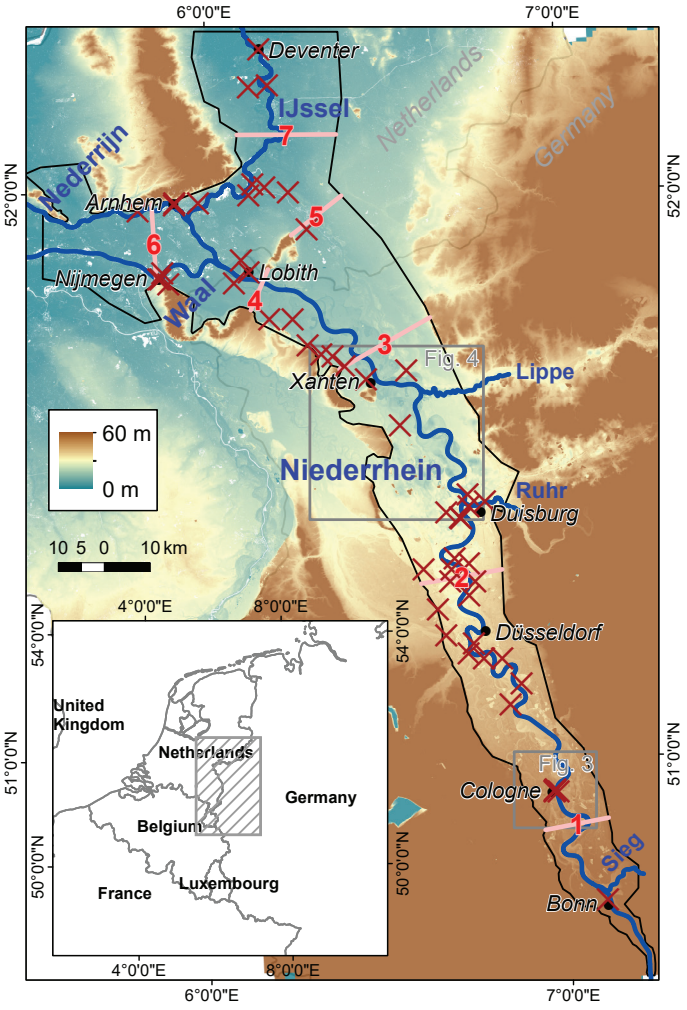

Fig. 6.1. Extent of model area and numbered profiles on LiDAR DEM of North Rhine-Westphalia and the Netherlands (modified from van der Meulen et al., 2020). The red crosses indicate the locations of observational data on palaeoflood levels (Supplementary Table). The grey boxes centred on Cologne and Duisburg-Xanten indicate the extents of Figs. 6.3 and 6.4.

The purpose of this study is to constrain past flooding patterns and magnitudes in the Lower Rhine river valley and upper delta (Fig. 6.1). Specifically, we aim to quantify the peak discharge of the most extreme ('millennial') floods that occurred. Likely, this value is in between the largest measured flood discharge (~12,000 m^3/s) and the largest discharges generated by stochastic weather simulations coupled to hydrological models (GRADE project: ~24,000 m^3/s; Hegnauer et al., 2014; Hegnauer et al., 2015). We set up a 1D–2D coupled hydraulic model with reconstructed terrain and roughness as input to simulate the propagation of extreme discharge waves in the past landscape setting. Subsequently, we compare the output water levels with geological, geomorphological, and archaeological observations informing on minimum and maximum palaeoflood levels in the study area. In addition to calculating a Late Holocene millennial flood magnitude for the Lower Rhine river, this study demonstrates for the first time the potential and the difficulties of spatially continuous palaeoflood modelling in large lowland areas. At the least, such research requires (1) an accurate reconstruction of the river and floodplain, (2) a numerical model with a two-dimensional component, and (3) a collection of spatially-distributed palaeoflood levels.

6.2 Materials and methods

The overall 'inverse modelling' approach applied in this study comprises three major steps (Fig. 6.2). The first step includes the reconstruction of the landscape, which encompasses floodplain topography, river position and bathymetry, and roughness values matching past land cover. Further, an inventory of palaeoflood levels was generated based on earlier geological and archaeological investigations. The second step consists of hydraulic modelling, using the past landscape as input. Next to terrain and roughness, the model set-up requires upstream and downstream boundary conditions, and a rasterization of the model area consisting of a 2D grid on the floodplain and 1D profiles in the channels. Key to the 'inverse modelling' approach is that multiple model runs are conducted with discharge waves of increasing magnitude as upstream boundary condition. In the third step, the output of the successive model runs is compared to the inventory of palaeoflood levels. The match between observed and simulated flood levels (m) is used to evaluate the model output resulting from different peak flows (m^3/s), thus constraining the maximum discharge that occurred in the studied period.

The upstream boundary of the model area is at river km 638 between Andernach and Bonn, Germany, where the Rhine changes from a bedrock-confined river to an alluvial meandering river in a terraced valley floor (Fig. 6.1). From here, the model area covers the entire floodplain of the Lower Rhine valley and the delta apex region. The downstream boundaries are placed at river km 908 (Waal), km 912 (Nederrijn), and km 950 (IJssel), where the delta plain widens substantially and water level slopes of the river branches are influenced by tides (Kleinhans et al., 2011; Stouthamer et al., 2011). Laterally, the area extends up to the edges of the valley floor and delta plain, where the terrain steeply rises (Fig. 6.1), covering all fluvial geomorphological units of Holocene age and latest Pleistocene terrace surfaces. These lateral boundaries were selected to prevent simulations of hypothetically extreme floods from requiring additional outflow locations, even though realistic extreme floods did not inundate the full width of the area according to geological and historical evidence. In the present situation, the model area can be clearly subdivided into embanked floodplains along the river channels and flood-protected areas on the other sides of the dikes. Such a distinction cannot be made for early medieval times when dikes were not yet present and floodplains were much wider.

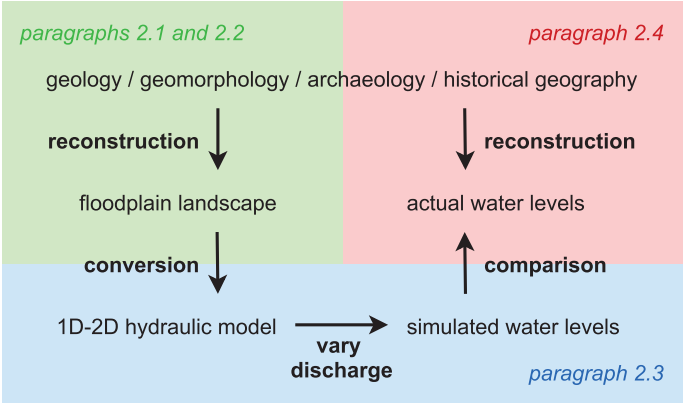

Fig. 6.2. Overview of the 'inverse modelling' approach applied in this study.

6.2.1 Topography and bathymetry

The most important component of the model schematisation is the terrain, represented by a Digital Elevation Model (DEM) of the past situation: a palaeo-DEM. We used a recently produced reconstruction of the topography, river position, and channel bathymetry of the Lower Rhine valley and upper delta in early medieval times (circa 800 CE; Fig. 6.3). This palaeo-DEM was constructed by stripping a modern LiDAR DEM from all changes to the topography by anthropogenic activities (van der Meulen et al., 2020), after correcting for recent mining-induced subsidence (Harnischmacher and Zepp, 2014). In addition, the river position and channel bathymetry were reconstructed by combining available historical, archaeological and geological data, and the natural floodplain elevation along the river was restored using geomorphological interpolations (van der Meulen et al., 2020).

The early medieval target age of the palaeo-DEM predates any major direct modifications to the terrain by humans. Therefore, the distal floodplain topography is representative for the entire Late Holocene period up to late medieval times (van der Meulen, 2020). The proximal floodplain topography and river position are considerably more variable through time, but within the Late Holocene the fluvial style and channel dimensions of the Rhine have been fairly stable (Klosterman, 1990; Erkens et al., 2011). Furthermore, local morphological change due to fluvial erosion and deposition likely did not alter the overall conveyance capacity for peak discharges at the scale of the entire valley. Similarly, indirect human impacts on the topography, most notably changes in sediment budget (Hoffmann et al., 2007; 2009; Middelkoop et al., 2010; Notebaert and Verstraeten, 2010), affected the area during the Late Holocene, but probably hardly influenced the propagation of extreme discharge waves over the full model area. As precisely these extremes are the focus of our simulations and analyses, we regard the simulation results produced using the early medieval palaeo-DEM representative for older Late Holocene times.

6.2.2 Hydraulic roughness

The next component of the model schematisation is hydraulic roughness, expressed as Manning's *n* values. Vegetation distribution and land use are broadly known for early medieval times in the study area, but detailed constraints are scarce (Gouw-Bouman, in prep.). Therefore, we developed a simplified land cover reconstruction. We distinguished five landscape classes based on distance to the river and relative floodplain elevation (with respect to a second-order polynomial trend surface), each associated with different natural vegetation and land use characteristics, and hence different average hydraulic roughness values (Fig. 6.4; Table 6.1). We used standard values for different vegetation types (Chow, 1959) as starting point to assign *n* values to landscape classes based on their estimated overall land cover composition.

The areas located more than 5 m above the trend surface (high grounds, class H) were mostly covered by forest, resulting in high *n* values. Note that class H covers only a small area (Table 6.1), because we cut off the model area where elevation significantly rises. The river itself (polygon obtained from palaeo-DEM, class R) consisted mostly of bare gravel and sand, resulting in low *n* values. The proximal floodplain (class P), which we defined as a 1-km-wide zone next to the river (Fig. 6.4), had dispersed riparian vegetation of the type modern floodplain-ecologists aim to restore (van Oorschot, 2017) and was assigned relatively high *n* values. Realistically, the width of this zone

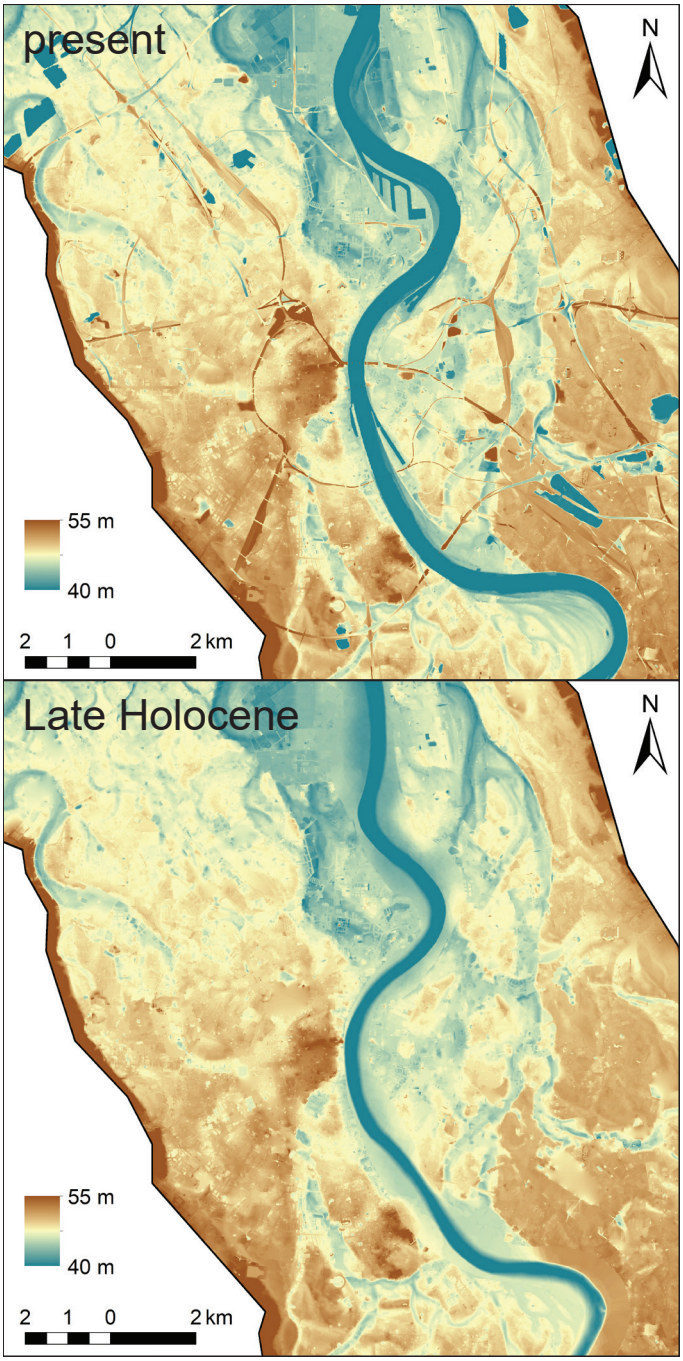

Fig. 6.3. LiDAR ground level DEM and palaeo-DEM of model area around Cologne, Germany (modified from van der Meulen et al., 2020). All anthropogenic modifications, such as embankments for roads and railroads, dump sites and quarry pits, have been removed, and the 'original' topography has been restored by various interpolation techniques. The river position has been reconstructed by combining historical and archaeological sources with geological–geomorphological insights. The extent of the figure is indicated in Fig. 6.1.

greatly varied along the river and thus our definition is a major simplification. However, given the large study area, a detailed reconstruction was not feasible. The higher parts of the distal floodplain (class DH) were used most intensively for settlement and agriculture (Pierik and van Lanen, 2019),

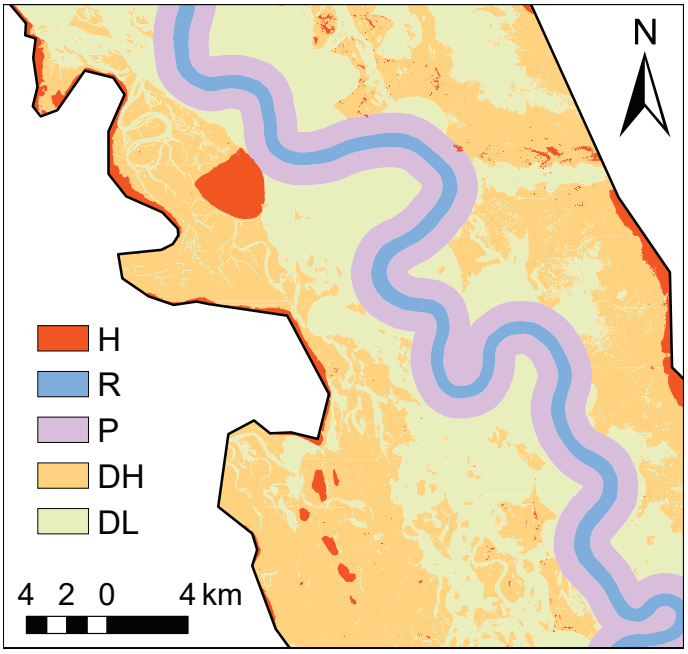

Fig. 6.4. Model area around Wesel, Germany, showing distribution of landscape classes. The abbreviations and Manning's *n* values assigned to the different classes are given in Table 6.1. The extent of the figure is indicated in Fig. 6.1.

Table 6.1. Landscape classes and assigned Manning's *n* values.

class		definition	% area	n_{min}	n_{best}	n_{max}
H	high grounds	area > trend surface + 5 m vertical	4.1	0.1	0.1	0.1
R	river bed and banks	river polygons + 100 m buffer	5.0	0.025	0.03	0.045
P	proximal floodplain	border of R + 1000 m buffer	14.7	0.06	0.07	0.08
DH	distal floodplain, high	remaining area > trend surface	38.6	0.04	0.05	0.06
DL	distal floodplain, low	remaining area < trend surface	37.6	0.035	0.04	0.055

and thus had little natural vegetation. Agricultural land in early medieval times consisted of smaller fields than today, with abundant hedges and local stands of trees. Therefore, we assigned higher *n* values to this class than used for agricultural land in models of present situations. The lower parts of distal floodplain (class DL) were, and still are, relatively wet and mostly used as meadows for grazing and hay production. In these areas, open grasslands prevailed, but locally swamp forests (carr) occurred as well (Gouw-Bouman et al., in prep). Grasslands have low *n* values, but the characteristically dense swamp forests have high *n* values. However, it is not possible to reconstruct the precise spatial distribution of grasslands and swamp forests within this zone. Overall, this class mainly consisted of grass; therefore, we assigned it low *n* values throughout the model area.

Besides average roughness values (n_{best}), we assigned lower (n_{min}) and upper estimates (n_{max}) to all classes, except for class H with its marginal occurrence (Table 6.1). The n_{min} and n_{max} were assigned to account for the uncertainties inherent in assigning roughness values (Chow, 1959; Warmink et al., 2013; Bomers et al., 2019a). All landscape classes, expect class R, consist of a mixture of relatively open and forested parts. Because of the co-occurrence of different vegetation types, Manning's *n* values beyond the lower and upper estimates given in Table 6.1 are unlikely

to be correct for any Late Holocene situation. In the Rhine area, significant catchment-scale deforestation occurred since the Bronze Age circa 3.5 ka. There was a slight increase in natural vegetation cover in the Dark Ages around 1.5 ka, due to population decline and land abandonment following Roman times (Kaplan et al., 2009; Gouw-Bouman, in prep.). For these reasons, lower n values (between n_{min} and n_{best}) may be appropriate for Middle Holocene to early Late Holocene times, whereas higher values (between n_{best} and n_{max}) may be typical for Roman times and for late medieval times. We used the n_{best} values in the model runs, unless otherwise stated.

6.2.3 Model set-up

We set up a 1D–2D coupled hydraulic model in HEC-RAS (v. 5.0.3). The main channels of the Rhine river and its distributaries were schematised by 500-m-spaced 1D profiles, whereas the floodplains were discretised on a 2D grid with a resolution of 200 x 200 m (Fig. 6.5). Flexible grid shapes were used along the model domain boundaries and along the transition from reworked to inherited floodplain (van der Meulen et al., 2020; Fig. 6.5). Rectangular grid cells were used in the remainder of the model domain. The 1D profiles were coupled with the 2D grid using the weir equation. The weir coefficient was set to a value corresponding to overland flow to enable correct prediction of the flow transfer and to keep the model stable. We used the full momentum equations to solve the system, because these resulted in more accurate model results compared to the simplified diffusive wave equations.

The upstream boundary condition consists of a discharge time series (Fig. 6.6). An initial discharge of 1,000 m^3/s was used in all runs to avoid a dry channel at the start of the simulations. We selected the two largest measured discharge waves as input. These are the floods of December 1925 / January 1926 (Bomers et al., 2019a) and January 1995. For the palaeoflood simulations, we used the shape of the 1926 discharge wave as a representative standard hydrograph, because it closely resembles the average of modelled extreme flood waves of the Rhine near Andernach (Hegnauer et al., 2014; 2015). By scaling this hydrograph, we obtained a series of input waves with different peak

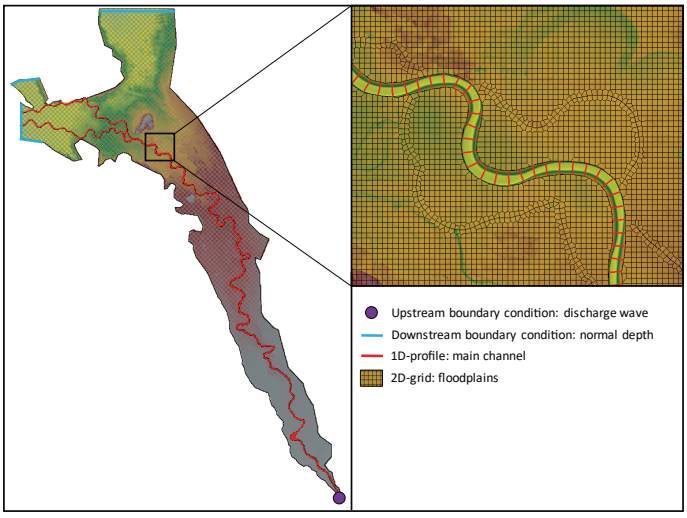

Fig. 6.5. Model set-up of the 1D–2D coupled hydraulic model on top of the palaeo-DEM. The close-up, between Rees and Emmerich, visualises the nature of the 1D–2D coupled grid.

discharges, from 10,000 to 30,000 m^3/s with intervals of 2,000 m^3/s (Fig. 6.6). We simplified the discharge waves of the Lower Rhine tributaries Sieg, Ruhr, and Lippe to constant input values of 250, 500, and 250 m^3/s respectively. Normal depths were used as downstream boundary conditions at the locations where water can potentially leave the model domain (Fig. 6.5). These normal depths were calculated using Manning's equation (Brunner, 2016).

In total, we conducted 15 simulations using the palaeoflood model set-up, one for each different peak discharge and two extra runs for both the 10,000 and 24,000 m^3/s input waves using the minimum and maximum Manning's *n* values for all classes (Table 6.1) to evaluate model sensitivity to roughness values. In addition to model runs on the Late Holocene pre-embanked landscape, we conducted model runs on the present landscape. For these we used a schematisation of river and floodplain geometry ('Baseline' dataset) provided by the Ministry of Infrastructure and Water Management (RWS) of the Netherlands and the Landesamt für Natur, Umwelt und Verbraucherschutz (LANUV) of North Rhine-Westphalia. The model set-up for the present landscape closely resembled the palaeoflood model set-up, but both the channel and the embanked floodplains were schematised by 1D profiles. The areas protected by embankments were discretised on a 2D grid (Bomers et al., 2019b).

6.2.4 Evaluation of model output and palaeoflood discharges

As a first step in analysing the model output, we plotted maps showing maximum water depths for each simulation. We used these to extract the maximum inundation extent for each different input discharge. Next, we plotted the simulated water levels and discharges at seven approximately equally-spaced profiles across the model area (Fig. 6.1). From the amounts of water passing these locations (discharge per time step), we determined flood wave propagation. Further, we plotted for all profile locations the relation between input discharge and water level.

To determine the maximum discharge that occurred in the Late Holocene to early medieval time period, we compared the simulated flood levels to an inventory of observational data (Supplementary Table) that inform whether or not different locations in the area were flooded in

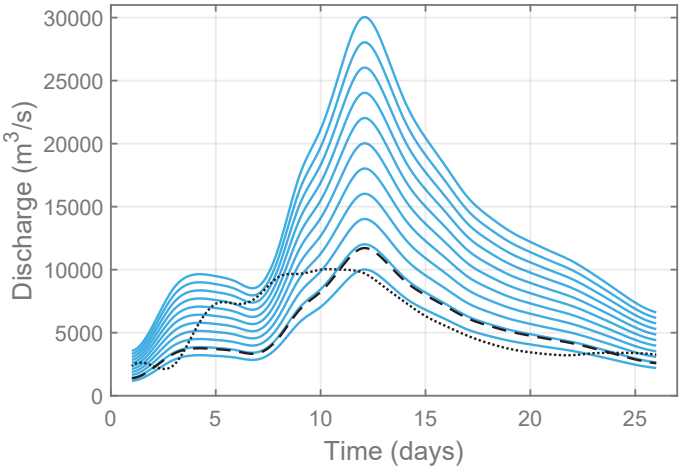

Fig. 6.6. Discharge waves used as upstream boundary condition. The dashed black line is the discharge wave of winter 1925/1926 at Andernach (peak 11,700 m^3/s), and the dotted black line is the discharge wave of January 1995 at Andernach (peak 10,100 m^3/s).

this period. We extracted these data from existing studies, most of which did not aim to reconstruct flood levels from their observations. The inventory consists of 96 flood level markers at 55 locations, spread throughout the study area (Fig. 6.1). The supplementary table gives for each location its coordinates, the exceeded (MinElev) or non-exceeded (MaxElev) level, its source type and references, and notes on the interpretation of the flood level. Identification and dating of MinElev (e.g. elevation of highest flood deposit) and MaxElev (e.g. lowest elevation of flood-free historic site) values were based on geological, archaeological, and historical sources, whereas corresponding elevations were mostly based on geomorphological indicators such as a nearby terrace surface level. The collected markers mostly date in the first millennium CE. The largest floods in this period are representative for the millennial flood magnitude in Late Holocene to early medieval times (Toonen, 2013; Cohen et al., 2016).

For each model run, we determined for all 55 locations whether minimum and maximum elevations were exceeded by the simulated local peak water level. In a theoretical 'perfect match' situation, the flood patterns produced by a certain peak flow exceed all MinElev points, but do not exceed any MaxElev points. A too low peak flow results in water levels not exceeding MinElev markers, whereas a too high peak flow results in water levels exceeding MaxElev markers. For each simulated discharge wave, we averaged the percentages of exceeded MinElev and non-exceeded MaxElev values as a simple measure for the goodness-of-fit between modelled and observed water levels. In this way, we used the complete inventory of MinElev and MaxElev values in the ranking of input discharges, increasing the confidence in our analysis and reducing the effects of potential errors in the observational data. This led to an optimal estimate for the millennial flood magnitude of the Lower Rhine system in Late Holocene to early medieval times.

6.3 Results

6.3.1 Inundation depth and extent

The effect of topography on flooded area is extensive. In the present landscape setting, an extreme flood such as that of January 1995 only inundates the embanked floodplains, amounting to about 450 km^2, given that no dike breaches occur (Fig. 6.7A). In contrast, a similar flood inundates about 2,370 km^2 in the pre-embanked landscape setting (Fig. 6.7C). Conversely, inundation depths are much higher in the flooded area between the embankments in the present situation (Fig. 6.7B) than in the past situation when overbank flow was unconfined (Fig. 6.7D).

The water depths in the pre-embanked landscape are generally larger in the upstream part of the model area than in the downstream part (Fig. 6.7C; Fig. 6.8). This is because elevation differences decrease in downstream direction, resulting in wider and relatively lower floodplains (Fig. 6.1). This is especially clear in the delta apex where the floodplain divides, circa 50 km upstream of the channel bifurcations (Fig. 6.8).

Both water depth and inundation extent increase with discharge (Fig. 6.8; Fig. 6.9). Interestingly, the increase in inundation extent is nearly linear for extreme discharges (Fig. 6.9). Most of the model area consists of a terraced valley, where additional surfaces flood with each step in simulated discharge, although water depths at the newly flooded locations are small. This is different in the present embanked situation, where the inundation extent ceases to increase when all areas between

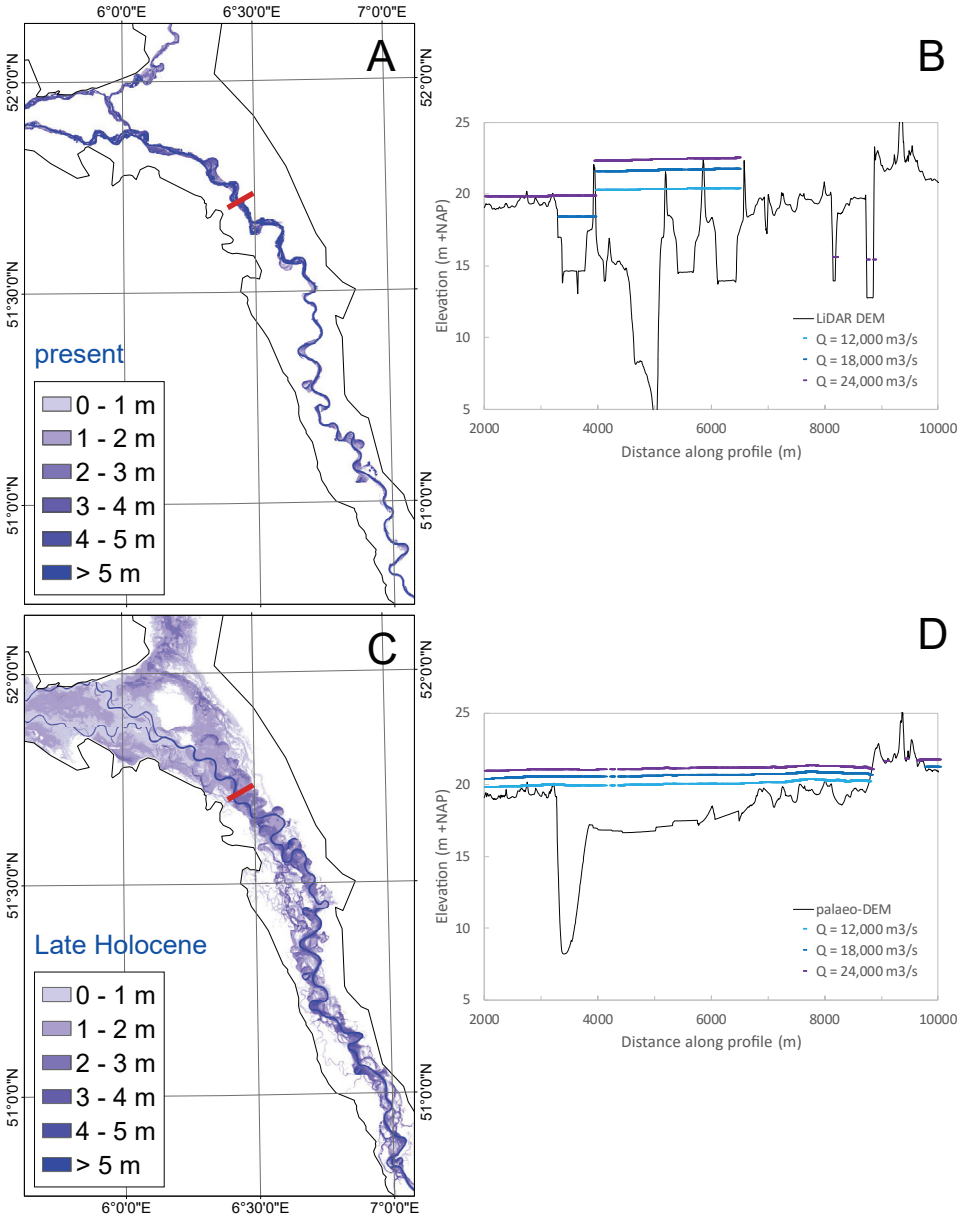

Fig. 6.7. Flooded area and water depths resulting from the 1995 discharge wave, in: (A, B) the present situation with modern DEM and roughness values and (C, D) the past situation with palaeo-DEM and reconstructed roughness values. The sections are located along profile 3 and show maximum flood levels resulting from discharge waves of 12,000, 18,000 and 24,000 m^3/s. The depth scales of the maps (A, C) are the same. The locations of the sections (B, D) are the same and indicated by a red bar in the maps. NAP (or NN) is the standard vertical datum in the Netherlands and Germany; 0 m is approximately mean sea level.

embankments are flooded (Fig. 6.7A). Despite this terrace effect, the graph does not appear stepwise (Fig. 6.9). The expected incremental trend is obscured due to the large size of the area (>4,500 km^2) with many small elevation differences and local terrace relief (Fig. 6.3).

When hydraulic roughness values are raised, the inundation extent increases (Fig. 6.9). The total spread in extent resulting from varying the roughness in all landscape classes between n_{min} and n_{max} is approximately 15%. This value is rather stable for different discharges, amounting to 15.5% for a peak discharge of 10,000 m^3/s and 14.5% for a peak discharge of 24,000 m^3/s (Fig. 6.9).

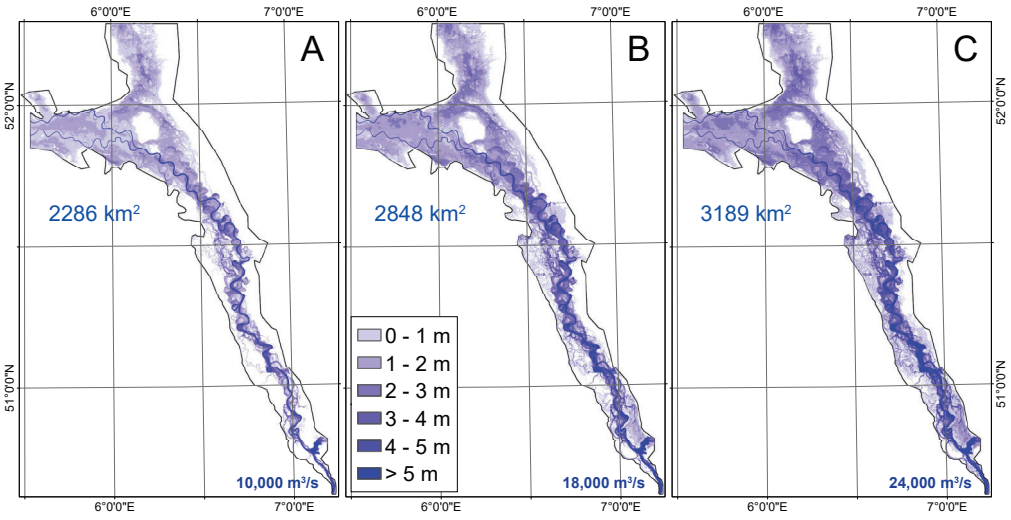

Fig. 6.8. Flooded area and maximum water depths for three different peak discharge scenarios: (A) 10,000 m^3/s, (B) 18,000 m^3/s and (C) 24,000 m^3/s. The depth scale is the same for all plots. The km^2 values inside the figures give the inundation extents of the different scenarios, which are plotted in Fig. 6.9.

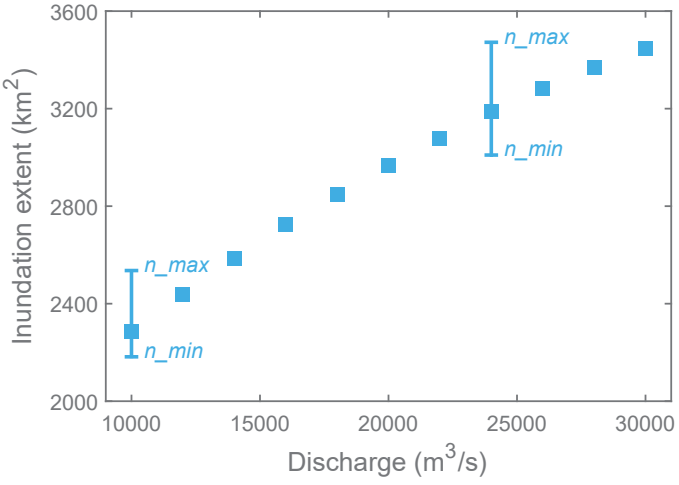

Fig. 6.9. Inundation extent plotted against peak discharge. The uncertainty bands at peak discharges of 10,000 and 24,000 m^3/s show results with all roughness classes set to minimum and maximum Manning's *n* values.

6.3.2 Flood wave propagation

Simulated peak discharges in the pre-embanked landscape remain remarkably constant along the Lower Rhine (Fig. 6.10). Retention in upstream parts of the area is apparently small and balanced by the discharge contribution of tributaries, indicating that nearly the complete floodplain conveys water downstream. The rise in water levels with discharge is largest in the upstream part of the study area (Fig. 6.11), which is related to the floodplain widening in downstream direction. An increase in peak discharge from 10,000 to 30,000 $m^{3/}s$ leads to a 1.5 to 3 m rise in maximum water levels in the river valley (Profiles 1 to 3 in Fig. 6.11), but less than 1 m in the delta (Profile 6 in Fig. 6.11). Both extent and depth of inundation exhibit slightly declining (concave down) increasing trends with discharge (Fig. 6.9; Fig. 6.11), because flow velocities increase as water depths across the floodplain rise.

In all model runs, the westward route in the delta (Waal and Nederrijn rivers and associated floodplain) carries more water than the northward route (IJssel valley). The division ratio is approximately 2:1 for a 10,000 m^3/s input discharge wave, but reduces to approximately 3:2 for 18,000 m^3/s (Fig. 6.10). For discharges lower than 10,000 m^3/s (not the focus of this study), an increasingly larger share of the flood water takes the westward route. After approximately 6,000 m^3/s enters the model area at the start of the modelled time period in the 18,000 m^3/s run, only one-fifth of total discharges flows northward (Fig. 6.10). The Q-h curve in the upstream part of the westward route (Profile 4 in Fig. 6.11; 'Gelderse Poort') is similar to those in the upstream (Profile 5 in Fig. 6.11; 'Oude IJssel') and downstream (Profile 7 in Fig. 6.11; 'IJssel') parts of the northward route. However, in the downstream part of the westward route (Profile 6 in Fig. 6.11; 'Betuwe'), the Q-h curve deviates and the rise in water level with discharge is significantly lower, owing to widening of the delta plain.

6.3.3 Peak discharge values

The difference between pairs of MinElev and MaxElev values is about 3 to 5 m in the Lower Rhine valley and about 1 to 2 m in the delta (Supplementary Table). The elevations of the flood

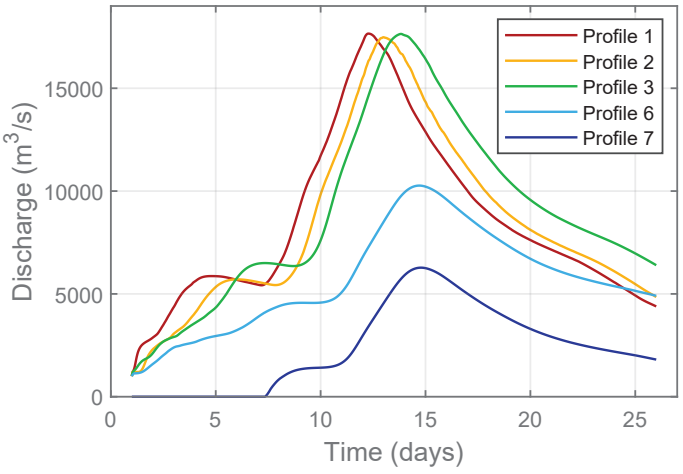

Fig. 6.10. Flood wave propagation in the pre-embanked situation. The graph shows the discharge that passes through the model area at different profile locations, for an initial peak discharge of 18,000 m^3/s. The profile locations are indicated in Fig. 6.1.

level markers roughly exhibit an overall downstream gradient of 0.25 m/km measured along the valley axis (Fig. 6.12). The data show a large amount of spread, reflecting the variety of sources and uncertainty in their relation to palaeoflood levels (Supplementary Table). Somewhat in line with the observational data, the simulated water levels for large (10,000 m^3/s) and extreme (30,000 m^3/s) discharges differ in general by about 2 to 3 m in the upstream part of the study area and by about 1 to 2 m in the downstream part (Fig. 6.12). This indicates that water levels are less sensitive to discharge in the downstream and delta parts of the study area, which is attributable to the wider floodplain in these areas.

The large spread in the observational data implies that for a simulated discharge some MaxElev values are already exceeded whereas some MinElev values are not (Fig. 6.12). For example, around Düsseldorf several MaxElev values plot below the model results of the 10,000 m^3/s simulation. These markers mostly derive from 'flood-free' terrace levels (Supplementary Table), which apparently at this location may not actually represent a non-exceeded elevation for the very largest floods that occurred. On the other hand, the MinElev values at some other sites plot disproportionally high, for example near Arnhem (Fig. 6.12), where archaeological observations provided flood markers (Supplementary Table). Despite these uncertainties, we still trust the robustness of the comparison step in our approach as it employs the complete inventory consisting of a large amount of markers obtained over a large area and derived from various sources and various types of sources.

Obviously, the larger the discharge, the more elevation markers are exceeded by simulated water levels. Ideally, for the maximum flood that occurred, all MinElev values would plot above the modelled-observed 1:1 line and all MaxElev values below it (Fig. 6.13). However, this result is complicated by the spread in elevation marker data and by the relatively small sensitivity of water level to discharge, especially in the downstream part of the study area, and presumably also by inaccuracies and simplifications in model input and numerical calculations. For the smallest simulated extreme discharge (10,000 m^3/s), the flood water levels already exceed more than half

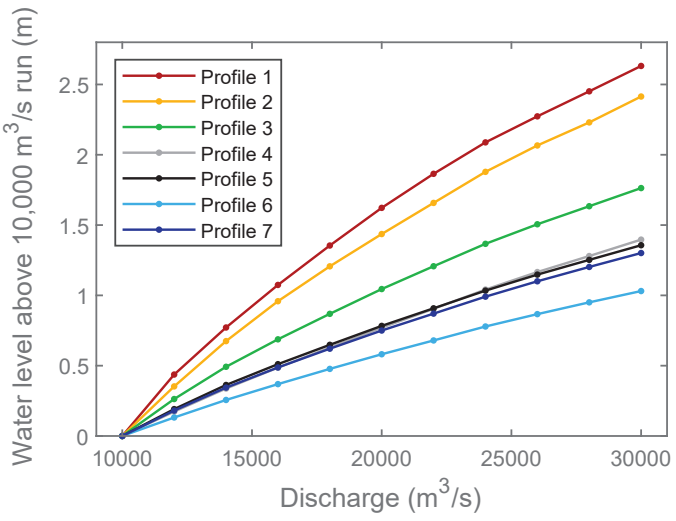

Fig. 6.11. Maximum water depths, averaged over each profile, for the different input discharges. The data are plotted relative to the water level reached in the 10,000 m^3/s run, which is about 10 m above the channel bottom in profiles 1, 2, 3 (Lower Rhine valley), 4 and 6 (westward route in delta) and about 2 m above the valley centre in profiles 5 and 7 (northward route in delta). The profile locations are indicated in Fig. 6.1.

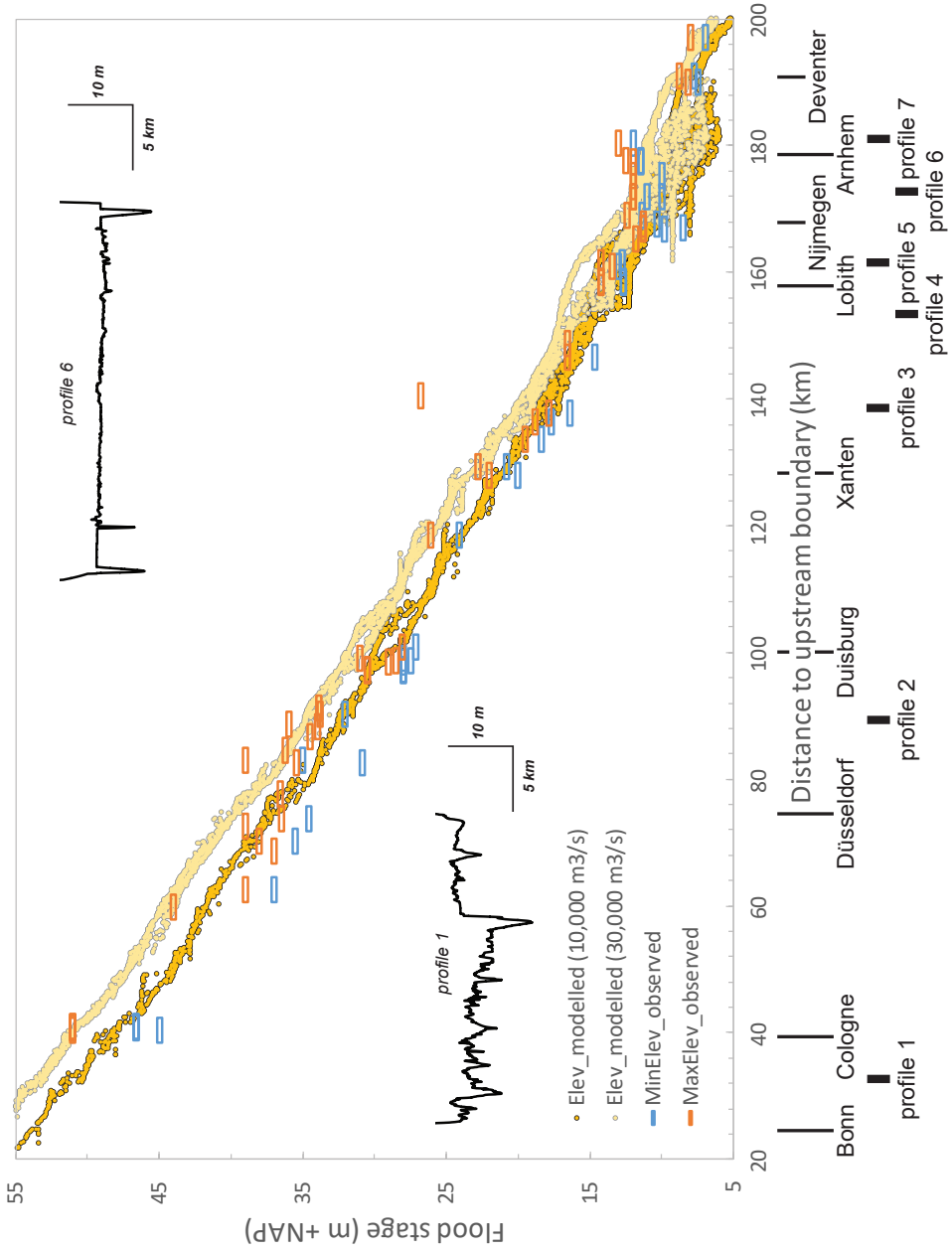

Fig. 6.12. Longitudinal profile of the study area with minimum and maximum flood levels extracted from observational data (blue and orange rectangles) and modelled output for the 10,000 and 30,000 m^3/s palaeoflood simulations (yellow with black and light yellow with grey data points). The flood levels in the model output were read from 10,000 randomly distributed points across the study area. NAP (or NN) is the standard vertical datum in the Netherlands and Germany; 0 m is approximately mean sea level.

MinElev values, but hardly any MaxElev values (Fig. 6.13A). This indicates that the lower end of our simulations realistically occurred. For the largest simulated discharge (30,000 m^3/s), the flood water levels exceed all but a few MinElev and MaxElev values (Fig. 6.13B), indicating that the upper end of our simulations surpasses the largest floods that actually occurred in the Late Holocene.

To determine which simulated discharge best matches the observational data, we calculated the percentages of exceeded MinElev and non-exceeded MaxElev values for each simulation, and used the average of these as a measure for the goodness-of-fit between modelled and observed water levels. This combined value peaks at a discharge of 14,000 m^3/s and drops considerably above 18,000 m^3/s (Fig. 6.14). Thus, our results suggest a millennial flood magnitude around 14,000 m^3/s. Simulations with larger input discharges increasingly exceed the upper limits defined by observational data, and our results strongly suggest that floods exceeding 18,000 m^3/s did not occur in the period under investigation.

6.4 Discussion

6.4.1 Late Holocene flooding patterns in the Lower Rhine valley and upper delta

Comparing flood simulations for past and present landscape settings allows to quantify combined effects of landscape changes and engineering impacts on flood characteristics (Bronstert et al., 2007; Remo et al., 2009). In the past, discharge wave propagation along the undivided Lower Rhine river took circa two days (Fig. 6.10), which is remarkably similar to present floods (Hegnauer

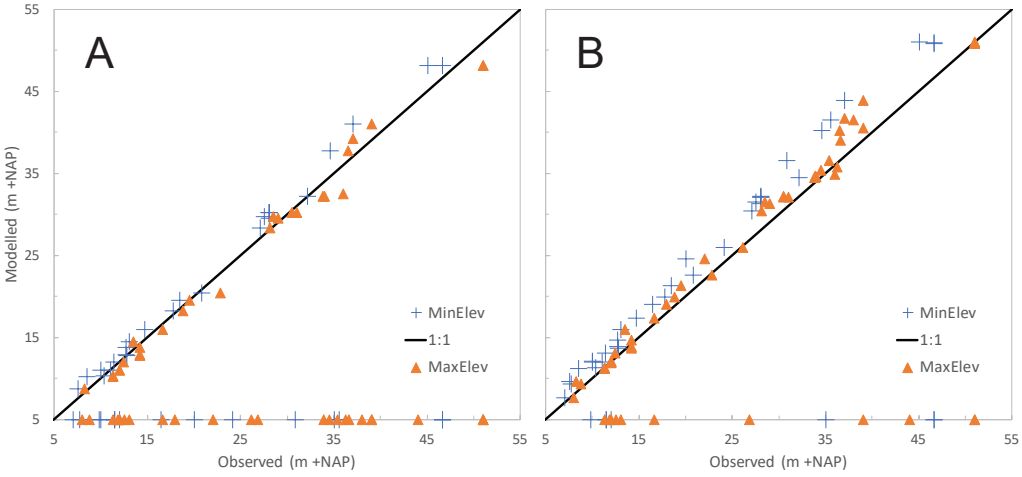

Fig. 6.13. Observed versus modelled palaeoflood levels for input discharges of (A) 10,000 m^3/s and (B) 30,000 m^3/s. The observed MinElev and MaxElev values are provided in the Supplementary Table. The symbols plotted on top of the x-axis indicate non-flooded locations. NAP (or NN) is the standard vertical datum in the Netherlands and Germany; 0 m is approximately mean sea level.

et al., 2014; Serinaldi et al., 2018). Large amounts of water flowed over the floodplain (Fig. 6.7, Fig. 6.8), but did not cause a downstream decrease in peak discharge up to the delta (Fig. 6.10), because floodplain connectivity was high (van der Meulen et al., 2020). At present, upstream flooding can reduce the discharge peak as flood water is stored in embanked areas with up to 4,000 m^3/s between Bonn and Wesel for extreme floods (>12,000 m^3/s; Hegnauer et al., 2015). Peak flow attenuation in the main river channel reduces the risks along downstream reaches (Lammersen et al., 2002; te Linde et al., 2010; Skublics et al., 2016). Although the floodplains along the Lower Rhine are currently seen as retention basins in flood risk management, these areas hardly served as such in the past situation and instead contributed to discharge routing.

In the Lower Rhine delta apex, the floodplain splits into two distributive systems (Fig. 6.1), resulting in a larger area for floodwater dispersal than in the Lower Rhine valley. In the present situation (Fig. 6.7A), the water diverges where the river bifurcates, close to Lobith. However, in the past situation (Fig. 6.7C), floodwater diversion occurred considerably further upstream, close to the city of Wesel. Current river management in the Netherlands mainly accounts for water entering the country near Lobith, but potential dike breaches in the German-Dutch border region and consequent floodwater diversion upstream of the river bifurcation can greatly affect the discharge distribution of the Rhine river branches (Parmet et al., 2001; te Linde et al., 2011; Bomers et al., 2019b). Our palaeoflood simulations underline this often overlooked importance of the delta apex area in flood risk analyses.

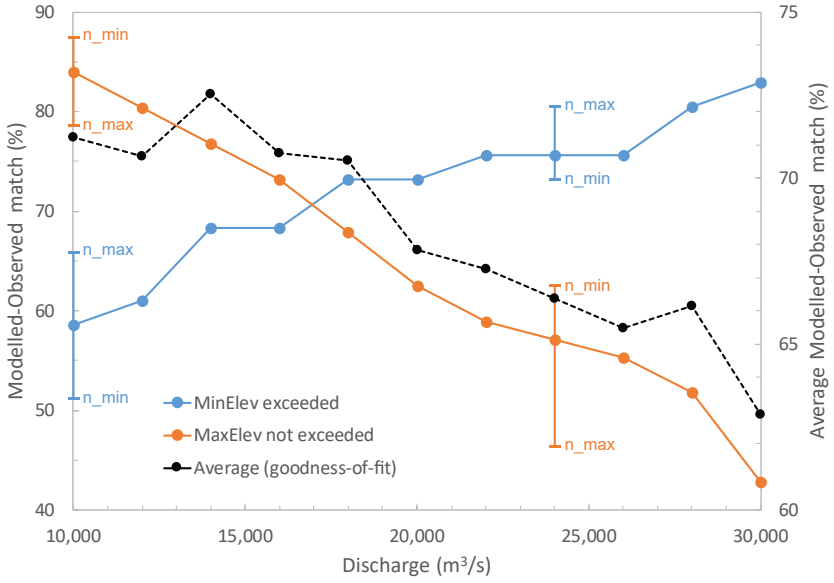

Fig. 6.14. Number of exceeded minimum and non-exceeded maximum elevation markers for each input discharge. The average of the two values is given by the dotted line, plotted on the secondary axis. The uncertainty bands at 10,000 and 24,000 m^3/s are derived from the model runs conducted with all roughness classes set to minimum and maximum Manning's *n* values (Table 6.1).

6.4.2 Palaeoflood magnitudes in the Lower Rhine valley and upper delta

Our 'inverse modelling' approach has enabled us to translate geological, archaeological and historical data on past flood levels into discharge values (Fig. 6.2; Figs. 6.12 to 6.14). Comparison of the palaeoflood simulations with observational data suggests a Late Holocene to early medieval millennial flood magnitude lower than 18,000 m^3/s, most probably around 14,000 m^3/s. This value is larger than any measured flood in the instrumental record (approximately 12,000 m^3/s in 1925-1926 CE). Accordingly, a peak discharge of 14,000 m^3/s is our best estimate for the geologically-recognised event in 785 CE (Toonen, 2013; Cohen et al., 2016) as well as for the flood cluster episode (cf. Toonen et al., 2017) that is dendrologically identified (Sass-Klaassen and Hanraets, 2006; Jansma, 2020) and that is thought to have initiated the IJssel northward deltaic branch in the sixth to seventh century CE (Makaske et al. 2008; Cohen et al., 2009; Groothedde, 2010). Note that the IJssel river channel is absent in the palaeo-DEM and model schematisation, as it had not matured before late medieval times (circa 1100 CE).

In late medieval times, the sedimentary record reveals one event of greater apparent magnitude than any in the millennia before (Toonen, 2013; Cohen et al., 2016). This event is linked to the year 1374 CE, which is also recognised in historical sources as a year of extreme water levels and major flooding damage along the Lower Rhine (Weikinn, 1958; Gottschalk, 1971; Buisman, 1996). A cross-sectional calculation of the 1374 CE event near Cologne by Herget and Meurs (2010) resulted in an estimated peak discharge of almost 24,000 m^3/s (18,800 $m^3/s < Q < 29,000$ m^3/s). Our findings suggest that only the very lower end of that estimate may be realistic, even though the event is outside the period covered by our simulations as it postdates embankment in downstream parts of the study area. Future reconstruction and modelling efforts are underway to specifically address the magnitude of the 1374 CE flood.

In the study area, embankments and other river management works are currently designed to accommodate peak discharges with recurrence times varying from hundreds to thousands of years, with differences between German and Dutch safety standards (te Linde et al., 2011; Hegnauer et al., 2015). The associated peak discharge has been set to 16,000 m^3/s at Lobith after the Lower Rhine flood of 1995 (Chbab, 1996). Although this value is subject of discussion and the newly adopted risk approach no longer identifies a single peak flow as standard (Deltacommissie, 2008; van Alphen, 2016), the design discharges in the German-Dutch border region exceed our estimate of 14,000 m^3/s for the millennial flood in the Lower Rhine river system. However, this does not necessarily imply that the current flood protection standards are too high, because the safety recurrence period set for some dike sections exceeds the time period spanned by the Late Holocene. Furthermore, changes in landscape significantly affect discharge routing (Section 6.4.1) and likely influence the magnitude of peak discharges. In addition, our methods cannot account for the aggravating effects of future climate change on the magnitudes and recurrence times of millennial floods.

6.4.3 Additional applications of model output

The model output supports our understanding of geological and geomorphological characteristics of the study area. For example, the coarsening of the river sediment since the onset of embankment (Frings et al., 2009) can be explained by the larger water depths and flow velocities that arise when

flood waters are concentrated between embankments (Fig. 6.7). The principle of constraining simulated discharges by observational data such as flood deposits can be applied the other way around, i.e. the model output provides the potential extent of Rhine flood deposits. For example, a Late Holocene clay cover is expected at topographic levels about 1 m below the maximum water level in the 14,000 m^3/s (millennial flood) simulation. Future modelling efforts may incorporate sediment transport and morphological processes to explain overbank deposition patterns in the natural landscape setting, such as oxbow lake infilling (Toonen et al., 2012; Ishii and Hori, 2016) and natural levee formation (Pierik et al., 2017; Johnston et al., 2019). However, modelling floodplain sedimentation in detail is largely limited to local studies for present landscape situations (Middelkoop and van der Perk, 1998; Nicholas et al., 2006; Thonon et al., 2007).

The palaeoflood model can contribute to palaeoecological research as vegetation types are related to number of inundation days per year in lowland river areas (van Oorschot, 2017; Gouw-Bouman et al., in prep.). Resulting land cover reconstructions may in turn be used to iteratively improve the currently oversimplified distribution of roughness classes (Fig. 6.4). Varying the roughness values did not introduce excessive uncertainty (Fig. 6.9), which is similar in palaeoflood studies applying 1D models (Machado et al., 2017). More extensive sensitivity analyses (Abu-Aly et al., 2014; Papaioannou et al., 2016; Bomers et al., 2019a) may focus on changing the roughness values of individual classes independently, stochastically varying the distribution of land cover within different classes (P, DH, DL), or changing the spatial definitions of the classes (Table 6.1, Fig. 6.4). Such additions may not only improve the palaeoflood model, but also contribute to improved understanding of natural vegetation patterns and early historical land use in the Lower Rhine region.

Insights into past flood extents and maximum water levels are valuable to test hypotheses in archaeological and historical research, for example regarding the preservation of auxiliary forts of the Roman Limes (first century BCE to third century CE) in relative proximity to the Lower Rhine. Long-known major sites of the Roman military border including legionary camps and urban centres (e.g. Cologne, Neuss, Xanten, Nijmegen; Fig. 6.1) and the main connecting road were founded on terrains just outside floodable areas (thus providing MaxElev values for this study; Supplementary Table), which is similar in other parts of the Roman Empire (Obrocki et al., 2020; O'Shea and Lewin, 2020). Smaller Roman military installations including fortlets and watchtowers (e.g. Haus Buergel, Till-Moyland, Herwen) were located closer to the rivers. These sites are presently conserved within a top soil that incorporates flood deposits of post-Roman age (thus providing MinElev values for this study). Their archaeological significance and conservation are receiving increased attention in light of pending UNESCO cultural heritage status. Flooding may have been both a taphonomic factor affecting preservation and an archaeological factor affecting post-Roman land use and settlement continuity.

The upper delta and especially the Betuwe area (between the Waal and Nederrijn rivers) flooded rapidly in all palaeoflood simulations, before arrival of the discharge peak. This explains the habitation patterns that occurred in the first millennium CE, which were mostly limited to former natural levees (Pierik and van Lanen, 2019). Further, it illustrates the importance of 'zijdewendes' (local dikes perpendicular to the river), which were constructed already prior to dikes along the river and have continued to play a role in flood mitigation (van de Ven, 1993; Alkema and Middelkoop, 2005).

6.4.4 Modelling advancements in palaeoflood hydrology

Our study shows that upscaling palaeoflood reconstructions to multiple dimensions provides important information that cross-sectional or longitudinal approaches cannot resolve (Webb and Jarrett, 2002; Baker, 2008, Benito and Díez-Herrero, 2015). Models with a 2D component can account for spatial flow patterns, such as velocity and direction (Tayefi et al., 2007; Liu et al., 2015). Especially in a delta setting, the incorporation of multiple dimensions is crucial, as discharge diversions can otherwise not be properly resolved. Another aspect not incorporated by 1D models is that the maximum water level is rarely horizontal in a direction perpendicular to the main flow. The two-dimensional nature of flood flows may cause some deposits to be placed above the cross-sectional average water surface, resulting in an often ignored inaccuracy factor in palaeoflood studies (Benito and O'Connor, 2013). This offset is significant (up to 1 m; Fig. 6.7D) and thus relevant when comparing observational levels to simulated output (Fig. 6.12).

A major benefit of 1D–2D modelling compared to cross-sectional 1D analyses (Herget and Meurs, 2010; Toonen et al., 2013; Herget et al., 2014) is that not only the peak discharge, but also the shape of the discharge wave may be varied (Fig. 6.6). This is important in palaeoflood research, since hydrograph characteristics such as volume affect the flooding patterns and water levels (Vorogushyn et al., 2010; Bomers et al 2019c). Choosing a discharge wave requires identifying a shape that is representative for an extreme flood in the river system under study, as we did in Section 6.2.3.

Besides the reconstructed landscape and selected hydrograph, future research may focus on the resolution and shape of the model grid (e.g. Caviedes-Voullième et al., 2012; Costabile et al., 2020). We decided on an optimal coupled grid with 1D profiles in the rivers and 2D cell rasters over the floodplains. Comparable set-ups were used to model recent flood events of the Po river in 1951 (Masoero et al., 2013) and 2005 (Morales-Hernández et al., 2016), demonstrating good agreement between modelled and observed inundation extents and timing. Effects of different grid sizes and shapes may be tested in a meaningful way by further aligning the grid to geomorphological features (Fig. 6.5). Such detailed work, similar to the suggested studies into the floodplain geology of the area and human-landscape interactions related to past flood hydrology (Section 6.4.3), warrant abundant further research.

Due to its large size, the study area (Fig. 6.1) covers different geomorphological settings, which respond differently to extreme floods. An increase in discharge results in a larger water level rise in the valley than in the delta (Fig. 6.11). This is related both to the lowering of the gradient and to differences in cross-sectional morphology (visualised in Fig. 6.12). Because of this low sensitivity of water level to discharge, determining palaeoflood magnitudes from geological or historical observations alone, without the use of a two-dimensional model, is practically impossible in a delta setting. The results further indicate that geological-geomorphological, archaeological and historical inferences on past flood levels show a large range in values and may contain significant errors (Fig. 6.13), and thus cannot individually constrain palaeoflood magnitudes in alluvial settings. Instead, such analyses require a collection of many observational points, as we used in this study (Fig. 6.1; Supplementary Table). This again implies that accurately constraining palaeoflood magnitudes in lowland settings demands two dimensions, not only the hydraulic calculations but also the other steps in the 'inverse modelling' approach (Fig. 6.2), including the comparison between model output and observational data.

6.5 Conclusion

We substantially expand upon previous palaeoflood modelling approaches by making the step to spatially continuous 1D–2D coupled modelling of past floods in the large and dynamic Lower Rhine valley and upper delta. Major effects of landscape changes, notably anthropogenic elements, on flooding patterns necessitates reconstruction in palaeoflood modelling of lowland rivers. Moreover, 2D approaches account for variations in flood water levels in directions perpendicular to the main channel, significantly reducing the risks of incorrect correlations between observed flood markers and simulated flood levels, particularly for distal floodplain sites. In addition to resolving past floods, 2D palaeoflood modelling can substantially support further geological, archaeological, historical and palaeoecological studies.

A large discharge increase in the delta causes only a small increase in water level, which complicates the comparison between flood markers and model output. We have solved this issue by providing a large dataset (96 points at 55 locations) of various observational data, which do not indicate precise maximum flood levels, but exceeded or non-exceeded elevations at critical locations just within or outside of flooding range. According to our results, the largest floods of the Lower Rhine that occurred in the Late Holocene up to medieval times (before the first embankments) had a peak discharge lower than 18,000 m^3/s, with a best estimate of 14,000 m^3/s. This millennial flood magnitude is larger than the most extreme measured discharge in the instrumental record, but lower than the magnitudes accounted for in flood risk management of the modern, engineered Rhine.

Acknowledgements

This work is part of the research programme 'Floods of the Past, Design for the Future' with project number 14506, which is financed by the Dutch Research Council (NWO). We presented earlier versions of our results at FLAG 2018, Liège, and INQUA 2019, Dublin, and we thank everyone with whom we discussed our research following the talks at these conferences. In October 2019, we presented our results for a mixed Dutch and German audience at the Ministry for Infrastructure and Water Management of the Netherlands (Rijkswaterstaat, Arnhem), where we had useful exchanges with river managers from both countries. We thank Marjolein Gouw-Bouman for discussions on past vegetation patterns in the study area, which helped us to determine roughness classes and values. For general input and discussions on past floods of the Lower Rhine river, we thank Willem Toonen, Jürgen Herget, Roy Dierx, Ralph Schielen, and Suzanne Hulscher. Two anonymous reviewers and the ESPL editor are thanked for their constructive commentary.

Chapter 7

Synthesis

How many PhD students does it take to change a lightbulb? Only one, but it takes four years.

uncredited

7.1 Floods of the past

Determining magnitudes of past extreme floods is important, because it contributes to fluvial system understanding and flood risk assessments (e.g. Benito et al., 2020; Liu et al., 2020; St. George et al., 2020). Natural archives used for palaeoflood reconstruction are usually fluvial, although recently other types of archives have been explored such as speleothems and tree rings (e.g. Ballesteros-Cánovas et al., 2015; Denniston and Luetscher, 2017; Wilhelm et al., 2018; Jansma, 2020). However, when it comes to large rivers, such as the Rhine, fluvial sediments and historical records are most suitable to obtain past flood magnitudes (Wilhelm et al., 2019).

The majority of palaeoflood studies have focused on geomorphologically stable confined fluvial settings, altough the alluvial reaches of most rivers are more densely populated and more at risk to flooding. In such lowland areas, sediment records in floodplain lakes have provided frequencies and relative magnitudes of past floods (Werritty et al., 2006; Cremer et al., 2010; Jones et al., 2010; 2010a; Toonen et al., 2015; Minderhoud et al., 2016; Fuller et al., 2018; Munoz et al., 2018; Peng et al., 2019; Toonen et al., 2020). However, the recorded events have to be calibrated to more recent events in the same series to arrive at absolute discharge estimates, which introduces significant uncertainties. Moreover, flood series based on sedimentological indices cannot in themselves account for changes in the landscape context, which further complicates the extraction of absolute magnitudes from such records (see discussion in Toonen et al., 2020). The approach applied in this thesis circumvents both of these problems, as it includes landscape reconstruction, and quantifies past floods from reconstructed water levels similar to traditional palaeoflood research approaches developed in confined fluvial settings (e.g. Kochel and Baker, 1982).

According to a recent review of palaeoflood research, "the principal sources of error are (1) the assumption that present channel geometry represents the channel conditions at the time of flooding and (2) an underestimate of the palaeodischarge due to the unknown level of the floodwaters above the palaeostage indicator" (Benito and Díez-Herrero, 2015). In downstream lowland areas, such as the Lower Rhine valley and delta, these sources of error are even more problematic than in confined upstream reaches. Thus, both had to be extensively addressed in the *Floods of the Past, Design for the Future* project (Chapter 1). Since the first assumption of landscape stability certainly does not hold for the Lower Rhine region at time scales above a few decennia, I created detailed reconstructions of channel and floodplain geometry (Chapters 4 and 5). To address the second issue of water levels above depositional indicators of past floods, I obtained detailed constraints on flood heights from raised grounds in urban archaeological contexts (Chapter 2), and applied combinations of exceeded and non-exceeded elevations to constrain palaeoflood model output (Chapter 6).

7.2 Main findings

This thesis isolates the three research steps that are typical for quantitative palaeoflood studies, namely flood level reconstruction, landscape reconstruction, and discharge calculation. Each step is conducted to an unparalled extent for the large and dynamic Lower Rhine valley and delta (Fig. 1.1). A major innovation concerns the spatial coverage, as my research produced two-dimensional results in each step, whereas earlier studies (those involving flood level reconstructions as well as those based on proxy record time series) generally concentrate on only one or a few sites (see overviews in Wilhem et al., 2018; 2019; Benito et al., 2020; Toonen et al., 2020).

7.2.1 Flood level reconstructions

The first objective of this research was to determine the water levels reached during the largest floods of the Lower Rhine in Late Holocene to historic times. I used both natural and historical archives to achieve this. The thesis provides flood level inventories for the Late Holocene period up to the last millennium (about 50 locations spread across the Lower Rhine valley and upper delta; Chapter 6), for the millennial flood event in 1374 (about 10 locations spread across the Rhine delta; Chapter 2), and for the largest floods since the late sixteenth century (about 50 locations spread across the Rhine delta; Chapter 3).

Past flood levels can be obtained from various sources, depending on the targeted time period (Fig. 7.1). Instrumental measurement records provide direct observations of water levels, but only date back to around 1800 along the Lower Rhine and its distributaries, which is already far back in time compared to what is available for most other river systems. Historic water level measurements are often considered reliable (e.g. Toonen, 2015), but a comparison to flood mark elevations suggests that measured peak levels in the nineteenth century may be off by up to 1 m (Chapter 3). Presumably, the inaccuracies in measurement records are insignificant when applying yearly average water levels in hydrological analyses, but they should be taken into account when specifically extracting peak levels for analyses of extreme floods. Epigraphic marks not only serve as a check on measured water levels for the largest events, but also extend the record back in time by about two centuries (Fig. 3.23). Maximum water levels in the central delta gradually rose up to circa 1850 and then dropped, demonstrating a significant influence of river normalisation on flood levels.

In addition to measurement records and epigraphic marks, historical descriptions and geological or archaeological data can be used to determine past flood levels (Fig. 7.1). Major floods are, similar to other disasters, often mentioned in documentary sources such as chronicles and newspapers (e.g. Buisman, 1995–2019; Brázdil et al., 2006). These mentions are usually biased to large events and large river basins (e.g. Kjeldsen et al., 2014; Wetter et al., 2017), which works out well considering the focus of this thesis. Historical descriptions are only suitable for flood level identification when they describe the maximum water level with respect to a landmark, and the mentioned level may be unreliable (Chapter 2). Geological observations, on the other hand, provide objective indicators of past flood levels. However, deriving maximum water levels from flood deposits requires quantifying elevation differences between deposits and water surfaces, which is often uncertain and varies with hydraulic setting (e.g. House et al., 2002; Jarret and England, 2002; Benito et al., 2003; 2004; Guo et al., 2017). Based on medieval raised ground levels in archaeological stratigraphy, the elevation difference between the highest-occurring flood deposits and the maximum water surface at the time amounts to about 1 m in the Rhine delta (Fig. 2.5; Fig. 2.10). Furthermore, the uncertainty regarding this difference can be circumvented in modelling by applying both minimum (exceeded) and maximum (non-exceeded) elevations at multiple locations (Appendix C).

7.2.2 Landscape reconstructions

The second objective of this research was to reconstruct the landscape context in which past extreme floods occurred. The thesis provides realistic reconstructions of river morphology before normalisation in the Rhine delta (Chapter 4) and floodplain morphology before embankment in the Lower Rhine valley and upper delta (Chapter 5).

In this part of my research, I distinguished between the river (position and bathymetry) and the floodplain (topography), because these ask for disparate reconstruction strategies (Fig. 7.1). The interpolative techniques deployed for most of the floodplain (Fig. 5.5; Fig. 5.6) are of no use in reconstructing channel geometry. Furthermore, the timing of the main alterations differs between the river and the floodplain. The largest changes to the river channels that affected flow dynamics occurred in the nineteenth century, during the process of normalisation (e.g Kalweit et al., 1993; van Heezik, 2007; Hudson et al., 2008), while the largest changes to the floodplain that affected flow patterns occurred much earlier, in medieval times when the first embankments were constructed (e.g. van de Ven, 1993; Tol and Langen, 2000; Hesselink, 2002).

For the Rhine river branches in the Netherlands, the re-discovered nineteenth-century systematic depth measurement data enabled a reconstruction of the semi-natural bathymetry at unprecedented detail (Chapter 4). These results are essential to numerical simulations of historic flood events, as was demonstrated for the 1809 casus (Bomers et al., 2019). Importantly, the bathymetry was not only expressed as relative elevations with respect to the water surface, but also as absolute elevations with respect to NAP (Appendix B). For the Lower Rhine region in Germany, the recently available

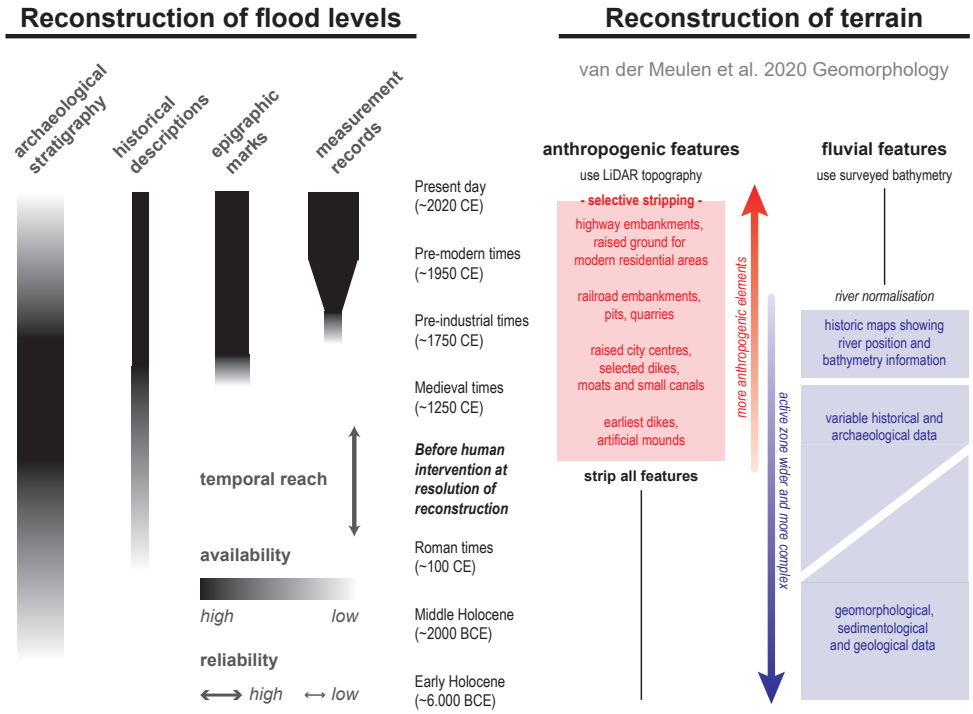

Fig. 7.1. Availability and reliability of sources for flood level reconstruction. Chapter 2 discusses flood levels obtained from archaeological stratigraphy and historical descriptions in more detail, and Chapter 3 discusses flood levels obtained from epigraphic marks and measurement records in more detail. The overview is plotted next to the temporal applicability of different palaeo-DEM construction methods, discussed in Chapter 5.

high-resolution LiDAR ground level DEM enabled the GIS operations required for palaeo-DEM construction (Chapter 5). The first operation was to strip all anthropogenic terrain elements from the DEM, including road and railroad networks, which often act as flow barriers in the landscape (e.g. Alkema and Middelkoop, 2005; Blanton and Marcus, 2009; Kumar et al., 2014). This was followed by restorative interpolations to the proximal floodplain and adding river position and bathymetry reconstructed from existing historical geographical and geological datasets (Chapter 5). Overall, the terrain reconstruction strategies strongly correlate to the geomorphological and hydrological properties of the landscape (Fig. 7.2).

The pre-embanked floodplain topography is generally very realistic in the palaeo-DEM (Fig. 5.9), but the channel bathymetry is somewhat more schematic. It does not include bars, although these were present in the Rhine up till the mid-nineteenth century (Fig. 4.5; Fig. 4.11). However, proper reconstruction of river bars in a medieval or older DEM is impossible, because the preservation of such features in the geological-geomorphological record is poor. For modelling purposes, bars may be implemented stochastically, placing them in the river in a pattern similar to the situation around 1835 (Chapter 4). In that case, the results would not serve as a scientific reconstruction, but as a first step in numerical analyses of palaeoflood model sensitivity to river landscape features.

7.2.3 Discharge calculations

The final objective of this research was to simulate the largest past floods in order to determine the associated discharge magnitudes. This was achieved in a modelling case study of an early nineteenth-century flood in the Rhine delta (Chapter 4) and in a comprehensive analysis of flood magnitudes in the Late Holocene before river embankment across the entire Lower Rhine valley and upper delta (Chapter 6).

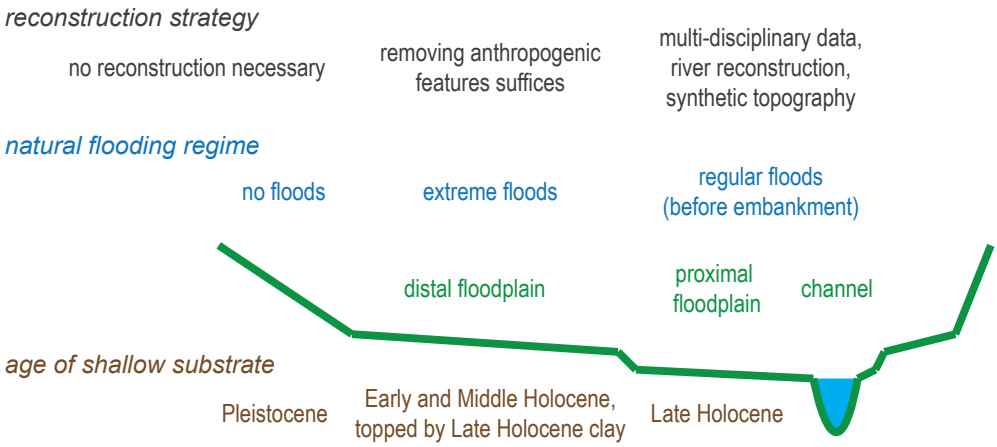

Fig. 7.2. Schematic cross-section of an alluvial river valley with terrain reconstruction strategies (above) related to the geological-geomorphological setting (below) and overall Late Holocene flooding regime (middle).

The study in Chapter 6 differs from 'traditional' palaeoflood modelling studies on several fronts due to the geomorphological context. Large and dynamic alluvial settings such as the Lower Rhine region are more demanding than incised river reaches in all steps of the palaeoflood research (red bars in Fig. 7.3), but are important to study given the nowadays major consequences of flooding in these often densely populated and flood-prone lowland regions (green bars in Fig. 7.3).

Especially in delta settings, palaeoflood hydraulic calculations require taking into account more than one dimension in order to resolve spatially complex overland flow patterns and discharge division over different river branches. In confined settings, 1D calculations suffice, although 2D models may still be beneficial (e.g. Denlinger et al., 2002).

Because the Lower Rhine valley and delta are geomorphologically dynamic and intensively utilized, resulting in both natural and anthropogenic alterations to the terrain, any palaeoflood calculations demand extensive landscape reconstruction (Fig. 7.3). Earlier palaeoflood studies that accounted for landscape instability limited their efforts to local cross-sectional reconstructions (e.g. Herget and Meurs, 2010; Toonen et al., 2013; Machado et al., 2017), whereas I created complete, i.e. spatially continuous, reconstructions for a large river system (Chapters 4 and 5).

An increase in discharge leads to a considerably larger rise in water level in a valley setting than in a delta setting (Fig. 6.12). The lowered sensitivity of water level to discharge complicates the assessment of palaeoflood magnitudes in laterally extensive fluvial settings (Fig. 7.3).

While the issues of landscape instability and model complexity can be solved by dedicated investments of effort and expertise, the issue of water level sensitivity is not 'solvable'. However, it can be accounted for by improving the precision of water level reconstructions (Chapter 2) and by incorporating large numbers of palaeoflood level observations (Chapters 3 and 6). Still, the issue of water level sensitivity is the main limiting factor to applying palaeoflood discharge calculations even farther downstream (Fig. 7.3).

7.3 Next steps

The palaeo-DEM construction and palaeoflood simulation in this study largely focused on the time period before embankment (Chapters 5 and 6). To simulate floods that occurred in more recent times, the research should involve reconstructing former dike dimensions and dike breach locations. By focusing on the pre-embanked period, I avoided this complicating factor. Still, I obtained peak flood levels for the period after embankment (1342, 1374, 1595 onwards) to enable future simulations of the largest historic floods in this period. Especially the 1374 flood event, with an estimated return period >>1000 years, calls for further quantification (Chapter 2).

The 1374 flood magnitude has been estimated at 23,800 m^3/s based on a cross-sectional calculation in Cologne (Herget and Meurs, 2010), although a value around 18,000 m^3/s has been deemed more likely (van Doornik, 2013; Toonen et al., 2016). Sedimentary records from oxbow lake deposits in the delta apex suggest an even lower peak magnitude of 'only' 15,500 m^3/s, although this lower value may in part be related to the more downstream position of the sites compared to the location of Cologne (Toonen, 2013). Based on all available evidence, the 1374 flood magnitude is rather poorly constrained between 14,000 m^3/s (Late Holocene millennial flood discharge; Chapter 6)

and 29,000 m^3/s (upper end of uncertainty band for the cross-sectional calculation in Cologne; Herget and Meurs, 2010). Future work involving a multi-dimensional palaeoflood analysis can provide a more accurate and precise estimate, using the maximum flood levels presented in Chapter 2 and the palaeoflood model set-up presented in Chapter 6, after adjustments to the landscape context presented in Chapter 5.

The outline for adapting the palaeo-DEM to other time periods (Fig. 5.12; Fig. 7.1) enables the construction of a late medieval DEM with relative ease. In addition, the late medieval river position can be extracted from early historic river maps (e.g. Fig. 4.1; Fig. 4.2; Fig. 4.3; Fig. 4.4; Overmars, 2020). However, additional model sensitivity tests may be prioritised before further landscape reconstruction. Chapter 6 provides suggestions for such tests (e.g. roughness distribution, hydrograph characteristics, model schematization). Simulations of the 1374 flood may apply a discharge wave shape conforming to historical mentions, which describe a prolonged period of high water levels with three peaks occurring in early January, late January, and mid-February (Buisman, 1996; Herget and Meurs, 2010). Furthermore, an optimal calculation of the discharge asks for as many local flood level reconstructions as possible. This too may be prioritised before extended landscape reconstruction. Building on the findings in Chapter 2, future archaeological research may identify additional medieval extreme flood signatures (thin flood deposits and thick raised grounds) in German and Dutch river cities along the floodplains of the Lower Rhine, leading to the large dataset that is required for model validation in a lowland setting.

7.4 Design for the future

Reconstructing floods of the past is not only of scientific importance, but also of societal relevance. Most importantly, it contributes to assessments of current and future flood risks. In fact, this was the primary motivation behind the research project (Chapter 1). Estimates of annual probabilities of extreme floods are often hampered by major statistical uncertainties, which can be reduced by incorporating past events (Cohen and Lodder, 2007; Toonen, 2013; Bomers, 2020).

Palaeoflood research has been applied in various river systems to test whether recent extreme events are of unique magnitude (e.g. Sanderock et al., 2005; Brázdil et al., 2006a; Sheffer et al., 2008; Blöschl et al., 2013; Elleder et al., 2013; Cloete et al., 2018). In the case of the Lower Rhine river, my research shows that the largest measured discharges have been exceeded in the past millennia (Chapter 6). This confirms earlier results based on sedimentary records from floodplain lakes in the delta apex (Toonen, 2013; Cohen et al., 2016; Toonen et al., 2016). Note however that maximum water levels of the most extreme floods in medieval times did not exceed water levels observed in the instrumental period in the central delta (Table 2.1). This apparent contradiction is caused by different flooding patterns arising from major changes in the landscape context (Fig. 2.11; Fig. 6.7), and stresses the importance of terrain reconstructions in lowland palaeoflood research.

The reference point for fluvial hydrological research and flood risk management in the Netherlands is the gauging station near the town of Lobith (e.g. Silva et al., 2001). From a palaeoflood perspective, this makes little sense. Instead, a point near the city of Wesel in Germany (~40 km upstream of Lobith) would be a better choice, because the floodplain divided near this city and so did the water that flowed over the floodplain during past extreme events (Fig. 5.11; Fig. 6.8). Furthermore, the shape and magnitude of the flood wave passing at Wesel still resembled that in

the upstream part of the valley (Fig. 6.10), which may allow for potential simplifications related to discharge wave attenuation in palaeoflood hydraulic analyses.

Flood protection standards are high across the study area, although the recurrence interval of the flood that is used to design embankments varies, with lower intervals for crucial dike sections in the delta (annual exceedance probabilities of 1/1,000 yr^{-1} and lower; e.g. Kind, 2013; Klijn et al., 2015; Slomp, 2016; Slootjes and van der Most, 2016; van Alphen, 2016). It is difficult to accurately assess the discharge of a flood with such a large return period. We do not want to underestimate this 'design discharge' for obvious reasons. However, overestimation is also undesirable, because the economic and other consequences (ecology, cultural heritage) of river management are high. While the choice of a recurrence interval largely derives from policy decisions, the determination of the associated discharge is an applied scientific problem. Since both the accuracy and the precision of frequency–magnitude relations can improve by incorporating historic floods (e.g. Parkes and Demeritt, 2016; Lam et al., 2017a; Schendel and Thongwichian, 2017; Bomers et al., 2019c; Reinders and Muñoz, 2021), my results may contribute to future efforts of constraining sizes and uncertainties of design discharges for the study area.

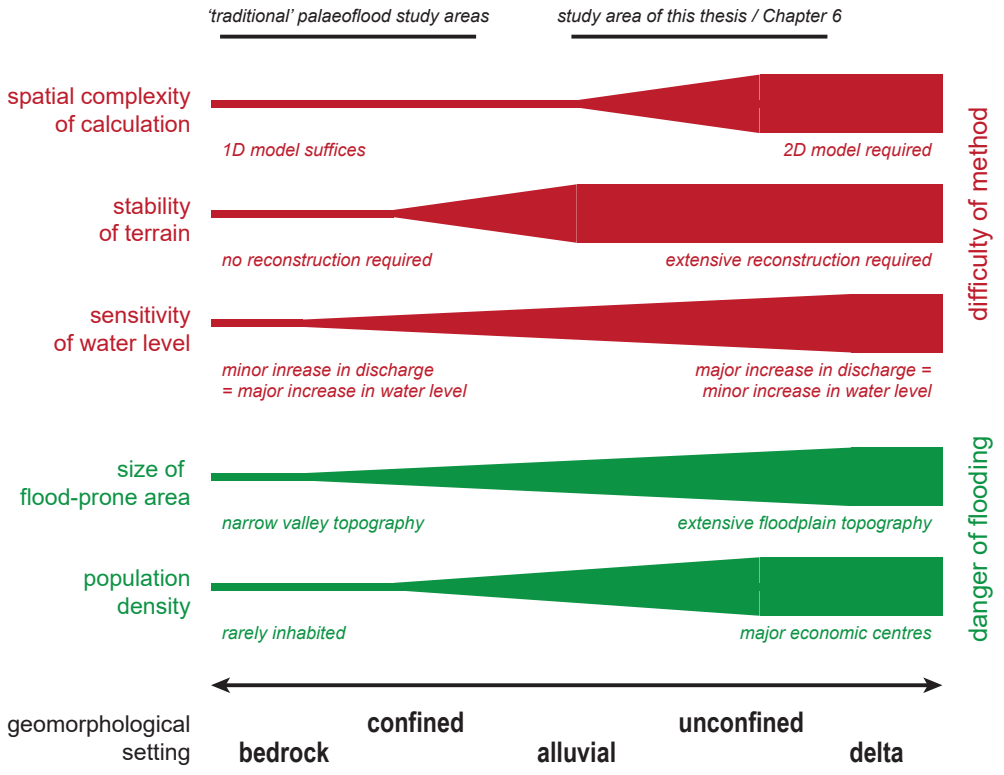

Fig. 7.3. Relative importance of palaeoflood modelling aspects for different geomorphological settings, ranging from typical upstream and narrow fluvial settings on the left-hand side of the figure to downstream and wide fluvial settings on the right-hand side.

Next to improving risk assessments, studies into past extreme floods (events that actually occurred instead of abstract extrapolations) can serve to raise public awareness. History shows that societal and political interest toward river floods mainly occurred directly following extreme events (e.g. van de Ven et al., 1995). This was also the case in medieval times, when grounds were raised in cities along the river shortly after an extreme flood (Chapter 2). Even in recent times, flood protection has been mostly reactive. This is illustrated by the Room for the River program that was set up directly following the high water events in late 1993 and early 1995 (e.g. Rijke et al., 2012; Straatsma et al., 2017; Berends et al., 2019). Improved understanding of past extreme floods may help to shift from a dominantly 'post-disaster' reactive approach to a more proactive approach, stimulating investments in research and flood protective measures during decades with no threats of extreme high water conditions. Public support can invigorate from the "common-sense recognition that what has actually occurred in the past could happen again" (Wilhelm et al., 2019). This may be achieved especially by visual results, such as the natural and anthropogenic flood marks (Chapters 2 and 3) and the palaeoflood model output (Chapter 6).

7.5 Concluding remarks

The central objective of my research was to quantify past extreme floods of the Lower Rhine. To approach this problem as good as possible, I integrated various methods and disciplines (Fig. 1.2). As a result, the thesis as a whole as well as some of the individual chapters combine physical geography and geology with archaeology and historical geography to answer an ultimately hydrological question. Multidisciplinarity is increasingly being recognized as very important in palaeoflood hydrological research (Woodward et al., 2010; Fontana et al., 2020a), and this thesis underlines that idea.

The successive chapters explore various methodologies and create multiple data products. The main products deriving from this thesis are flood level inventories (for Late Holocene to early medieval times based on geological data, for the extreme flood of 1374 based on archaeological data, for historic times based on epigraphic data) and landscape reconstructions (river bathymetry based on georeferenced historic data, floodplain topography based on geomorphological interpolations). The methods cultivated in this thesis are not only relevant to the Lower Rhine valley and delta but also to other lowland river areas. Specifying flood levels from archaeological stratigraphy (Chapter 2) has potential in urbanized areas along many rivers, provided that their banks have been occupied for at least hundreds of years. Collecting and measuring flood marks (Chapter 3) has already been done in many countries, but integrations for entire river systems are still rare. Reconstructing bathymetry from historic river maps (Chapter 4) is relevant to comprehend flow dynamics before major river engineering, but is only possible when such data are available, rendering this approach difficult or impossible for most other rivers. The methods for palaeo-DEM construction (Chapter 5) on the other hand are easier for most other regions, as human impact on floodplain morphology is almost nowhere as extensive as in the Lower Rhine valley and delta. The palaeoflood modelling (Chapter 6) is the final step to understand past flooding patterns and resolve palaeoflood magnitudes, which for lowland areas first of all requires an accurate representation of the past landscape. Hopefully, with the guidelines developed in this thesis (e.g. Fig. 5.4; Fig. 5.12; Fig. 6.2), such efforts are now within reach for other study areas.


Rheinstraße and Eisenbahnbrücke, Griethausen, Germany
January 2018
Q_{Lobith} ~ 7500 m^3/s


Rheinstraße and Eisenbahnbrücke, Griethausen, Germany
August 2020
Q_{Lobith} ~ 1000 m^3/s

Appendix A
Supplementary information to Chapter 2

In the south-central part of the medieval city centre of Arnhem, we have documented flood beds that were deposited in 1374, when the largest flood of the Lower Rhine river occurred in historic times and possibly in the entire Holocene (see Introduction of main text). The north-eastern part of the medieval city centre, characterized by a small valley formed by the Jansbeek brook tributary, is located at an elevation similar to the terrain in the south-central part (Fig. 2.3 of main text). Because of this topographic similarity, we also expect traces of the 1374 flood in this part of the city. To test this hypothesis, we thoroughly checked all field sketches of the largest archaeological excavation campaign conducted in this area for potential palaeoflood evidence. This excavation was carried out in 2003–2004 in the Musiskwartier (van der Mark et al., 2006), located in the northeast of Arnhem city centre at an elevation of about 13 to 14 m NAP.

From the field sketches (over 200 sheets with often multiple profile sketches), we selected all profiles showing a potential flood mark or specifically mentioning clay, which in the coarse sandy context of this site strongly suggests a fluvial origin (see Materials of main text). Then, we traced all artefacts collected from these locations to constrain the ages of the potential flood layers (Figs. A1a–5a). If such a layer dates to the late fourteenth century, matching with the most extreme Lower Rhine river flood, this strongly corroborates its tentative identification as a flood level. From the potential flood layers themselves, no finds were recovered, but underlying and overlying strata did yield artefacts, although usually only few pieces, resulting in relatively broad age ranges. For each profile, we constructed a simple Harris matrix to give the relative age of the potential flood layer with respect to surrounding strata (Figs. A1b–5b). Based on their stratigraphic context, appearance, and dating information, we determined for all potential flood layers if they represent an actual flood signature to be used in resolving the water level reached in 1374 (see Results of main text). The field sketches and the recovered artefacts from the Musiskwartier excavation campaign are stored in the depot of Arnhem municipality.

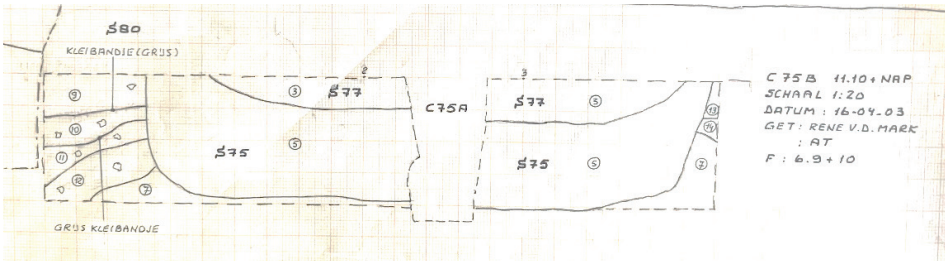

Fig. A1a. Pit 2, profile 75B. The two grey clay drapes ('kleibandjes'), positioned between layers 9 and 10 and between layers 10 and 11, may be flood deposits. RD: 190976, 443850.

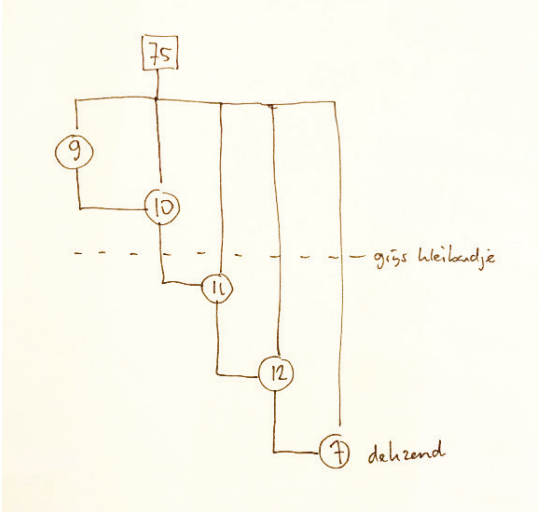

Fig. A1b. Available age constraints for the potential flood beds in Fig. A1a. Below these layers, no artefacts are recovered. Layer 7 is the subsurface consisting of Pleistocene sand. Above the layers, trace S75 (Fig. A1a) dates to circa 1500, based on two pieces of glass (Maigelein) collected from this layer. This trace further yielded two pieces of brick and four roof tile fragments.

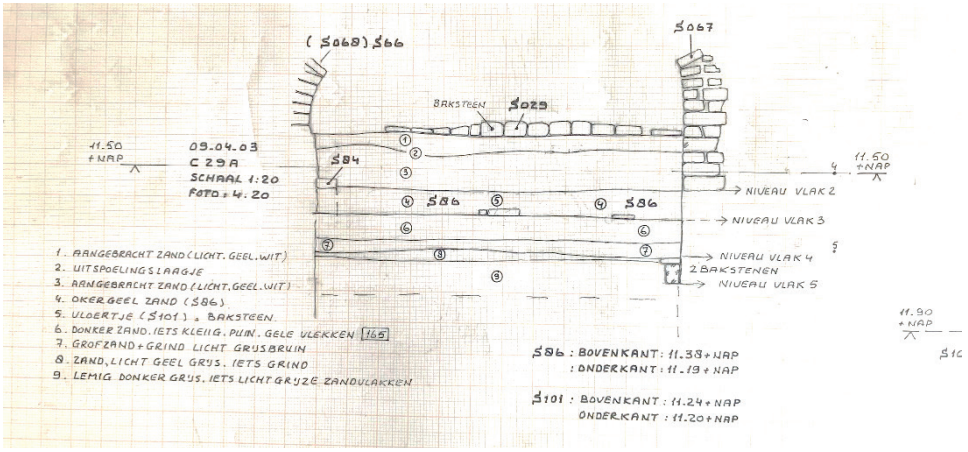

Fig. A2a. Pit 1, profile 29A. Layer 2 is a washed-out horizon ('uitspoelingslaag'), potentially indicating a flooded level at 11.6 m NAP. Layer 1 is raised ground ('aangebracht'), consisting of light-coloured sand (compare Fig. 2.6 of main text). RD: 190969, 443839.

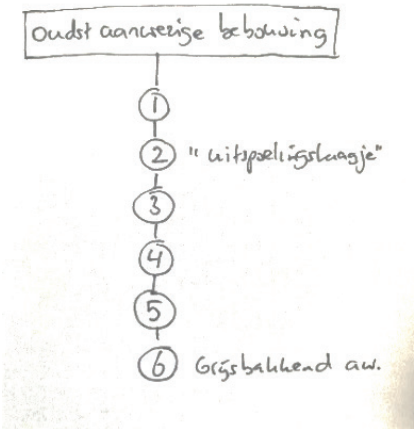

Fig. A2b. Available age constraints for the potential flood layer in Fig. A2a. Layer 6 is dated to 1250–1525, based on six shards of non-specific grey pottery collected from this layer. Layer 1 is dated to 1400–1425, based on the oldest documentation for the buildings on top of this level.

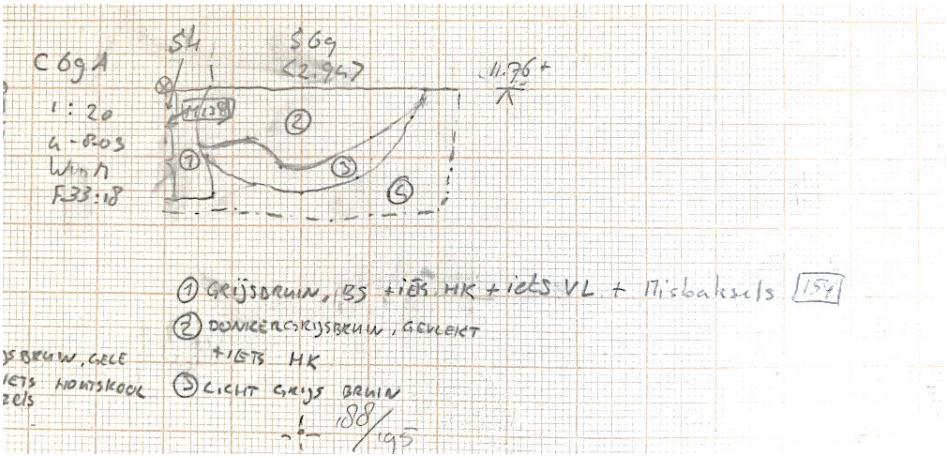

Fig. A3a. Pit 7, profile 69A. Layer 3 is described as light-coloured grey-brown. Based on its appearance (compare Fig. 2.7 of main text), this layer may be a flood deposit. RD: 191032, 443863.

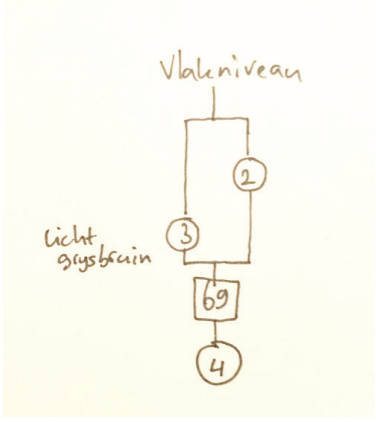

Fig. A3b. Available age constraints for the potential flood beds in Fig. A3a. Layers 2 and 3 fill in trace S69 (Fig. A3a), which is dated to 1280-1400 based on a pottery shard.

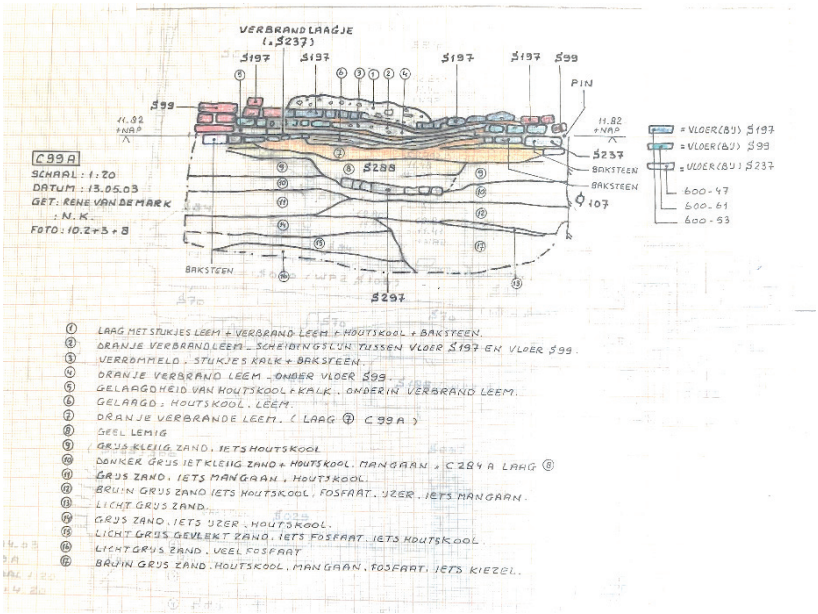

Fig. A4a. Pit 2, profile 99A. Layer 9 consists of grey clayey sand. Potentially, the clayey component in this layer originated from an extreme flood. RD: 190974, 443848.

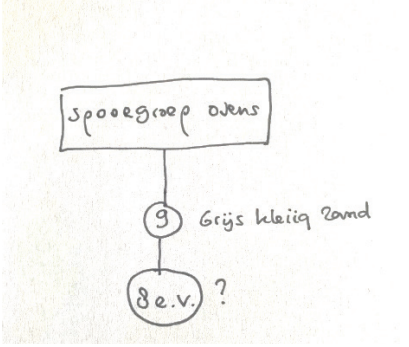

Fig. A4b. Available age constraints for the potential flood layer in Fig. A4a. Below layer 9, no artefacts were recovered. The material above layer 9 is related to ovens that were present at this site, identifiable from the brickwork and the abundance of burned loam and charcoal ('houtskool', Fig. A4a). This layer dates to 1575–1600, based on the oldest documentation for the buildings on top of this level.

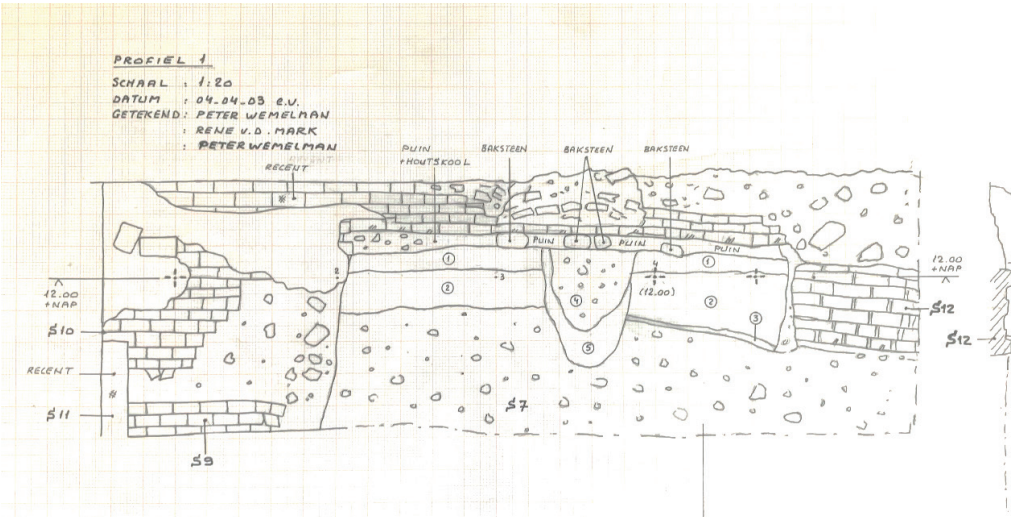

Fig. A5a. Pit 3, profile 1. Layer 3 consists of grey clayey sand. Potentially, the clayey component in this layer originated from an extreme flood. RD: 191022, 443866.

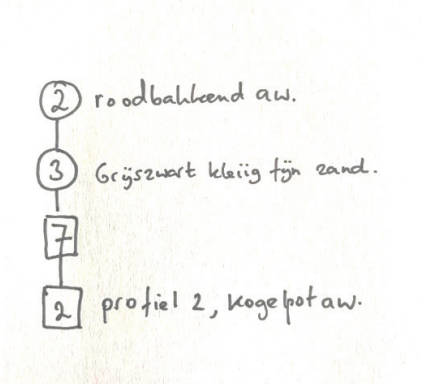

Fig. A5b. Available age constraints for the potential flood layer in Fig. A5a. The lower layer 2 dates to 700–1300, based on two non-specific spherical cooking pots ('kogelpotten') collected from this layer. The upper layer 2 dates to 1200–1900 based on two pieces of non-specific red pottery with glazing collected from this layer. Based on the glazing on the shards, a sharper albeit tentative date for this layer is the period 1400/1450–1650/1700. A brick well that was dug into trace S7 (Fig. A5a) dates to 1650–1700.

Appendix B
Supplementary information to Chapter 4

De waterstand van 26 Augustus 1812, welke in de verzameling van Hydrographische en Topographische waarnemingen van den Heer Lt.-Gen. KRAYENHOFF, aan onderscheidene peilschalen opgegeven is, plagt voor den middelbaren rivierstand aangenomen te worden, als nabij overeenstemmmende met den middelbaren zomerstand van den 1sten Mei tot den 31sten October, opgemaakt uit de dagelijksche waarnemingen gedurende 29 achtereenvolgende jaren.

Fig. B1. Excerpt of the registers belonging to the *Algemene Rivierkaart* providing the background of the 'Middelbare Rivierstand' (MR) to which the depth measurements were corrected.

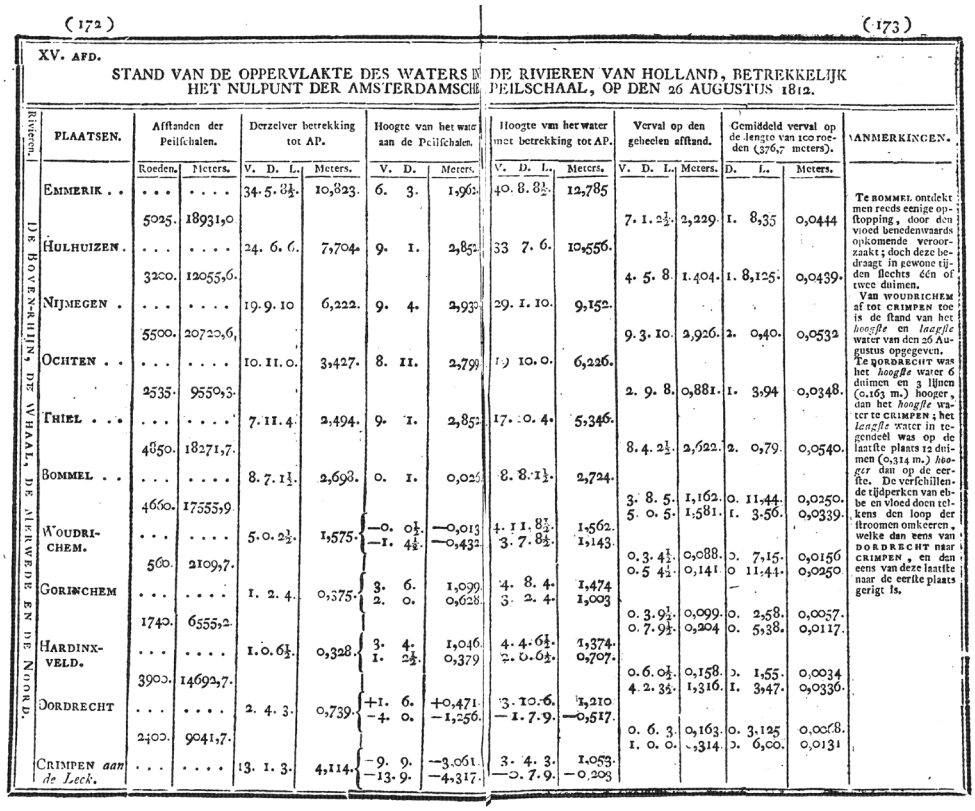

(172) (173)

XV. AFD.

STAND VAN DE OPPERVLAKTE DES WATERS IN DE RIVIEREN VAN HOLLAND, BETREKKELIJK HET NULPUNT DER AMSTERDAMSCHE PEILSCHAAL, OP DEN 26 AUGUSTUS 1812.

Rivieren.	PLAATSEN.	Afstanden der Peilschalen. Roeden.	Meters.	Derzelver betrekking tot AP. V. D. L.	Meters.	Hoogte van het water aan de Peilschalen. V. D.	Meters.	Hoogte van het water met betrekking tot AP. V. D. L.	Meters.	Verval op den geheelen afstand. V. D. L.	Meters.	Gemiddeld verval op de lengte van 100 roeden (376,7 meters). D. L.	Meters.	ANMERKINGEN.
DE BOVENRIJN, DE WAAL, DE NEERWEDE EN DE NOORD.	EMMERIK . .	. . .	. . . .	34. 5. 8½.	10,823.	6. 3.	1,962.	40. 8. 8½.	12,785					Te BOMMEL ontdekt men reeds eenige opstopping, door den vloed benedenwaards opkomende veroorzaakt; doch deze bedraagt in gewone tijden slechts één of twee duimen. Van WOUDRICHEM af tot CRIMPEN toe is de stand van het *hoogste* en *laagste* water van den 26 Augustus opgegeven. Te DORDRECHT was het *hoogste* water 6 duimen en 3 lijnen (0,163 m.) hooger, dan het *hoogste* water te CRIMPEN; het *laagste* water in tegendeel was op de laatste plaats 12 duimen (0,314 m.) *hooger* dan op de eerste. De verschillende tijdperken van ebbe en vloed doen telkens den loop der stroomen omkeeren, welke dan eens van DORDRECHT naar CRIMPEN, en dan eens van deze laatste naar de eerste plaats gerigt is.
		5025.	18931,0							7. 1. 2½.	2,229.	1. 8,35	0,0444	
	HULHUIZEN .	. . .	. . . .	24. 6. 6.	7,704.	9. 1.	2,852.	33 7. 6.	10,556.					
		3200.	12055,6.							4. 5. 8	1.404.	1. 8,125.	0,0439.	
	NIJMEGEN .	. . .	. . . .	19. 9. 10	6,222.	9. 4.	2,932	29. 1. 10.	9,152.					
		5500.	20720,6,							9. 3. 10.	2,926.	2. 0,40.	0,0532	
	OCHTEN . .	. . .	. . . .	10. 11. 0.	3,427.	8. 11.	2,799	19 10. 0.	6,226.					
		2535.	9550,3.							2. 9. 8.	0,881.	1. 3,94	0,0348.	
	THIEL . . .	. . .	. . . .	7. 11. 4.	2,494.	9. 1.	2,852.	17. 0. 4.	5,346.					
		4850.	18271,7.							8. 4. 2½.	2,522.	2. 0,79	0,0540.	
	BOMMEL . .	. . .	. . . .	8. 7. 1½.	2,698.	0. 1.	0,026	8. 8. 1½.	2,724.					
		4660.	17555,9							3. 8. 5.	1,162.	0. 11,44.	0,0250.	
										5. 0. 5.	1,581.	1. 3.56.	0,0339.	
	WOUDRICHEM.	. . .	. . . .	5. 0. 2½.	1,575.	—0. 0½.	—0,013	4. 11. 8½.	1,562.					
						—1. 4½.	—0,432	3. 7. 8½.	1,143.					
		560.	2109,7.							0. 3. 4½.	0,088.	0. 7,15.	0,0156	
										0. 5 4½.	0,141	0 11,44.	0,0250	
	GORINCHEM	. . .	. . . .	1. 2. 4.	0,375.	3. 6.	1,099	4. 8. 4.	1,474					
						2. 0.	0,628	3. 2. 4.	1,003					
		1740.	6555,2.							0. 3. 9½.	0,099.	0. 2,58.	0,0057.	
										0. 7. 9½.	0,204	0. 5,38.	0,0117.	
	HARDINX-VELD.	. . .	. . . .	1. 0. 6½.	0,328.	3. 4.	1,046	4. 4. 6½.	1,374.					
						1. 2½.	0,379	2. 0. 6½.	0,707.					
		3900.	14692,7.							0. 6. 0½.	0,158.	0. 1,55.	0,0034	
										4. 2. 3½.	1,316.	1. 3,47.	0,0336.	
	DORDRECHT	. . .	. . . .	2. 4. 3.	0,739.	+1. 6.	+0,471	3. 10. 6.	1,210					
						—4. 0.	—1,256.	— 1. 7. 9.	—0,517.					
		2400.	9041,7.							0. 6. 3.	0,163.	0. 3,125	0,0078.	
										1. 0. 0.	0,314.	0. 6,00.	0,0131	
	CRIMPEN *aan de Leek.*	. . .	. . . .	13. 1. 3.	4,114.	—9. 9.	—3,061.	3. 4. 3.	1,053.					
						—13. 9.	—4,317.	—0. 7. 9.	—0,208					

Fig. B2. Information in the *Hydrografische en topografische waarnemingen* by C.R.T. Krayenhoff, providing data of measurement stations in both MR and AP.

Table B1. Conversion of MR to AP using the data given in the *Hydrografische en topografische waarnemingen* by Krayenhoff combined with the early nineteenth-century river kms (profile locations) and measurement stations indicated on the *Algemene Rivierkaart*.

	Krayenhoff (used in Alg. Rivierkaart)		Read from georeferenced Alg. Rivierkaart	Krayenhoff (used in Alg. Rivierkaart)		Calculated from georeferenced Alg. Rivierkaart ...	... combined with data of Krayenhoff	
Location*	**Distance (r)**	**Distance (m)**	**Distance along Waal (Rhine km)**	**Level w.r.t. AP****	**Water level w.r.t. AP****	**Distance along Waal (m)**	**Slope (-)**	**Slope given by Krayenhoff ...**	**... / 376.7**
Emmerich	5025	18931	-16	10.823	12.785	18900	-1.18E-04	0.0444	1.18E-04
Hulhuizen	3200	12055.6	2.9	7.704	10.556	12900	-1.09E-04	0.0439	1.17E-04
Nijmegen	5500	20720.6	15.8	6.222	9.152	22100	-1.32E-04	0.0532	1.41E-04
Ochten	2535	9550.3	37.9	3.427	6.226	9600	-9.17E-05	0.0348	9.24E-05
Tiel	4850	18271.7	47.5	2.494	5.346	18300	-1.43E-04	0.054	1.43E-04
Zaltbommel	4660	17555.9	65.8	2.698	2.724	N/A	N/A	N/A	N/A

r = roeden

NB. 19th-century Rhine kms significantly differ from present Rhine kms

NB. Krayenhoff gives slope in r/km

*measurement locations ('peilschalen') indicated on Alg. Rivierkaart

**AP is assumed equal to NAP, although there are local dm-scale differences

colours:

read from Krayenhoff (national levelling campaign with focus on river water levels, 1797-1812), used in river mapping campaign (see e.g. Bosch and van der Ham, 2015 p. 56)

read from Goudriaan / van der Kun (national river mapping campaign, 1829-1866, Waal map sheets circa 1830-1835)

combined

Appendix C
Supplementary information to Chapter 6

Supplementary Table available at:
https://onlinelibrary.wiley.com/doi/full/10.1002/esp.5071

Direct download link:
https://onlinelibrary.wiley.com/action/downloadSupplement?doi=10.1002%2Fesp.5071&file=esp5071-sup-001-Table_S1.xlsx

Location					Palaeoflood level, exceeded			Palaeoflood level, non-exceeded		
Name	River km (di	Distance to ı	Latitude	Longitude	MinElev (m)	Type References	Notes	MaxElev (m)	Type References	Notes
Bonn	RH656	17104	50.745	7.100				59	A LGL UNESCO nomination files, 2019	LiDAR elevation, "The Bonna legionary fortress, which existed
Cologne - Deutz	RH688	40417	50.938	6.970	45	A LGL UNESCO nomination files, 2019	LiDAR elevation of ground surface near surviving wall fragme	51	A LGL UNESCO nomination files, 2019	Bridgehead fortress opposite of Cologne Praetorium, MaxEle
Cologne - Alter Markt	RH688	40761	50.939	6.960	46.6	A Höltken and Wagner, 2014; UNESCO nomination files for Low	Harbour quarters of Roman Cologne on bank of Rhine, MinEle	51	A Höltken and Wagner, 2014; LGL UNESCO nomination files, 20	Harbour quarters of Roman Cologne on bank of Rhine, MaxEl
Cologne - Praetorium	RH688	40793	50.939	6.959	46.6	A see Cologne Am Domhof		51	A Höltken and Wagner, 2014; LGL UNESCO nomination files, 20	Roman governor palace on flood-free terrace, also in use in m
Cologne - Am Domhof	RH688	40947	50.941	6.960	46.6	A Höltken and Wagner, 2014	Excavations identifying early medieval 'black earth' layers on	51	A see Cologne Praetorium	
Cologne - St. Maria ad Gradus	RH689	40982	50.941	6.961	46.6	A Höltken and Wagner, 2014	Romanasque church between Dom church and Rhine river, de	51	A Höltken and Wagner, 2014	Romanasque church between Dom church and Rhine river, de
Dormagen	RH712	59850	51.093	6.841				44	A LGL UNESCO nomination files, 2019	Roman fort Durnomagus, "situated on a flood-free terrace"
Monheim - Haus Buergel	RH717	62619	51.129	6.873	37	A LGL UNESCO nomination files, 2019	Terrace surface surrounding Roman fort with standing walls i	39	A LGL UNESCO nomination files, 2019	Terrace surface surrounding Roman fort with standing walls i
Holthausen	RH730	68625	51.174	6.820				37	G Zhou, 2000	Terrace level NT3-Suden (Ebinger Terrasse)
Neuss - Reckberg	RH733	70221	51.175	6.769	35.5	A LGL UNESCO nomination files, 2019	Fortlet, watchtower, Roman road on inland dune of Lateglaci	38	A LGL UNESCO nomination files, 2019	Fortlet, watchtower, Roman road on inland dune of Lateglaci
Neuss - Koenenlager	RH736	72502	51.184	6.726				39	A LGL UNESCO nomination files, 2019	Roman legionary fortress Novaesium, "located on a flood-fre
Hamm - Fiehe	RH737	73679	51.201	6.742	34.6	G Zhou, 2000	Clayey hm2 terrace, surface elevation ~ 0.4 m ploughed horiz	36.5	G Zhou, 2000	MaxElev based on nearby NT3 terrace with Parabraunerde so
Neuss - Weissenberg	RH740	77709	51.216	6.665				36.6	G Zhou, 2000	Terrace level NT2-Suden
Leuchtenberg	RH754	82499	51.285	6.731	30.85	G Zhou, 2000	Clayey hm2 terrace, surface elevation ~ 0.4 m ploughed horiz	35.4	G Zhou, 2000	MaxElev based on nearby NT3 terrace with Parabraunerde so
Bovert	RH752	82909	51.261	6.642	35	G Zhou, 2000	Terrace level NT2	39	G Zhou, 2000	Terrace surface with Parabraunerde soil
Kaiserwerth - Einbrungen	RH757	84535	51.310	6.748				36.25	G Zhou, 2000	Terrace level NT3-Norden (Ebinger Terrasse)
Lank-Latum	RH758	86625	51.311	6.678				34.5	G Zhou, 2000	Terrace level NT3-Insel at Lank-Latum
Holtumer Hof	RH760	88264	51.342	6.731				34	G Zhou, 2000	Terrace level NT3-Insel near Holtumer Hof
Krefeld - Gellep	RH761	88707	51.333	6.682				36	A LGL UNESCO nomination files, 2019	Roman fortress at battlefield site of 'Gelduba' 69 CE Batavian
Muendelheim	RH763	90344	51.352	6.692	32.1	G Zhou, 2000	Clayey hm1 terrace, surface elevation ~ 0.4 m ploughed horiz	33.8	G Zhou, 2000	MaxElev based on nearby NT3 terrace with Parabraunerde so
Krefeld - Botanical Garden	RH764	91159	51.333	6.604				33.9	G Zhou, 2000	Terrace level NT2-Norden
Werthausen (fortlet)	RH777	97036	51.422	6.711	28	A LGL UNESCO nomination files, 2019; subsidence corrections: I	Roman fortlet site "located on the former right bank of the Rh	30.5	A LGL UNESCO nomination files, 2019; subsidence corrections: I	Roman fortlet site "located on the former right bank of the Rh
Werthausen (brandgrab)	RH777	97257	51.424	6.708	28	G,H Scheller, 1957; subsidence corrections: Harnischmacher and 2	Truncated floodplain sequence overlying Roman cremation gr	30.5	G,H Scheller, 1957; subsidence corrections: Harnischmacher and 2	Truncated floodplain sequence overlying Roman cremation gr
Ruhrmuendung	RH780	98409	51.451	6.780	28	G,H Scheller, 1957	Scheller mentions 29.3 m +NN as present maximum flood lev	29	G,H Scheller, 1957	see MinElev, estimate +1 m
Kasslerfeld	RH779	98672	51.443	6.734	27.5	G,H Scheller, 1957	Scheller cites and reproduces cross-sections measured in 190	28.5	G,H Scheller, 1957	Scheller cites and reproduces cross-sections measured in 190
Moers - Asberg	RH778	99111	51.432	6.670	28	A LGL UNESCO nomination files, 2019	Roman fort "situated on the flood-free left bank of the Rhine,	31	A LGL UNESCO nomination files, 2019	Roman fort ('castellum') from 1st cy CE, in late Roman times a
Muehlenfeld	RH781	100821	51.463	6.732	27.1	G,H Scheller, 1957	Scheller mentions 27.6 m +NN (read from the 1892 topograhi	28.1	G,H Scheller, 1957	Scheller mentions 27.6 m +NN (read from the 1892 topograhi
Alpen - Druept	RH807	118461	51.587	6.544	24.1	A LGL UNESCO nomination files, 2019; subsidence corrections: I	LiDAR elevation at Roman marching camp corrected for 20th-	26.1	A LGL UNESCO nomination files, 2019; subsidence corrections: I	LiDAR elevation at Roman marching camp corrected for 20th-
Wesel - Flueren	RH819	127873	51.684	6.564	20	A LGL UNESCO nomination files, 2019	Roman army camps on Germanic side of Rhine, earth works p	22	A LGL UNESCO nomination files, 2019	Roman army camps on Germanic side of Rhine, earth works p
Xanten	RH824	129397	51.669	6.450	20.8	A UNESCO nomination files for Lower German Limes, 2019	Roman city COLONIA ULPIA TRAIANA located on lower terrace	22.8	A LGL UNESCO nomination files, 2019	Roman city COLONIA ULPIA TRAIANA located on lower terrace
Vossekuhl upstream	RH830	133609	51.693	6.390	18.4	G Toonen et al., 2013	Middle Holocene minimum flood level of Toonen et al. (18.4 a	19.5	G Toonen et al., 2013	Middle Holocene maximum flood level of Toonen et al. (19.5
Vossekuhl downstream	RH832	136314	51.710	6.356	17.7	G Toonen et al., 2013	Middle Holocene minimum flood level of Toonen et al. (18.4 a	18.8	G Toonen et al., 2013	Middle Holocene maximum flood level of Toonen et al. (19.5
Kalkar - Bornsches Feld	RH836	137711	51.714	6.325	16.4	A LGL UNESCO nomination files, 2019	Roman fortress known as Burginatum, "The elements are situ	17.9	A LGL UNESCO nomination files, 2019	Roman fortress known as Burginatum, "The elements are situ
Kalkarberg	RH842	140493	51.730	6.286				26.8	A LGL UNESCO nomination files, 2019	LiDAR elevation at very foot of push-ridge complex, a few m b
Till-Moyland	RH848	146514	51.777	6.244	14.7	G,A Erkens et al., 2011; Drechsler, 2013; LGL UNESCO nomination	LiDAR elevation of Early Holocene terrace (NT3), hosting Rom	16.6	G Drechsler, 2013	Drechsler, 2013: "Der Platz auf einem hochwasserfreien Plate
Kleve - Qualburg	RH854	148760	51.778	6.179				16.6	G Erkens et al., 2011	LiDAR elevation of 'flood-free' terrace hosting Qualburg
Kleve - Keeken	RH863	158302	51.841	6.079	12.7	A same as Lobith Dorpsdijk		14.2	A same as Herwen	
Lobith - Dorpsdijk	RH861	158648	51.859	6.120	12.7	A Schabbink, 2006	Levee clay sedimentats below Lobith town dike	14.2	A same as Herwen	
Doetinchem - Waalse Water	RH860	160906	51.934	6.287	13	G Cohen et al., 2009	Geomorphological interpretation LiDAR relief: breach channe	13.5	G Cohen et al., 2009	Geomorphological interpretation LiDAR relief: aeolian dune la
Herwen	RH865	161466	51.881	6.099	12.8	G van Renswoude and van Kampen, 2019; pers. obs. (KMC)	Crest of medieval levee deposits + 1 m	14.2	A LGL UNESCO nomination files, 2019	Roman fort Carvium positioned on Late Holocene levee comp
Nijmegen - Circul van de Ooij	WA880	165173	51.841	5.892				11.8	G Willemse, 2019	Gravelly colluvium covered by recent (1926 CE) flood bed
Nijmegen - Waalkade Bastei	WA884	166795	51.849	5.870	9.8	G pers. obs. (KMC), pers. comm. (F. de Roode, municpal archaec	Riverine clay drape in otherwise colluvial and archaeological s	11.3	A de Roode, 2019; in prep.	Merovingian occupation of river bank below hillslope of Valkh
Nijmegen - Waalkade Rozengas	WA884	167108	51.850	5.864	8.5	G Teunissen, 1988; Teunissen, 1990; Cohen et al., in prep.	Washed-in debris at 7.5 m +NAP, +1 m reasonable water dep	11.3	A same as Nijmegen Waalkade Bastei	
Nijmegen - Lent	WA882	167559	51.860	5.876	10.3	A,G Heunks and van Hemmen, 2016; Heirbaut and Koot, 2016; Wi	Crest of crevasse splays / levee build-up, overlying a Roman-M	11.3	A same as Nijmegen Waalkade Bastei	
Keppel	IJ875	169079	52.000	6.235	11.4	G Cohen et al., 2009	Geomorphological interpretation LiDAR relief: breach channe	12.4	G Cohen et al., 2009	Geomorphological interpretation LiDAR relief: aeolian dune la
Drempt	IJ880	171886	52.009	6.168	11	G Cohen et al., 2009	Geomorphological interpretation LiDAR relief: breach channe	12	G Cohen et al., 2009	Geomorphological interpretation LiDAR relief: aeolian dune la
Doesburg - Beinum	IJ900	171990	51.996	6.122	10	A Fermin and van Straten, 2009	Early medieval wooden water wells preserved up to 10 m +NA	12	A,H Haans, 2008; Cohen et al., 2016	Resettlement to Doesburg centre after early medieval and lat
Doesburg - Centre	IJ902	173569	52.015	6.134				12	A,H Haans, 2008; Cohen et al., 2016	Top of raised ground above clay drapes
Velp -Velperbroekdrcuit	IJ883	175323	51.982	5.979	10	G Teunissen, 1990	Dated compacted sample at 8.8 m, overlain by 1.2 m clay	12	G Teunissen, 1960; Teunissen, 1990	LiDAR readings (floodplain - alluvial fan transition, verified by
Arnhem - Broerenstraat	NR883	177437	51.979	5.910	11.5	A,G pers. obs. (BvdM, KMC), pers. comm. (M. Defilet, city archaec	Clay deposits in otherwise anthropogenic stratigraphy + 0.5 m	12	A,G pers. obs. (BvdM, KMC), pers. comm. (M. Defilet, city archaec	Raised ground above clay deposits
Arnhem - Sint-Jansbeek	NR883	177722	51.982	5.910	11.5	A Baetsen and Zielman, 2020	Clay deposits in otherwise anthropogenic stratigraphy + 0.5 m	12.5	A Baetsen and Zielman, 2020	Raised ground above clay deposits
Heveadorp	NR890	180391	51.970	5.806	12	G Teunissen, 1960	Raised ground at very foot of push moraine ~ 0.5 m (Teunisse	13	G Teunissen, 1960	Raised ground at very foot of push moraine + 0.5 m
Gorssel	IJ935	189981	52.190	6.179	7.5	G Cohen et al., 2009, in prep.	Geomorphological interpretation LiDAR relief: breach channe	8.2	G Cohen et al., 2009, in prep.	Geomorphological interpretation LiDAR relief: aeolian dune la
Voorst	IJ935	191037	52.186	6.124	7.75	G Cohen et al., 2009, in prep.	Geomorphological interpretation LiDAR relief: breach channe	8.75	G Cohen et al., 2009, in prep.	Geomorphological interpretation LiDAR relief: aeolian dune la
Deventer	IJ943	196980	52.252	6.155	7	H,A Buisman, 1996	Lebuinus church original floor level estimate ~ 0.5 m	8	H,A Buisman, 1996	Lebuinus church original floor level estimate + 0.5 m

Type of information used to extract flood level: H = Historical, A = Archaeological, G = Geological

Not all sites have MinElev, but all have MaxElev, as this can be determined with relative ease and confidence from nearby sites in the absence of local direct information on (non-exceeded) flood level

References

Abu-Aly, T.R., Pasternack, G.B., Wyrick, J.R., Barker, R., Massa, D., Johnson, T., 2014. Effects of LiDAR-derived, spatially distributed vegetation roughness on two-dimensional hydraulics in a gravel-cobble river at flows of 0.2 to 20 times bankfull. Geomorphology 206, 468-482. DOI:10.1016/j.geomorph.2013.10.017

Alkema, D., Middelkoop, H., 2005. The influence of floodplain compartmentalization on flood risk within the Rhine–Meuse Delta. Natural Hazards 36, 125–145. DOI:10.1007/s11069-004-4545-8

Apel, H., Aronica, G.T., Kreibich, Z.A., Thieken, H., 2009. Flood risk analyses—how detailed do we need to be? Natural Hazards 49, 79–98. DOI:10.1007/s11069-008-9277-8

Arnaud, F., Sehen Chanu, L., Grillot, J., Riquier, J., Piégay, H., Roux-Michollet, D., Carrel, G., Olivier, J.M., 2020. Historical cartographic and topo-bathymetric database on the French Rhône River (17th–20th centuries). Earth System Science Data Discussions. DOI:10.5194/essd-2020-274

Arnaud-Fassetta, G., Carcaud, N., Castanet, C., Salvador, P.G., 2010. Fluviatile palaeoenvironments in archaeological context: Geographical position, methodological approach and global change – Hydrological risk issues. Quaternary International 216, 93–117. DOI:10.1016/j.quaint.2009.03.009

Baetsen, W.A., Zielman, G., (Eds.), 2020. Wat de nieuwe Sint Jansbeek boven water bracht: dood en leven in het Arnhemse verleden: archeologisch onderzoek Sint Jansbeek te Arnhem. RAAP report 4476.

Baker, V.R., 1987. Paleoflood hydrology and extreme flood events. Journal of Hydrology 96, 79–99.

Baker, V.R., Webb, R.H., House, P.K., 2002. The scientific and societal value of paleoflood hydrology. Ancient Floods, Modern Hazards: Principles and Applications of Paleoflood Hydrology. Water Science and Application 5, 1–19. DOI:10.1029/WS005p0001

Baker, V.R., 2008. Paleoflood hydrology: Origin, progress, prospects. Geomorphology 101, 1–13. DOI:10.1016/j.geomorph.2008.05.016

Balasch, J.C., Pino, D., Ruiz-Bellet, J.L., Tuset, J., Barriendos, M., Castelltort, X., Peña, J.C., 2019. The extreme floods in the Ebro River basin since 1600 CE. Science of the Total Environment 646, 645–660. DOI:10.1016/j.scitotenv.2018.07.325

Ballesteros, J.A., Bodoque, J.M., Díez-Herrero, A., Sanchez-Silva, M., Stoffel, M., 2011. Calibration of floodplain roughness and estimation of flood discharge based on tree-ring evidence and hydraulic modelling. Journal of Hydrology 403, 103–115. DOI:10.1016/j.jhydrol.2011.03.045

Ballesteros-Cánovas, J.A., Stoffel, M., St. George, S., Hirschboeck, K., 2015. A review of flood records from tree rings. Progress in Physical Geography 39, 794–816. DOI:10.1177/0309133315608758

Barriendos, M., Ruiz-Bellet, J.L., Tuset, J., Mazón, J., Balasch, J.C., Pino, D., Ayala, J.L., 2014. The "Prediflood" database of historical floods in Catalonia (NE Iberian Peninsula) AD 1035–2013, and its potential applications in flood analysis. Hydrology and Earth System Sciences 18, 4807–4823. DOI:10.5194/hess-18-4807-2014

Barriendos, M., Gil-Guirado, S., Pino, D., Tuset, J., Pérez-Morales, A., Alberola, A., Costa, J., Balasch, J.C., Castelltort, X., Mazón, J., Ruiz-Bellet, J.L., 2019. Climatic and social factors behind the Spanish Mediterranean flood event chronologies from documentary sources (14th–20th centuries). Global and Planetary Change 182, 102997. DOI:10.1016/j.gloplacha.2019.102997

Baubiniene, A., Morkunaite, R., Bauza, D., Vaitkevicius, G., Petrosius, R., 2015. Aspects and methods in reconstructing the medieval terrain and deposits in Vilnius. Quaternary International 386, 83–88. DOI:10.1016/j.quaint.2014.09.068

Bechert, T., 2007. Germania Inferior. Eine Provinz an der Nordgrenze des Römischen Reiches. Verlag Philipp von Zabern, Mainz am Rhein.

Begbie, D., Roberts, G., 2014. Bridging in the Second World War: an imperative to victory. Proceedings of the Institution of Civil Engineers-Engineering History and Heritage 167, 111–121. DOI:10.1680/ehah.13.00022

Benito, G., Sopeña, A., Sánchez-Moya, Y., Machado, M. J., Pérez-González, A., 2003. Palaeoflood record of the Tagus River (central Spain) during the Late Pleistocene and Holocene. Quaternary Science Reviews 22, 1737–1756. DOI:10.1016/S0277-3791(03)00133-1

Benito, G., Lang, M., Barriendos, M., Llasat, M.C., Francés, F., Ouarda, T., Thorndycraft, V.R., Enzel, Y., Bardossy, A., Coeur, D., Bobée, B., 2004. Use of systematic, palaeoflood and historical data for the improvement of flood risk estimation. Review of scientific methods. Natural Hazards 31, 623–643. DOI:10.1023/B:NHAZ.0000024895.48463.eb

Benito, G., Thorndycraft, V.R., 2005. Palaeoflood hydrology and its role in applied hydrological sciences. Journal of Hydrology 313, 3–15. DOI:10.1016/j.jhydrol.2005.02.002

Benito, G., O'Connor, J.E., 2013. Quantitative paleoflood hydrology. In: Shroder, J., Wohl, E., (Eds.). Treatise on Geomorphology 9, Fluvial Geomorphology, 459–474. DOI:10.1016/B978-0-12-374739-6.00250-5

Benito, G., Brázdil, R., Herget, J., Machado, M.J., 2015a. Quantitative historical hydrology in Europe. Hydrology and Earth System Sciences 19, 3517–3539. DOI:10.5194/hess-19-3517-2015

Benito, G., Díez-Herrero, A., 2015. Palaeoflood hydrology: Reconstructing rare events and extreme flood discharges. In: Schroder, J., Paron, P., Di Baldassarre, G., (Eds.). Hydro-Meteorological Hazards, Risks and Disasters. pp. 65–104. DOI:10.1016/B978-0-12-394846-5.00003-5

Benito, G., Macklin, M.G., Panin, A., Rossato, S., Fontana, A., Jones, A.F., Machado, M.J., Matlakhova, E., Mozzi, P., Zielhofer, C., 2015. Recurring flood distribution patterns related to short-term Holocene climatic variability. Scientific Reports 5, 16398. DOI:10.1038/srep16398

Benito, G., Harden, T.M., O'Connor, J.E., 2020. Quantitative paleoflood hydrology. In: Shroder, J., Wohl, E., (Eds.). Treatise on Geomorphology 9, Fluvial Geomorphology, 459–474. DOI:10.1016/B978-0-12-409548-9.12495-9

Berends, K.D., Straatsma, M.W., Warmink, J.J., Hulscher, S.J.M.H., 2019. Uncertainty quantification of flood mitigation predictions and implications for interventions, Natural Hazards and Earth System Sciences 19, 1737–1753. DOI:10.5194/nhess-19-1737-2019

Berendsen, H.J.A., (Ed.), 1986. Het landschap van de Bommelerwaard. Nederlandse Geografische Studies 10.

Berendsen, H.J., Stouthamer, E., 2000. Late Weichselian and Holocene palaeogeography of the Rhine–Meuse delta, the Netherlands. Palaeogeography, Palaeoclimatology, Palaeoecology

161, 311–335. DOI:10.1016/S0031-0182(00)00073-0
Berendsen, H.J.A., Stouthamer, E., 2001. Palaeogeographic development of the Rhine-Meuse delta, the Netherlands. Koninklijke Van Gorcum, Assen.
Bini, M., Rossi, V., Amorosi, A., Pappalardo, M., Sarti, G., Noti, V., Capitani, M., Fabiani, F., Gualandi, M.L., 2015. Palaeoenvironments and palaeotopography of a multilayered city during the Etruscan and Roman periods: early interaction of fluvial processes and urban growth at Pisa (Tuscany, Italy). Journal of Archaeological Science 59, 197–210. DOI:10.1016/j.jas.2015.04.005
Blanton, P., Marcus, W.A., 2009. Railroads, roads and lateral disconnection in the river landscapes of the continental United States. Geomorphology 112, 212–227.
Blauw, M., 2005. 'Eene aanschouwelijke voorstelling van den waterstaat.' De Waterstaatskaart van Nederland, 1865–1992. Caert-Thresoor 24, 112–119.
Blöschl, G., Nester, T., Komma, J., Parajka, J., Perdigão, R.A.P., 2013. The June 2013 flood in the Upper Danube basin, and comparisons with the 2002, 1954 and 1899 floods. Hydrology and Earth System Sciences 10, 9533–9573. DOI:10.5194/hess-17-5197-2013
Blöschl, G., Hall, J., Parajka, J., Perdigão, R.A.P., Merz, B., Arheimer, B., Aronica, G., Bilibashi, A., Bonacci, O., Borga, M., Canjevac, I., Castellarin, A., Chirico, G., Claps, P., Fiala, K., Frolova, N., Gorbachova, L., Gül, A., Hannaford, J., Harrigan, S., Kireeva, M., Kiss, A., Kjeldsen, T., Kohnová, S., Koskela, J., Ledvinka, O., Macdonald, N., Mavrova-Guirguinova, M., Mediero, L., Merz, R., Molnar, P., Montanari, A., Murphy, C., Osuch, M., Ovcharuk, V., Radevski, I., Rogger, M., Salinas, J., Sauquet, E., Šraj, M., Szolgay, J., Viglione, A., Volpi, E., Wilson, D., Zaimi, K., Živkovic, N., 2017. Changing climate shifts timing of European floods. Science 357, 588–590. DOI:10.1126/science.aan2506
Blöschl, G., Hall, J., Viglione, A., Perdigão, R.A.P., Parajka, J., Merz, B., Lun, D., Arheimer, B., Aronica, G.T., Bilibashi, A., Boháč, M., Bonacci, O., Borga, M., Čanjevac, I., Castellarin, A., Chirico, G.B., Claps, P., Frolova, N., Ganora, D., Gorbachova, L., Gül, A., Hannaford, J., Harrigan, S., Kireeva, M., Kiss, A., Kjeldsen, T.R., Kohnová, S., Koskela, J.J., Ledvinka, O., Macdonald, N., Mavrova-Guirguinova, M., Mediero, L., Merz, R., Molnar, P., Montanari, A., Murphy, C., Osuch, M., Ovcharuk, V., Radevski, I., Salinas, J.L., Sauquet, E., Šraj, M., Szolgay, J., Volpi, E., Wilson, D., Zaimi, K., Živković, N., 2019. Changing climate both increases and decreases European river floods. Nature 573, 108–111. DOI:10.1038/s41586-019-1495-6
Bomers, A., Schielen, R.M.J., Hulscher, S.J.M.H., 2019a. Application of a lower-fidelity surrogate hydraulic model for historic flood reconstruction. Environmental Modelling & Software 117, 223–236. DOI:10.1016/j.envsoft.2019.03.019
Bomers, A., Schielen, R.M.J., Hulscher, S.J.M.H., 2019b. Consequences of dike breaches and dike overflow in a bifurcating river system. Natural Hazards 97, 309–334. DOI:10.1007/s11069-019-03643-y
Bomers, A., Schielen, R. M., Hulscher, S. J., 2019c. Decreasing uncertainty in flood frequency analyses by including historic flood events in an efficient bootstrap approach. Natural hazards and earth system sciences 19, 1895–1908. DOI:10.5194/nhess-19-1895-2019
Bomers, A., van der Meulen, B., Schielen, R.M.J., Hulscher, S.J.M.H., 2019. Historic flood reconstruction with the use of an Artificial Neural Network. Water Resources Research 55, 1–16. DOI:10.1029/2019WR025656
Bomers, A., 2020. Hydraulic modelling approaches to decrease uncertainty in flood frequency relations. PhD thesis, University of Twente. DOI:10.3990/1.9789036549288

Boode, M.F., 1979. 150 jaar rivierkaarten van Nederland. Report of the Meetkundige Dienst, Rijkswaterstaat. Delft, the Netherlands.
Bosch, A., van de Ven, G.P., 1993. Rivierverbetering. In: Lintsen, H.W., (Ed.). Geschiedenis van de techniek in Nederland. De wording van een moderne samenleving 1800–1890. Deel II. Walburg Pers, Zutphen.
Brázdil, R., Kotyza, O., Dobrovolný, P., 2006a. July 1432 and August 2002—two millennial floods in Bohemia? Hydrological Sciences Journal 51, 848–863. DOI:10.1623/hysj.51.5.848
Brázdil, R., Kundzewicz, Z.W., Benito, G., 2006. Historical hydrology for studying flood risk in Europe. Hydrological Sciences Journal 51, 739–764. DOI:10.1623/hysj.51.5.739
Brázdil, R., Kundzewicz, Z.W., Benito, G., Demarée, G., Macdonald, N., Roald, L.A., 2012. Historical floods in Europe in the past millennium. In: Kundzewicz, Z.W., (Ed.). Changes in Flood Risk in Europe. Taylor & Francis Group. pp. 121–166. DOI:10.1201/b12348-9
Breeze, D.J., Jilek, S., Graafstal, E.P., Willems, W.J.H., Bödecker, S., 2018. Frontiers of the Roman Empire; the Lower German Limes. Sidestone Press, Leiden.
Briant, R.M., Cohen, K.M., Cordier, S., Demoulin, A.J.A.G., Macklin, M.G., Mather, A.E., Rixhon, G., Veldkamp, T., Wainwright, J., Whittaker, A., Wittmann, H., 2018. Applying Pattern Oriented Sampling in current fieldwork practice to enable more effective model evaluation in fluvial landscape evolution research. Earth Surface Processes and Landforms 43, 2964–2980. DOI: 10.1002/esp.4458
Bronstert, A., Bárdossy, A., Bismuth, C., Buiteveld, H., Disse, M., Engel, H., Fritsch, U., Hundecha, Y., Lammersen, R., Niehoff, D., Ritter, N., 2007. Multi-scale modelling of land-use change and river training effects on floods in the Rhine basin. River Research and Applications 23, 1102–1125. DOI:10.1002/rra.1036
Brouwer Burg, M., 2013. Reconstructing "total" paleo-landscapes for archaeological investigation: an example from the central Netherlands. Journal of Archaeological Science 40, 2308–2320. DOI:10.1016/j.jas.2013.01.008
Brown, A.G., Tooth, S., Bullard, J.E., Thomas, D.S.G., Chiverrell, R.C., Plater, A.J., Murton, J., Thorndycraft, V.R., Tarolli, P., Rose, J., Wainwright, J., Downs, P., Aalto, R., 2017. The geomorphology of the Anthropocene: emergence, status and implications. Earth Surface Processes and Landforms 42, 71–90. DOI:10.1002/esp.3943
Brunner, G.W., 2016. HEC-RAS, River Analysis System Hydraulic Reference Manual, Version 5.0. US Army Corps of Engineers Hydrologic Engineering Center (HEC), Davis, USA.
Buisman, J., 1995–2019. Duizend jaar weer, wind en water in de Lage Landen. Deel 1–7. Van Wijnen, Franeker.
Buisman, J., 1996. Duizend jaar weer, wind en water in de Lage Landen. Deel 2: 1300–1450 AD. Van Wijnen, Franeker.
Busschers, F.S., Cohen, K.M., Vandenberghe, J., Van Balen, R.T., Kasse, C., Wallinga, J., Weerts, H.J., 2011. Comment on 'Causes, consequences and chronology of large-magnitude palaeoflows in Middle and Late Pleistocene river systems of northwest Europe' by Westaway and Bridgland (2010). Earth Surface Processes and Landforms 36, 1836–1840. DOI:10.1002/esp.2204
Calenda, G., Calvani, L., Mancini, C.P., 2003. Simulation of the great flood of December 1870 in Rome. Water and Maritime Engineering 156, 305–312. DOI:10.1680/wame.2003.156.4.305
Camuffo, D., della Valle, A., Becherini, F., 2020. A critical analysis of the definitions of climate and hydrological extreme events. Quaternary International 538, 5–13. DOI:10.1016/j.

quaint.2018.10.008.
Caviedes-Voullième D, García-Navarro, P., Murillo, J., 2012. Influence of mesh structure on 2D full shallow water equations and SCS Curve Number simulation of rainfall/runoff events. Journal of Hydrology 448, 39–59. DOI:10.1016/j.jhydrol.2012.04.006
Chbab, E.H., 1996. How extreme were the 1995 flood waves on the rivers Rhine and Meuse? Physics and Chemistry of the Earth 20, 455–458.
Chow, V.T., 1959. Open channel hydraulics. McGraw-Hill, New York.
Cloete, G., Benito, G., Grodek, T., Porat, N., Enzel, Y., 2018. Analyses of the magnitude and frequency of a 400-year flood record in the Fish River Basin, Namibia. Geomorphology 320, 1–17. DOI:10.1016/j.geomorph.2018.07.025
Cohen, K.M., 2005. 3D geostatistical interpolation and geological interpretation of palaeo-groundwater rise in the coastal prism in the Netherlands. In: Giosan, L., Bhattacharaya, J.P., (Eds.). River Deltas: Concepts, Models, and Examples. SEPM Special Publication 83, 341–364. DOI:10.2110/pec.05.83.0341
Cohen, K.M., Lodder, Q.J., 2007. Paleogeografie en veiligheid tegen overstromen. De bruikbaarheid van inzichten in de ontwikkeling van de Nederlandse delta in de laatste 5000 jaar voor het kwantitatief begrenzen van overstromingsmagnitudes en -frequenties. Rijkswaterstaat report 2007.016.
Cohen, K.M., Stouthamer, E., Hoek, W.Z., Berendsen, H.J.A., Kempen, H.F.J., 2009. Zand in Banen - Zanddieptekaarten van het Rivierengebied en het IJsseldal in de provincies Gelderland en Overijssel. Provincie Gelderland, Arnhem.
Cohen, K.M., Stouthamer, E., Pierik, H.J., Geurts, A.H., 2012. Rhine-Meuse Delta Studies' Digital Basemap for Delta Evolution and Palaeogeography. DOI:10.17026/dans-x7g-sjtw
Cohen, K.M., Arnoldussen, S., Erkens, G., van Popta, Y.T., Taal, L.J., 2014. Archeologische verwachtingskaart uiterwaarden rivierengebied. Deltares, Utrecht. DOI:10.17026/dans-zbt-xcck
Cohen, K.M., Schielen, R., van der Meulen, B., Bomers, A., Hulscher, S.J.M.H., Middelkoop, H., 2016a. Floods of the Past, Design of Tomorrow – Project Introduction. In: Fontana, A., Rossata, S., (Eds.). Palaeohydrological extreme events: evidence and archives. Abstract volume EX-AQUA 2016.
Cohen, K.M., Toonen, W.H.J., Weerts, H.J.T., 2016. Overstromingen van de Rijn gedurende het Holoceen – Relevantie van de grootste overstromingen voor archeologie van het Nederlandse rivierengebied. Deltares, Utrecht.
Cohen, K.M., Dambrink, R., De Bruijn, R., Marges, V.C., Erkens, G., Pierik, H.J., Koster, K., Stafleu, J., Schokker, J., Hijma, M.P., 2017. Mapping buried Holocene landscapes: past lowland environments, palaeoDEMs and preservation in GIS. In: Lauwerier, R.C.G.M., Eerden, M.C., Groenewoudt, B.J., Lascaris, M.A., Rensink, E., Smit, B.I., Speleers, B.P., Van Doesburg, J., (Eds.). Knowledge for Informed Choices: Tools for more effective and efficient selection of valuable archaeology in the Netherlands. Netherlands Archeological Reports 55, 73–93.
Cook, A., Merwade, V., 2009. Effect of topographic data, geometric configuration and modeling approach on flood inundation mapping. Journal of Hydrology 377, 131–142. DOI:10.1016/j.jhydrol.2009.08.015
Costabile, P., Costanzo, C., De Lorenzo, G., Macchione, F., 2020. Is local flood hazard assessment in urban areas significantly influenced by the physical complexity of the hydrodynamic inundation model? Journal of Hydrology 580, 2020, 124231. DOI:10.1016/j.

jhydrol.2019.124231
Cremer, H., Bunnik, F.P.M., Donders, T.H., Hoek, W.Z., Koolen-Eekhout, M., Koolmees, H.H., Lavooi, E., 2010. River flooding and landscape changes impact ecological conditions of a scour hole lake in the Rhine-Meuse delta, The Netherlands. Journal of Paleolimnology 44, 789–801. DOI:10.1007/s10933-010-9452-2
Crosato, A., Mosselman, E., 2020. An integrated review of river bars for engineering, management and transdisciplinary research. Water 12, 596. DOI:10.3390/w12020596
Cyberski, J., Grześ, M., Gutry-Korycka, M., Nachlik, E., Kundzewicz, Z.W., 2006. History of floods on the River Vistula. Hydrological Sciences Journal 51, 799–817. DOI:10.1623/hysj.51.5.799
Czuba, J.A., David, S.R., Edmonds, D.A., Ward, A.S., 2019. Dynamics of surface-water connectivity in a low-gradient meandering river floodplain. Water Resources Research 55, 1849–1870. DOI:10.1029/2018WR023527
de Roode, F., Kuppens, W.J.A., 2012. De Oude Haven, de Rode Toren en de stadsmuur herontdekt. Archeologisch onderzoek op de westelijke Waalkade. Archeologische Berichten Nijmegen 36. DOI:10.17026/dans-285-5aes
de Roode, F., 2018. Naar het ideaal van een ommuurde stad. Stadsmuren uit de 13e en 16e eeuw aan de Nieuwe Markt, Nijmegen. Archeologische Berichten Nijmegen 74. DOI:10.17026/dans-zm7-y75n
Defilet, M.P., van den Berghe, K.J., 2011. Archeologisch onderzoek Vijzelstraat (VIJ19) te Arnhem, basisrapport. Archeologisch Rapport Arnhem 52. DOI:10.17026/dans-xqj-d74k
Deltacommissie, 2008. Advies: Samen werken met water. Een land dat leeft, bouwt aan zijn toekomst. Bevindingen van de Deltacommissie.
den Hartog, E., Glaudemans, R., 2013. De Sint-Eusebiuskerk te Arnhem. Bouwsculptuur en bouwgeschiedenis. Uitgeverij WBOOKS.
Denis, S., Gjesfjeld, E., Moreau, L., 2019. Post-Linear Pottery cultural boundary and repopulation of the German Rhineland: Revisiting the Western contacts hypothesis. Journal of Archaeological Science: Reports 23, 946–952. DOI:10.1016/j.jasrep.2018.11.037
Denlinger, R.P., O'Connell, D.R.H., House, P.K., 2002. Robust determination of stage and discharge: an example from an extreme flood on the Verde River, Arizona. In: House, P.K., Webb, R.H., Baker, V.R., Levish, D.R., (Eds.). Ancient Floods, Modern Hazards: Principles and Applications of Paleoflood Hydrology, Water Science and Application Series 5, 127–147. DOI:10.1029/WS005p0127
Denniston, R.F., Luetscher, M., 2017. Speleothems as high-resolution paleoflood archives. Quaternary Science Reviews 170, 1–13. DOI:10.1016/j.quascirev.2017.05.006
Departement van Waterstaat, 1926. Verslag van het voorgevallene tijdens het hooge opperwater op de Nederlandsche rivieren in den winter van 1925 op 1926. Algemene Landsdrukkerij, 's Gravenhage.
Deutsch, M., Grünewald, U., Rost, K.T., 2006. Historische Hochwassermarken – Ausgangssituation, Probleme und Möglichkeiten bei der heutigen Nutzung. In: Disse, M., Guckenberger, K., Pakosch, S., Yörük, A., Zimmermann, A., (Eds.). Risikomanagement extremer hydrologischer Ereignisse. Beiträge zum Tag der Hydrologie 2006. Forum für Hydrologie und Wasserbewirtschaftung, Heft 15.06. pp. 59–70.
Dezileau, L., Terrier, B., Berger, J.F., Blanchemanche, P., Latapie, A., Freydier, R., Bremond, L., Paquier, A., Lang, M., Delgado, J.L., 2014. A multidating approach applied to historical slackwater flood deposits of the Gardon River, SE France. Geomorphology 214, 56–68.

DOI:10.1016/j.geomorph.2014.03.017
Donkersloot–de Vrij, Y.M., 1981. Topografische kaarten van Nederland vóór 1750. PhD thesis, University of Groningen.
Dottori, F., Di Baldassarre, G., Todini, E., 2013. Detailed data is welcome, but with a pinch of salt: Accuracy, precision, and uncertainty in flood inundation modeling. Water Resources Research 49, 6079–6085. DOI:10.1002/wrcr.20406
Driessen, A.M.A.J., 1994. Watersnood tussen Maas en Waal: overstromingsrampen in het rivierengebied tussen 1780 en 1810. PhD thesis, University of Amsterdam.
Elleder, L., Herget, J., Roggenkamp, T., Nießen, A., 2013. Historic floods in the city of Prague – a reconstruction of peak discharges for 1481–1825 based on documentary sources. Hydrology Research, 44, 202–214. DOI:10.2166/nh.2012.161
Engeland, K., Wilson, D., Borsányi, P., Roald, L., Holmqvist, E., 2018. Use of historical data in flood frequency analysis: a case study for four catchments in Norway. Hydrology Research 49, 466–486. DOI:10.2166/nh.2017.069
England, J.F. Jr., Velleux, M.L., Julien, P.Y., 2007. Two-dimensional simulations of extreme floods on a large watershed. Journal of Hydrology 347, 229–241. DOI:10.1016/j.jhydrol.2007.09.034
England, J.F. Jr., Godaire, J.E., Klinger, R.E., Bauer, T.R., Julien, P.Y., 2010. Paleohydrologic bounds and extreme flood frequency of the Upper Arkansas River, Colorado, USA. Geomorphology 124, 1–16. DOI:10.1016/j.geomorph.2010.07.021
Enzel, Y., Ely, L.L., House, P.K., Baker, V.R., Webb, R.H., 1993. Paleoflood evidence for a natural upper bound to flood magnitudes in the Colorado River Basin. Water Resources Research 29, 2287–2297. DOI:10.1029/93WR00411
Erkens, G. 2009. Sediment dynamics in the Rhine catchment: quantification of fluvial response to climate change and human impact. PhD thesis, Utrecht University.
Erkens, G., Hoffmann, T., Gerlach, R., Klostermann, J., 2011. Complex fluvial response to Lateglacial and Holocene allogenic forcing in the Lower Rhine Valley (Germany). Quaternary Science Reviews 30, 611–627. DOI:10.1016/j.quascirev.2010.11.019
Ewijk, H., 1809. Geschiedkundig verslag der dijkbreuken en overstroomingen langs de rivieren in het Koningrijk Holland, voorgevallen in Louwmaand 1809. Joh. Allart & Jac. Ruys, Amsterdam.
Fermin, H.A.C.., Groothedde, M., van Krimpen, G.W., 2006. De middeleeuwen op straat (2). Laat-middeleeuwse straatdekken in de Oude Wand in Zutphen. Zutphense Archeologische Publicaties 24. DOI:10.17026/dans-276-shh9
Fermin, H.A.C., Groothedde, M., 2008. Doesburg Diachroon. Bewoningsgeschiedenis in de Korte Koepoortstraat te Doesburg van prehistorie tot heden. Doesburgse Archeologische Publicaties 3. DOI:10.17026/dans-xcv-9mxu
Flokstra, L.M., Schuurman, E.I., 2008. Plangebied Eltenseweg te Lobith, gemeente Rijnwaarden; archeologisch bureau- en inventariserend veldonderzoek (verkenning en kartering). RAAP report 1611.
Fontana, A., Frassine, M., Ronchi, L., 2020. Geomorphological and geoarchaeological evidence of the medieval Deluge in the Tagliamento River (NE Italy). In: Herget, J., Fontana, A., (Eds.). Palaeohydrology: Traces, Tracks and Trails of Extreme Events. Geography of the Physical Environment, pp. 97–116. DOI:10.1007/978-3-030-23315-0_5
Fontana, A., Herget, J., Toonen, W.H.J., Sinha, R., 2020a. EX-AQUA 2016: Palaeohydrological extreme events, evidence and archives. Quaternary International 538, 1–4. DOI:10.1016/j.

quaint.2020.02.011
Frings, R.M., Berbee, B.M., Erkens, G., Kleinhans, M.G., Gouw, M.J.P., 2009. Human-induced changes in bed shear stress and bed grain size in the River Waal (The Netherlands) during the past 900 years. Earth Surface Processes and Landforms 34, 503–514. DOI:10.1002/esp.1746
Frings, R.M., Hillebrand, G., Gehres, N., Banhold, K., Schriever, S., Hoffmann, T. 2019. From source to mouth: Basin-scale morphodynamics of the Rhine River. Earth-Science Reviews 196, 102830. DOI:10.1016/j.earscirev.2019.04.002
Fuller, I.C., Macklin, M.G., Toonen, W.H.J., Holt, K.A., 2018. Storm-generated Holocene and historical floods in the Manawatu River, New Zealand. Geomorphology 310, 102–124. DOI:10.1016/j.geomorph.2018.03.010
Furlanetto, P., Bondesan, A., 2015. Geomorphological evolution of the plain between the Livenza and Piave Rivers in the sixteenth and seventeenth centuries inferred by historical maps analysis (Mainland of Venice, Northeastern Italy). Journal of Maps 11, 261–266. DOI:10.1080/17445647.2014.947341
Gerlach, R., 2003. Historische Auenmorphologie und ihre Nutzung im Duisburger Altstadtgebiet. In: Schirmer, W., (Ed.). Landschaftsgeschichte im europäischen Rheinland. GeoArcheoRhein 4, 461–481.
Gerlach, R., 2006. Holozän: Die Umgestaltung der Landschaft durch den Menschen seit dem Neolithikum. In: Kunow, J., Wegner, H., (Eds). Urgeschichte im Rheinland. Verlag des Rheinischen Vereins für Denkmalpflege und Landschaftsschutz, Köln. pp. 87–98.
Glaser, R., Stangl, H., 2003. Historical floods in the Dutch Rhine Delta. Natural Hazards and Earth System Sciences 3, 605–613.
Glaser, R., Stangl, H., 2004. Climate and floods in central europe since AD 1000: Data, methods, results and consequences. Surveys in Geophysics 25, 485–510. DOI:10.1007/s10712-004-6201-y
Gorissen, F., 1956. Stede-atlas van Nijmegen. Werken uitgegeven door Gelre: Vereeniging tot beoefening van Geldersche geschiedenis, oudheidkunde en recht 29.
Gottschalk, M.K.E., 1971. Stormvloeden en rivieroverstromingen in Nederland. Deel 1: De periode voor 1400. Van Gorcum, Assen.
Gottschalk, M.K.E., 1971–1977. Stormvloeden en rivieroverstromingen in Nederland. Deel 1–3. Van Gorcum, Assen.
Gouw, M.J.P., Erkens, G., 2007. Architecture of the Holocene Rhine-Meuse delta (the Netherlands) – A result of changing external controls. Netherlands Journal of Geosciences 86, 23–54. DOI:10.1017/S0016774600021302
Gouw-Bouman, M.T.I.J., in prep. Late-Holocene vegetation dynamics: intensity and regional patterns of the Dark Age reforestation (AD 300 – 700) in the Netherlands. Vegetation history and Archaeobotany.
Gouw-Bouman, M.T.I.J., Pierik H.J., van Lanen R.J., in prep. Reforestation in the Rhine-Meuse delta (the Netherlands) during the Migration period visualised using vegetation reconstruction maps from the Roman and Early Medieval period. Netherlands Journal of Geosciences.
Grabowski, R.C., Gurnell, A.M., 2016. Using historical data in fluvial geomorphology. In: Kondolf, G.M., Piégay, H., (Eds.). Tools in Fluvial Geomorphology. Second Edition. John Wiley & Sons, Ltd. pp. 56–75. DOI:10.1002/9781118648551.ch4
Grimm, U., Heinrich, J., 2019. Leipzig 1015 CE – a multiproxy study to reconstruct the

palaeorelief of Leipzig's city centre. Archaeological Prospection 26, 225–237. DOI:10.1002/arp.1736
Groenhuijzen, M.R., Verhagen, P., 2017. Comparing network construction techniques in the context of local transport networks in the Dutch part of the Roman limes. Journal of Archaeological Science: Reports 15, 235–251. DOI:10.1016/j.jasrep.2017.07.024
Groothedde, M., 2010. De 'nieuwe' IJssel: Wat vertellen de geschreven bronnen en archeologische vondsten? Bijdragen en mededelingen historisch jaarboek voor Gelderland 101, 7–26.
Groothedde, M., 2013. Een vorstelijke palts te Zutphen? Macht en prestige op en rond het plein 's-Gravenhof van de Karolingische tijd tot aan de stadsrechtverlening. PhD thesis, Leiden University.
Guo, Y., Huang, C.C., Pang, J., Zhou, Y., Zha, X., Mao, P., 2017. Reconstruction palaeoflood hydrology using slackwater flow depth method in the Yanhe River valley, middle Yellow River basin, China. Journal of Hydrology 544, 156–171. DOI: 10.1016/j.jhydrol.2016.11.017
Haans, F., 2008. Historische ontwikkeling van Doesburg. In: Haans, F., (Ed.). Monumentengids Doesburg. Monumenten in Gelderland 7, 22–85.
Hansmann, A., Elikker, A., Justenhoven, J., Milz, H., 1973. Geschichte der Stadt und des Amtes Zons. Pädagogischer Verlag Schwann, Düsseldorf.
Harenberg, E., 2008. Archeologie in Doesburg. In: Haans, F., (Ed.). Monumentengids Doesburg. Monumenten in Gelderland 7, 86–95.
Harnismacher, S., Zepp, H., 2010. Bergbaubedingte Höhenänderungen im Ruhrgebiet – Eine Analyse auf Basis digitalisierter historischer Karten. Zeitschrift für Geodäsie, Geoinformation und Landmanagement 6, 386–397.
Harnischmacher, S., Zepp, H., 2014. Mining and its impact on the earth surface in the Ruhr District (Germany). Zeitschrift für Geomorphologie 58, 3–22. DOI:10.1127/0372-8854/2013/s-00131
Heere, E., Storms, M., 2002. Kartobibliografie van de Waterstaatskaart (1865–1991). Report of the Meetkundige Dienst, Rijkswaterstaat. Delft, the Netherlands.
Hegnauer M., Beersma J.J., van den Boogaard H.F.P., Buishand T.A., Passchier R.H., 2014. Generator of Rainfall and Discharge Extremes (GRADE) for the Rhine and Meuse Basins. Final report of GRADE 2.0. Deltares report 1209424-004.
Hegnauer, M., Kwadijk, J., Klijn, F., 2015. The plausibility of extreme high discharges in the river Rhine. Deltares report 1220042-004.
Heine, K., Siebertz, H., 1980. Abriß der paläogeographischen Entwicklung des unteren Niederrheingebietes. Arbeiten zur Rheinischen Landeskunde 46, 1–13.
Herget, J., Meurs, H., 2010. Reconstructing peak discharges for historic flood levels in the city of Cologne, Germany. Global and Planetary Change 70, 108–116. DOI:10.1016/j.gloplacha.2009.11.011
Herget, J., 2012. Am Anfang war die Sintflut: Hochwasserkatastrophen in der Geschichte. Wissenschaftliche Buchgesellschaft, Darmstadt.
Herget, J., Roggenkamp, T., Krell, M., 2014. Estimation of peak discharges of historical floods. Hydrology and Earth System Sciences 18, 4029–4037. DOI:10.5194/hess-18-4029-2014
Herget, J., Kapala, A., Krell, M., Rustemeier, E., Simmer, C., Wyss, A., 2015. The millennium flood of July 1342 revisited. Catena 130, 82–94. DOI:10.1016/j.catena.2014.12.010
Herget, J., 2020. Palaeostage indicators in rivers—an illustrated review. In: Herget, J., Fontana, A., (Eds.). Palaeohydrology: Traces, Tracks and Trails of Extreme Events. Geography of the

Physical Environment, pp. 187–211. DOI:10.1007/978-3-030-23315-0
Hesselink, A.W., 2002. History makes a river. Morphological changes and human interference in the river Rhine, the Netherlands. PhD thesis, Utrecht University.
Hesselink, A.W., Stelling, G.S., Kwadijk, J.C., Middelkoop, H., 2003. Inundation of a Dutch river polder, sensitivity analysis of a physically based inundation model using historic data. Water resources research 39, 1–17. DOI:10.1029/2002WR001334
Hesselink, A.W., Kleinhans, M.G., Boreel, G.L., 2006. Historic discharge measurements in three Rhine branches. Journal of Hydraulic Engineering 132, 140–145. DOI:10.1061/(ASCE)0733-9429(2006)132:2(140)
Heunks, E., van Hemmen, F., 2016. In het krachtenspel van Mens en Waal. Een biografie van het Lentse land. Archeologische Berichten Nijmegen, Gemeente Nijmegen.
Hobo, N., Makaske, B., Wallinga, J., Middelkoop, H., 2014. Reconstruction of eroded and deposited sediment volumes of the embanked River Waal, the Netherlands, for the period AD 1631–present. Earth Surface Processes and Landforms 39, 1301–1318. DOI:10.1002/esp.3525
Hobo, N., 2015. The sedimentary dynamics in natural and human-influenced delta channel belts. PhD thesis, Utrecht University.
Hoffmann, T., Erkens, G., Cohen, K.M., Houben, P., Seidel, J., Dikau, R., 2007. Holocene floodplain sediment storage and hillslope erosion within the Rhine catchment. The Holocene 17, 105–118. DOI:10.1177/0959683607073287
Hoffmann, T., Erkens, G., Gerlach, R., Klostermann, J., Lang, A., 2009. Trends and controls of Holocene floodplain sedimentation in the Rhine catchment. Catena 77, 96–106. DOI:10.1016/j.catena.2008.09.002
Höltken, T., Wagner, G., 2015. Frühmittelalterliche Funde am Fuß des Domes. In: Aufleger, M., Schmidt, C., (Eds.). Archäologie im Rheinland 2014. Wissenschaftlichen Buchgesellschaft, Darmstadt. pp. 162–165.
Hoppe, C., 1970. Die großen Flußverlagerungen des Niederrheins in den letzten zweitausend Jahren und ihre Auswirkungen auf Lage und Entwicklung der Siedlungen. PhD thesis, University of Cologne.
Horritt, M.S., Bates, P.D., 2002. Evaluation of 1D and 2D numerical models for predicting river flood inundation. Journal of Hydrology 268, 87–99. DOI:10.1016/S0022-1694(02)00121-X
House, P.K., Pearthree, P.A., Klawon, J.E., 2002. Historical flood and paleoflood chronology of the lower Verde River, Arizona: Stratigraphic evidence and related uncertainties. In: House, P.K., Webb, R.H., Baker, V.R., Levish, D.R., (Eds.). Ancient Floods, Modern Hazards: Principles and Applications of Paleoflood Hydrology. Water Science and Application 5, 267–293. DOI:10.1029/WS005p0267
Hu, G., Huang, C.C., Zhou, Y., Pang, J., Zha, X., Guo, Y., Zhang, Y., Zhao, X., 2016. Extreme paleoflood events 3200–3000 a BP in the Jingyuan–Jingtai reaches of the upper Yellow River, China. The Holocene 26, 790–800. DOI:10.1177/0959683615618257
Huang, C.C., Pang, J., Zha, X., Su, H., Jia, Y., 2011. Extraordinary floods related to the climatic event at 4200 a BP on the Qishuihe River, middle reaches of the Yellow River, China. Quaternary Science Reviews 30, 460–468. DOI:10.1016/j.quascirev.2010.12.007
Hudson, P.F., Middelkoop, H., Stouthamer, E., 2008. Flood management along the Lower Mississippi and Rhine Rivers (The Netherlands) and the continuum of geomorphic adjustment. Geomorphology 101, 209–236. DOI:10.1016/j.geomorph.2008.07.001
Hutchinson, M.F., 1993. Development of a continent-wide DEM with applications in terrain and

climate analysis. In: Goodchild, M.F., Parks, B.O., Steyaert, L.T., (Eds.). Environmental Modeling with GIS, 392–399.
Ishii, Y., Hori, K., 2016. Formation and infilling of oxbow lakes in the Ishikari lowland, northern Japan. 2016. Quaternary International 397, 136–146. DOI:10.1016/j.quaint.2015.06.016.
Jansma, E., 2020. Hydrological disasters in the NW-European Lowlands during the first millennium AD: a dendrochronological reconstruction. Netherlands Journal of Geosciences 99, e11. DOI:10.1017/njg.2020.10
Jarrett, R.D., England Jr., J.F., 2002. Reliability of paleostage indicators for paleoflood studies. In: House, P.K., Webb, R.H., Baker, V.R., Levish, D.R., (Eds.). Ancient Floods, Modern Hazards: Principles and Applications of Paleoflood Hydrology. Water Science and Application 5, 91–109. DOI:10.1029/WS005p0091
Johnston, G.H., David, S.R., Edmonds, D.A., 2019. Connecting fluvial levee deposition to flood-basin hydrology. Journal of Geophysical Research: Earth Surface 124,1996–2012. DOI:10.1029/2019JF005014
Jones, A.F., Brewer, P.A., Macklin, M.G., 2010. Geomorphological and sedimentological evidence for variations in Holocene flooding in Welsh river catchments. Global and Planetary Change 70, 92–107. DOI:10.1016/j.gloplacha.2009.11.010.
Jones, A.F., Lewin, J., Macklin, M.G., 2010. Flood series data for the later Holocene: Available approaches, potential and limitations from UK alluvial sediments. The Holocene 20, 1123-1135. DOI:10.1177/0959683610369501
Kadetova, A.V., Radziminovich, Y.B., 2020. Historical floods within the Selenga river basin: chronology and extreme events. Natural Hazards 103, 579–598. DOI: 10.1007/s11069-020-04001-z
Kalweit, H., Buck, W., Felkel, K., Gerhard, H., van Malde, J., Nippes, K.-R., Ploeger, B., Schmitz, W., 1993. Der Rhein unter der Einwirkung des Menschen – Ausbau, Schiffahrt, Wasserwirtschaft. International Commission for the Hydrology of the Rhine Basin (CHR/KHR) report I-11.
Kaplan, J.O., Krumhardt, K.M., Zimmermann, N., 2009. The prehistoric and preindustrial deforestation of Europe. Quaternary Science Reviews 28, 3016–3034. DOI:10.1016/j.quascirev.2009.09.028.
Kind, J.M., 2013. Economically efficient flood protection standards for the Netherlands. Journal of Flood Risk Management 7, 103–117. DOI:10.1111/jfr3.12026
Kirchner A., Zielhofer C., Werther L., Schneider M., Linzen S., Wilken, D., Wunderlich, T., Rabbel, W., Meyer, C., Schmidt, J., Schneider, B., Berg-Hobohm, S., Ettel, P., 2017. A multidisciplinary approach in wetland geoarchaeology: Survey of the missing southern canal connection of the Fossa Carolina (SW Germany). Quaternary International 473, 3–20. DOI:10.1016/j.quaint.2017.12.021
Kiss, A., Laszlovszky, J., 2013. 14th–16th-century Danube floods and long-term water-level changes in archaeological and sedimentary evidence in the Western and Central Carpathian Basin: an overview with documentary comparison. Journal of Environmental Geography 6, 1–11. DOI:10.2478/jengeo-2013-0001
Kjeldsen, T.R., Macdonald, N., Lang, M., Mediero, L., Albuquerque, T., Bogdanowicz, E., Brázdil, R., Castellarin, A., David, V., Fleig, A., Gül, G.O., Kriauciuniene, J., Kohnová, S., Merz, B., Nicholson, O., Roald, L.A., Salinas, J.L., Sarauskiene, D., Šraj, M., Strupczewski, W., Szolgay, J., Toumazis, A., Vanneuville, W., Veijalainen, N., Wilson, D., 2014. Documentary evidence of past floods in Europe and their utility in flood frequency estimation. Journal of

Hydrology 517, 963–973. DOI:10.1016/j.jhydrol.2014.06.038
Kleinhans, M.G., Cohen, K.M., Hoekstra, J., IJmker, J.M., 2011. Evolution of a bifurcation in a meandering river with adjustable channel widths, Rhine delta apex, The Netherlands. Earth Surface Processes and Landforms 36, 2011–2027.
Klijn, F., Kreibich, H., de Moel, H., Penning-Rowsell, E., 2015. Adaptive flood risk management planning based on a comprehensive flood risk conceptualisation. Mitigation and Adaptation Strategies for Global Change 20, 845–864. DOI:10.1007/s11027-015-9638-z
Klostermann, J., 1986. Rheinstromverlagerungen bei Xanten während der letzten 10000 Jahre. Natur am Niederrhein 1, 5–16.
Klostermann, J., 1992. Das Quartär der Niederrheinischen Bucht. Geologisches Landesamt Nordrhein-Westfalen, Krefeld.
Knol, W.C., Kramer, H., Gijsbertse, H., 2004. Historisch Grondgebruik Nederland: een landelijke reconstructie van het grondgebruik rond 1900. Alterra report 573.
Kochel, R.C., Baker, V.R., 1982. Paleoflood hydrology. Science 215, 353–361. DOI:10.1126/science.215.4531.353
Koeman, C., 1983. Geschiedenis van de kartografie van Nederland. Zes eeuwen land- en zeekaarten en stadsplattegronden. Canaletto, Alphen aan den Rijn.
Koomen, A.J.M., Maas, G.J., 2004. Geomorfologische Kaart Nederland (GKN); Achtergronddocument bij het landsdekkende digitale bestand. Alterra, Wageningen.
Kosian, M.C., van Lanen, R.J., Weerts, H.J.T., 2016. Een nieuwe kaart van Nederland in 1575. Rijksdienst voor het Cultureel Erfgoed, Amersfoort.
Koster, K., Stafleu, J., Cohen, K.M., 2017. Generic 3D interpolation of Holocene base-level rise and provision of accommodation space, developed for the Netherlands coastal plain and infilled palaeovalleys. Basin Research 29, 775–797. DOI:10.1016/j.earscirev.2013.10.014
Krahe, P., Larina, M., 2010. Hoch- und Niedrigwasser in Köln seit AD 1000. Geographische Rundschau 62, 34–41.
Krause, G., 1997. Archaeological evidence of medieval shipping from the Old Town of Duisburg, Lower Rhineland. Papers of the Medieval Europe conference. pp. 101–116.
Krause, G., 1999. Duisburg, Lower Rhineland – the harbour and the topography of the town from the Merovingian period to c. 1600. Papers of the 5th International Conference on Waterfront Archaeology. pp. 109–118.
Krause, G., 2003. Duisburg and its environs at the confluence of Rhine and Ruhr from the Late Antiquity to the Industrial Age – Essential aspects of its development according to archaeological and historical sources. Papers of the Medieval Europe conference. pp. 155–165.
Kreßner, L., 2009. Digitale Analyse der Genauigkeit sowie der Erfassungs- und Darstellungsqualität von Altkarten aus Mecklenburg Vorpommern - dargestellt an den Kartenwerken von Wiebeking (ca. 1786) und Schmettau (ca. 1788). PhD thesis, University of Rostock.
Kumar, R., Jain, V., Prasad Babu, G., Sinha, R., 2014. Connectivity structure of the Kosi megafan and role of rail-road transport network. Geomorphology 227, 73–86. DOI:10.1016/j.geomorph.2014.04.031
Kuys, J., de Leeuw, L., Paquay, V., van Schaïk, R., 1983. De Tielse Kroniek. Verloren, Amsterdam.
Lam, D., Croke, J., Thompson, C., Sharma, A., 2017. Beyond the gorge: Palaeoflood reconstruction from slackwater deposits in a range of physiographic settings in subtropical Australia. Geomorphology 292, 164–177. DOI:10.1016/j.geomorph.2017.05.008

Lam, D., Thompson, C., Croke, J., Sharma, A., Macklin, M., 2017a. Reducing uncertainty with flood frequency analysis: The contribution of paleoflood and historical flood information. Water Resources Research 53, 2312–2327.
Lambeek, J.J.P., Mosselman, E., 1998. Huidige en historische rivierkundige parameters van de Nederlandse Rijntakken. WL | Delft Hydraulics.
Lammersen, R., Engel, H., van de Langemheen, W., Buiteveld, H., 2002. Impact of river training and retention measures on flood peaks along the Rhine. Journal of Hydrology 267, 115–124. DOI:10.1016/S0022-1694(02)00144-0.
Le, T.B., Crosato, A., Montes Arboleda, A., 2020. Revisiting Waal River Training by Historical Reconstruction. Journal of Hydraulic Engineering 146, 05020002. DOI:10.1061/(ASCE)HY.1943-7900.0001688
Lewin, J., 2013. Enlightenment and the GM floodplain. Earth Surface Processes and Landforms 38, 17–29. DOI:10.1002/esp.3230
Lewin, J., Ashworth, P.J., 2014. The negative relief of large river floodplains. Earth-Science Reviews 129, 1–23. DOI:10.1016/j.earscirev.2013.10.014
Li, T., Li, J., Zhang, D.D., 2020. Yellow River flooding during the past two millennia from historical documents. Progress in Physical Geography 44, 661–678. DOI:10.1177/0309133319899821
Lindenschmidt, K.E., Huokuna, M., Burrell, B.C., Beltaos, S., 2018. Lessons learned from past ice-jam floods concerning the challenges of flood mapping. International Journal of River Basin Management 16, 457–468. DOI:10.1080/15715124.2018.1439496
Liu, Q., Qin, Y., Zhang, Y., Li, Z., 2015. A coupled 1D–2D hydrodynamic model for flood simulation in flood detention basin. Natural Hazards 75, 1303–132. DOI:10.1007/s11069-014-1373-3
Liu, T., Greenbaum, N., Baker, V.R., Ji, L., Onken, J., Weisheit, J., Porat, N., Rittenour, T., 2020. Paleoflood hydrology on the lower Green River, upper Colorado River Basin, USA: An example of a naturalist approach to flood-risk analysis. Journal of Hydrology 580, 124337. DOI:10.1016/j.jhydrol.2019.124337
Louwe Kooijmans, L.P., 2007. The gradual transition to farming in the Lower Rhine Basin. Proceedings of the British Academy 144, 287–309.
Macdonald, N., Werritty, A., Black, A.R., McEwen, L.J., 2006. Historical and pooled flood frequency analysis for the River Tay at Perth, Scotland. Area 38, 34–46. DOI:10.1111/j.1475-4762.2006.00673.x
Macdonald, N., 2007. On epigraphic records: a valuable resource in reassessing flood risk and long-term climate variability. Environmental History 12, 136–140. DOI:10.1093/envhis/12.1.136
Macdonald, N., 2013. Reassessing flood frequency for the River Trent through the inclusion of historical flood information since AD 1320. Hydrology Research 44, 215–233. DOI:10.2166/nh.2012.188
Machado, M.J., Botero, B.A., López, J., Francés, F., Díez-Herrero, A., Benito, G., 2015. Flood frequency analysis of historical flood data under stationary and non-stationary modelling. Hydrology and Earth System Sciences 19, 2561–2576. DOI:10.5194/hess-19-2561-2015
Machado, M.J., Medialdea, A., Calle, M., Rico, M.T., Sánchez-Moya, Y., Sopeña, A., Benito, G., 2017. Historical palaeohydrology and landscape resilience of a Mediterranean rambla (Castellón, NE Spain): Floods and people. Quaternary Science Reviews 171, 182–198. DOI:10.1016/j.quascirev.2017.07.014

Makaske, B., Maas, G.J., van Smeerdijk, D.G., 2008. The age and origin of the Gelderse IJssel. Netherlands Journal of Geosciences 87, 323–337. DOI:10.1017/S0016774600023386
Masoero, A., Claps, P., Asselman, N.E.M., Mosselman, E., Di Baldassarre, G., 2013. Reconstruction and analysis of the Po River inundation of 1951. Hydrological Processes 27, 1341–1348. DOI:10.1002/hyp.9558
Medialdea, A., Thomsen, K.J., Murray, A.S., Benito, G., 2014. Reliability of equivalent-dose determination and age-models in the OSL dating of historical and modern palaeoflood sediments. Quaternary Geochronology 22, 11–24. DOI:10.1016/j.quageo.2014.01.004
Meurers-Balke, J., Knörzer, K.H., Glasmacher, H.A., Berke, H., Gerlach, R., Tegtmeier, U., 1999. Ein spätmittelalterlicher Brunnen in der Duisburger Niederstrasse. Bonner Jahrbücher 199, 347–396.
Middelkoop, H., 1997. Embanked floodplains in the Netherlands: geomorphological evolution over various time slices. PhD thesis, Utrecht University.
Middelkoop, H., van der Perk, M., 1998. Modelling spatial patterns of overbank sedimentation on embanked floodplains. Geografiska Annaler: Series A, Physical Geography 80, 95–109. DOI:10.1111/j.0435-3676.1998.00029.x
Middelkoop, H., Erkens, G., van der Perk, M., 2010. The Rhine delta—a record of sediment trapping over time scales from millennia to decades. Journal of Soils and Sediments 10, 628–639. DOI:10.1007/s11368-010-0237-z
Mijnssen-Dutilh, M., 2006. 'Zwaar met ijs bezet en bovenmate met water bezwaard.' De doorbraak van de Grebbedijk op 5 maart 1855 en wat daaraan voorafging. Flehite 7, 98–135.
Minderhoud, P.S.J., Cohen, K.M., Toonen, W.H.J., Erkens, G., Hoek, W.Z., 2016. Improving age-depth models of fluvio-lacustrine deposits using sedimentary proxies for accumulation rates. Quaternary Geochronology 33, 35–45. DOI:10.1016/j.quageo.2016.01.001
Montes Arboleda, A., Crosato, A., Middelkoop, H., 2010. Reconstructing the early 19th-century Waal River by means of a 2D physics-based numerical model. Hydrological Processes 24, 3661–3675. DOI:10.1002/hyp.7804
Morales-Hernández, M., Petaccia, G., Brufau, P., García-Navarro, P., 2016. Conservative 1D–2D coupled numerical strategies applied to river flooding: The Tiber (Rome). Applied Mathematical Modelling 40, 2087–2105. DOI:10.1016/j.apm.2015.08.016
Mozzi, P., Ferrarese, F., Zangrando, D., Gamba, M., Vigoni, A., Sainati, C., Fontana, A., Ninfo, A., Piovan, S., Rossato, S., Veronese, F., 2018. The modeling of archaeological and geomorphic surfaces in a multistratified urban site in Padua, Italy. Geoarchaeology 33, 67–84. DOI:10.1002/gea.21641
Munoz, S.E., Giosan, L., Therrell, M.D., Remo, J.W.F., Shen, Z., Sullivan, R.M., Wiman, C., O'Donnell, M., Donnelly, J.P., 2018. Climatic control of Mississippi River flood hazard amplified by river engineering. Nature 556, 95–98. DOI:10.1038/nature26145
Munzar, J., Deutsch, M., Elleder, L., Ondráček, S., Kallabová, E., Hrádek, M., 2006. Historical floods in Central Europe and their documentation by means of floodmarks and other epigraphical monuments. Moravian Geographical Reports 14, 26–44.
Naulet, R., Lang, M., Ouarda, T.B.M.J., Coeur, D., Bobée, B., Recking, A., Moussay, D., 2005. Flood frequency analysis on the Ardèche river using French documentary sources from the last two centuries. Journal of Hydrology 313, 58–78. DOI:10.1016/j.jhydrol.2005.02.011.
Neal, J.C., Bates, P.D., Fewtrell, T.J., Hunter, N.M., Wilson, M.D., Horritt, M.S., 2009. Distributed whole city water level measurements from the Carlisle 2005 urban flood event and comparison with hydraulic model simulations. Journal of Hydrology 368, 42–55.

DOI:10.1016/j.jhydrol.2009.01.026
Nicholas, A.P., Walling, D.E., Sweet, R.J., Fang, X., 2006. New strategies for upscaling high-resolution flow and overbank sedimentation models to quantify floodplain sediment storage at the catchment scale. Journal of Hydrology 329, 577–594. DOI:10.1016/j.jhydrol.2006.03.010
Nienhuis, P. H., Buijse, A. D., Leuven, R. S. E. W., Smits, A. J. M., De Nooij, R. J. W., Samborska, E. M., 2002. Ecological rehabilitation of the lowland basin of the river Rhine (NW Europe). Hydrobiologia 478, 53–72. DOI:10.1023/A:1021070428566
Noordzij, G.A., 2018. Gelre: dynastie, land en identiteit in de late middeleeuwen. PhD thesis, Leiden University.
Notebaert, B., Verstraeten, G., 2010. Sensitivity of West and Central European river systems to environmental changes during the Holocene: A review. Earth-Science Reviews 103, 163–182. DOI:10.1016/j.earscirev.2010.09.009.
Obrocki, L., Becker, T., Mückenberger, K., Finkler, C., Fischer, P., Willershäuser, T., Vött, A., 2020. Landscape reconstruction and major flood events of the River Main (Hesse, Germany) in the environs of the Roman fort at Grosskrotzenburg. Quaternary international 538, 94–109. DOI:10.1016/j.quaint.2018.08.009
Olthuis, J., 2018. An overview and analysis of ice jam formations in the Rhine and Meuse in the period of 1750–1870. BSc thesis, Utrecht University.
O'Shea, T.E., Lewin, J., 2020. Urban flooding in Britain: an approach to comparing ancient and contemporary flood exposure. Natural Hazards 104, 581–591. DOI:10.1007/s11069-020-04181-8
Overmars, W., 2020. Een Waal verhaal. Historisch-morfologische atlas van de Rhein en de Waal: 1500–1700 Emmerich-Nijmegen. PhD thesis, VU Amsterdam.
Papaioannou, G., Loukas, A., Vasiliades, L., Aronica, G.T., 2016. Flood inundation mapping sensitivity to riverine spatial resolution and modelling approach. Natural Hazards 83, 117–132. DOI:10.1007/s11069-016-2382-1
Parkes, B., Demeritt, D., 2016. Defining the hundred year flood: A Bayesian approach for using historic data to reduce uncertainty in flood frequency estimates. Journal of Hydrology 540, 1189–1208, DOI:10.1016/j.jhydrol.2016.07.025
Parmet, B.W.A.H., van de Langemheen, W., Chbab, E.H., Kwadijk, J.C.J., Diermanse, F.L.M., Klopstra, D., 2001. Analyse van de maatgevende afvoer van de Rijn te Lobith. RIZA report 2002.012.
Pekárová, P., Halmová, D., Bačová Mitková, B., Miklánek, P., Pekár, J., Škoda, P., 2013 Historic flood marks and flood frequency analysis of the Danube River at Bratislava, Slovakia. Journal of Hydrology and Hydromechanics 61, 326–333. DOI:10.2478/johh-2013-0041
Peng, F., Prins, M.A., Kasse, C., Cohen, K.M., Van der Putten, N., van der Lubbe, J., Toonen, W.H.J., van Balen, R.T., 2019. An improved method for paleoflood reconstruction and flooding phase identification, applied to the Meuse River in the Netherlands. Global and Planetary Change 177, 213–224. DOI:10.1016/j.gloplacha.2019.04.006
Pennington, B.T., Bunbury, J., Hovius, N., 2016. Emergence of civilization, changes in fluvio-deltaic style, and nutrient Redistribution forced by Holocene sea-level rise. Geoarchaeology 31, 194–210. DOI:10.1002/gea.21539
Pierik, H.J., Stouthamer, E., Cohen, K.M., 2017. Natural levee evolution in the Rhine–Meuse delta, the Netherlands, during the first millennium CE. Geomorphology 295, 215–234. DOI:10.1016/j.geomorph.2017.07.003

Pierik, H.J., van der Meulen, B., van Lanen, R., Cohen, K., 2018. Holocene palaeoDEMs for the Rhine valley and delta plain, the Netherlands and Germany. EGU General Assembly Conference Abstracts 20, 8155.

Pierik, H.J., van Lanen, R.J., 2019. Roman and early-medieval occupation patterns in a delta landscape: the link between settlement elevation and landscape dynamics. Quaternary International 501, 379–392. DOI:10.1080/17445647.2019.1590248

Pinter, N., Ickes, B.S., Wlosinski, J.H., van der Ploeg, R.R., 2006. Trends in flood stages: Contrasting results from the Mississippi and Rhine River systems. Journal of Hydrology 331, 554–566. DOI:10.1016/j.jhydrol.2006.06.013.

Piotte, O., Boura, C., Cazaubon, A., Chaléon, C., Chambon, D., Guillevic, G., Pasquet, F., Perherin, C., Raimbault, E., 2016. Collection, storage and management of high-water marks data: praxis and recommendations. E3S Web of Conferences 7, 16003. DOI:10.1051/e3sconf/20160716003

Ploeger, B., 1992. Bouwen aan de Rijn. Menselijke ingrepen op de Rijn en zijn takken. Rijkswaterstaat report 53.

Polak, M., Bödecker, S., Berger, L., Zandstra, M., Leene, T., 2019. Frontiers of the Roman Empire – The Lower Germanic Limes. Nomination File for Inscription on the UNESCO World Heritage List.

Pröschel, B., Lehmkuhl, F., 2019. Paleotopography and anthropogenic deposition thickness of the city of Aachen, Germany. Journal of Maps 15, 269–277. DOI:10.1080/17445647.2019.1590248

Quik, C., Wallinga, J., 2018. Reconstructing lateral migration rates in meandering systems – a novel Bayesian approach combining optically stimulated luminescence (OSL) dating and historical maps. Earth Surface Dynamics 6, 705–721. DOI:10.5194/esurf-2018-30

Reinders, J.B., Muñoz, S.E., 2021. Improvements to flood frequency analysis on alluvial rivers using paleoflood data. Water Resources Research, e2020WR028631. DOI:10.1029/2020WR028631

Remo, J.W.F., Pinter, N., Heine, R., 2009. The use of retro-and scenario-modeling to assess effects of 100+ years river of engineering and land-cover change on Middle and Lower Mississippi River flood stages. Journal of Hydrology 376, 403–416. DOI:10.1016/j.jhydrol.2009.07.049

Reuter, H.I., Nelson, A., Jarvis, A. 2007. An evaluation of void-filling interpolation methods for SRTM data. International Journal of Geographical Information Science, 21, 983–1008.

Rijke, J., van Herk, S., Zevenbergen, C., Ashley, R., 2012. Room for the River: delivering integrated river basin management in the Netherlands. International Journal of River Basin Management 10, 369–382. DOI:10.1080/15715124.2012.739173

Röbke, B.R., Schüttrumpf H., Vött, A., 2016. Effects of different boundary conditions and palaeotopographies on the onshore response of tsunamis in a numerical model – A case study from western Greece. Continental Shelf Research 124, 182–199. DOI:10.1016/j.csr.2016.04.010

Roggenkamp, T., Herget, J., 2014. Reconstructing peak discharges of historic floods of the river Ahr, Germany. Erdkunde 68, 49–59. DOI:10.3112/erdkunde.2014.01.05

Rondags, E.J.N., 2019. Lent zones K en L, archeologisch dijkonderzoek, gemeente Nijmegen. RAAP report 3207. DOI:10.17026/dans-ze9-ars8

Sandercock, P., Wyrwoll, K.H., 2005. The historical and palaeoflood record of Katherine river, northern Australia: evaluating the likelihood of extreme discharge events in the context of the 1998 flood. Hydrological Processes 19, 4107–4120. DOI:10.1002/hyp.5875

Sass-Klaassen, U., Hanraets, E., 2006. Woodlands of the past — The excavation of wetland woods at Zwolle-Stadshagen (the Netherlands): Growth pattern and population dynamics of oak and ash. Netherlands Journal of Geosciences 58, 61–71. DOI:10.1017/S0016774600021429
Schabbink, M., 2006. Voormalig Hotel De Leeuw te Lobith, Gemeente Rijnwaarden. Definitief Onderzoek (noodopgraving). RAAP report 1430. DOI:10.17026/dans-xed-w567
Scheller, H., 1957. Der Rhein bei Duisburg im Mittelalter. In: von Roden, G., Tischler, F., (Eds.). Duisburger Forschungen Band 1. Verlag für Wirtschaft und Kultur Werner Renckhoff KG, Duisburg-Ruhrort. pp. 45–87.
Scheller, H., 1965. Laufänderungen des Rheins bei Neuß. Beiträge zur Rheinkunde 17, 3–11.
Schendel, T., Thongwichian, R., 2017. Considering historical flood events in flood frequency analysis: Is it worth the effort? Advances in Water Resources 105, 144–153, DOI:10.1016/j.advwatres.2017.05.002
Schmidt, J., Werther, L., Zielhofer, C., 2018. Shaping pre-modern digital terrain models: The former topography at Charlemagne's canal construction site. PLoS ONE 13, e0200167. DOI:10.1371/journal.pone.0200167
Schneider, J., 1886. Die alten Heer- und Handelswege der Germanen, Römer und Franken im deutschen Reiche; Fünftes Heft. T.O. Weigel, Leipzig.
Schneider, A., Hirsch, F., Wechler, K.-P., Raab, A., Raab, T., 2017. Reconstruction of a palaeosurface and archaeological site location in an anthropogenic drift sand area. Archaeological Prospection 24, 297–310. DOI:10.1002/arp.1571
Schoor, M.M., Wolfert, H.P., Maas, G.J., Middelkoop, H., Lambeek, J.J.P., 1999. Potential for floodplain rehabilitation based on historical maps and present-day processes along the River Rhine, The Netherlands. In: Marriott, S.B., Alexander, J., (Eds.), 1999. Floodplains: Interdisciplinary Approaches. Geological Society of London Special Publications 163, 123–137.
Schulte, L., Schillereff, D., Santisteban, J.I., 2019. Pluridisciplinary analysis and multi-archive reconstruction of paleofloods: Societal demand, challenges and progress. Global and Planetary Change 177, 225–238. DOI: 10.1016/j.gloplacha.2019.03.019
Serinaldi, F., Loecker, F., Kilsby, C.G., Bast, H., 2018. Flood propagation and duration in large river basins: a data-driven analysis for reinsurance purposes. Natural Hazards 94, 71–92. DOI:10.1007/s11069-018-3374-0
Shala, B., 2001. Jungquartäre Talgeschichte des Rheins zwischen Krefeld und Dinslaken. PhD thesis, Düsseldorf.
Sheffer, N.A., Enzel, Y., Benito, G., Grodek, T., Poart, N., Lang, M., Naulet, R., Coeur, D., 2003. Historical and palaeofloods of the Ardeche river, France. Water Resources Research 39, 7-1–7-13. DOI:10.1029/2003WR002468
Sheffer, N.A., Rico, M., Enzel, Y., Benito, G., Grodek, T., 2008. The palaeoflood record of the Gardon River, France: a comparison with the extreme 2002 flood event. Geomorphology 98, 71–83. DOI:10.1016/j.geomorph.2007.02.034
Shen, D., Wang, J., Cheng, X., Rui, Y., Ye, S., 2015. Integration of 2-D hydraulic model and high-resolution lidar-derived DEM for floodplain flow modeling. Hydrology and Earth System Sciences 19, 3605–3616. DOI:10.5194/hess-19-3605-2015
Silva, W.F., Klijn, F., Dijkman, J.P.M., 2001. Room for the Rhine Branches in The Netherlands. What the research has taught us. RIZA report 2001.031 and Delft Hydraulics report R3294.
Skublics, D., Blöschl, G., Rutschmann, P., 2016. Effect of river training on flood retention of the

Bavarian Danube. Journal of Hydrology and Hydromechanics 64, 349-356. DOI:10.1515/johh-2016-0035
Slomp, R., 2016. Implementing risk based flood defence standards. Rijkswaterstaat.
Slootjes, N., van der Most, H., 2016. Achtergronden bij de normering van de primaire waterkeringen in Nederland. Ministerie van Infrastructuur en Milieu.
Spitzers, T.A., van de Venne, A.C., 2020. Archeologische opgraving Beekstraat/Kromme Elleboogsteeg te Arnhem, gemeente Arnhem (GD). Laagland Archeologie Rapport 333. DOI:10.17026/dans-zam-yx6d
Springer, G.S., Kite, S.J., 1997. River-derived slackwater sediments in caves along Cheat River, West Virginia. Geomorphology 18, 91–100. DOI:10.1016/S0169-555X(96)00022-0
St. George, S., Mudelsee, M., 2019. The weight of the flood-of-record in flood frequency analysis. Journal of Flood Risk Management 12, e12512. DOI:10.1111/jfr3.12512
St. George, S., Hefner, A.M., Avila, J., 2020. Paleofloods stage a comeback. Nature Geoscience. DOI:10.1038/s41561-020-00664-2
Stamataki, I. Kjeldsen, T., 2020. Reconstructing a hydraulic model for historic flood levels in the city of Bath, United Kingdom. EGU General Assembly Conference Abstracts 3751.
Stouthamer, E., Cohen, K.M., Gouw, M.J.P., 2011. Avulsion and its implications for fluvial-deltaic architecture: insights from the Holocene Rhine–Meuse delta. SEPM special publication 97, 215–232.
Straatsma, M.W., Bloecker, A.M., Lenders, H.R., Leuven, R.S., Kleinhans, M.G., 2017. Biodiversity recovery following delta-wide measures for flood risk reduction. Science advances 3, e1602762. DOI:10.1126/sciadv.1602762
Strasser, R., 1989. Geschichtlicher Atlas der Rheinlande Beiheft I/6. Veränderungen des Rheinlaufs zwischen Wupper- und Düsselmündung seit der Römerzeit. Gesellschaft für Rheinische Geschichtskunde, Köln.
Strasser, R., 1992. Die Veränderungen des Rheinstromes in historischer Zeit. Band 1. Zwischen der Wupper- und der Düsselmündung. Publikationen der Gesellschaft für Rheinische Geschichtskunde 68.
Sudhaus, D., Seidel, J., Bürger, K., Dostal, P., Imbery, F., Mayer, H., Glaser, R., Konold, W., 2008. Discharges of past flood events based on historical river profiles. Hydrology and Earth System Sciences 5, 323–344. DOI:10.5194/hess-12-1201-2008
Syrovatko, A.S., Panin, A.V., Troshina, A.A., Zaretskaya, N.E., 2019. Magnitude and chronology of extreme floods in the last 2 ka based on the stratigraphy of a riverine archeological site (Schurovo settlement, middle Oka River, Central European Russia). Quaternary International 516, 83–97. DOI:10.1016/j.quaint.2018.10.002
Tarolli, P., Sofia, G., 2016. Human topographic signatures and derived geomorphic processes across landscapes. Geomorphology 255, 140–161. DOI:10.1016/j.geomorph.2015.12.007
Tayefi, V., Lane, S.N., Hardy, R.J., Yu, D., 2007. A comparison of one- and two-dimensional approaches to modelling flood inundation over complex upland floodplains. Hydrological Processes 21, 3190–3202. DOI:10.1002/hyp.6523.
te Linde, A.H., Aerts, J.C.J.H., Kwadijk, J.C.J., 2010. Effectiveness of flood management measures on peak discharges in the Rhine basin under climate change. Journal of Flood Risk Management 3, 248–269. DOI:10.1111/j.1753-318X.2010.01076.x
te Linde, A.H., Bubeck, P., Dekkers, J.E.C., de Moel, H., Aerts, J.C.J.H., 2011. Future flood risk estimates along the river Rhine. Natural Hazards and Earth System Science 11, 459–473. DOI:10.5194/nhess-11-459-2011

Teunissen, D., 1990. Palynologisch onderzoek in het oostelijk rivierengebied; een overzicht. Mededelingen van de Afdeling Biogeologie van de Discipline Biologie van de Katholieke Universiteit van Nijmegen 16.
Thonon, I., de Jong, K., van der Perk, M., Middelkoop, H., 2007. Modelling floodplain sedimentation using particle tracking. Hydrological Processes 21, 1402–1412. DOI:10.1002/hyp.6296
Thorndycraft, V.R., Barriendos, M., Benito, G., Rico, M., Casas, A., 2006. The catastrophic floods of AD 1617 in Catalonia (northeast Spain) and their climatic context. Hydrological Sciences Journal 51, 899–912. DOI:10.1623/hysj.51.5.899
Tol, R.S., Langen, A., 2000. A concise history of Dutch river floods. Climatic Change 46, 357–369. DOI:10.1023/A:1005655412478
Toonen, W.H.J., Kleinhans, M.G., Cohen, K.M., 2012. Sedimentary architecture of abandoned channel fills. Earth Surf. Process. Landforms 37, 459–472. DOI:10.1002/esp.3189
Toonen, W.H.J., 2013. A Holocene flood record of the Lower Rhine. PhD thesis, Utrecht University.
Toonen, W.H.J., de Molenaar, M.M., Bunnik, F.P., Middelkoop, H., 2013. Middle Holocene palaeoflood extremes of the Lower Rhine. Hydrology Research 44, 248–263. DOI:10.2166/nh.2012.162
Toonen, W.H.J., 2015. Flood frequency analysis and discussion of non-stationarity of the Lower Rhine flooding regime (AD 1350-2011): Using discharge data, water level measurements, and historical records. Journal of Hydrology 528, 490–502. DOI:10.1016/j.jhydrol.2015.06.014
Toonen, W.H.J., Winkels, T.G., Cohen, K.M., Prins, M.A., Middelkoop, H., 2015. Lower Rhine historical flood magnitudes of the last 450 years reproduced from grain-size measurements of flood deposits using End Member Modelling. Catena 130, 69–81. DOI:10.1016/j.catena.2014.12.004
Toonen, W.H.J., Middelkoop, H., Konijnendijk, T.Y.M., Macklin, M.G., Cohen, K.M., 2016. The influence of hydroclimatic variability on flood frequency in the Lower Rhine. Earth Surface Processes and Landforms. 41, 1266–1275. DOI:10.1002/esp.3953
Toonen, W.H.J., Foulds, S.A., Macklin, M.G., Lewin, J., 2017. Events, episodes, and phases: Signal from noise in flood-sediment archives. Geology 45, 331–334. DOI:10.1130/G38540.1
Toonen, W.H.J., Munoz, S.E., Cohen, K.M., Macklin, M.G., 2020. High-resolution sedimentary paleoflood records in alluvial river environments: a review of recent methodological advances and application to flood hazard assessment. In: Herget, J., Fontana, A., (Eds.). Palaeohydrology: Traces, Tracks and Trails of Extreme Events. Geography of the Physical Environment, pp. 213–228. DOI:10.1007/978-3-030-23315-0_11
Uribelarrea, D., Pérez-González, A., Benito, G., 2003. Channel changes in the Jarama and Tagus rivers (central Spain) over the past 500 years. Quaternary Science Reviews 22, 2209–2221. DOI:10.1016/S0277-3791(03)00153-7.
van Alphen, J., 2016. The Delta Programme and updated flood risk management policies in the Netherlands. Journal of Flood Risk Management 9, 310–319. DOI:10.1111/jfr3.12183
van de Ven, G.P., 1976. Aan de wieg van Rijkswaterstaat. Het graven van het Pannerdens Kanaal. PhD thesis, Radboud University Nijmegen.
van de Ven, G.P. 1993. Man-made lowlands. History of water management and land reclamation in the Netherlands. Matrijs, Utrecht.
van de Ven, G.P., Driessen, A.M.A.J., Wolters, W., Wasser, J., 1995. Niets is bestendig…

Geschiedenis van de rivieroverstromingen in Nederland. Matrijs, Utrecht.
van den Brink, P.P.W.J., 1998. 'In een opslag van het oog': de Hollandse rivierkartografie en waterstaatszorg in opkomst, 1725–1754. PhD thesis, Utrecht University.
van den Brink, P.P.W.J., 2002. Kartobibliografie van de Rivierkaart (1830–1961). Report of the Meetkundige Dienst, Rijkswaterstaat. Delft, the Netherlands.
van den Brink, V.B., van Renswoude, J., 2017. Een opgraving in het plangebied Tiel-Fabriekslaantje. Sporen van bewoning en bedijking uit de Volle Middeleeuwen en de Nieuwe Tijd. Zuidnederlandse Archeologische Notities 466. DOI:10.17026/dans-xqz-7dkv
van Denderen, R.P., Schielen, R.M.J., Blom, A., Hulscher, S.J.M.H., Kleinhans, M.G., 2018. Morphodynamic assessment of side channel systems using a simple one-dimensional bifurcation model and a comparison with aerial images. Earth Surface Processes and Landforms 43, 1169–1182. DOI:10.1002/esp.4267
van der Ham, W., van de Ven, G.P., 2004. Afleiden of opruimen: De strijd om de beste aanpak tegen het rivierbederf, een beschouwing van 300 jaar rivierverbetering in het kader van de spankrachtstudie. Rijkswaterstaat, Lelystad.
van der Mark, R., Wemerman, P.J.L., van de Venne, A., 2006. Aan de Beek, op de Beek. BAAC report 06.218. DOI:10.17026/dans-2b2-wnzw
van der Mark, R., 2016. Arnhem Kerkplein: Inventariserend veldonderzoek door middel van proefsleuven (IVO-P). BAAC report A-16.0030. DOI:10.17026/dans-zec-vnnq
van der Meulen, B., Deggeller, T.S., Bomers, A., Cohen, K.M., Middelkoop, M., 2018. The historical river: morphology of the Rhine before river normalization. In: Huismans, Y., Berends, K.D., Niesten, I., Mosselman, E., (Eds.). The future river: Netherlands Centre for River Studies conference proceedings. NCR publication 42-2018, 44–45.
van der Meulen, B., Cohen, K.M., Pierik, H.J., Zinsmeister, J.J., Middelkoop, H., 2020. LiDAR-derived high-resolution palaeo-DEM construction workflow and application to the early medieval Lower Rhine valley and upper delta. Geomorphology 370, 107370. DOI:10.1016/j.geomorph.2020.107370
van der Meulen, B., Bomers, A., Cohen, K.M., Middelkoop, H., 2021. Late Holocene flood dynamics and magnitudes in the Lower Rhine river valley and upper delta resolved by a two-dimensional hydraulic modelling. Earth Surface Processes and Landforms 46, 853–868. DOI:10.1002/esp.5071
van der Monde, N., 1835. Tijdschrift voor geschiedenis, oudheden en statistiek van Utrecht. Jaargang 1. Publicly available through Utrecht University library at http://hdl.handle.net/1874/9802.
van der Wal., M., 2015. Archeologisch proefonderzoek in het portaal van de Lebuïnuskerk. Interne Rapportages Archeologie Deventer 88.
van Dinter, M., Cohen, K.M., Hoek, W.Z., Stouthamer, E., Jansma, E., Middelkoop, H., 2016. Late Holocene lowland fluvial archives and geoarchaeology: Utrecht's case study of Rhine river abandonment under Roman and Medieval settlement. Quaternary Science Reviews 166, 227–265. DOI:10.1016/j.quascirev.2016.12.003
van Doornik, W.E., 2013. Reconstructie van het hoogwater in de Rijn van 1374 en de gevolgen voor de huidige situatie: 18000 m^3/s – waan of werkelijkheid? MSc thesis, University of Twente.
van Engeldorp Gastelaars, H.J.N. (Ed.), 2019. Aan de rand van de stad: Arnhem Bartok. Een archeologische begeleiding en opgraving. ADC Monografie 27.
van Heezik, A.A.S., 2007. Strijd om de rivieren: 200 jaar rivierenbeleid in Nederland of de opkomst

en ondergang van het streven naar de normale rivier. PhD thesis, Delft.
van Lanen, R.J., Jansma, E., van Doesburg, J., Groenewoudt, B.J., 2016. Roman and early-medieval long-distance transport routes in north-western Europe: Modelling frequent-travel zones using a dendroarchaeological approach. Journal of Archaeological Science 73, 120–137. DOI:10.1016/j.jas.2016.07.010
van Lanen, R.J., de Kleijn, M.T.M., Gouw-Bouman, M.T.I.J., Pierik, H.J., 2018. Exploring Roman and early-medieval habitation of the Rhine–Meuse delta: modelling large-scale demographic changes and corresponding land-use impact. Netherlands Journal of Geosciences 97, 45–68. DOI:10.1017/njg.2018.3
van Lanen, R.J., Pierik, H.J., 2019. Calculating connectivity patterns in delta landscapes: modelling Roman and early-medieval route networks and their stability in dynamic lowlands. Quaternary International 501, 393–412. DOI:10.1016/j.quaint.2017.03.009
van Leeuwen, J.D., 1789. Chronicon Tielense. B. Wild & J. Altheer, Utrecht.
van Oorschot, M., 2017. Riparian vegetation interacting with river morphology: modelling long-term ecosystem responses to invasive species, climate change, dams and river restoration. PhD thesis, Utrecht University.
van Renswoude, J., van Kampen, J.C.G., 2019. Waardering van de Romeinse vindplaats. Een aanvullend proefsleuvenproject Bijland-Noordoost Herwen. Zuidnederlandse Archeologische Notities.
van Wees, M. 2020. Het Hart van Doesburg: Archeologisch onderzoek in de bouwput van het Doesburgse gemeentehuis. Doesburgse Archeologische Publicaties 22.
van Zellem, J., 2003. 'Nooyt gehoorde hooge waeteren' Bestuurlijke, technische en sociale aspecten, in het bijzonder de hulpverlening, van de overstromingsramp in de Over-Betuwe in 1740–1741. Tijdschrift voor Waterstaatsgeschiedenis 12, 11–20.
Verhagen, J., Kluiving, S.J., Anker, E., van Leeuwen, L., Prins, M.A., 2017. Geoarchaeological research for Roman waterworks near the late Holocene Rhine-Waal delta bifurcation, the Netherlands. Catena 149, 460–473. DOI:10.1016/j.catena.2016.03.027
Vermeer, J.A.M., Finke, P.A., Zwertvaegher, A., Gelorini, V., Bats, M., Antrop, M., Verniers, J., Crombé, P., 2014. Reconstructing a prehistoric topography using legacy point data in a depositional environment. Earth Surface Processes and Landforms 39, 632–645. DOI:10.1016/j.eswa.2010.12.162
Vorogushyn, S., Merz, B., Lindenschmidt, K.E., Apel, H., 2010. A new methodology for flood hazard assessment considering dike breaches. Water Resources Research 46, 1–17. DOI:10.1029/2009WR008475
Waalewijn, A., 1979. De tweede nauwkeurigheidswaterpassing van Nederland, 1926-1940. Publication of the Netherlands Geodetic Commission. W.D. Meinema B.V., Delft.
Waalewijn, A., (Ed.), 1987. Drie eeuwen Normaal Amsterdams Peil. Rijkswaterstaat publication 48.
Warmink, J.J., Straatsma, M.W., Huthoff, F., Booij, M.J., Hulscher, S.J.M.H., 2013. Uncertainty of design water levels due to combined bed form and vegetation roughness in the Dutch River Waal. Journal of Flood Risk Management 6, 302–318. DOI:10.1111/jfr3.12014
Webb, R.H., Jarrett, R.D., 2002. One-dimensional estimation techniques for discharges of paleofloods and historical floods. In: House, P.K., Webb, R.H., Baker, V.R., Levish, D.R., (Eds.). Ancient Floods, Modern Hazards: Principles and Applications of Paleoflood Hydrology. Water Science and Application 5, 111–125.
Weber, H., 1977. Hochwasser im Rheingebiet. Beiträge zur Rheinkunde 29, 50–62.

Weikinn, C., 1958. Quellentexte zur Witterungsgeschichte Europas von der Zeitwende bis zum Jahre 1850. Teil 1: Zeitwende – 1500. Akademie-Verlag, Berlin.
Weikinn, C., 1958–1963. Quellentexte zur Witterungsgeschichte Europas von der Zeitwende bis zum Jahre 1850. Teil 1–4. Akademie-Verlag, Berlin.
Werbrouck I., Antrop M., van Eetvelde V., Stal C., de Maeyer P., Bats M., Bourgeois .J, Court-Picon M., Crombé P., de Reu J., de Smedt P., Finke P.A., van Meirvenne M., Verniers J., Zwertvaegher A., 2011. Digital Elevation Model generation for historical landscape analysis based on LiDAR data, a case study in Flanders (Belgium). Expert Systems with Applications 38, 8178–8185. DOI:10.1016/j.eswa.2010.12.162
Werritty, A., Paine, J.L., Macdonald, N., Rowan, J.S., McEwen, L.J., 2006. Use of multi-proxy flood records to improve estimates of flood risk: Lower River Tay, Scotland. Catena 66, 107–19. DOI:10.1016/j.catena.2005.07.012
Wetter, O., 2017. The potential of historical hydrology in Switzerland. Hydrological and Earth System Sciences 21, 5781–5803. DOI:10.5194/hess-21-5781-2017
Wetter, O., Pfister, C., Weingartner, R., Luterbacher, J., Reist, T., Trösch, J., 2011. The largest floods in the High Rhine basin since 1268 assessed from documentary and instrumental evidence. Hydrological Sciences Journal 56, 733–758. DOI:10.1080/02626667.2011.583613
Wierda, M., Zweerus, L., 1994. Omzetting rivierkaarten 1830–1860 naar GIS. RIZA working document 94.105X.
Wijbenga, J.H.A., Lambeek, J.J.P., Mosselman, E., Nieuwkamer, R.L.J., Passchier, R., 1993. Toetsing uitgangspunten rivierdijkversterkingen. Deelrapport 2: Maatgevende belastingen. Ministerie van Verkeer en Waterstaat.
Wilhelm, B., Ballesteros-Cánovas, J.A., Corella, J.P., Kämpf, L., Swierczynski, T., Stoffel, M., Støren, E., Toonen, W.H.J., 2018. Recent advances in paleoflood hydrology: from new archives to data compilation and analysis. Water Security 3, 1–8. DOI:10.1016/j.wasec.2018.07.001
Wilhelm, B., Ballesteros-Cánovas, J.A., Macdonald, N., Toonen, W.H.J., Baker, V.R. Barriendos, M., Benito, G., Brauer, A., Corella, J.P., Denniston, R.F., Glaser, R., Ionita, M., Kahle, M., Liu, T., Luetscher, M., Macklin, M.G., Mudelsee, M., Munoz, S.E., Schulte, L., St. George, S., Stoffel, M., Wetter, O., 2019. Interpreting historical, botanical, and geological evidence to aid preparations for future floods. WIREs Water 6, e1318. DOI:10.1002/wat2.1318
Willemse, N.W., 2019. De vroege Waal bij Nijmegen. Stratigrafie, sedimentologie en genese van laatholocene rivierafzettingen tussen Nijmegen en Lent. RAAP report 3208.
Willmes, C., Niedziółka, K., Serbe, B., Grimm, S.B., Groß, D., Miebach, A., Märker, M., Henselowsky, F., Gamisch, A., Rostami, M., Mateos, A., Rodríguez, J., Limberg, H., Schmidt, I., Müller, M., Hölzchen, E., Holthausen, M., Klein, K., Wegener, C., Weninger, B., Nielsen, T.K., Otto, T., Weniger, G.-C., Bubenzer, O., Bareth, G., 2020. State of the Art in Paleoenvironment Mapping for Modeling Applications in Archeology—Summary, Conclusions, and Future Directions from the PaleoMaps Workshop. Quaternary 3, 13. DOI:10.3390/quat3020013
Winsemius, H.C., Aerts, J.C.J.H., van Beek, L.P.H., Bierkens, M.F.P., Bouwman, A., Jongman, B., Kwadijk, J.C.J., Ligtvoet, W., Lucas, P.L., van Vuuren, D.P., Ward, P.J., 2016. Global drivers of future river flood risk. Nature Climate Change 6, 381–385. DOI:10.1038/nclimate2893
Witte, W., Krahe, P., Liebscher, H.J., 1995. Rekonstruktion der Witterungsverhältnisse im Mittelrheingebiet von 1000 n. Chr. bis heute anhand historischer hydrologischer Ereignisse. International Commission for the Hydrology of the Rhine Basin report II-9.

Wolfert, H.P., Maas, G.J., 2007. Downstream changes of meandering styles in the lower reaches of the River Vecht, the Netherlands. Netherlands Journal of Geosciences 86, 257–271. DOI:10.1017/S0016774600077842

Woodward, J.C., Tooth, S., Brewer, P.A., Macklin, M.G., 2010. The 4th International Palaeoflood Workshop and trends in palaeoflood science. Global and Planetary Change 70, 1–4. DOI:10.1016/j.gloplacha.2009.11.002

Wronna, M., Baptista, M.A., Götz, J., 2017. On the construction and use of a paleo-DEM to reproduce tsunami inundation in a historical urban environment – the case of the 1755 Lisbon tsunami in Cascais. Geomatics, Natural Hazards and Risk 8, 841–862. DOI:10.1080/19475705.2016.1271832

Ylla Arbós, C., Blom, A., Viparelli, E., Reneerkens, M., Frings, R. M., Schielen, R. M. J., 2021. River response to anthropogenic modification: Channel steepening and gravel front fading in an incising river. Geophysical Research Letters 48, e2020GL091338. DOI:10.1029/2020GL091338

Zanoni, L., Gurnell, A., Drake, N., Surian, N., 2008. Island dynamics in a braided river from analysis of historical maps and air photographs. River Research and Applications 24, 1141–1159. DOI:10.1002/rra.1086

Zhang, Y., Huang, C.C., Pang, J., Zha, X., Zhou, Y., Wang, X., 2015. Holocene palaeoflood events recorded by slackwater deposits along the middle Beiluohe River valley, middle Yellow River basin, China. Boreas 44, 127–138. DOI:10.1111/bor.12095

Zhou, D., 2000. Jungquartäre Talgeschichte des mittleren Niederrheins. PhD thesis, Düsseldorf.

Zimmermann, E., Quiring, H., Fuchs, A., 1930. Erläuterungen zur Geologischen Karte von Preußen und benachbarten deutschen Ländern. Blatt Hilden, Nr. 2780. Preußisches Geologisches Landesanstalt, Berlin.

Summary

This thesis examines the largest floods of the Lower Rhine river over the past centuries to millennia (Late Holocene to historic time frame). Its central objective is to quantify these events. First, the thesis determines maximum water levels in the past based on sedimentological interpretation of archaeological stratigraphy and geographical survey of epigraphic marks. Next, it provides detailed reconstructions of the alluvial terrain of the Lower Rhine valley and delta, covering the early modern channel bathymetry restored from historic maps and the medieval floodplain topography restored from geomorphological analysis and interpolation. The past landscape context then serves to set up a palaeoflood hydraulic model that resolves the discharges of the largest floods by linking the simulation results to reconstructed water levels. The insights gained in this thesis may ultimately contribute to the design of future flood protection measures.

The overarching findings demonstrate that reliable quantification of past floods in lowland river settings necessitates a two-dimensional approach, when it comes to the required flood level and landscape reconstructions and the discharge calculations. Furthermore, the findings show that palaeoflood research benefits from a multidisciplinary approach, with the primary methodological focus depending on the selected casus and targeted time period. The results include successfully reconstructed pre-instrumental flood levels across the Lower Rhine valley and delta by integrating archaeological, geological, and historical sources (Chapters 2, 3, and 6). Additionally, the results encompass successful reconstructions of the landscape for two key periods: before the onset of river normalisation in the mid-nineteenth century and before the onset of embankment in medieval times (Chapters 4 and 5). Finally, the thesis provides an estimate for the 'millennial' discharge in the Late Holocene by numerical flood simulations in the pre-embanked landscape context, resulting in a value of 14,000 m^3/s (Chapter 6). Further output of the *Floods of the Past, Design for the Future* project shows that the landscape context prior to normalisation is crucial to constraining discharge magnitudes of individual historic flood events (Chapter 4).

Chapter 2 — Medieval extreme flood levels

Reconstructing water levels reached during past floods contributes to fluvial system understanding and flood risk assessments. For methodological restrictions, this type of research is usually conducted in confined valley settings. In this study, we expand upon that geomorphological context by reconstructing extreme flood levels in a lowland delta setting. We used the archaeological stratigraphy of medieval river cities in the Rhine delta to determine water levels for the largest historic flood in the year 1374. We obtained minimum estimates by identifying thin fluvial deposits interbedded with anthropogenic layers, and further constrained peak flood levels using fourteenth-century raised ground layers directly overlying these deposits. First, we tested the proposed method for extracting flood levels from urban archaeological stratigraphy in the city of Arnhem. Then, we complemented those results with archaeological and historical data in other cities to arrive at a complete overview for the Rhine delta. This overview shows that the 1374 flood levels exceed the highest levels in the instrumental record along the northern distributary (IJssel river), but not

along the western distributaries in the central delta (Nederrijn and Waal rivers). This pattern is explained by changes in the discharge division over the different river branches and by the rise of embankments since late medieval times, which considerably decreased the flooded area. Thus, this study demonstrates not only the potential of palaeoflood reconstructions in lowland floodplain settings (see Chapter 6), but also the pitfalls, resulting from spatially complex flooding patterns and anthropogenic terrain modifications (see Chapter 3 and Chapter 5).

Chapter 3 — Flood marks on buildings

This chapter presents an inventory of historic flood levels marked on buildings and other structures in the Rhine delta. These flood marks provide maximum water levels across the area from the late sixteenth to twentieth centuries, complementing instrumental measurement records in both space and time. The main goals of the chapter are to explain how I created this inventory and to unlock the resulting flood level dataset for hydrological analyses.

Chapter 4 — Historic river morphology

This chapter describes a reconstruction I made of the Rhine river branches and their surrounding floodplains based on historic maps and measurement data. The results have been used in numerical simulations of an early nineteenth-century extreme flood event. The reconstruction covers all relevant river landscape elements in the delta, but the focus of the chapter is on the historical morphology of the river branches.

Chapter 5 — Digital Elevation Model reconstruction

Reconstruction of past topography in palaeo-DEMs serves various geomorphological analyses. Constructing a palaeo-DEM by stripping young elements from a LiDAR DEM can provide results for large study areas at high resolution. However, such a 'top-down' approach is more suited to recent periods and geomorphologically static parts of the landscape than to geomorphologically dynamic areas and periods farther back in time. Here, we explore this approach by reconstructing the early medieval (circa 800 CE) topography of the Lower Rhine river valley and upper delta in Germany and the Netherlands. The large (~4,500 km^2) study area contains abundant anthropogenic terrain modification and stretches across geomorphologically active as well as inactive zones. The active zone, close to the river, is characterized by meander activity and cut-offs in the last 1200 years. The inactive zone is the remainder of the floodplain. We first removed all anthropogenic relief elements from the LiDAR DEM, using separate procedures for linear and non-linear elements. These steps were sufficient to obtain the palaeotopography of the inactive zone, characterized by inherited natural relief. Then, we reconstructed the topography and bathymetry in the fluvially-reworked active zone by incorporating geological and historical geographical information. We present and evaluate zonal averages of elevation differences between the modern and past valley floor topography in this densely populated area with complex land-use history, which allows us to approximate total anthropogenic volumetric change. Further comparisons with the modern LiDAR DEM indicate large changes in floodplain negative-relief connectivity, demonstrating the importance of palaeo-DEMs for research into past river floods. Our palaeo-DEM construction

workflow is deployable at diverse spatial scales and widely applicable to other lowland areas, because of its top-down and generic nature. The relative importance of different workflow aspects depends on the time period that is targeted. Beyond a target age of 10–15 ka, large valley floors are considered geomorphologically dynamic and a top-down approach to palaeo-DEM construction is no longer advisable.

Chapter 6 — Palaeoflood simulation

Palaeoflood hydraulic modelling is essential for quantifying 'millennial flood' events not covered in the instrumental record. Palaeoflood modelling research has largely focused on one-dimensional analysis for geomorphologically stable fluvial settings, because two-dimensional analysis for dynamic alluvial settings is time-consuming and requires a detailed representation of the past landscape. In this study, we make the step to spatially continuous palaeoflood modelling for a large and dynamic lowland area. We applied advanced hydraulic model simulations (1D–2D coupled set-up in HEC-RAS with 950 channel sections and 108 × 10^3 floodplain grid cells) to quantify the extent and magnitude of past floods in the Lower Rhine river valley and upper delta. As input we used a high-resolution terrain reconstruction (palaeo-DEM) of the area in early medieval times, complemented with hydraulic roughness values. After conducting a series of model runs with increasing discharge magnitudes at the upstream boundary, we compared the simulated flood water levels to an inventory of exceeded and non-exceeded elevations extracted from various geological, archaeological and historical sources. This comparison demonstrated a Lower Rhine millennial flood magnitude of approximately 14,000 m^3/s for the Late Holocene period before late medieval times. This value exceeds the largest measured discharges in the instrumental record, but not the design discharges currently accounted for in flood risk management.

Samenvatting

Dit proefschrift onderzoekt de grootste overstromingen van de Benedenrijn in de afgelopen eeuwen tot millennia (Laat Holoceen tot historisch tijdsbestek), met als belangrijkste doelstelling deze te kwantificeren. Om te beginnen achterhaalt het proefschrift maximale waterstanden in het verleden door sedimentologische interpretatie van archeologische stratigrafie en geografische opmeting van hoogwatermarkeringen. Daarna geeft het gedetailleerde reconstructies van het rivierlandschap in de Benedenrijnse laagvlakte en de Rijndelta. Deze beslaan de vroegmoderne rivierbedding gebaseerd op historische kaarten en de middeleeuwse topografie gebaseerd op geomorfologische analyse en interpolatie. De vroegere landschapscontext dient vervolgens om een hydraulisch model op te zetten dat de afvoeren van de grootste overstromingen bepaalt door de simulatieresulaten aan gereconstrueerde waterstanden te koppelen. De inzichten verkregen in dit proefschrift kunnen op termijn bijdragen bij aan het ontwerp van toekomstige hoogwaterbeschermingsmaatregelen.

De overkoepelende bevindingen tonen aan dat een tweedimensionale aanpak vereist is om vroegere overstromingen in laaglandgebieden betrouwbaar te kwantificeren. Dit geldt voor de benodigde waterstands- en landschapsreconstructies en de afvoerberekeningen. De bevindingen laten verder zien dat onderzoek naar vroegere overstromingen gebaat is bij een multidisciplinaire aanpak, waarbinnen het zwaartepunt afhangt van de geselcteerde casus en tijdsperiode. De resultaten omvatten succesvol gereconstrueerde hoogwaterstanden in de Benedenrijnse laagvlakte en de Rijndelta door archeologische, geologische en historische bronnen te integreren (Hoofdstukken 2, 3 en 6). Daarnaast bestaan de resultaten uit succesvolle reconstructies van het landschap voor twee sleutelperiodes: voor de riviernormalisatie in het midden van de negentiende eeuw en voor de bedijking in de middeleeuwen (Hoofdstukken 4 en 5). Tenslotte geeft het proefschrift een schatting van de 'duizendjarige' afvoer in het Laat Holoceen aan de hand van numerieke overstromingssimulaties in de onbedijkte landschapscontext, resulterend in een waarde van 14,000 m^3/s (Hoofdstuk 6). Verdere uitkomsten van het *Floods of the Past, Design for the Future* project wijzen uit dat de landschapscontext voor de normalisatie een cruciale rol speelt in het verfijnen van afvoergroottes van individuele historische overstromingen (Hoofdstuk 4).

Hoofdstuk 2 — Waterstanden van extreme overstromingen in de middeleeuwen

Het reconstrueren van waterstanden van vroegere extreme overstromingen draagt bij aan het begrip van fluviatiele systemen en aan het afschatten van overstromingsrisico's. Wegens methodologische beperkingen wordt zulk onderzoek meestal uitgevoerd in nauwe rivierdalen. In deze studie breiden we die geomorfologische context uit door extreme waterstanden te reconstrueren in een laaglandsetting. We gebruiken de archeologische stratigrafie van middeleeuwse riviersteden in de Rijndelta om de maximale waterstanden te bepalen van de grootste historische overstroming, in het jaar 1374. Minimumschattingen komen van dunne fluviatiele afzettingen en maximumschattingen van veertiende-eeuwse ophooglagen direct boven deze afzettingen. We hebben de voorgestelde methode om hoogwaterstanden uit stedelijke archeologische stratigrafie te halen eerst getest in de binnenstad van Arnhem. Deze resultaten hebben we vervolgens aangevuld met archeologische

en historische observaties in andere steden om tot een compleet overzicht voor de Rijndelta te komen. Dit overzicht toont aan dat de maximale waterstanden in 1374 de hoogste waterstanden in instrumentale meetreeksen overschrijden langs de noordelijke riviertak (IJssel), maar niet langs de westelijke riviertakken (Nederrijn en Waal). Dit kan worden verklaard door veranderingen in de afvoerverdeling over de takken en door dijkverzwaringen sinds de late middeleeuwen, waardoor het gebied dat overstroomde aanzienlijk is afgenomen. Deze studie toont niet alleen het potentieel van overstromingsreconstructies in laaggelegen gebieden (zie Hoofdstuk 6), maar ook de valkuilen als gevolg van ruimtelijk complexe overstromingspatronen en antropogene ingrepen in het landschap (zie Hoofdstuk 3 en Hoofdstuk 5).

Hoofdstuk 3 — Hoogwatermarkeringen op gebouwen

Dit hoofdstuk geeft een inventarisatie van historische waterstanden gemarkeerd op gebouwen en andere constructies in de Rijndelta. Deze hoogwatermarkeringen tonen maximale waterstanden van de late zestiende tot twintigste eeuw en komen verspreid over het gebied voor. Zodoende vormen ze een aanvulling op instrumentale meetgegevens in zowel ruimte als tijd. De hoofddoelen van het hoofdstuk zijn om duidelijk te maken hoe ik deze gegevens heb verzameld en om de resulterende dataset van hoogwaterstanden te ontsluiten voor hydrologische analyses.

Hoofdstuk 4 — Historische riviermorfologie

Dit hoofdstuk beschrijft een reconstructie van de Rijntakken en de omliggende gebieden op basis van historische kaarten en meetgegevens. De resultaten zijn gebruikt in numerieke simulaties van een vroeg-negentiende-eeuwse extreme overstroming. De reconstructie omvat alle relevante landschapselementen in de delta, maar de focus van het hoofdstuk ligt op de historische morfologie van de riviertakken.

Hoofdstuk 5 — Reconstructie van een digitaal hoogtemodel (DEM)

De reconstructie van vroegere topografie in een 'paleo-DEM' dient verschillende geomorfologische doeleinden. Een palaeo-DEM kan op hoge resolutie voor een groot studiegebied worden gemaakt door jonge elementen uit een LiDAR-DEM te verwijderen. Een dergelijke 'top-down' benadering is echter meer geschikt voor recente perioden en voor geomorfologisch statische delen van het landschap dan voor dynamische gebieden en voor perioden verder terug in de tijd. Hier onderzoeken we deze benadering door de vroegmiddeleeuwse (circa 800) topografie van de Benedenrijnse laagvlakte en de Rijndelta te reconstrueren. Dit grote (~4,500 km^2) studiegebied bevat veel antropogene terreinveranderingen en beslaat zowel geomorfologisch actieve als inactieve zones. De actieve zone, dicht langs de rivier, kende rivierbochtverplaatsingen en -afsnijdingen in de laatste 1200 jaar. De inactieve zone is de rest van de overstromingsvlakte. We hebben eerst alle antropogene reliëfelementen uit het LiDAR-DEM verwijderd met afzonderlijke procedures voor lineaire en niet-lineaire elementen. Deze stappen waren afdoende voor de inactieve zone met overgeërfd natuurlijk reliëf. Vervolgens hebben we de topografie en bathymetrie in de door de rivier herwerkte actieve zone gereconstrueerd aan de hand van geologische en historisch geografische gegevens. We bepalen en evalueren zonale hoogteverschillen tussen de moderne en de vroegere

topografie, wat leidt tot een benadering van het totale volume van antropogene veranderingen in dit dichtbevolkte gebied met complexe geschiedenis van landgebruik. Verdere vergelijkingen met het huidige terrein wijzen op grote veranderingen in de connectiviteit van negatief reliëf, wat het belang aantoont van paleo-DEMs voor onderzoek naar vroegere rivieroverstromingen. Onze workflow is breed toepasbaar op laaglandgebieden op diverse ruimtelijke schaalniveaus vanwege de generieke insteek en de benadering die overwegend top-down is. Het relatieve belang van de verschillende workflowaspecten hangt samen met de beoogde tijdsperiode. Verder dan tien- tot vijftienduizend jaar terug kunnen grote riviervlaktes als geomorfologisch dynamisch worden beschouwd en is een top-down benadering voor het maken van een paleo-DEM niet meer geschikt.

Hoofdstuk 6 — Simulatie van vroegere overstromingen

Hydraulische modellering van vroegere overstromingen is essentieel voor het kwantificeren van extreme afvoeren die niet voorkomen in instrumentale meetreeksen. Dit type onderzoek houdt zich voornamelijk bezig met eendimensionale analyses voor geomorfologisch stabiele gebieden, omdat tweedimensionale analyses voor geomorfologisch dynamische gebieden veel tijd kosten en een gedetailleerde weergave van het vroegere landschap vereisen. In deze studie maken we de stap naar ruimtelijke modellering van vroegere overstromingen voor een groot en dynamisch laaglandgebied. We gebruiken geavanceerde hydraulische simulaties (1D–2D gekoppelde structuur in HEC-RAS met 950 secties in de geul en 108×10^3 cellen in de overstromingsvlakte) om de omvang en afvoergrootte te bepalen van vroegere overstromingen in de Benedenrijnse laagvlakte en de Rijndelta. Als invoer gebruiken we een gedetailleerde reconstructie van het gebied in de vroege middeleeuwen, aangevuld met hydraulische ruwheidswaarden. Na het uitvoeren van een serie modelruns met toenemende bovenstroomse afvoerpiek, vergelijken we de gesimuleerde hoogwaterstanden met een inventarisatie van overschreden en niet-overschreden niveaus bepaald uit verschillende geologische, archeologische en historische bronnen. Dit geeft een waarde van ongeveer 14.000 m^3/s voor de 'duizendjarige' afvoer van de Benedenrijn in het Laat Holoceen tot aan de bedijking. Deze waarde overtreft de hoogste gemeten afvoeren, maar niet de ontwerpwaardes waarmee rekening wordt gehouden in de huidige hoogwaterbescherming.

About the author

Bas van der Meulen was born in Amersfoort on September 9, 1991. He attended high school at the *stedelijk gymnasium Johan van Oldenbarnevelt*, where he graduated in 2009. Without much of a doubt, Bas decided to study Earth Sciences in Utrecht. This turned out to be an excellent choice, as he liked all aspects of the study. Still, he broadened his view by taking classes at different institutes on top of the regular curriculum, including a course on historical geography at the Human Geography department, a minor in climate physics at the Science faculty, and an archaeological field campaign to Greece led by Ghent University. This already showed the wide interest that Bas later applied in his PhD research, combining different aspects of Earth science (geomorphology, sedimentology, stratigraphy) with historical geography, archaeological fieldwork, and hydrological modelling. Bas obtained his BSc degree in 2013 and his MSc degree in 2015, both with distinction (*cum laude*, GPA >4).

During his studies, Bas received funding by the KNAW (Royal Netherlands Academy of Arts and Sciences) to work as an assistant in the project *River flood record from fresh core material of abandoned Rhine channels* at the department of Physical Geography, where he conducted various laboratory measurements (organic content, grain size, palaeomagnetism) and Bayesian age modelling analyses. Furthermore, he was a teaching assistant in several undergraduate courses, mainly in the field of sedimentary geology, but also in the fields of chemistry and mathematics. Both the laboratory assistantship and the teaching activities motivated Bas to continue in academia. In the last year of his studies, Bas was applied part-time by the Freudenthal Institute, where he developed education materials on long-term climate changes and taught these to upper level high school students (*U-Talent programme*). In addition, he was applied by the Geosciences faculty where he assisted in starting up the archival campaign of the lacquer peel sample collection.

Before starting his PhD at the department of Physical Geography, Bas worked for six months as a junior researcher at the department of Earth Sciences in the Stratigraphy and Palaeontology group. Here, he studied fluvial sedimentary rocks of the Bighorn Basin in Wyoming, which eventually led to a first-authored publication. He combined stratigraphic records obtained in the field with isotope measurements and palaeontological data, resulting in an integrative reconstruction of climate change and mammalian evolution at the Palaeocene–Eocene boundary. Although this research was very interesting to Bas, he wanted to work on scientific problems with more direct societal relevance. Furthermore, he wished to integrate his interests in historical geography and archaeology into his research. Therefore, he started a PhD in the project *Floods of the Past, Design for the Future*, which culminated in the thesis that is in front of you.

Bas has always loved the tangible and outdoors nature of his education and career. He has conducted abundant fieldwork and participated in many excursions, both as a student or researcher and as a teacher. Bas likes to explore nature and culture in his free time as well, and thoroughly enjoys road trips and cycling tours. Other hobbies include playing board games, writing and performing comedy (Bas occasionally contributes to Dutch satirical website *De Speld*), and playing ultimate frisbee at UFO ('Utregse Frisbee Organisatie'). At the moment, Bas is looking for a job that aligns with his interests, in which he can combine teaching and supervising at an academic level with setting up excursions and field trips.

List of publications

in reverse chronological order

Dierkx, J.R., Bomers, A., **van der Meulen, B.,** Cohen, K.M., Hulscher, S.J.M.H., 2021 (submitted). Modelling early medieval flood-induced breaching of a coversand ridge in the IJssel valley, Rhine delta, the Netherlands. Geomorphology, under review.

van der Meulen, B., Defilet, M.P., Tebbens, L.A., Cohen, K.M., 2021 (submitted). Palaeoflood level reconstructions in a lowland setting from urban archaeological stratigraphy, Rhine river delta, the Netherlands. Catena, under review.

van der Meulen, B., 2021. Historic flood level inventory from epigraphic marks in the Rhine river delta. DANS dataset.
DOI:10.17026/dans-2zz-kpka

van der Meulen, B., Bomers, A., Cohen, K.M., Middelkoop, H., 2021. Late Holocene flood dynamics and magnitudes in the Lower Rhine river valley and upper delta resolved by a two-dimensional hydraulic modelling approach. Earth Surface Processes and Landforms 46, 853–868.
DOI:10.1002/esp.5071

Bomers, A., Hulscher, S.J.M.H., **van der Meulen, B.**, Schielen, R.M.J., 2020. Historic flood reconstructions for a safer future: the use of three types of surrogate models. Proceedings of the 10th International Conference on Fluvial Hydraulics.
DOI:10.1201/b22619-263

van der Meulen, B., Cohen, K.M., Pierik, H.J., Zinsmeister, J.J., Middelkoop, H., 2020. LiDAR-derived high-resolution palaeo-DEM construction workflow and application to the early medieval Lower Rhine valley and upper delta. Geomorphology 370, 107370.
DOI:10.1016/j.geomorph.2020.107370

van der Meulen, B., Zielman, G., 2020. Hoofdstuk 3. Fysisch-geografisch onderzoek. In: Baetsen, W.A., Zielman, G., (Eds.). Wat de nieuwe Sint Jansbeek boven water bracht: dood en leven in het Arnhemse verleden. Archeologisch onderzoek Sint Jansbeek te Arnhem. RAAP report 4476, 33–43.

van der Meulen, B., Gingerich, P.D., Lourens, L.J., Meijer, N., van Broekhuizen, S., van Ginneken, S., Abels, H.A., 2020. Carbon isotope and mammal recovery from extreme greenhouse warming at the Paleocene–Eocene boundary in astronomically-calibrated fluvial strata, Bighorn Basin, Wyoming, USA. Earth and Planetary Science Letters 534, 116044.
DOI:10.1016/j.epsl.2019.116044
Press release: www.uu.nl/nieuws/reconstructie-van-een-broeikasperiode (Dutch),
www.uu.nl/en/news/reconstruction-of-a-greenhouse-warming-period (English)

Bomers, A., **van der Meulen, B.**, 2019. Reconstructed data on the 1809 historic flood event of the Rhine river. 4TU.Centre for Research Data.
DOI:10.4121/uuid:2068ddc3-1726-4d9d-bbe7-37477767b220

Bomers, A., **van der Meulen, B.**, Schielen, R.M.J., Hulscher, S.J.M.H., 2019. Historic flood reconstruction with the use of an Artificial Neural Network. Water Resources Research 55, 9673–9688.
DOI:10.1029/2019WR025656

van der Meulen, B., Pierik, H.J., Middelkoop, H., Cohen, K.M., 2019. Reconstruction of early historic topography of a large lowland area for palaeo-hydraulic analyses. International Union for Quaternary Research (INQUA) 20th Congress.

van der Meulen, B., 2019. Insights into fluvial morphological processes from historic maps of Rhine river branches. International Conference on the History of Cartography (ICHC) and International Cartographic Association (ICA) joined pre-ICHC event. Controlling the waters: seas, lakes and rivers on historic maps and charts.

van der Meulen, B., Cohen, K.M., Pierik, H.J., Middelkoop, H., 2019. Early historic topography of the Lower Rhine valley and upper delta. Nederlands Aardwetenschappelijk Congres 15.

van der Meulen, B., Zinsmeister, J.J., Pierik, H.J., Cohen, K.M., 2018. Reconstructing floodplain topography and river bathymetry of the Lower Rhine for palaeoflood hydraulic studies. Fluvial Archives Group (FLAG) Biennial Meeting 2018.

Pierik, H.J., **van der Meulen, B.**, van Lanen, R.J., Cohen, K.M., 2018. Holocene palaeoDEMs for the Rhine valley and delta plain, the Netherlands and Germany. EGU General Assembly 20.
https://meetingorganizer.copernicus.org/EGU2018/EGU2018-8155.pdf

van der Meulen, B., Cohen, K.M., 2018. Historic extreme flood levels and archaeological excavations. Nederlands Aardwetenschappelijk Congres 14.

van der Meulen, B., Deggeller, T.S., Bomers, A., Cohen, K.M., Middelkoop, H., 2018. The historical river: morphology of the Rhine before river normalization. In: Huismans, Y., Berends, K.D., Niesten, I., Mosselman, E., (Eds.). The future river: Netherlands Centre for River Studies conference proceedings.
https://cdn.bullit.digital/ncr-web/20200918091508/ncr-42-ncrdays2018_bookofabstracts-web.pdf

Cohen, K.M., Koster, K., Pierik, H.J., **van der Meulen, B.**, Hijma, M.P., Schokker, J., Stafleu, J., 2017. Holocene palaeoDEMs for coastal and delta plain landscape reconstructions. EGU General Assembly 19.
https://meetingorganizer.copernicus.org/EGU2017/EGU2017-5559-1.pdf

Cohen, K.M., Schielen, R., **van der Meulen, B.**, Bomers, A., Hulscher, S.J.M.H., Middelkoop, H., 2016. Floods of the Past, Design of Tomorrow – Project Introduction. In: Fontana, A., Rossata, S., (Eds.). Palaeohydrological extreme events: evidence and archives. EX-AQUA abstracts, Università degli Studi di Padova.

van der Meulen, B., Abels, H.A., Meijer, N., Gingerich, P.D., Lourens, L.J., 2016. Carbon isotope signature and precession-scale chronology of the PETM in a terrestrial setting. International Conference on Paleoceanography 12.

van der Meulen, B., Abels, H.A., Meijer, N., Gingerich, P.D., Lourens, L.J., 2016. Constraints on the duration of the Paleocene–Eocene Thermal Maximum by orbitally-influenced fluvial sediment records of the northern Bighorn Basin, Wyoming, USA. EGU General Assembly 18.
https://meetingorganizer.copernicus.org/EGU2016/EGU2016-15040.pdf

van der Meulen, B., Abels, H.A., Meijer, N., Gingerich, P.D., Lourens, L.J., 2016. Constraints on the duration of the PETM by orbitally-influenced fluvial sediment records of the northern Bighorn Basin, Wyoming, USA. Nederlands Aardwetenschappelijk Congres 13.

van der Meulen, B., 2015. PETM chronology by orbitally-influenced fluvial sediment records. MSc thesis, Utrecht University.
(Grade 9/10)
http://dspace.library.uu.nl/handle/1874/324355

Toonen, W.H.J., Donders, T.H., **van der Meulen, B.**, Cohen, K.M., Prins, M.A., 2013. A composite Holocene palaeoflood chronology of the Lower Rhine. In: Toonen, W.H.J., 2013. A Holocene flood record of the Lower Rhine. PhD thesis, Utrecht University.
https://dspace.library.uu.nl/bitstream/1874/282871/2/toonen.pdf

van der Meulen, B., 2013. Global expression of the 4.2 ka event. BSc thesis, Utrecht University.
(Grade 9/10)